Deltares

Enabling Delta Life

Derivation of the semi-probabilistic safety assessment for piping

WTI 2017: Cluster C, piping failure mechanism

Deltares

Derivation of the semi-probabilistic safety assessment for piping

WTI 2017: Cluster C, piping failure mechanism

Ana Teixeira
Karolina Wojciechowska
Wouter ter Horst

1220080-002

Deltares

Title
Derivation of the semi-probabilistic safety assessment for piping

Client	Projectnumber	Reference	Pages
Rijkswaterstaat Water, Verkeer en Leefomgeving Locatie Lelystad	1220080-002	1220080-002-ZWS-0006	165

Classification
1220080-002-ZWS-0006 - final

Keywords
WTI 2017, safety factors, calibration, piping, heave, uplift, probabilistic analysis, reliability

Summary

In the Netherlands, all primary flood defences are periodically tested against statutory safety standards. The new safety assessment framework WTI 2017 (defined in terms of allowable probability of flooding) allows for probabilistic as well as semi-probabilistic assessments, where the latter are based on a partial safety factor approach. To ensure consistency between probabilistic and semi-probabilistic assessments, the currently in use semi-probabilistic rules have to be (re)calibrated based on probabilistic analyses.

This report presents the procedure and results of the calibration of the semi-probabilistic assessment rules for the piping failure mechanism. The calibration is performed with the new piping kernel and information (schematisations and geotechnical parameter values) from the VNK2-project (Flood Risks and Safety in the Netherlands, in Dutch *Veiligheid Nederland in Kaart*), with exception of the uncertainty of the permeability and grain size parameters which were fixed by experts and recommended in the schematisation guidelines of the piping mechanism.

The piping failure mechanism consists of three sub-mechanisms: heave, uplift and backward erosion. The latter is often referred to as piping. A calibration has been performed for all three sub-mechanisms. In the WTI framework, sub-soil scenarios were introduced to account for various possible sub-soils, each having a certain likelihood. One of the subjects of this report is the description of the semi-probabilistic assessment with various sub-soil scenarios.

The result of the calibration is an exponential relation (defined per sub-mechanism) between the reliability β and the safety factor γ, which has to be applied in the semi-probabilistic assessment. The relation is given in terms of two reliability indices β_{cross} (cross-section level) and β_{norm} (norm requirement, or safety standard). Figure 1, 2 and 3 give the derived relations for all three sub-mechanisms. Note that the relations have been derived separately for different safety levels (β_{norm}). This was done to prevent the semi-probabilistic assessment rules from becoming overly conservative.

As a final step, the allowable probability of failure on the cross-section level has been derived from the safety standard of the considered dike segment. For that we recommend the following length-effect parameters: $b = 350$ m and $a = 1$. This assumes that the entire dike segment is sensitive to piping (since $a = 1$) and that the length of an equivalent independent dike section is equal to 350 m. If this is not the case, the user can lower the value of a.

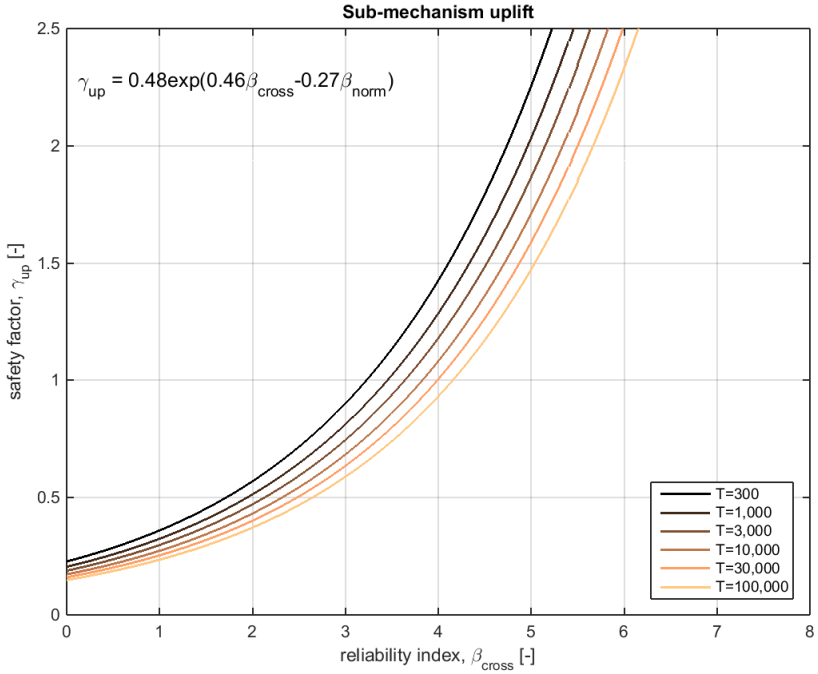

Figure 1: Relation between the required reliability and the safety factor for the uplift sub-mechanism.

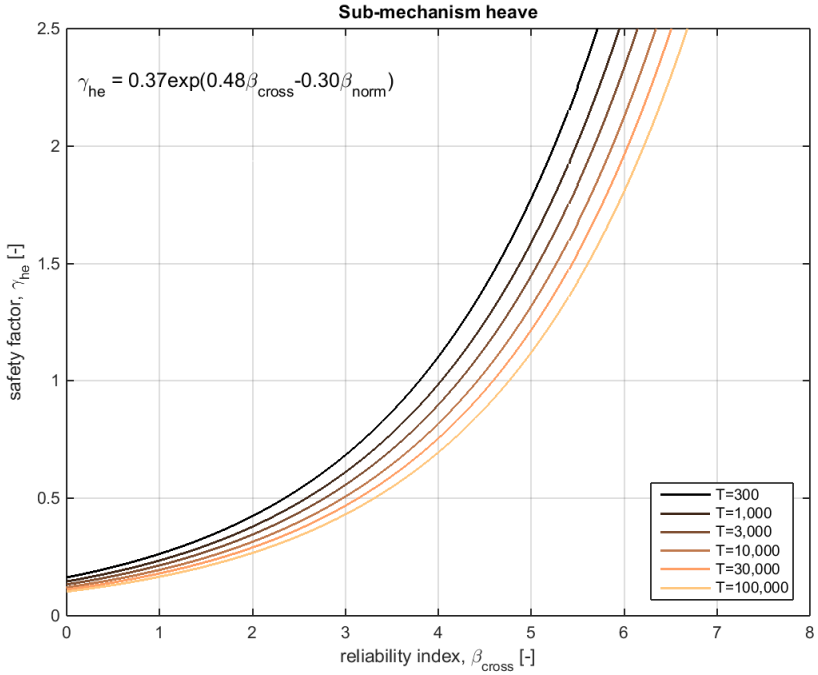

Figure 2: Relation between the required reliability and the safety factor for the heave sub-mechanism.

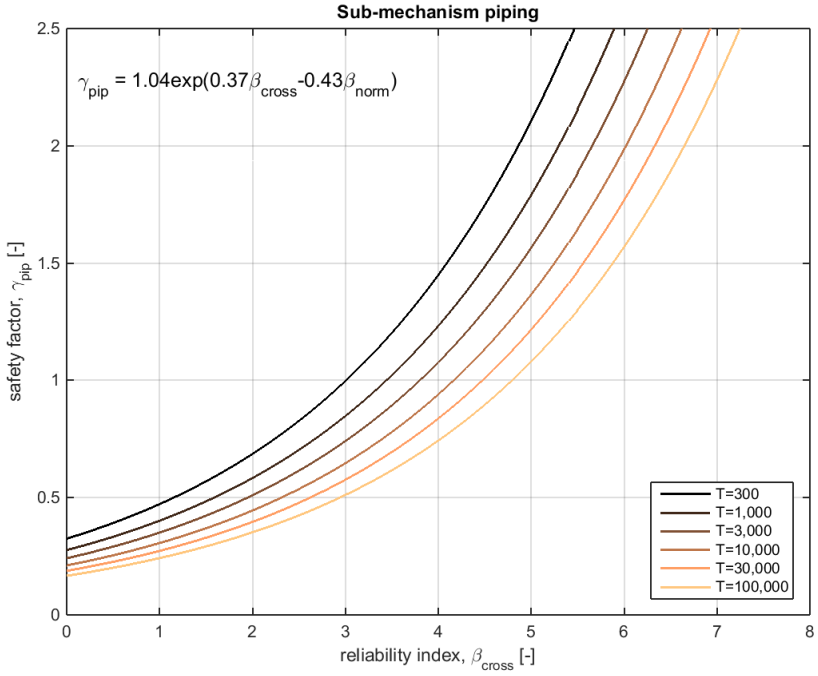

Figure 3: Relation between the required reliability and the safety factor for the piping sub-mechanism.

Samenvatting

In Nederland worden alle primaire waterkering getoetst, waarbij wordt gekeken of ze voldoen aan de wettelijke veiligheidsnormen. Binnen het nieuwe wettelijke toetsinstrumentarium (WTI 2017), gedefineerd in termen van toelaatbare overstromingskansen, is het mogelijk om zowel een volledig probabilistische toets als een semi-probabilistische toets uit te voeren. Bij de semi-probabilistische toets wordt gebruik gemaakt van veiligheidsfactoren, die de mate van veiligheid weergeven. Om ervoor te zorgen dat de probabilistische toets en de semi-probabilistische toets goed op elkaar aansluiten zijn de toe te passen veiligheidsfactoren van de semi-probabilistische toets gekalibreerd met behulp van een probabilistische analyse.

In dit rapport worden de werkwijze en de resultaten van de kalibratie van de semi-probabilistische toetsregel voor piping beschreven. De kalibratie is uitgevoerd met behulp van de nieuwe piping rekenkern, waarbij gebruik gemaakt is van informatie (schematiseringen en parameters) uit het project Veiligheid Nederland in Kaart (VNK2) met uitzondering van de onzekerheden in doorlatendheid en korreldiameter. Deze waren vastgesteld door experts en aanbevolen in de schematiseringshandleiding van het piping faalmechanisme.

Het faalmechanisme piping bestaat uit de drie submechanismen: heave, opbarsten en terugschrijdende (interne) erosie. Het laatste wordt ook vaak als piping aangeduid. Voor alle drie de sub-mechanismen is de kalibratie uitgevoerd. Bij de kalibratie is rekening gehouden met het feit dat binnen het WTI wordt gewerkt met verschillende ondergrondscenario's die een bepaalde kans van voorkomen hebben. Dit rapport beschrijft ook de semi-probabilistische beoordeling met verschillende ondergrondsce-

nario's.

Het resultaat van de kalibratie is een exponentiele relatie tussen de betrouwbaarheid β en de veiligheidsfactor γ, die moet worden toegepast in de semi-probabilistische beoordeling. De relatie wordt gegeven in de vorm van twee betrouwbaarheidsindexen β_{cross} (dijkdoorsnedeniveau) en β_{norm} (dijktrajectnorm). In Figure 1, 2 en 3 zijn de relaties voor de drie submechanismen weergegeven. De relaties zijn afgeleid voor afzonderlijke waarden van de trajectnorm. Dit is gedaan om te voorkomen dat de semi-probabilistische toets onnodig conservatief wordt.

Ten slotte dient de toelaatbare overstromingskans op doorsnedeniveau te worden bepaald op basis van de wettelijke norm, die voor het normtraject geldt. Voor dit adviseren wij het volgende lengte-effect parameters: $b = 350$ m en $a = 1$. Dit veronderstelt dat de gehele dijk traject piping gevoelig is (omdat $a = 1$) en dat de lengte van een equivalente onafhankelijke dijkstrekking gelijk is aan 350 m. Indien dit niet het geval is, kan de gebruiker de waarde van a verlagen.

References
No references.

Version	Date	Author	Initials	Review	Initials	Approval	Initials
2.1	28-08-15	A. Teixeira K. Wojciechowska W.L.A. ter Horst		F. Diermanse		-	
3.0	24-09-15	A. Teixeira K. Wojciechowska W.L.A. ter Horst		E. Calle			
4.0	16-12-15	A. Teixeira K. Wojciechowska W.L.A. ter Horst		E. Calle			
4.1	16-02-16	A. Teixeira K. Wojciechowska W.L.A. ter Horst		E. Calle			

Status
final
No disclaimer.

Contents

1 Introduction **3**
- 1.1 WTI project context . . . 3
- 1.2 Objectives and scope . . . 3
- 1.3 Outline . . . 4

2 Basic concepts **5**
- 2.1 Failure probabilities, reliability indices and influence coefficients . . . 5
- 2.2 The relations between probabilistic and semi-probabilistic assessments 6

3 Piping failure mechanism **9**
- 3.1 Uplift . . . 10
- 3.2 Heave . . . 10
- 3.3 Piping - Sellmeijer 2011 . . . 10

4 Calibration procedure **13**

5 Step 1: Establishing reliability requirement **15**
- 5.1 Maximum allowable probabilities of flooding . . . 15
- 5.2 Reliability requirement for piping in general . . . 15

6 Step 2: Establishing the safety format **17**
- 6.1 Establishing a test set . . . 17
- 6.2 Defining representative influence coefficients . . . 18
- 6.3 Representative values and safety factors . . . 20
- 6.4 The resulting safety format . . . 21

7 Step 3: Establishing safety factors **23**
- 7.1 The calibration criterion . . . 23
- 7.2 The Beta-invariant permeability factor . . . 24
- 7.3 Calibrating Beta-dependent safety factors . . . 24

8 Calibration results **27**
- 8.1 Results per sub-mechanism . . . 28
  - 8.1.1 Piping . . . 28
  - 8.1.2 Heave . . . 30
  - 8.1.3 Uplift . . . 31
- 8.2 Established functional relations . . . 32
  - 8.2.1 Piping . . . 33
  - 8.2.2 Heave . . . 34
  - 8.2.3 Uplift . . . 35

9 Semi-probabilistic assessment steps and comparison with other assessments **37**
- 9.1 Piping semi-probabilistic assessment steps . . . 37
- 9.2 Comparison with present-day relations . . . 41

10 Conclusions and recommendations **45**

References **47**

A Final test set **49**
- A.1 General definitions and assumptions . . . 49

A.2 Test set 49
A.3 Design water levels 57

B Translation of inputs from PC-Ring to Hydra-Ring 65

C Study on the length-effect parameters - Case 1 69

D Semi-proababilistic rules 75

E Designed values derived in the calibration - Case 1 and 2 79
E.1 Uplift calibration: cover thickness 79
E.2 Heave calibration: cover thickness 80
E.3 Piping calibration: seepage lengths 81

F Cluster alternatives study - Case 1 85
F.1 Clustering alternatives 85
F.2 Rationalization of the results and clustering combination 87

G Uplift: calibration results per cluster W, T and C - Case 1 95

H Heave: calibration results per cluster W, T and C - Case 1 99

I Piping: calibration results per cluster W, T and C - Case 1 103

J Influence coefficients (Step 3) - Case 1 107
J.1 Uplift - clustering per water system 107
J.2 Uplift - clustering per cover thickness class 110
J.3 Heave - clustering per water system 112
J.4 Heave - clustering per cover thickness class 115
J.5 Piping - clustering per water system 117
J.6 Piping - clustering per cover thickness class 120

K Variables in the calibration 123
K.1 Decimate heights 123
K.2 Uplift - clustering per water system 124
K.3 Uplift - clustering per cover thickness class 127
K.4 Heave - clustering per water system 130
K.5 Heave - clustering per cover thickness class 133
K.6 Piping - clustering per water system 136
K.7 Piping - clustering per cover thickness class 141

L Uplift: calibration results and cluster alternatives - Case 1 147

M Heave: calibration results and cluster alternatives - Case 1 153

N Piping: calibration results and cluster alternatives - Case 1 159

O Calibration for Eastern Scheldt - Case 1 165

List of Figures

1 Relation between the required reliability and the safety factor for the uplift sub-mechanism. . . . iv
2 Relation between the required reliability and the safety factor for the heave sub-mechanism. . . . iv
3 Relation between the required reliability and the safety factor for the piping sub-mechanism. . . . v

2.1 The probability density functions of load (S) and strength (R), and the design values of load and strength (S_d) and (R_d). . . . 7

3.1 Definitions of geometrical properties, phreatic and piezometric levels for uplift, heave and piping. . . . 9
3.2 Fault tree for internal erosion - piping failure mechanism. . . . 9

4.1 Schematic overview of the calibration, adopted from Jongejan (2013). 14

6.1 Statistics of the influence coefficients per random variable for 3.5<β<6.5 - uplift failure mechanism. . . . 18
6.2 Statistics of the influence coefficients per random variable for 3.5<β<6.5 - heave sub-mechanism. . . . 19
6.3 Statistics of the influence coefficients per random variable for 3.5<β<6.5 - piping failure mechanism (Case 1 - all inputs from the VNK2-databases). 19
6.4 Statistics of the influence coefficients per random variable for 3.5<β<6.5 - piping failure mechanism (Case 2 - adjusted cov values of k and d_{70}). 20

8.1 Piping results including histograms and 20%-quantile curve - Case 1. 28
8.2 Piping calibration results for Case 1 (all inputs come from the VNK2 databases) and average of the cross-sectional failure probabilities curve (black line). . . . 29
8.3 Piping calibration results for Case 2 (adjusted cov values of k and d_{70}) and average of the cross-sectional failure probabilities curve (black line). 29
8.4 Comparison of the average of the cross-sectional failure probabilities curves for piping with Cases 1 and 2. . . . 30
8.5 Heave calibration results and average of the cross-sectional failure probabilities curve (black line). . . . 31
8.6 Uplift calibration results and average of the cross-sectional failure probabilities curve (black line). . . . 31
8.7 Derived functional $\gamma_{pip} - \beta_{cross}$ relation for the piping sub-mechanism. 33
8.8 Derived functional $\gamma_{he} - \beta_{cross}$ relation for the heave sub-mechanism. 34
8.9 Derived functional $\gamma_{up} - \beta_{cross}$ relation for the uplift sub-mechanism. . 35

9.1 Schematised semi-probabilistic assessment for the piping mechanism in WTI 2017 (as in Jongejan and Klerk (2015)). . . . 37
9.2 Comparison of the functional relations (Calibration 2015) and the present-day relations for the uplift sub-mechanism. . . . 41
9.3 Comparison of the functional relations (Calibration 2015, Case 2) and the present-day relations for the piping sub-mechanism. . . . 42

A.1 Overview of available VNK2 databases per DPV segment. . . . 50
A.2 DPV segments in the final test set for uplift, heave and piping (differentiation per hydraulic region). . . . 51
A.3 DPV segments in the final test set for uplift, heave and piping (differentiation per safety standard). . . . 52

A.4 Number of dike cross-sections (sub-soil scenarios) in the final test set per DPV segment. . . . 53
A.5 Number of dike cross-sections (sub-soil scenarios) in the final test set with cover layer per DPV segment. . . . 54
A.6 Number of dike cross-sections (sub-soil scenarios) in the final test set without cover layer per DPV segment. . . . 55
A.7 Design water levels for HR stations considered in the calibration exercise. 57
A.8 Overview of water levels corresponding to T=300 years. . . . 58
A.9 Reliability differences in the water level calculations for T=300 years. . 58
A.10 Overview of water levels corresponding to T=1,000 years. . . . 59
A.11 Reliability differences in the water level calculations for T=1,000 years. 59
A.12 Overview of water levels corresponding to T=3,000 years. . . . 60
A.13 Reliability differences in the water level calculations for T=3,000 years. 60
A.14 Overview of water levels corresponding to T=10,000 years. . . . 61
A.15 Reliability differences in the water level calculations for T=10,000 years. 61
A.16 Overview of water levels corresponding to T=30,000 years. . . . 62
A.17 Reliability differences in the water level calculations for T=30,000 years. 62
A.18 Overview of water levels corresponding to T=100,000 years. . . . 63
A.19 Reliability differences in the water level calculations for T=100,000 years. 63

B.1 Translation of a dike segment schematisation from PC-Ring to Hydra-Ring. 66
B.2 Permeability values in the VNK2-databases (ordered). . . . 67
B.3 Histogram of the permeability ratios $\mu(k_1)/\mu(k_{1,ave})$. . . . 67

C.1 Intermediate results of the length-effect parameters' analysis. . . . 72
C.2 Final results of the algorithm that studies the parameters of the length-effect in piping sub-mechanism. . . . 73
C.3 Histogram of a values, all DPV segments considered in the calibration study. . . . 74

E.1 Cumulative distribution functions of the designed cover layer thickness for different safety factors, uplift calibration. . . . 80
E.2 Cumulative distribution functions of the designed cover thickness for different safety factors, heave calibration. . . . 81
E.3 Cumulative distribution functions of the designed seepage lengths for different safety factors, piping calibration (Case 1 - all inputs from the VNK2-databases). . . . 82
E.4 Cumulative distribution functions of the designed seepage lengths for different safety factors, piping calibration (Case 2 - adjusted cov values of k and d_{70}). . . . 82
E.5 Overview of the designed seepage lengths for $\gamma_{\beta,pip}$ = 1.5, piping calibration (Case 1 - all inputs from the VNK2-databases). . . . 83

F.1 Representation of the clusters in a summarised way (left) and schematic representation of possible combinations of clusters (right), as the basis for the rationalisation and recommendation for the semi-probabilistic assessment of piping. . . . 86
F.2 Cluster step 1 example: Heave calibration results with 20%-quantile curve (all results - black line), and curves per class return period (Cluster T). . . . 88
F.3 Cluster step 2 example: Heave calibration results with 20%-quantile curves per region and water system for T = 1,000 years. . . . 88
F.4 Cluster step 3 example: Heave calibration results with 20%-quantile curves per water system for low safety standard (Cluster S+W). . . . 89

F.5 Cluster step 4 example: Heave calibration results with 20%-quantile curves per water system for low safety standard (Cluster S+W'). . . . 89
F.6 Cluster step 5 example: Heave calibration results with 20%-quantile curves for low safety standard (Cluster S+W'+C). 90
F.7 Cluster S+W' and respective 20%-quantile curves, uplift calibration. The black line represents the 20%-quantile curve based on all data points in the respective plot. Notice that for the medium and high safety standard levels, the brown and black curves overlap. 91
F.8 Cluster S+W' and respective 20%-quantile curves, heave calibration. The black line represents the 20%-quantile curve based on all data points in the respective plot. Notice that for the medium safety standard level, the brown and black curves overlap. 92
F.9 Cluster S+W' and respective 20%-quantile curves, piping calibration. The black line represents the 20%-quantile curve based on all data points in the respective plot. Notice that for the low safety standard level, the brown and black curves overlap. 93

G.1 Uplift calibration results with 20%-quantiles - Cluster W. 95
G.2 Uplift calibration results with 20%-quantiles - Cluster T. 96
G.3 Uplift calibration results with 20%-quantiles - Cluster C. 97

H.1 Heave calibration results with 20%-quantiles - Cluster W. 99
H.2 Heave calibration results with 20%-quantiles - Cluster T. 100
H.3 Heave calibration results with 20%-quantiles - Cluster C. 101

I.1 Piping calibration results with 20%-quantiles - Cluster W. 103
I.2 Piping calibration results with 20%-quantiles - Cluster T. 104
I.3 Piping calibration results with 20%-quantiles - Cluster C. 105

J.1 Analysis of influence coefficients for $\gamma_{\beta,up}$ = 1.5, uplift calibration. . . . 107
J.2 Analysis of influence coefficients for $\gamma_{\beta,up}$ = 1.5, uplift calibration. . . . 108
J.3 Analysis of influence coefficients for $\gamma_{\beta,up}$ = 1.5, uplift calibration. . . . 109
J.4 Analysis of influence coefficients for $\gamma_{\beta,up}$ = 1.5, uplift calibration. . . . 110
J.5 Analysis of influence coefficients for $\gamma_{\beta,up}$ = 1.5, uplift calibration. . . . 111
J.6 Analysis of influence coefficients for $\gamma_{\beta,he}$ = 1.5, heave calibration. . . 112
J.7 Analysis of influence coefficients for $\gamma_{\beta,he}$ = 1.5, heave calibration. . . 113
J.8 Analysis of influence coefficients for $\gamma_{\beta,he}$ = 1.5, heave calibration. . . 114
J.9 Analysis of influence coefficients for $\gamma_{\beta,he}$ = 1.5, heave calibration. . . 115
J.10 Analysis of influence coefficients for $\gamma_{\beta,he}$ = 1.5, heave calibration. . . 116
J.11 Analysis of influence coefficients for $\gamma_{\beta,pip}$ = 1.5, piping calibration. . . 117
J.12 Analysis of influence coefficients for $\gamma_{\beta,pip}$ = 1.5, piping calibration. . . 118
J.13 Analysis of influence coefficients for $\gamma_{\beta,pip}$ = 1.5, piping calibration. . . 119
J.14 Analysis of influence coefficients for $\gamma_{\beta,pip}$ = 1.5, piping calibration. . . 120
J.15 Analysis of influence coefficients for $\gamma_{\beta,pip}$ = 1.5, piping calibration. . . 121

K.1 Decimate heights. 123
K.2 Analysis of mean values of variables, uplift calibration. 124
K.3 Analysis of mean values of variables, uplift calibration. 125
K.4 Analysis of mean values of variables, uplift calibration. 126
K.5 Analysis of mean values of variables, uplift calibration. 127
K.6 Analysis of mean values of variables, uplift calibration. 128
K.7 Analysis of mean values of variables, uplift calibration. 129
K.8 Analysis of mean values of variables, heave calibration. 130
K.9 Analysis of mean values of variables, heave calibration. 131
K.10 Analysis of mean values of variables, heave calibration. 132

K.11 Analysis of mean values of variables, heave calibration. 133
K.12 Analysis of mean values of variables, heave calibration. 134
K.13 Analysis of mean values of variables, heave calibration. 135
K.14 Analysis of mean values of variables, piping calibration. 136
K.15 Analysis of mean values of variables, piping calibration. 137
K.16 Analysis of mean values of variables, piping calibration. 138
K.17 Analysis of mean values of variables, piping calibration. 139
K.18 Analysis of mean values of variables, piping calibration. 140
K.19 Analysis of mean values of variables, piping calibration. 141
K.20 Analysis of mean values of variables, piping calibration. 142
K.21 Analysis of mean values of variables, piping calibration. 143
K.22 Analysis of mean values of variables, piping calibration. 144
K.23 Analysis of mean values of variables, piping calibration. 145

L.1 Uplift calibration results with 20%-quantiles - clustering per hydraulic region within a cluster per return period (T+R). 147
L.2 Uplift calibration results with 20%-quantiles - clustering per water system within a cluster per return period (T+W). 148
L.3 Uplift calibration results with 20%-quantiles - clustering per water system within a cluster per safety standard level (S+W). 149
L.4 Uplift calibration results with 20%-quantiles - clustering per water system (Wb) within a cluster per safety standard level (S+Wb). 150
L.5 Uplift calibration results with 20%-quantiles - clustering per cover layer class (Cb) within a water system (Wb) which is within a safety standard level (S+Wb+Cb). 151

M.1 Heave calibration results with 20%-quantiles - clustering per hydraulic region within a cluster per return period (T+R). 153
M.2 Heave calibration results with 20%-quantiles - clustering per water system within a cluster per return period (T+W). 154
M.3 Heave calibration results with 20%-quantiles - clustering per water system within a cluster per safety standard level (S+W). 155
M.4 Heave calibration results with 20%-quantiles - clustering per water system (Wb) within a cluster per safety standard level (S+Wb). 156
M.5 Heave calibration results with 20%-quantiles - clustering per cover layer class (Cb) within a water system (Wb) which is within a safety standard level (S+Wb+Cb). 157

N.1 Piping calibration results with 20%-quantiles - clustering per hydraulic region within a cluster per return period (T+R). 159
N.2 Piping calibration results with 20%-quantiles - clustering per water system within a cluster per return period (T+W). 160
N.3 Piping calibration results with 20%-quantiles - clustering per water system within a cluster per safety standard level (S+W). 161
N.4 Piping calibration results with 20%-quantiles - clustering per water system (Wb) within a cluster per safety standard level (S+Wb). 162
N.5 Piping calibration results with 20%-quantiles - clustering per cover layer class (Cb) within a water system (Wb) which is within a safety standard level (S+Wb+Cb). 163

O.1 Piping calibration results, 20%-quantile curve for dike segment 28-1 (red line) and remaining areas (black line), Case 1. 165

List of Tables

3.1 Input parameters for piping failure mechanism. 11

5.1 Maximum allowable failure probabilities per failure mechanism, defined as a fraction of the maximum allowable probability of flooding - Jongejan (2013). 15
5.2 Reliability requirement for a range of safety standards - piping mechanism. 16

9.1 Input parameters for piping analyses (norm = normal, log = log-normal). 40
9.2 Overview of the present-day relations for uplift and piping sub-mechanisms. 41

A.1 Statistics of the final test set per hydraulic region. 56
A.2 Statistics of the final test set per safety standard. 56

B.1 Translation of random variables from `PC-Ring` to `Hydra-Ring`. . . . 65

C.1 Input for the study on the length-effect parameters. 70
C.2 Analysis of a values per hydraulic region 74

D.1 Input parameters for piping analyses (norm = normal, log = log-normal). 77

E.1 Statistics of the designed cover thickness results for different safety factors, uplift calibration. 79
E.2 Statistics of the designed cover thickness results for different safety factors, heave calibration. 80
E.3 Statistics of the designed seepage lengths results for different safety factors, piping calibration (Case 1 - all inputs from the VNK2-databases). 81
E.4 Statistics of the designed seepage lengths results for different safety factors, piping calibration (Case 2 - adjusted cov values of k and d_{70}). 81

Symbols (Latin)

Symbol	Definition	Unit
a	Fraction of the length that is sensitive to the failure under study	-
b	Length-effect factor for piping failure	m
cov	Coefficient of variation (σ/μ)	-
D	Total thickness of the aquifer layer	m
D_{cover}	Effective thickness of the cover layer (aquitard)	m
d_{70}	70%-quantile of the grain size distribution of the piping-sensitive layer	m
$d_{70.m}$	Mean value of d_{70} in small scale tests (reference value in Sellmeijer formula)	m
$E(X)$	Expected value of the variable X	-(*)
F_i	Failure due to sub-mechanism i (uplift, heave or piping)	-
$F(\cdot)$	Standard normal distribution function	-
f	Failure probability factor (*faalruimtefactor*): target contribution of the failure mode to the probability of flooding	-
g	Gravitational constant	m/s^2
$g(\cdot)$	function of ($\cdot$)	-
h	River/outside water level at a particular moment relative to NAP	m
H_c	Critical head difference	m
h_{exit}	Polder/exit point phreatic level relative to NAP	m
i	Hydraulic gradient	-
$i_{c,h}$	Critical gradient for heave sub-mechanism	-
k	Darcy permeability of the aquifer layer	m/s
L	Seepage length	m
L_{segm}	Total length of the dike segment (*normtraject*)	m
m_u	Model factor for uplift	-
m_p	Model factor for piping	-
$P(\cdot)$	Probability of an event	-
P	Probability of failure	yr^{-1}
P_{norm}	Target failure probability (safety standard): target probability of flooding for a dike segment (*normtraject*) due to the series of events that lead to flooding	yr^{-1}
P_T	Target failure probability for piping: target probability of flooding for a dike segment due to the event of piping	yr^{-1}
$P_{T,cross}$	Cross-sectional target failure probability; the average cross-sectional probability of failure may not exceed $P_{T,cross}$	yr^{-1}
R	Resistance / Strength	-(*)
R_{char}	Characteristic value of random resistance/strength variable	-(*)
R_d	Design value of random resistance/strength variable	-(*)
r_{exit}	Damping factor at exit	-
r_c	Reduction factor for piping	-
S	Load	-(*)
S_{char}	Characteristic value of random load variable	-(*)
S_d	Design value of the random load variable	-(*)
S_i	Sub-soil scenario i	-
T	Return period that corresponds to the safety standard of a segment (*normtraject*)	yr
u	Standard normally distributed random variable (mean $\mu = 0$ and standard deviation $\sigma = 1$)	-
X	random variable	-(*)
X_d	Design value of the random variable X	-(*)
X_{char}	Characteristic or representative value of the random variable X	-(*)
Z_i	Limit state function of the mechanism i ($Z = R - S$)	-
Z_{II}	Linearised and normalized limit state function	-

Symbols (Greek)

Symbol	Definition	Unit
α_i	Influence coefficient for random variable X_i ($\Sigma\alpha_1^2 = 1$)	-
α_R	Influence coefficient of the resistance in limit state function	-
α_S	Influence coefficient of the load in limit state function	-
β	Reliability index	-
$\beta_{segm,HYR}$	Reliability index for a certain mechanism and segment (*normtraject*) taken from `Hydra-Ring` combined computations	-
β_{norm}	Reliability index that corresponds to the safety standard P_{norm}	-
β_T	Target reliability index: target reliability index for flooding in a dike segment (*normtraject*) due to piping, corresponds to P_T	-
$\beta_{T,cross}$	Cross-sectional reliability requirement (reliability index), corresponds to $P_{T,cross}$	-
β_{cross}	Cross-sectional reliability (reliability index)	-
γ_{inv}	β- invariant factor	-
γ_β	β- dependent safety factor	-
γ_{mec}	β- dependent safety factor for the individual failure mechanism mec	-
γ_R	Partial safety factor for random resistance/strength variable R	-
γ_S	Partial safety factor for random load variable S	-
γ_{water}	Water volumetric unit weight	kN/m^3
$\gamma_{sat,cover}$	Saturated volumetric unit weight of the cover layer	kN/m^3
$\gamma_{sub,particles}$	Submerged volumetric unit weight of the aquifer particles ($\gamma_{particles} - \gamma_{water}$)	kN/m^3
$\gamma_{particles}$	Volumetric unit weight of the aquifer particles	kN/m^3
$\Phi(\cdot)$	standard normal distribution function	-
ϕ	Hydraulic head	m
ϕ_c	Critical hydraulic head	m
$\theta_{sellmeijer,rev}$	Bedding angle of sand grains for the revised Sellmeijer rule (2011)	$^\circ$
μ	Mean value	-(*)
σ	Standard deviation	-(*)
σ_{eff}	Effective vertical stress	kN/m^2
η	White's drag coefficient	-
ν_{water}	Kinematic viscosity of water	m^2/s

(*) Unit depends on the variable concerned.

In this report, the maximum allowable probability of flooding of a dike segment refers to the target probability of failure (safety standard).

1 Introduction

1.1 WTI project context

The Dutch primary flood defences are periodically tested against statutory safety standards. These standards were, until recently, defined in terms of design loads. Nowadays, policy-makers decided to move towards safety standards defined in terms of target probabilities of flooding. To facilitate such a move, a new set of instruments for assessing the safety of flood defences is currently being developed: the WTI 2017.

The WTI 2017 will include probabilistic as well as semi-probabilistic assessment procedures. The latter rests on a partial safety factor approach and allows engineers to evaluate the reliability of flood defences without having to resort to probability calculus. To ensure consistency between probabilistic and semi-probabilistic assessments, the currently used safety factors have to be (re)calibrated. Important aspects within the standard WTI 2017 calibration procedure concern the derivation of reliability requirements, the definition of design values on the basis of influence coefficients, and the handling of spatial correlations.

1.2 Objectives and scope

This report concerns the final derivation of the semi-probabilistic assessment for WTI 2017 and the respective safety factors' calibration regarding the piping failure mechanism for dikes in the Netherlands.

Besides the calibration exercise, this report comprises the following activities:

- determination and analysis of test set used for the calibration;
- study of the intermediate results of the calibration procedure;
- derivation of functional relations for the semi-probabilistic dike safety assessments regarding uplift, heave and piping;
- study of the length-effect for uplift, heave and piping;
- comparison of the achieved semi-probabilistic assessment rules with the present-day relations.

The scope of this study is:

- The calibration exercise concerns three sub-mechanisms of the piping failure mechanism: uplift, heave and piping. The calibration is performed separately for each of these sub-mechanisms.[1]
- The probabilistic calculations are made with `Hydra-Ring` versions that were available during the study (from January until July 2015). We note that `Hydra-Ring` is under development (see Diermanse *et al.* (2013)).
- The data used for the calibration come from the VNK2-project (type of the databases is *2e referentiesituatie* [2]).

[1] The effort to establish semi-probabilistic rules, accounting for the combined effect of uplift and heave and piping, is considered to be disproportional compared with the benefit.

[2] The second reference situation takes into account new insights. The databases include implementation of the current improvement projects and programs (in 2015/2020) - VNK2 (2013).

- The hydraulic databases, used for derivation of design water levels with `Hydra-Ring`, are TMR2006 databases.
- Except for the Eastern Scheldt (*Oosterschelde*), all water systems in the Netherlands are included in the calibration. All piping sensitive dike sections within these water systems, according to the VNK2-study, are considered as test set.
- Even though Eastern Scheldt was not included in the main calibration, computations for one dike segment in this area were made. Results of these computations as well as the recommendations are presented in Appendix O.
- All safety standards, as proposed in DPV (2015), are included in the calibration exercise.
- The length-effect is studied for 12 dike segments (*normtraject*) that were considered in the preliminary calibration in 2014 (see ter Horst *et al.* (2014)).
- In the calibration the cover thickness is the effective thickness. The calibration results are also valid for dikes with a ditch (*teensloot*), under the assumption that in that case the effective cover thickness is determined according to the functional design of the piping kernel (see Visschedijk and Schweckendiek (2013)).

1.3 Outline

The report is organized as follows.

- Chapter 2 introduces some basic concepts in reliability engineering.
- Chapter 3 provides description of the piping failure mechanism together with the corresponding limit state functions.
- An overview of the calibration procedure is given in Chapter 4. The first step of this procedure, *i.e.* the definition of reliability requirements, is discussed in Chapter 5. The second step, *i.e.* the establishment of the safety formats, is considered in Chapter 6. The third step, *i.e.* the establishment of safety factors, is described in Chapter 7.
- Results of the calibration are presented in Chapter 8.
- In Chapter 9, a summary of the semi-probabilistic assessment steps and comparison with the present-day relations are given.
- Chapter 10 summaries conclusions and recommendations following from this study.

2 Basic concepts

2.1 Failure probabilities, reliability indices and influence coefficients

A flood defence will fail when the load exceeds its resistance. The resistance parameters of a flood defence are, in principle, deterministic. In practice, however, they are uncertain due to spatial variability, a limited number of measurements and measurement uncertainties. Also, the models used to predict critical combinations of parameter values (*i.e.* combinations that would lead to failure), might produce outcomes that are besides the (unknown) truth. Such model uncertainties also have to be taken into consideration in reliability analyses. This means that the resistance of a flood defence should be treated as a random variable, just like the uncertain loads.

The probability of failure (P_f) equals the probability that load (S) exceeds resistance / strength (R):

$$P_f = P(R < S) \tag{2.1}$$

or:

$$P_f = P(Z < 0) \text{ with } Z = R - S \tag{2.2}$$

where Z is the limit state function.

The First Order Reliability Method ($FORM$, described by Rackwitz (2001)) is an efficient method to compute failure probabilities. It is also known as a level II approach. In a $FORM$-analysis, the limit state function is normalized and linearized in the design point. The design point is the combination of parameter values with the highest probability density for which $Z = 0$. The linearized and normalized limit state function (Z_{II}) resulting from a $FORM$-analysis has the following form:

$$Z_{II} = \beta + \sum_{i=1}^{n} \alpha_i \cdot u_i \tag{2.3}$$

where:

β	is the reliability index,
α_i	is the influence coefficient for random variable X_i ($\sum \alpha_i^2 = 1$) and
u_i	is a standard normally distributed random variable (mean $\mu = 0$ and standard deviation $\sigma = 1$) representing the variable X_i .

An influence coefficient is a measure for the relative importance of the uncertainty related to a random variable. The squared value of an influence coefficient corresponds to the fraction of the variance (σ^2) of the linearized and normalized limit state function that can be attributed to a random variable.

Generally, a $FORM$-analysis yields a close approximation of the probability of failure:

$$P(Z_{II} < 0) \approx P(Z < 0) \tag{2.4}$$

Note that the failure probability estimate $P(Z_{II} < 0)$ is equal to $P(Z < 0)$ when the limit state function is linear and all random variables are independent and normally distributed.

From eq. (2.3) and the fact that the sum of the squares of the influence coefficients is equal to one, it follows that:

$$P(Z_{II} < 0) = \Phi(-\beta) \tag{2.5}$$

where $\Phi(.)$ is the standard normal cumulative distribution function.

It also follows from eq. (2.3) that the design point value ($X_{d,i}$) of a normally distributed random variable X_i equals:

$$X_{d,i} = \mu_i - \alpha_i \cdot \beta \cdot \sigma_i \tag{2.6}$$

where:

μ_i is the mean value of random variable X_i and
σ_i is the standard deviation.

The design point values are of interest for semi-probabilistic assessment rules, as will be clarified in the next section.

2.2 The relations between probabilistic and semi-probabilistic assessments

Semi-probabilistic and probabilistic safety assessments are closely related. Both rely on predefined safety standards, limit state functions, and the statistical properties of the random variables that represent the uncertain load and strength parameters. The same uncertainties play a role in semi-probabilistic and probabilistic assessments. Yet a semi-probabilistic assessment rests on a number of simplifications and approximations, giving it the appearance of a deterministic procedure.

In probabilistic safety assessments, analysts consider the probability that the ultimate limit state is exceeded, *i.e.* that load (S) exceeds resistance (R). The probability of failure, $P(S > R)$, should not exceed some target value (P_T).

In semi-probabilistic assessments, analysts consider the difference between the design values of load (S_d) and strength (R_d): S_d should not exceed R_d. Design values are defined in terms of characteristic values (e.g. 5% or 95%-quantiles or nominal values) and (partial) safety factors. This use of terminology is consistent with the Eurocode EN 1990 (CEN, 2002). Readers should be aware that similar terms may have different definitions in other international standards.

The design values should be calibrated such that the condition $S_d \leq R_d$ implies that the probability of failure meets the reliability requirement: $P(S > R) \leq P_T$. The relationship between probabilistic and semi-probability safety assessments is illustrated in Figure 2.1.

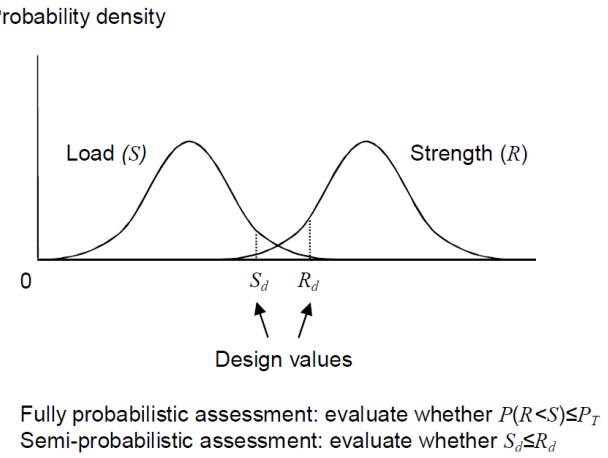

Figure 2.1: The probability density functions of load (S) and strength (R), and the design values of load and strength (S_d) and (R_d).

The design values of normally distributed resistance and load variables are:

$$R_d = \mu_R - \alpha_R \cdot \beta_T \cdot \sigma_R = R_{char}/\gamma_R \quad \text{(resistance / strength parameter)} \tag{2.7}$$

$$S_d = \mu_S - \alpha_S \cdot \beta_T \cdot \sigma_S = S_{char} \cdot \gamma_S \quad \text{(load parameter)} \tag{2.8}$$

where:

μ_R, μ_S	are the expected values of R and S,
α_R, α_S	are the values of the influence coefficients for R and S,
β_T	the target (required) reliability index, corresponding with the target (allowable) probability of failure P_T,
σ_R, σ_S	are the standard deviations of R and S,
R_{char}, S_{char}	are the characteristic values of R and S, (e.g. 5%-quantile for strength and 95%-quantile for load) and
γ_R, γ_S	are the (partial) safety factors.

Note that $\alpha_S \leq 0$ while $\alpha_R \geq 0$.

In short, probabilistic and semi-probabilistic assessments both require:

- A failure mechanism model,
- Probability density functions for all random variables (based on statistical data and / or engineering judgment) and
- A reliability requirement (”target”).

The essential differences between probabilistic and semi-probabilistic assessments are:

- In a probabilistic assessment, a failure mechanism model is fed with all possible parameter values and their probabilities (*i.e.* probability density functions),
- In a semi-probabilistic assessment, a failure mechanism model is fed with unique, ”sufficiently safe” values (*i.e.* design values). How safe ”sufficiently safe” is, depends ultimately on the reliability requirement and a calibration criterion.

As such, to ensure consistency between probabilistic and semi-probabilistic assessments, calibration exercises are indispensable.

3 Piping failure mechanism

The piping failure mechanism consists of three sub-mechanisms: uplift, heave and piping[1]. Failure due to uplift, heave or piping is in principal caused by excessive pore pressures. These excessive pore pressures will develop in sand layers due to high (river) water levels. The piezometric head difference over a dike determines the load on the dike. The resistance of the dike depends on several soil characteristics such as cover layer thickness (the so-called "cover" - cohesive layer) and weight, permeability of the sand layer and the available seepage length. An overview of relevant parameters and definitions is given in Figure 3.1.

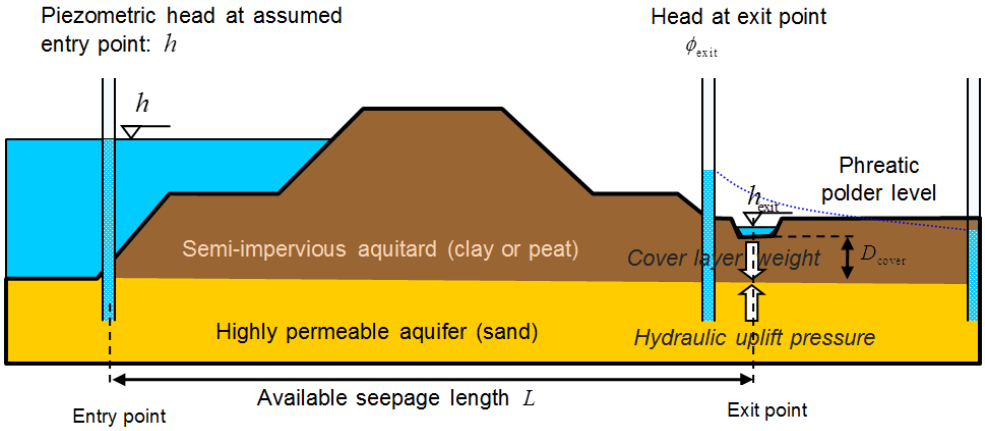

Figure 3.1: Definitions of geometrical properties, phreatic and piezometric levels for uplift, heave and piping.

Each sub-failure mechanism is translated in the limit state function, for further reliability analyses. This function is called Z_{up} for uplift, Z_{he} for heave and Z_{pip} for piping (Sellmeijer revised model - see Sellmeijer *et al.* (2011)). It is considered that piping failure only occurs if all sub-mechanisms occur, which can be modelled by a parallel system and it is represented in a fault tree by means of an AND-gate (see Figure 3.2).

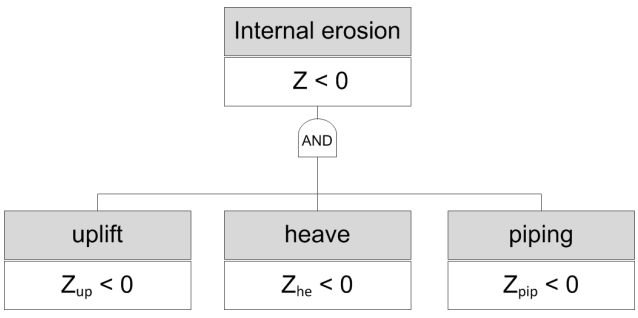

Figure 3.2: Fault tree for internal erosion - piping failure mechanism.

[1]The last sub-mechanism is also called backward erosion. Care was taken in this report to avoid the possible misunderstanding. Hence, *piping failure mechanism* refers to the three sub-mechanisms whereas *piping sub-mechanism* refers to the backward erosion only.

3.1 Uplift

Uplift is a necessary condition for piping to occur, if a cover layer is present at the land side of the dike. If intact, this cover layer acts as a low-permeability cover. Uplift is the breaching of the cover layer because of excessive upwards pressure in the underlying aquifer. The limit state function for uplift (Z_{up}) is based on a comparison of the (downward) pressure exerted by the weight of the cover layer (strength) and the (upward) water pressure in the aquifer (load):

$$Z_{up} = m_u \cdot \Delta\phi_{c,u} - (\phi_{exit} - h_{exit}) \tag{3.1}$$

where:

$$\Delta\phi_{c,u} = \frac{D_{cover} \cdot \gamma_{eff,cover}}{\gamma_{water}} \tag{3.2}$$

$$\gamma_{eff,cover} = \gamma_{sat,cover} - \gamma_{water} \tag{3.3}$$

$$\phi_{exit} = h_{exit} + (h - h_{exit}) \cdot r_{exit} \tag{3.4}$$

The meaning of each variable in the uplift equations can be consulted in Table 3.1.

3.2 Heave

Piping is internal erosion of sand through horizontal pipes towards the location of uplift breaching (the exit location). A condition for progressive erosion of the horizontal pipes is that vertical sand transport (heave) at the vertical parts must be possible. This transport can only occur if the vertical outflow gradient of the sand at the exit point exceeds a critical value for heave. The corresponding limit state function Z_{he} is:

$$Z_{he} = i_{c,h} - i \tag{3.5}$$

where:

$$i = (\phi_{exit} - h_{exit})/D_{cover} \tag{3.6}$$

$$\phi_{exit} = h_{exit} + (h - h_{exit}) \cdot r_{exit} \tag{3.7}$$

The meaning of each variable in the heave equations can be consulted in Table 3.1.

3.3 Piping - Sellmeijer 2011

Piping, as described in this chapter, concerns backward internal erosion under dikes with predominantly horizontal seepage paths. The general form of the limit state function is presented in eq. (3.8). The models by Bligh, Sellmeijer original or Sellmeijer revised can be applied. Only Sellmeijer 2011 (revised - de Bruijn *et al.* (2010) and Förster *et al.* (2012)) form will be used and therefore presented. Piping models are based on average gradients between the seepage entry and exit point. Together with the seepage length L, this leads to a critical head difference H_c, given by eq. (3.9) to (3.12), which can be compared with the actual head difference.

$$Z_{pip} = m_p \cdot H_c - (h - h_{exit} - r_c \cdot D_{cover}) \tag{3.8}$$

$$\frac{H_c}{L} = F_{resistance} \cdot F_{scale} \cdot F_{geometry} \tag{3.9}$$

where:

$$F_{resistance} = \eta \cdot \frac{\gamma_{sub,particles}}{\gamma_{water}} \cdot \tan\theta_{sellmeijer,rev} \tag{3.10}$$

$$F_{scale} = \frac{d_{70.m}}{\sqrt[3]{\kappa \cdot L}} \cdot \left(\frac{d_{70}}{d_{70.m}}\right)^{0.4} \text{ and } \kappa = \frac{\nu_{water}}{g} \cdot k \tag{3.11}$$

$$F_{geometry} = 0.91 \cdot \left(\frac{D}{L}\right)^{\frac{0.28}{\left(\frac{D}{L}\right)^{2.8}-1}+0.04} \tag{3.12}$$

The meaning of each variable in the piping equations can be consulted in Table 3.1.

Table 3.1: Input parameters for piping failure mechanism.

Symbol [unit]	Description	Uplift	Heave	Piping
m_u $[-]$	Model factor for uplift	x		
γ_{water} $[kN/m^3]$	Volumetric weight of water	x		x
$\gamma_{sat,cover}$ $[kN/m^3]$	Saturated volumetric weight of the cover layer	x		
r_{exit} $[-]$	Damping factor at exit	x	x	
$i_{c,h}$ $[-]$	Critical heave gradient		x	
D_{cover} $[m]$	Effective thickness of the cover layer	x	x	x
h_{exit} $[m+NAP]$	Phreatic level at the exit point	x	x	x
m_p $[-]$	Model factor for piping			x
h $[m+NAP]$	Outside water level	x	x	x
r_c $[-]$	Reduction factor			x
L $[m]$	Seepage length, from entry point to exit point			x
$\gamma_{sub,particles}$ $[kN/m^3]$	Submerged volumetric weight of sand particles			x
η $[-]$	White's drag coefficient			x
d_{70} $[m]$	70%-quantile of the grain size distribution of the piping-sensitive layer			x
k $[m/s]$	Darcy permeability of the aquifer layer			x
ν_{water} $[m^2/s]$	Kinematic viscosity of water			x
g $[m/s^2]$	Gravitational constant			x
D $[m]$	Thickness of the aquifer			x
$d_{70.m}$ $[m]$	Mean value of the d_{70} in small scale tests			x
$\theta_{sellmeijer,rev}$ $[°]$	Bedding angle of sand grains for the revised Sellmeijer rule (Sellmeijer *et al.*, 2011)			x

4 Calibration procedure

In this chapter, the following procedure is applied for calibrating the semi-probabilistic safety assessment rules for uplift, heave and piping sub-mechanisms. The procedure is based on Jongejan (2013) (see also Figure 4.1).

Step 1: Establish the reliability requirement. This requirement is defined as a maximum allowable probability of failure for the failure mechanism under consideration for an entire segment (*normtraject*). The length-effect is not yet considered in this step. This effect is taken into account in step 3(c), when deciding which safety factors may be considered sufficiently safe. *In this report, the maximum allowable probability of flooding of a dike segment refers to the target probability of failure (safety standard).*

Step 2: Establish the safety format. This step comprises the following activities:

(a) establish a test set that covers a wide range of cases. The test set members concern existing or fictitious cross-sections of dikes;

(b) calculate influence coefficients for each test set member, for a specific target failure probability or a range of values;

(c) based on the outcomes of the previous activity and practical considerations, define representative values (characteristic values) and decide on the safety factors that are to be included in the semi-probabilistic assessment rule.

Step 3: Establish safety factors. This step comprises the following activities:

(a) establish, on the basis of representative influence coefficients and a target reliability index, the values of all but one safety factor. Herein, these safety factors will be called $\beta-$invariant safety factors;

(b) for each test set member, determine the required seepage length (or cover layer thickness) so that $R_d = S_d$, for a range of values of the remaining $\beta-$dependent safety factor. When this condition is fulfilled, each (modified) test set member would just pass a semi-probabilistic assessment. Then calculate the probability of failure of each (modified) test set member. The objective of this step is to establish a relationship between the value of the $\beta-$dependent safety factor and the probability of failure (or reliability index), for each test set member;

(c) apply a calibration criterion to select the appropriate value of the $\beta-$dependent safety factor. The calibration criterion provides a reference for deciding which design values are sufficiently safe. An analysis of the length-effect is part of this evaluation. According to the criterion, the failure probability of a segment should be smaller than the target failure probability that applies to the segment. A dike segment typically consists of a number of different dike sections with a representative cross-section.

Step 4: Compare the calibrated semi-probabilistic assessment rule with the present-day $\gamma - \beta$ relations.

The calibration is performed using the Piping WTI 2017 kernel implemented in `Hydra-Ring` as well as several routines developed in `Matlab`.

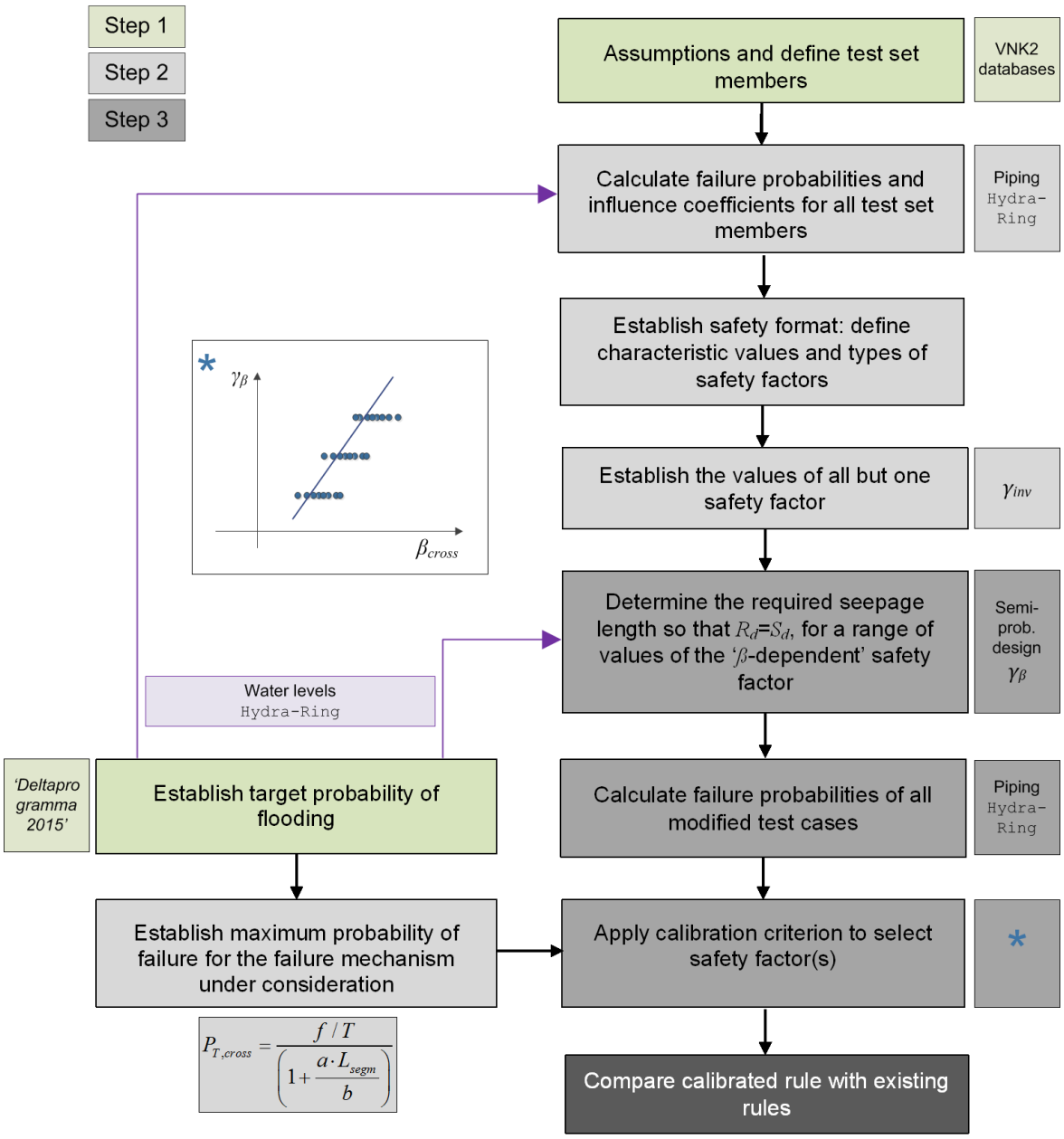

Figure 4.1: Schematic overview of the calibration, adopted from Jongejan (2013).

5 Step 1: Establishing reliability requirement

This chapter discusses the establishment of the reliability requirement that is needed for calibration purposes. It starts with a maximum allowable probability of flooding (section 5.1), from which the reliability requirement for piping is derived (section 5.2).

5.1 Maximum allowable probabilities of flooding

The flood safety standards are defined in terms of maximum allowable probabilities of flooding DPV (2015). These standards apply to dike segments (*normtraject*). A dike segment is a dike system or part thereof. Segments can be over 20 km long and are usually located in one water system. Segments may consist of numerous dike sections and/or hydraulic structures.

5.2 Reliability requirement for piping in general

For calibrating a semi-probabilistic assessment rule for a particular failure mechanism, a reliability requirement for that failure mechanism is needed. Such a reliability requirement can be derived from a fault tree analysis. Each failure mechanism may lead to flooding, the fault tree's top event. The combined probabilities of the various failure mechanisms may not exceed the maximum allowable probability of flooding. To ensure this requirement is met, the maximum allowable failure probabilities for the failure mechanisms, their 'failure probability factors', should be defined in such a manner that their combined value does not exceed the maximum allowable probability of flooding (Jongejan, 2013). The maximum allowable contributions of the different failure mechanisms to the maximum allowable probability of flooding are shown in Table 5.1. The fractions in Table 5.1 are based on the expected importance of the different failure mechanisms if all dike systems were to meet their (assumed) safety standards. These estimates are based on calculations with `PC-Ring` and VNK2-data as well as a number of expert sessions with representatives of research institutes (TNO, Deltares, Delft University of Technology), engineering consultancies, water boards, and Rijkswaterstaat. For further details about the maximum allowable failure probabilities per failure mechanism, the reader is referred to Jongejan (2013).

The failure probability factor f for the piping mechanism is 0.24. This factor applies to the combination of uplift, heave and piping sub-mechanisms. This factor leads to maximum allowable failure probabilities (P_T) as shown in Table 5.2. The reliability requirements are also expressed in terms of reliability indices (β_T). It should be noticed that the reliability requirements (P_T or β_T) in Table 5.2 apply to dike segments. These should not be confused with cross-sectional reliability requirements. Due to the length-effect, cross-sectional reliability requirements will

Table 5.1: Maximum allowable failure probabilities per failure mechanism, defined as a fraction of the maximum allowable probability of flooding - Jongejan (2013).

Type of flood defence	Failure mechanism	Failure probability factor (f)	
		Sandy coast	Other (dikes)
Dikes and structures	Overflow and wave overtopping	0	0.24
Dikes	**Uplift and piping**	0	**0.24**
	Macro instability of the inner slope	0	0.04
	Revetment failure and erosion	0	0.10
Structures	Non-closure	0	0.04
	Piping	0	0.02
	Structural failure	0	0.02
Dunes	-	0.70	0 or 0.10
Other	-	0.30	0.30 or 0.20
Total		1.00	1.00

have to be more stringent than reliability requirements for entire segments.

Table 5.2: Reliability requirement for a range of safety standards - piping mechanism.

f [−]	P_{norm} [y^{-1}]	$\beta_{norm} = -\Phi^{-1}(P_{norm})$ [on an annual basis]	Reliability requirement (entire dike segment) $P_T = f.P_{norm}$ [y^{-1}]	$\beta_T = -\Phi^{-1}(P_T)$ [on an annual basis]
0.24	1/300	2.71	8.0E-04	3.16
	1/1,000	3.09	2.4E-04	3.49
	1/3,000	3.40	8.0E-05	3.78
	1/10,000	3.72	2.4E-05	4.07
	1/30,000	3.99	8.0E-06	4.31
	1/100,000	4.26	2.4E-06	4.57

The difference between the reliability requirement for an entire segment and the reliability requirement for individual cross-sections will increase with decreasing spatial correlations and decrease with greater variability in cross-sectional reliabilities. The latter is because the failure probabilities of the weakest cross-sections will dominate the failure probability of the entire segment when the weakest cross-sections have relatively high probabilities of failure (Calle and Kanning, 2013).

The relationship between the reliability requirement for entire dike segments (P_T or β_T) and cross-sectional failure probabilities is discussed in greater detail in chapter 7 and Appendix C. By means of performing combined reliability computations for several dike segments, the length-effect parameters were studied in Appendix C. However, due to the complexity of the problem and the applied computation algorithm, the study led to no conclusive results.

Recommendations on the values of a and b are given in chapter 9.

6 Step 2: Establishing the safety format

The safety format concerns the definition of representative values (characteristic values) and the types of safety factors that are to be included in the semi-probabilistic assessment rule. The safety format depends on the relative importance of the uncertainties related to the various random variables (see also section 2.2). To obtain insight into the relative importance of the uncertainties, probabilistic analyses are indispensable. Section 6.1 first discusses the test set for which probabilistic analyses were carried out. The calculated influence coefficients are discussed in section 6.2. These lie at the heart of the safety format that is detailed in section 6.3. A summary is provided in section 6.4.

6.1 Establishing a test set

To obtain insight into the relative importance of the numerous random values, probabilistic analyses were carried out for a large number of test set members. The test set members reflect the wide variety of sub-soil conditions and loading conditions found throughout the Netherlands. The test set is composed of actual dikes from the VNK2-project that are linked to specific locations and hydraulic stations.

For uplift and heave, all inputs for the test set members come from the VNK2 databases. Whereas for the piping sub-mechanism, two cases are considered:

- Case 1: All inputs from the VNK2 databases (mean values and standard deviations),
- Case 2: All inputs from the VNK2 databases, except for the coefficients of variance (cov) values of the permeability k and grain size d_{70}. These cov values were taken equal to 0.50 and 0.12, respectively.

The cov values of k and d_{70} in Case 2 correspond to the values recommended in the schematisation guidelines of piping mechanism (Förster *et al.*, 2015), while for Case 1 the cov values of k varied between 10 and 200% and for d_{70} between 2 and 30% - see Teixeira and Wojciechowska (2015).

For further details about the test set, see Appendix A.

The final test set consists of 3321 dike sub-soil scenarios (63% with cover layer and 37% without cover layer). These fall into 92 DPV segments[1]. This final set refers to the primary dikes category A, in the Netherlands, as follows from the VNK2-project data. Except for the Eastern Scheldt, all hydraulic regions are represented in the set [2]. Furthermore, the considered safety standards cover the entire range of the safety standards as defined in DPV (2015).

6.2 Defining representative influence coefficients

The relative importance of the uncertainties related to random variables can be expressed in terms of influence coefficients (see also section 2.1). An inspection of influence coefficients provides useful clues about appropriate representative values (quantiles) and/or the variables for which partial safety factors should be introduced.

[1] *Normtrajecten van Deltaprogramma Veiligheid.*

[2] Even though Eastern Scheldt was not included in the main calibration, computations for one dike segment in this area were made. Results of these computations as well as the recommendations are presented in Appendix O.

Figure 6.1 to 6.3 show the influence coefficients (α's) for the random variables, resulting from the test set members with a reliability index in the order of 3.5<β_{cross}<6.5. This range corresponds with the rage of the (required) reliability indices that arise in the semi-probabilistic assessment.

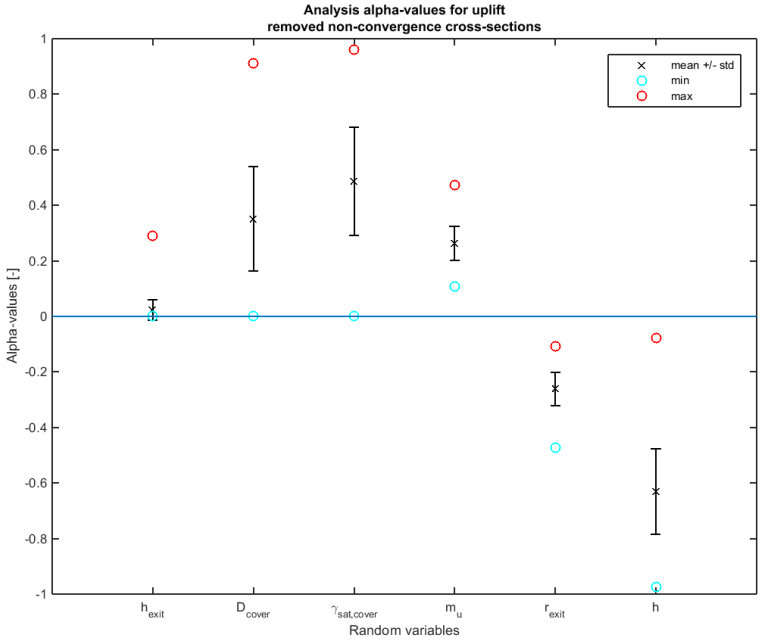

Figure 6.1: Statistics of the influence coefficients per random variable for 3.5<β_{cross}<6.5 - uplift failure mechanism.

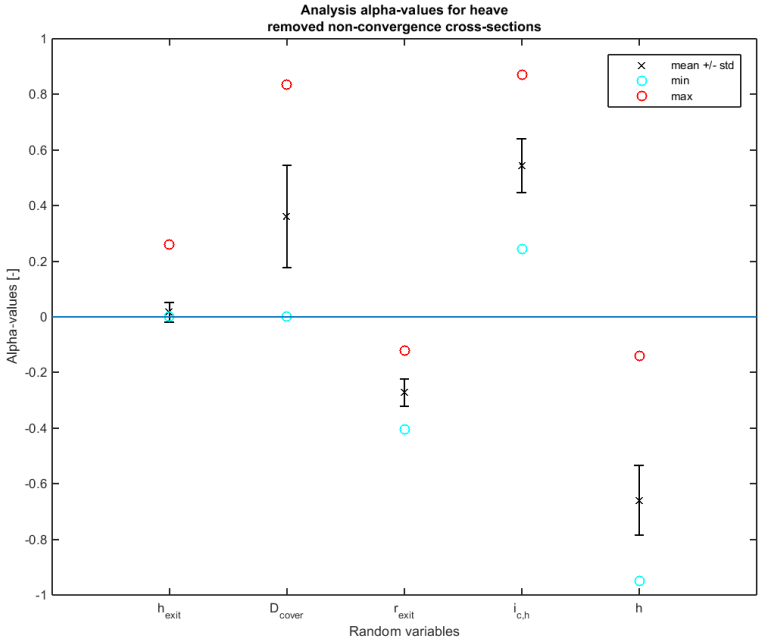

Figure 6.2: Statistics of the influence coefficients per random variable for 3.5<β_{cross}<6.5 - heave sub-mechanism.

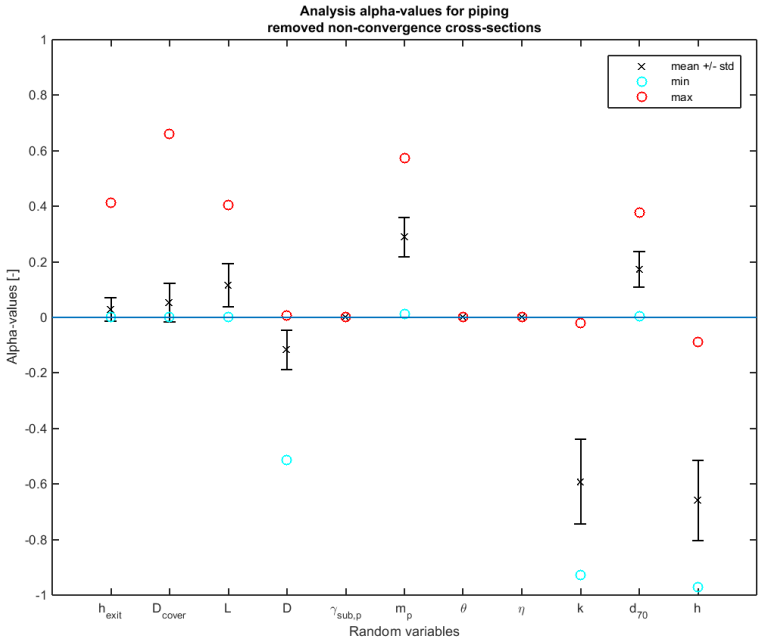

Figure 6.3: Statistics of the influence coefficients per random variable for 3.5<β_{cross}<6.5 - piping failure mechanism (Case 1 - all inputs from the VNK2-databases).

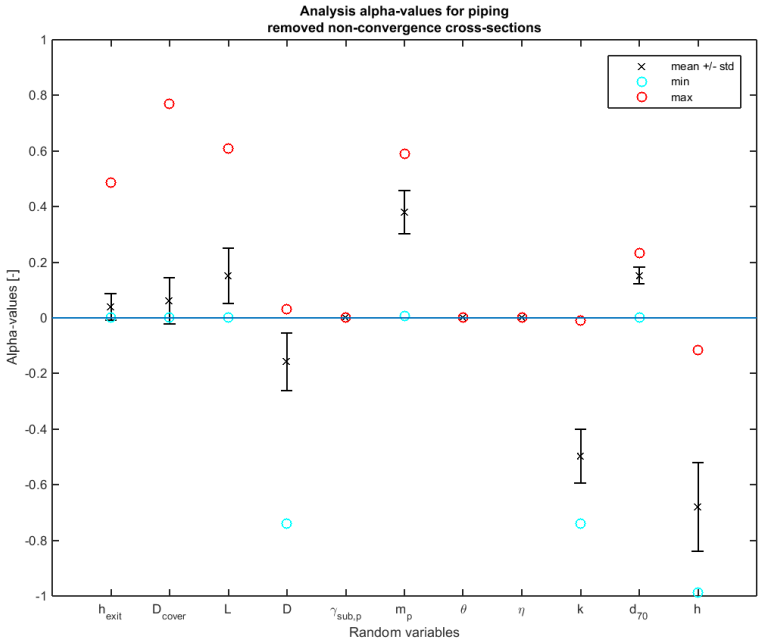

Figure 6.4: Statistics of the influence coefficients per random variable for 3.5<β_{cross}<6.5 - piping failure mechanism (Case 2 - adjusted cov values of k and d_{70}).

From Figure 6.1 to 6.3, the uncertainty related to the hydraulic loading conditions (outside water level h) appears to be most important for all three sub-mechanisms, $\alpha_h \simeq -0.65$. Furthermore, based on the influence coefficients results, the following can be concluded for each sub-mechanism:

- UPLIFT: the cover thickness D_{cover} and the saturated volumetric weight of the cover layer $\gamma_{sat,cover}$ are the most influential random strength variables (these are favourable variables, as an increase in its value decreases the failure probability), $\alpha_{D_{cover}} \simeq 0.35$ and $\alpha_{\gamma_{sat,cover}} \simeq 0.50$;
- HEAVE: the critical heave gradient $i_{c,h}$ and the cover thickness D_{cover} are the most influential random strength variables, $\alpha_{i_{c,h}} \simeq 0.55$ and $\alpha_{D_{cover}} \simeq 0.35$;
- PIPING: the influence of the permeability k and the outside water level h is quite substantial. Both random variables are unfavourable (*i.e.* an increase in values of these variables increases the failure probability) and their mean influence coefficients deviate significantly from zero $|\alpha| > 0.5$ (both Case 1 and 2). The model uncertainty m_p is a variable on the strength side $\alpha_{m_p} \simeq 0.3$ (Case 1) and $\alpha_{m_p} \simeq 0.4$ (Case 2), however its influence is not as high as k and h. Note that the variability of the α-values of k and d_{70} is lower in Case 2 than in Case 1, which was to be expected.

In case the uncertainty in the permeability k is reduced (piping sub-mechanism), the importance of other variables increases. When the uncertainty in k is reduced to zero, then the outside water level h and the piping model error m_p become the most important variables (Teixeira and Wojciechowska, 2015).

6.3 Representative values and safety factors

Design values should ideally be chosen on the basis of (target) reliability indices and influence coefficients, see section 2.2. Yet there are exceptions to this rule.

First, the decision to only introduce safety factors for the most important random variables, or even a single overall safety factor, may strongly simplify the semi-probabilistic assessment rule. Otherwise, analysts have to use a large number of safety factors, many of them close to 1. The selection of safety factors normally involves a trade-off between precision (minimal conservatism) and practicality. Yet in this case, reducing the number of safety factors would hardly reduce the accuracy of the semi-probabilistic assessment rule. This is because the uncertainties related to many of the random variables appear to be relatively unimportant, as seen in Figure 6.1 to 6.3, and also in the study on block revetments for WTI 2017.

Second, for pragmatic reasons, representative values should be defined as uniformly as possible. The consistent use of 5%-quantiles for strength parameters is preferable over the use of e.g. the 10%-quantile for variable X_1, the 25%-quantile for X_2, the 55%-quantile for variable X_3 and so on. Therefore, the use of the 5% (5%-quantile for resistance parameters and 95% for load parameters) as representative value is due to practical reasons (WTI 2017 uniformity).

Third, within the WTI 2017, the strategy, for reasons of uniformity, is to select the load with an exceedance probability equal to the allowable probability of flooding (Jongejan, 2013). For the piping mechanism, the representative values of the load (*i.e.* outside water level) will therefore be obtained for target probabilities equal to the maximum allowable probabilities of flooding. This ensures consistency across failure mechanisms and facilitates comparisons between today's rules and $\gamma - \beta$ relations, and the WTI 2017.

Fourth, representative values are normally defined as quantiles. Yet when it comes to the model uncertainty parameter, it seems practical to choose a representative value equal to 1. The design value of the model uncertainty parameter is then directly equal to the partial safety factor (if it exists). Analysts would otherwise have to combine a representative value (quantile) for the model uncertainty parameter with a partial safety factor.

Finally, in theory, all design values should depend on reliability requirements. That would be impractical, however. A pragmatic solution is to define a $\beta-$invariant model or permeability factor and a separate $\beta-$dependent safety factor to account for the stringency of the safety standard and the remaining uncertainties. This format is similar to the one used in semi-probabilistic slope stability assessments: there, a $\beta-$dependent damage factor is used

alongside $\beta-$invariant model, material and geometry factors. The $\beta-$dependent safety factor is to be applied to the ratio R_d/S_d for piping failure, the same as the present-day rule.

6.4 The resulting safety format

The safety format for the piping mechanism, *i.e.* sub-mechanism uplift, heave and piping (erosion), is defined as follows:

1 The representative values of all random strength variables[3] are 5%-quantiles, except for the model uncertainty parameter(s) and the critical heave gradient ($i_{c,h}$). This is in accordance with the current safety assessments;

2 The representative values of all random load variables[4] are 95%-quantiles, except for the outside water level (h). This is in accordance with the current safety assessments;

3 The representative value of the model uncertainty parameter(s) is equal to one;

4 The representative value of the critical heave gradient ($i_{c,h}$) is equal to 0.3, which is the recommendation after expert judgement (Förster *et al.*, 2015);

5 The representative value of the outside water level (h) (design water level) is defined as the water level with an exceedance probability equal to the maximum allowable probability of flooding for the considered dike segment;

6 Each random variable can have a corresponding $\beta-$invariant safety factor different than one. Due to the high importance, the permeability of the aquifer layer (k) is often considered as a potential random variable with a $\beta-$invariant safety factor (different than one). In this report, all random variables have the $\beta-$invariant safety factor equal to one however. This choice is motivated in section 7.2;

7 A $\beta-$dependent safety factor is introduced to cover all other uncertainties. It is applied to the ratio R_d/S_d for piping failure.

[3] Increase in values of these variables *decreases* the failure probability.
[4] Increase in values of these variables *increases* the failure probability.

7 Step 3: Establishing safety factors

This chapter discusses the derivation of partial safety factors for semi-probabilistic assessments of dikes with respect to the piping failure mechanism. Safety factors should be sufficiently safe but not unduly stringent. A calibration criterion is used to decide 'how safe is safe enough'. This criterion is introduced in section 7.1. Section 7.2 then deals with the $\beta-$invariant safety factor. The remaining uncertainties are covered by a $\beta-$dependent safety factor, and section 7.3 discusses the application of calibration criteria to define this factor.

7.1 The calibration criterion

According to the WTI 2017 calibration criterion, the failure probability of a dike segment should be smaller than the target failure probability that applies to this segment (*dijktraject*). This criterion is fulfilled, with a sufficient accuracy, when the average of cross-sectional failure probabilities in the segment is smaller than the target failure probability for a dike cross-section in this segment (Jongejan and Lopez de La Cruz, 2011). The average of cross-sectional failure probabilities is therefore used for the calibration of the safety factors. This average value roughly corresponds to the 20%-quantile values of the calculated reliability indices (on the cross-section level) for each value of the overall safety factor, based on modelled normal distributions[1].

When relating the cross-sectional reliabilities of individual test set members to reliability requirements/targets that apply to entire segments, the length-effect has to be accounted for. In the case of the piping failure mechanism, the length-effect is characterised by the parameters a and b, and the relation between the reliability requirement for a dike cross-section and the reliability requirement for a dike segment is given as follows:

$$P_T = P_{T,cross} \cdot \left(1 + \frac{a \cdot L_{segm}}{b}\right) \tag{7.1}$$

$$P_T = f \cdot P_{norm} = \frac{f}{T} \tag{7.2}$$

where:

P_T	is the target failure probability of a dike segment for piping mechanism [yr^{-1}],
$P_{T,cross}$	the target failure probability of a dike cross-section for piping mechanism [yr^{-1}],
T	is the return period that corresponds to the safety standard of a segment [yr],
L_{segm}	is the total length of the segment [m],
a	is a fraction of the length that is sensitive to piping [-],
b	is a measure for the intensity of the length-effect within the part of the segment that is sensitive to piping (the length of independent, equivalent dike sections) [m],
P_{norm}	is the target failure probability (safety standard) [yr^{-1}] and
f	is the failure probability factor for piping failure mechanism [-].

The value of f is equal to 0.24 for piping mechanism (as shown in Table 5.1).

According to OI (2015), the recommended value of b is equal to 300 m. The recommended values of a are: 0.9 for the upper-river area and 0.4 for the remaining hydraulic regions in the

[1] When cross-sectional reliability indices are normally distributed with a standard deviation of about 0.5, their 20%-quantile value corresponds to the average probability of failure.

Netherlands. According to Lopez de La Cruz *et al.* (2010), the recommendation for the length-effect parameters is $b = 350$ m and $a = 1$. This study assumes that the entire dike segment is sensitive to piping.

The definition of a entails that stretches within the segment, where piping is basically a relevant failure mechanism, contribute uniformly to the probability of piping. It may, however, be that only some of the stretches contribute significantly, while others contribute marginally. Therefore, there may be discussion on the definition of a.

In this study, computations are performed with `Hydra-Ring`[2], in order to verify whether the current values of a and b are suitable for the transformation of P_T into $P_{T,cross}$ for piping failure mechanism. Results of these computations and more information are presented in Appendix C (Case 1 results). During the analysis, two approaches to estimate a and b values were considered. However, none showed conclusive results. This could be explained by the selected data but also by the complexity of the problem. Recommendations on the values of a and b are given in chapter 9.

We emphasize that the parameters a and b do not play a role in deriving the $\gamma - \beta$ relations. Yet, these parameters are needed for the dike safety assessment regarding the piping failure mechanism within the WTI 2017.

The steps to perform a semi-probabilistic assessment of a dike cross-section regarding the piping mechanism are described in chapter 9.

7.2 The Beta-invariant permeability factor

The goal of having a $\beta-$invariant safety factor in the safety format is to decrease the spreading in the relation between the semi-probabilistic and the fully probabilisitc assessments. In Wojciechowska and Teixeira (2014), a semi-probabilistic piping rule with two safety factors was studied: $\beta-$invariant and $\beta-$dependent. The $\beta-$invariant safety factor was applied to the permeability k, since this is the random variable with the highest influence in piping sub-mechanism (together with the outside water level (h)).

However, the study of Wojciechowska and Teixeira (2014) showed no considerable differences between the assessments with the different options (1 versus 2 safety factors), even when different quantiles for the characteristic value of k and/or different values of $\beta-$invariant safety factor were considered. These findings were consulted with experts and it was decided to conduct the present calibration with no $\beta-$invariant safety factors. Furthermore, in previous calibration studies (Lopez de La Cruz *et al.*, 2010), also no $\beta-$invariant safety factors were selected in the derived semi-probabilistic rules for uplift nor piping. Keeping the same safety format makes a one-to-one comparison between the two calibrations possible.

7.3 Calibrating Beta-dependent safety factors

The greater the value of the overall safety factor for piping sub-mechanism, the greater the required seepage length and the greater the reliability index will be. If uplift or heave sub-mechanisms are considered, the greater the value of the overall safety factor, the greater the required cover layer thickness and the greater the reliability index will be. Since the permeability/$\beta-$invariant safety factor is set equal to 1 and no other safety factors are involved (see section 7.2), the $\beta-$dependent safety factor is equal to the overall safety factor.

The required seepage length (or cover layer thickness for uplift and heave) and corresponding reliability indices have been calculated for a range of values of the overall safety factors. In

[2] Reliability computations for a dike segment (the so-called combined or ring computations), where failure probabilities P_f for sections (within this segment) are combined with consideration of length-effects and a reliability index β for the dike segment is derived.

other words, the following algorithm is applied per test set member and sub-mechanism:

1 Given:
   (a) a value of the $\beta-$dependent safety factor (γ_β),
   (b) the water levels corresponding to the exceedance probability of $1/T$ per year, where T is the return period defined per dike segment,
   (c) the recommended representative values (characteristic values) of all variables present in the safety assessment except for the seepage length (L) for piping or the cover layer thickness (D_{cover}) for uplift and heave,

   apply the semi-probabilistic rule such that $S_{char} \cdot \gamma_\beta = R_{char}$ (details in Appendix D) to obtain L or D_{cover};
2 The obtained values of L or D_{cover} are used to back-calculate the mean values $\mu(L)$ or $\mu(D_{cover})$, which is subsequently used to perform probabilistic computations at cross-section level[3];
3 Repeat points 1 and 2 for different values of the $\beta-$dependent safety factor γ_β = [0.5; 1; 1.25; 1.5; 1.75; 2].

For an overview of the calculated reliability indices (β_{cross}) as a function of the overall safety factor (γ_β) see plots in chapter 8. The plots also present the average values of the computed cross-sectional failure probabilities, $-\Phi^{-1}(P_{cross,avg})$, for each value of the overall safety factor. This probability is roughly equal to the 20%-quantile value of the calculated reliability indices, $\beta_{cross,20\%}$, based on modelled normal distributions. Both metrics (*i.e.* $-\Phi^{-1}(P_{cross,avg})$ and $\beta_{cross,20\%}$) may be used in calibration exercises to relate cross-sectional reliability requirements to the results of probabilistic analyses (see Jongejan (2013)). Considerable differences between these two metrics can result from e.g. non-normal distribution of the reliability indices, the presence of outliers or a strong scatter.

The next step is to propose the $\gamma - \beta$ relation in a functional form.

[3] All cross-sections in the test set were designed, *i.e.* even the cross-sections that do not have a cover layer are considered for uplift and heave.

8 Calibration results

This chapter presents the results of the calibration of the semi-probabilistic rules for uplift, heave and piping, *i.e.* it presents the achieved $\gamma_\beta - \beta_{cross}$ relations per sub-mechanism to be applied in the piping safety assessment.

The calibration was carried out for a large number of test set members (see section 6.1), which reflect the variabilities in the Netherlands. For uplift and heave, all inputs for the calibration come from the VNK2 databases. Whereas for the piping sub-mechanism, two cases are considered:

- Case 1: All inputs for the calibration come from the VNK2 databases,
- Case 2: All inputs for the calibration come from the VNK2 databases, except for the cov values of the permeability k and grain size d_{70}. These cov values were taken equal to 0.5 and 0.12, respectively.

The cov values of k and d_{70} in Case 2 correspond to the values recommended in the schematisation guidelines of piping mechanism (Förster *et al.*, 2015), while for Case 1 the cov values of k varied between 10-200% and for d_{70} between 2-30% - see (Teixeira and Wojciechowska, 2015).

In the calibration, 11 out of 15 hydraulic regions are considered, which belong to 6 different water systems, and the safety standards cover the entire range defined by DPV (2015), textiti.e. return periods of $T =$ [300; 1,000; 3,000; 10,000; 30,000; 100,000] years.

It is important to remark that cases, where (i) $FORM$-convergence problems were found in the `Hydra-Ring` computations and/or (ii) have unexpected inputs, were excluded from the analysis. Therefore, all results presented exclude cases, which were considered unreliable. In total 2227 and 2178 case remain for uplift and heave. Whereas for piping, 2352 cases are considered in Case 1 and 2435 cases in Case 2 (adjusted cov values of k and d_{70}). The final test sets constitute around 70% of the original test set (with 3321 members). We notice that for the piping sub-mechanism, the $FORM$-convergence problems were mostly detected in the lower-river area, the deltas of the rivers Vecht and IJssel and in the lake area. For the uplift and heave sub-mechanisms, the problems were additionally found in the Wadden Sea.

The calibration results follow from step 3 of the calibration procedure, as described in chapter 7. Only one safety factor ($\beta-$dependent safety factor) is considered per sub-mechanism. Given a $\beta-$dependent safety factor, the semi-probabilistic rule is applied to find the corresponding designed[1] values of the seepage length (for piping) or the cover thickness (for uplift and heave) such that $S_{char} \cdot \gamma_\beta = R_{char}$. Design water levels are presented and discussed in Appendix A.

The designed seepage lengths and cover thickness values for all test cases can be consulted in Appendix E. We notice that the achieved designed seepage lengths are very long in most of the cases. The probability of obtaining a designed seepage length longer than 100 m varies from approximately 65% to 90%, depending on a safety factor. For the safety factor of 1.0, the designed seepage lengths are up to 366 m. We note that this is not a direct result of the calibration. This is a result of the combination of the used inputs, the new piping rule and more stringent safety standards. Application of the old Sellmeijer model leads to significantly lower designed seepage lengths, as shown in Teixeira and Wojciechowska (2015). Also, the designed cover thickness values are higher than expected. For the safety factor of 1.0, the designed cover thickness values are up to 68.5 m (uplift) and 43.5 m (heave). These results are caused by low values of the cover layer weight (which come from the VNK2-data), but also from the fact that we design for the 3 sub-mechanism individually[2].

[1] "designed" refers to the value that arises from a semi-probabilistic rule given a certain safety factor.

[2] In reality, when designing a dike resistant to piping mechanism, one would choose only one of the 3 designs (sub-mechanism designs) which is the optimal for the situation.

Subsequently, having the designed values, `Hydra-Ring` is used to perform full probabilistic computations.

The achieved relations between the safety factor and the cross-sectional reliability index are presented and analysed in this chapter including the comparison of Case 1 and Case 2 for piping. Also implications for the calibration criteria are discussed.

8.1 Results per sub-mechanism

8.1.1 Piping

In this section, the results of the calibration of the semi-probabilistic rule for piping sub-mechanism are presented and discussed. Both the results achieved for Case 1 and Case 2 are presented. Note that Case 2 is the one to be used to derive the functional relations.

Figure 8.1 shows the result for Case 1, where the scatter points correspond to the 2352 cases for which reliable probabilistic computations were carried out. The black curve in the figure refers to the 20%-quantiles of the reliability indices achieved per γ_β (as seen in the histograms), which represents the average of the cross-sectional probabilities in this case (see also Jongejan (2013)).

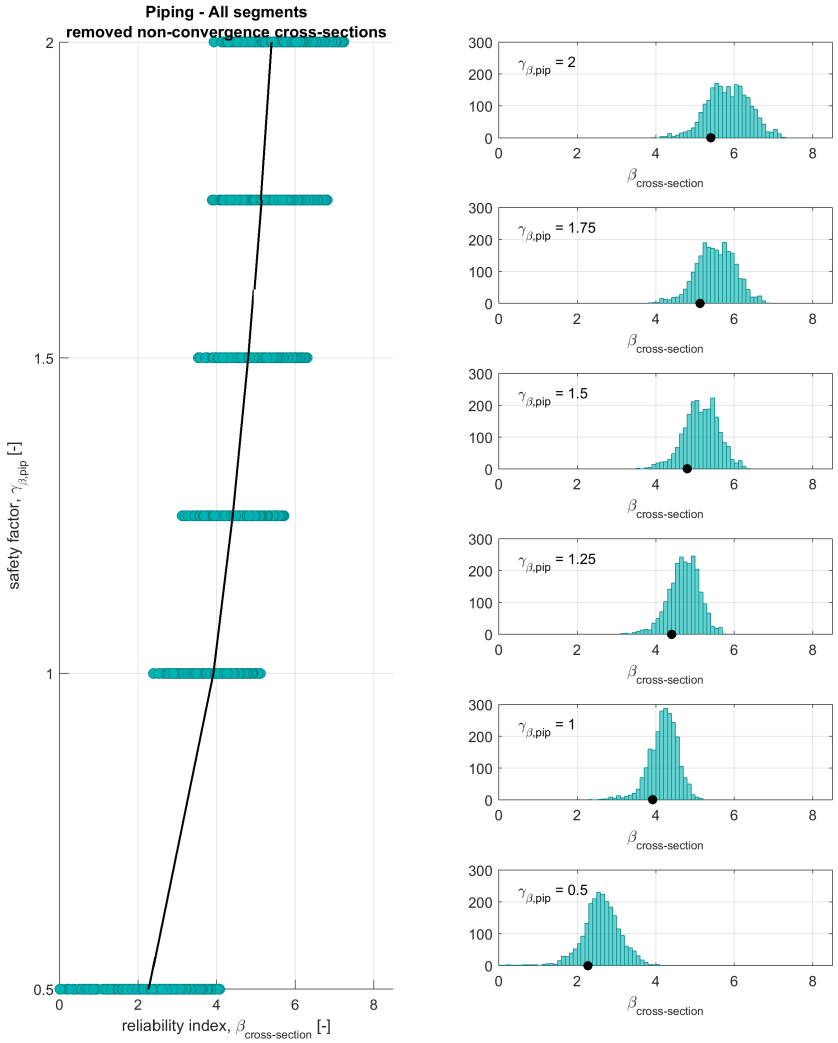

Figure 8.1: Piping results including histograms and 20%-quantile curve - Case 1.

The same principles apply for Case 2, where the uncertainties on the variables k and d_{70} were adjusted after several expert sessions. Figure 8.2 and 8.3 show the results of the calibration for Case 1 and Case 2, respectively. Again, the scatter points correspond to the test sets for which reliable probabilistic computations were carried out.

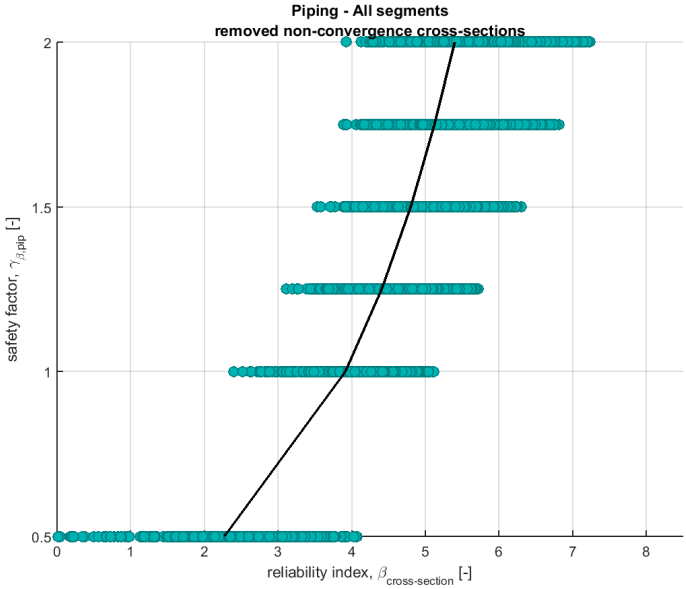

Figure 8.2: Piping calibration results for Case 1 (all inputs come from the VNK2 databases) and average of the cross-sectional failure probabilities curve (black line).

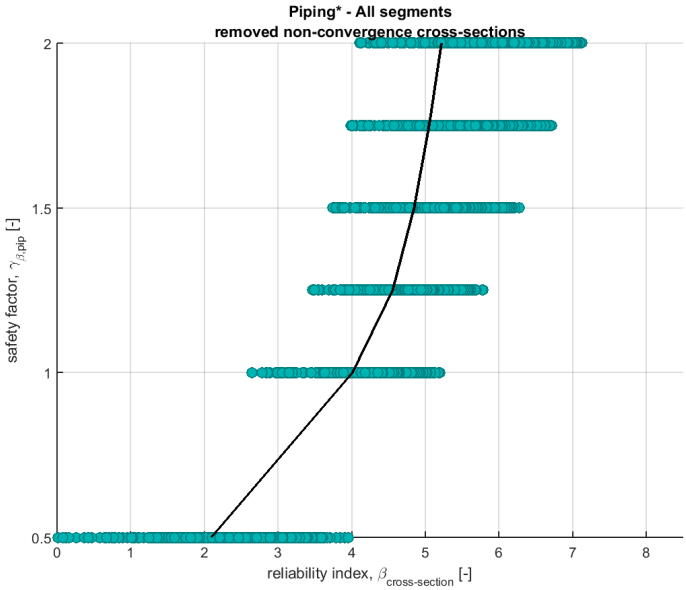

Figure 8.3: Piping calibration results for Case 2 (adjusted cov values of k and d_{70}) and average of the cross-sectional failure probabilities curve (black line).

As referred before, the average probability of failure value roughly corresponds to the 20%-quantile values of the calculated reliability indices (on the cross-section level) for each value of the overall safety factor, based on modelled normal distributions. This was true for Case 1 results, where the average probability of failure corresponds to the 20%-quantile values of the calculated reliability indices (notice the normally distributed results in Figure 8.1). On the other

hand, for Case 2, the resulted distributions were slightly skewed, and the average probability of failure value does not correspond well to the 20%-quantile values of the calculated reliability indices for each value of the overall safety factor. As such, both black lines in Figure 8.2 and 8.3 are based on the average cross-sectional probability of failure value for each value of the overall safety factor. Additionally, Figure 8.4 presents the effect of adjusting cov values of k and d_{70} in the calibration exercise, which shows to be marginal.

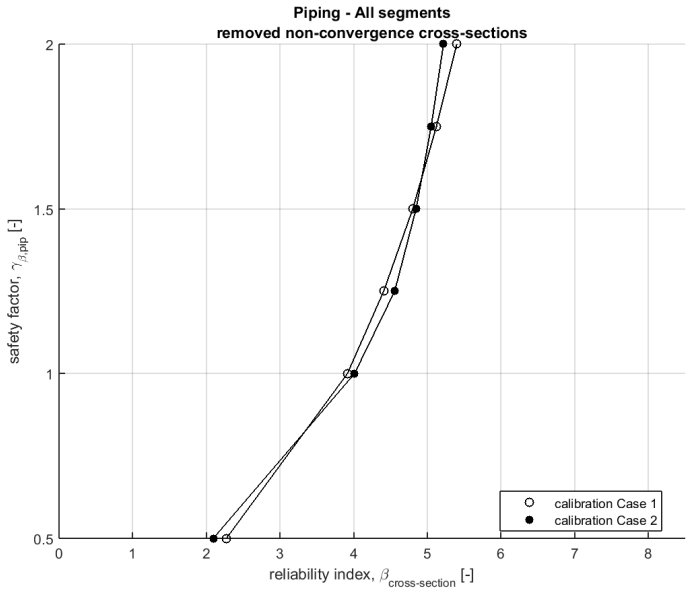

Figure 8.4: Comparison of the average of the cross-sectional failure probabilities curves for piping with Cases 1 and 2.

8.1.2 Heave

The results of the calibration of the semi-probabilistic rule for heave sub-mechanism are presented in Figure 8.5. The scatter points correspond to the results of the probabilistic computations and the black curve refers to the reliability indices that correspond to the average of the cross-sectional failure probabilities achieved per γ_β.

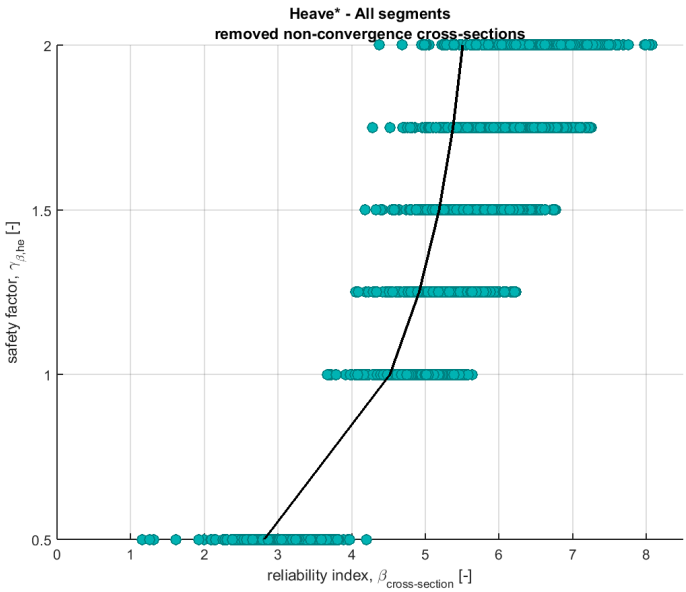

Figure 8.5: Heave calibration results and average of the cross-sectional failure probabilities curve (black line).

8.1.3 Uplift

The results of the calibration of the semi-probabilistic rule for uplift sub-mechanism are presented in Figure 8.6. The scatter points correspond to the results of the probabilistic computations and the black curve refers to the reliability indices that correspond to the average of the cross-sectional failure probabilities achieved per γ_β.

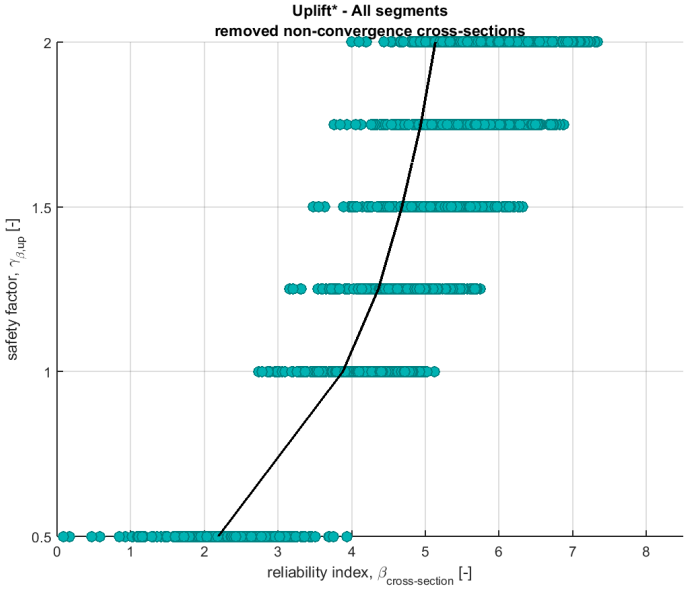

Figure 8.6: Uplift calibration results and average of the cross-sectional failure probabilities curve (black line).

For the 3 sub-mechanism, it can be observed that the reliability indices for all sub-mechanisms increase with increase in γ_β. This is as expected and can be explained by higher values of the designed variable that arise for higher γ_β's.

8.2 Established functional relations

In this section, relations between the reliability index and the safety factor are established in a functional form for uplift, heave and piping. In case of piping sub-mechanism, Case 2 is considered since it corresponds to the most recent recommendations in the schematisation guidelines of piping mechanism (Förster *et al.*, 2015).

Except for the Eastern Scheldt, all water systems in the Netherlands are included. In spite of this, computations for one dike segment in this area were made (see Appendix O). Further research was done in order to consider these results for the functional relations, and also study clustering alternatives, where the $\gamma - \beta$ relations are differentiated with respect to water systems, safety standards and situations with and without a blanket layer - see Appendix F.

The cluster that takes into account different return periods T (*i.e.* different safety standards) presented quite an intuitive behaviour - it is easy to understand the effect of T in the $\gamma - \beta$ relation. Given a safety factor, a higher required safety standard leads to a higher outside water level, which entails a higher seepage length or cover thickness according to the semi-probabilistic rules. This consequently leads to a higher reliability index.

Having in mind the conclusions on the two aforementioned points (Eastern Scheldt area and clustering consideration) and in order to find the best functional relations for each sub-mechanism, different functions were fitted to the results. More precisely, the functions were fitted to the average of the cross-sectional failure probabilities (per return period/safety standard).

Furthermore, since the safety assessment of WTI 2017 for piping mechanism requires a transformation from the occurring safety factor to the reliability index (β), the fits were made for the full range $0 \leq \gamma_\beta \leq 2$, including all the calibration points $\gamma_\beta = [0.5, 1.0, 1.25, 1.5, 1.75, 2.0]$. The resulting functional relations are presented next. The eq. (8.4), (8.5) and (8.6) give the formulas (uplift, heave and piping), with the reliability index corresponding to the safety factor of a dike section (β_{norm}) as one of the arguments. This form appears to be helpful in the semi-probabilistic assessment (see chapter 9). The values of β_{norm} can be consulted in Table 5.2 depending on the safety standard of a dike section under consideration.

For every sub-mechanism, good fits were achieved by an exponential function, which relates $\gamma - \beta$ and also includes the norm information (β_{norm}). Simplicity and comparison with the present-day recommendations would indicate the linear fit as the best option. However, one linear function (per sub-mechanism) would not provide a good fit in the full range and/or induce considerable over/under estimations of the reliability index, for a given safety factor. Furthermore, given the variability encountered in the test set, application of one relation (per sub-mechanism) can lead to too conservative/optimistic dike safety assessments.

The derived functions give one relation per sub-mechanism that comprises all calibration results and all the water systems in the Netherlands (including the Eastern Scheldt area).

8.2.1 Piping

The following Figure 8.7 shows the exponential function fitted to the the average of the cross-sectional probabilities, its equation is presented in eq.(8.1).

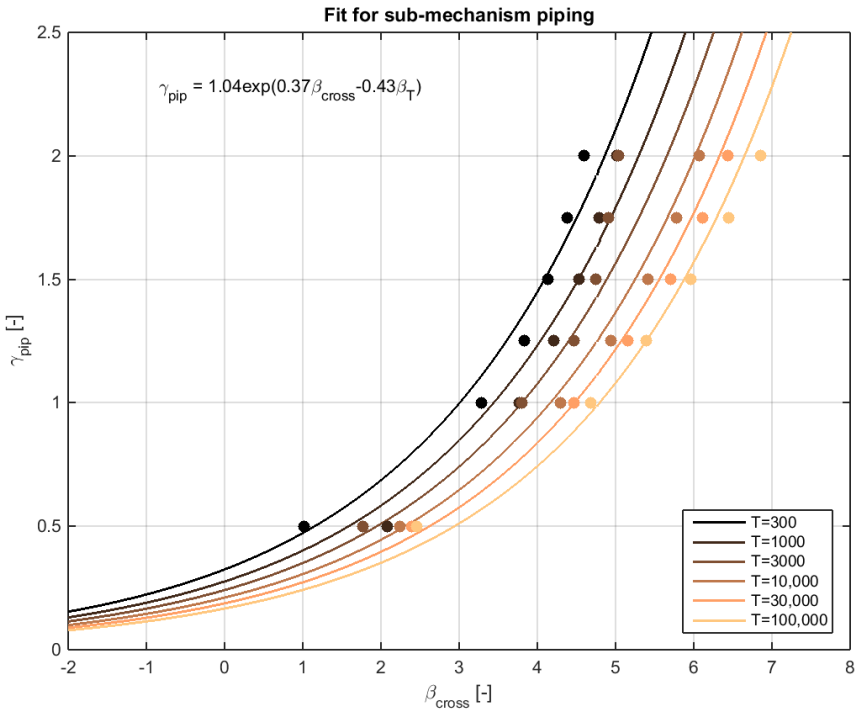

Figure 8.7: Derived functional $\gamma_{pip} - \beta_{cross}$ relation for the piping sub-mechanism.

$$\gamma_{pip} = 1.04 \cdot e^{(0.37 \cdot \beta_{cross} - 0.43 \cdot \beta_{norm})} \tag{8.1}$$

8.2.2 Heave

The following Figure 8.8 shows the exponential function fitted to the the average of the cross-sectional probabilities, its equation is presented in eq.(8.2).

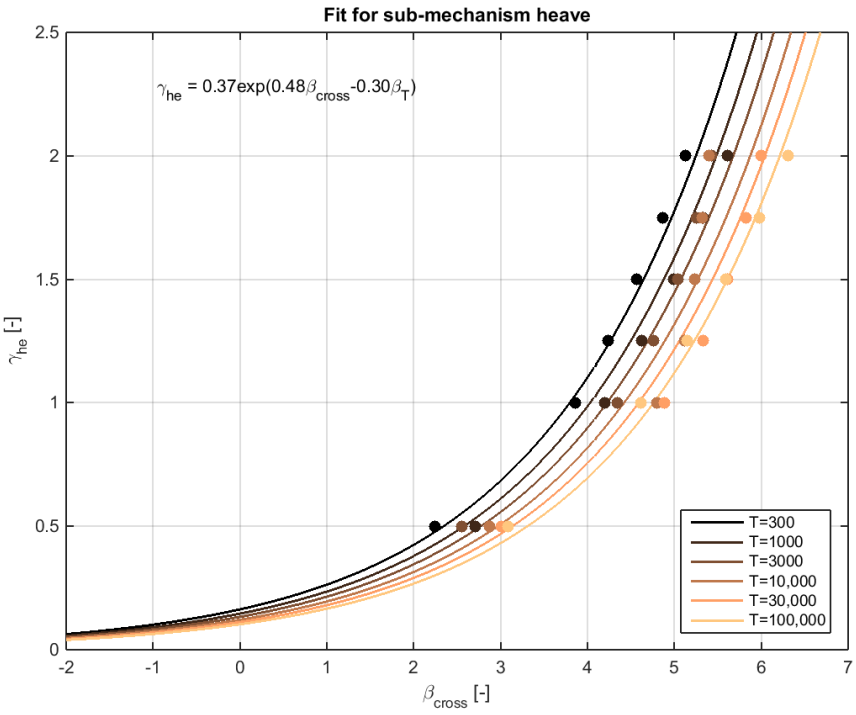

Figure 8.8: Derived functional $\gamma_{he} - \beta_{cross}$ relation for the heave sub-mechanism.

$$\gamma_{he} = 0.37 \cdot e^{(0.48 \cdot \beta_{cross} - 0.30 \cdot \beta_{norm})} \tag{8.2}$$

8.2.3 Uplift

The following Figure 8.9 shows the exponential function fitted to the the average of the cross-sectional probabilities, its equation is presented in eq.(8.3).

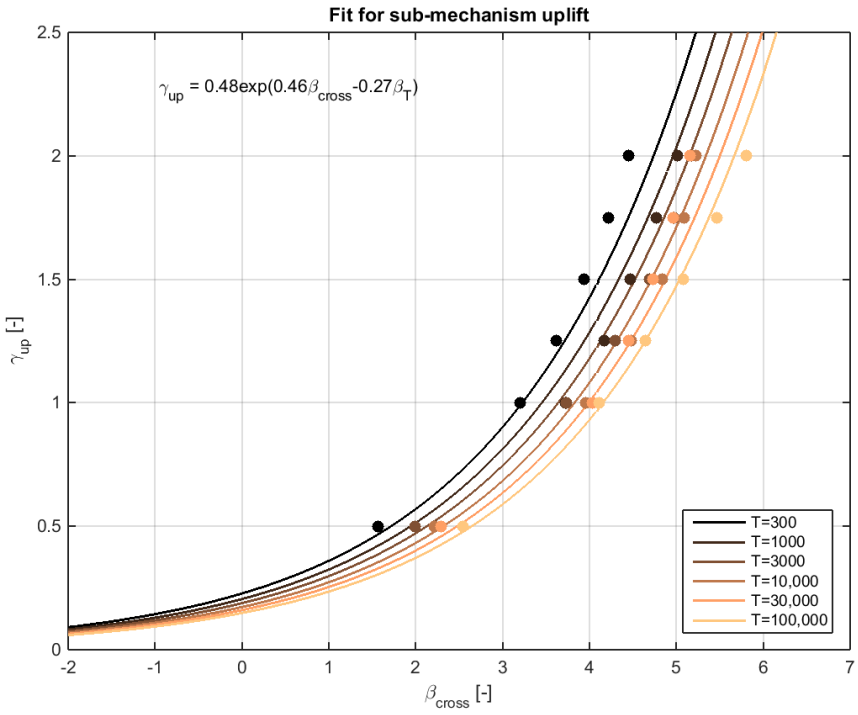

Figure 8.9: Derived functional $\gamma_{up} - \beta_{cross}$ relation for the uplift sub-mechanism.

$$\gamma_{up} = 0.48 \cdot e^{(0.46 \cdot \beta_{cross} - 0.27 \cdot \beta_{norm})} \tag{8.3}$$

In summary, the following equations provide the recommendation for the functional relationship for Uplift, Heave and Piping, with the safety factor as an argument; this form is needed for the semi-probabilistic assessment (as explained in chapter 9):

UPLIFT (UP)

$$\beta_{up} = \frac{1}{0.46}\left(\ln\left(\frac{\gamma_{up}}{0.48}\right) + 0.27\beta_{norm}\right) \tag{8.4}$$

HEAVE (HE)

$$\beta_{he} = \frac{1}{0.48}\left(\ln\left(\frac{\gamma_{he}}{0.37}\right) + 0.30\beta_{norm}\right) \tag{8.5}$$

PIPING (PIP)

$$\beta_{pip} = \frac{1}{0.37}\left(\ln\left(\frac{\gamma_{pip}}{1.04}\right) + 0.43\beta_{norm}\right) \tag{8.6}$$

9 Semi-probabilistic assessment steps and comparison with other assessments

This chapter presents in the first section (section 9.1) how to carry out a semi-probabilistic assessment for piping mechanism, including how to deal with sub-mechanisms and sub-soil scenarios. In the last section (section 9.2), comparison of the calibrated relations with the present-day ones, for piping assessment (piping and uplift sub-mechanisms) is presented and discussed.

9.1 Piping semi-probabilistic assessment steps

This section outlines steps of a semi-probabilistic assessment of a dike cross-section regarding the piping mechanism, following Jongejan and Klerk (2015) and as schematised in Figure 9.1. The failure mechanism consists of three sub-mechanisms: uplift, heave and piping. All sub-mechanisms have to occur before the dike fails. For each sub-mechanism, the assessment is carried out per sub-soil scenario. In the end, the combined results of the assessments per sub-mechanism and per sub-soil scenario are combined to an overall result. It is assumed that the dike cross-section is situated in a dike segment (*normtraject*) with the safety standard of $1/T$ years and n is the number of sub-soil scenarios. The reliability index corresponding to the safety standard of $1/T$ years is denoted by β_{norm} or β_T (if it includes the failure probability factor).

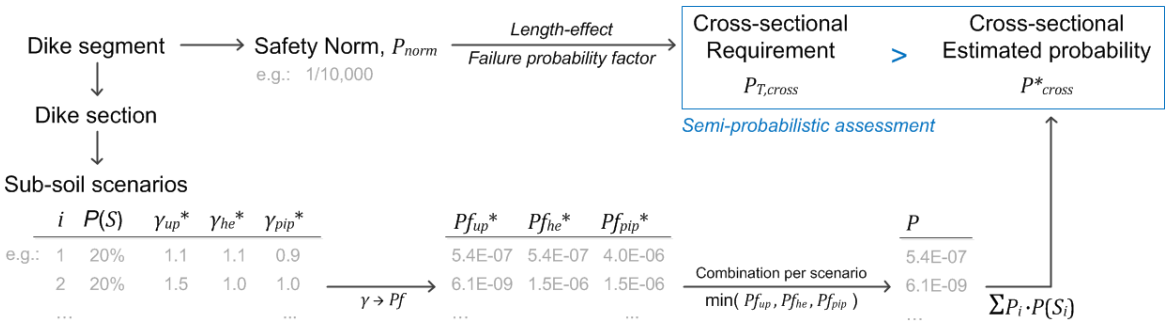

Figure 9.1: Schematised semi-probabilistic assessment for the piping mechanism in WTI 2017 (as in Jongejan and Klerk (2015)).

The goal is to compare the target safety with the occurring safety in terms of the reliability index or the probability of failure:

$$\beta^*_{cross} \geq \beta_{T,cross} \Leftrightarrow P^*_{cross} \leq P_{T,cross} \tag{9.1}$$

where $\beta_{T,cross}$ ($P_{T,cross} = \Phi(-\beta_{T,cross})$) is the target reliability index at the cross-section level and β^*_{cross} ($P^*_{cross} = \Phi(-\beta^*_{cross})$) is the derived/estimated reliability index for the dike cross-section.

For that, one should follow the steps below.

1 Determine characteristic values of variables involved in the semi-probabilistic rule(s), as specified in Table 9.1, for each sub-soil scenario. Characteristic values of random variables are marked with index $char$.

2 Derive the outside water level $h(T)$ corresponding to the safety standard of the dike segment.

3 With the characteristic values and design water level, determine the $\beta-$dependent safety factors for each sub-mechanism and each sub-soil scenario ($\gamma^*_{up,i}$, $\gamma^*_{he,i}$, $\gamma^*_{pip,i}$ and $i = 1, \ldots, n$, where n = the number of subsoil scenarios considered):

UPLIFT (UP)

$$\gamma^*_{up,i} = \frac{R_{char}}{S_{char}} = \frac{D_{cover,char} \cdot \gamma_{eff,cover,char}}{\gamma_{water,char} \cdot (h(T) - h_{exit,char}) \cdot r_{exit,char}} \tag{9.2}$$

HEAVE (HE)

$$\gamma^*_{he,i} = \frac{R_{char}}{S_{char}} = \frac{D_{cover,char} \cdot i_{c,h,char}}{(h(T) - h_{exit,char}) \cdot r_{exit,char}} \tag{9.3}$$

PIPING (PIP)

$$\gamma^*_{pip,i} = \frac{R_{char}}{S_{char}} = \frac{f(L_{char}, D_{char}, d_{70,char}, k_{char})}{h(T) - h_{exit,char} - r_{c,char} \cdot D_{cover,char}} \tag{9.4}$$

where $f(.)$ is the critical head difference according to Sellmeijer 2011 (see eq.(3.9)) and i refers to the sub-soil scenario i ($i = 1, \ldots, n$). The meaning of each variable in the above equations can be consulted in Table 9.1.

4 The calibrated $\gamma - \beta$ relation(s) may be used inversely to obtain a (safe) estimate of the conditional reliability index (or probability of failure) per sub-soil scenario. Accordingly, use the recommended rules to transform the occurring safety factors into reliability indices ($\beta_{up,i}$, $\beta_{he,i}$, $\beta_{pip,i}$ and $i = 1, \ldots, n$):

UPLIFT (UP)

$$\beta_{up,i} = \frac{1}{0.46} \cdot \left(\ln \left(\frac{\gamma^*_{up,i}}{0.48} \right) + 0.27 \cdot \beta_{norm} \right) \tag{9.5}$$

HEAVE (HE)

$$\beta_{he,i} = \frac{1}{0.48} \cdot \left(\ln \left(\frac{\gamma^*_{he,i}}{0.37} \right) + 0.30 \cdot \beta_{norm} \right) \tag{9.6}$$

PIPING (PIP)

$$\beta_{pip,i} = \frac{1}{0.37} \cdot \left(\ln \left(\frac{\gamma^*_{pip,i}}{1.04} \right) + 0.43 \cdot \beta_{norm} \right) \tag{9.7}$$

The values of β_{norm} can be consulted in Table 5.2 depending on the safety standard of the considered dike segment.

5 Transform the reliability indices to failure probabilities $P_{f,up,i} = \Phi(-\beta_{up,i})$, $P_{f,he,i} = \Phi(-\beta_{he,i})$ and $P_{f,pip,i} = \Phi(-\beta_{pip,i})$ for $i = 1, \ldots, n$.

6 To reach an overall verdict, the results of assessments for uplift, heave and piping for the different sub-soil scenarios have to be combined:

(a) For every sub-soil scenario, determine the minimum probability of failure ("combination" of sub-mechanisms):

$$P_{f,i} = \min\{P_{f,up,i}, P_{f,he,i}, P_{f,pip,i}\} \text{ and } i = 1, \ldots, n \tag{9.8}$$

Notice that the minimum probability of failure (corresponding to the maximum reliability index) is equal to the failure probability due to piping mechanism, under the assumption that the three sub-mechanisms are fully correlated[1]. This assumption is conservative.

(b) Having the failure probabilities for each sub-soil scenario, calculate the total occurring failure probability P^*_{cross} and reliability index β^*_{cross} by:

$$P^*_{cross} = \sum_{i=1}^{n} P_{f,i} \cdot P(S_i) \quad \text{and} \quad \beta^*_{cross} = -\Phi^{-1}(P^*_{cross}) \tag{9.9}$$

where $P(S_i)$ is the probability of sub-soil scenario i and $\sum_{i=1}^{n} P(S_i) = 1$. P^*_{cross} is a conservative (safe) estimate of the cross-sectional probability of failure.

7 To assess the cross-section, based on the safety standard T and the length-effect parameters for piping failure mechanism, determine the target failure probability (or reliability index) of the dike cross-section by using:

$$P_{T,cross} = \frac{f/T}{\left(1 + \frac{a \cdot L_{segm}}{b}\right)} \quad \text{and} \quad \beta_{T,cross} = -\Phi^{-1}(P_{T,cross}) \tag{9.10}$$

where L_{segm} is the total length of the segment [m], a is a fraction of the length that is sensitive to piping [-], b is a measure for the intensity of the length-effect within the part of the segment that is sensitive to piping (the length of independent, equivalent dike sections) [m] and f is the piping failure probability factor equal to 0.24.

Following the study of Lopez de La Cruz *et al.* (2010), the recommendation for the length-effect parameters is $b = 350$ m and $a = 1$, under the assumption that the *entire* dike segment is sensitive to piping. If this is not the case (*i.e.* if not the entire dike segment is sensitive to piping), the user can lower the value of a ($a \in [0, 1]$).

8 The considered dike cross-section complies to the safety standard regarding the piping failure mechanism if it fulfills eq.(9.1).

[1] The probability $P(A \cap B \cap C)$ is equal to $\min\{P(A), P(B), P(C)\}$ when the events A, B and C are fully correlated. On the other hand, the probability $P(A \cap B \cap C)$ is equal to $P(A) \cdot P(B) \cdot P(C)$ when the events are independent. It holds that $P(A) \cdot P(B) \cdot P(C) \leq P(A \cap B \cap C) \leq \min\{P(A), P(B), P(C)\}$. The probability $P(A \cap B \cap C)$ corresponds here to $P(\text{uplift} \cap \text{heave} \cap \text{piping})$.

Table 9.1: Input parameters for piping analyses (norm = normal, log = log-normal).

Symbol [unit]	Description	Uplift	Heave	Piping	Distribution type	Default	$char$ value
m_u $[-]$	Model factor for uplift	x			log	μ 1.0 ,σ 0.10	1.0
γ_{water} $[kN/m^3]$	Volumetric weight of water	x		x	-	10	10
$\gamma_{sat,cover}$ $[kN/m^3]$	Saturated volumetric weight of the cover layer	x			shifted log (+10)	-	5%
r_{exit} $[-]$	Damping factor at exit	x	x		log	-	95%
$i_{c,h}$ $[-]$	Critical heave gradient		x		log	μ 0.5 ,σ 0.10	0.3
D_{cover} $[m]$	Effective thickness of the cover layer	x	x	x	log	-	5%
h_{exit} $[m + NAP]$	Phreatic level at the exit point	x	x	x	norm	-	5%
m_p $[-]$	Model factor for piping			x	log	μ 1.0 ,σ 0.12	1.0
h $[m+NAP]$	Outside water level	x	x	x	`Hydra-Ring`	-	Design water level*
r_c $[-]$	Reduction factor			x	-	0.3	0.3
L $[m]$	Seepage length, from entry point to exit point			x	log	-	5%
$\gamma_{sub,particles}$ $[kN/m^3]$	Submerged volumetric weight of sand particles			x	-	16.5	16.5
η $[-]$	White's drag coefficient			x	-	0.25	0.25
d_{70} $[m]$	70%-quantile of the grain size distribution of the piping-sensitive layer			x	log	cov 0.12	5%
k $[m/s]$	Darcy permeability			x	log	cov 0.50	95%
ν_{water} $[m^2/s]$	Kinematic viscosity of water			x	-	1.33×10^{-6}	1.33×10^{-6}
g $[m/s^2]$	Gravitational constant			x	-	9.81	9.81
D $[m]$	Thickness of the aquifer			x	log	-	95%
$d_{70,m}$ $[m]$	Mean value of the d_{70} in small scale tests			x	-	2.08×10^{-4}	2.08×10^{-4}
$\theta_{sellmeijer,rev}$ $[^\circ]$	Bedding angle of sand grains for the revised Sellmeijer rule (Sellmeijer *et al.*, 2011)			x	-	37	37

*Design water level is defined as the water level with an exceedance probability equal to the maximum allowable probability of flooding of a dike segment.

9.2 Comparison with present-day relations

In this section, the exponential relations for uplift and piping sub-mechanisms, achieved in the previous chapter, are compared with present-day relations found in the following literature[2]:

- *Voorschrift toetsen op Veiligheid Primaire Waterkeringen 2006*, called further VTV 2006 (see VTV (2007)),
- *Ontwerpinstrumentarium 2014* (based on study from 2010), called further OI 2014/study 2010 (see OI (2013) and Lopez de La Cruz *et al.* (2010)),
- *Ontwerpinstrumentarium 2014 version 3*, called further OI 2014 v3 (see OI (2015)).

An overview of the present-day relations is given in Table 9.2. Figures 9.2 and 9.3 present the comparisons for uplift and piping sub-mechanisms, respectively.

Table 9.2: Overview of the present-day relations for uplift and piping sub-mechanisms.

Study	Sub-mechanism	Relation
VTV 2006	Piping	Safety factor has to be at least 1.2 (old Sellmeijer rule)
	Uplift	Safety factor has to be at least 1.0, 1.1 or 1.2, depending on the way pore water pressure is determined.
OI 2014/study 2010	Piping	$\gamma_{pip} = 0.60 \cdot \beta_{T,cross} - 1.50$ for $\beta_{T,cross} \in [4.5, 5.5]$ $\gamma_{pip} = 1.20$ for $\beta_{T,cross} < 4.5$ $\gamma_{pip} = 1.80$ for $\beta_{T,cross} > 4.5$
	Uplift	$\gamma_{up} = 0.57 \cdot \beta_{T,cross} - 1.20$ for $\beta_{T,cross} \in]4.0, 5.5[$
OI 2014 v3	Piping	$\gamma_{pip} = 0.80 \cdot \beta_{T,cross} - 2.4$ for $\gamma_{pip} \geq 1.2$

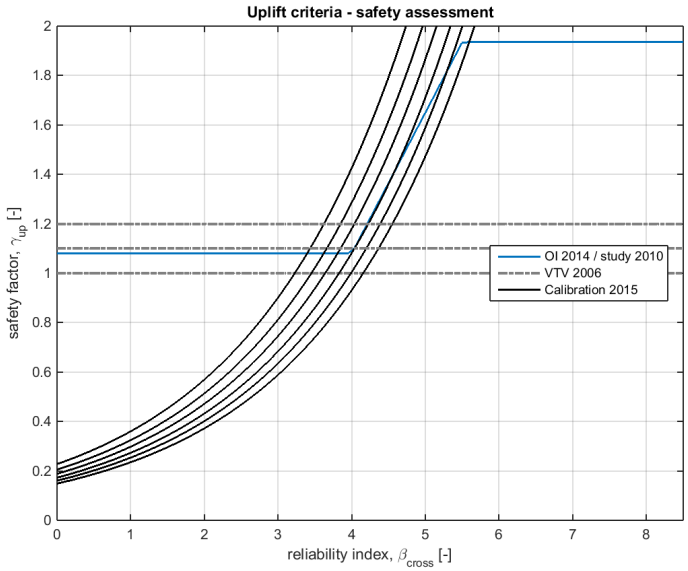

Figure 9.2: Comparison of the functional relations (Calibration 2015) and the present-day relations for the uplift sub-mechanism.

[2] In these studies, the heave sub-mechanisms is not considered.

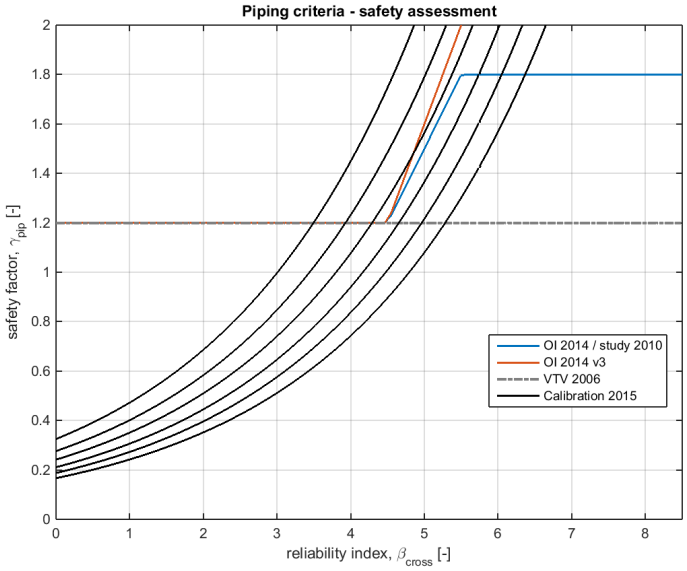

Figure 9.3: Comparison of the functional relations (Calibration 2015, Case 2) and the present-day relations for the piping sub-mechanism.

The comparison between the relations achieved in this study and the present-day relations is difficult due to the following reasons:

1 The achieved relations depend on the cross-sectional reliability index. This is also the case for OI 2014/study 2010 and OI 2014 v3. The relations according to VTV 2006 do not depend on the cross-sectional reliability index and hence this comparison is here not suitable.

2 The achieved relations depend on the required reliability index corresponding to the safety standard of a dike segment *i.e.* β_{norm}. Whereas, none of the present-day relations depend on β_{norm}.

For uplift, the relation according to OI 2014/study 2010 crosses the relations from this report found for the safety standards $T = 10,000$ and $T = 30,000$ years (*i.e.* the fourth and the fifth black lines from the left in Figure 9.2). For piping, the relations according to OI 2014/study 2010 and OI 2014 v3 corresponds with the relation for the safety standard $T = 3,000$ years (*i.e.* the third black line from the left in Figure 9.3).

The fact that the relations from this report depend on the required reliability index of a dike segment differs from the "average approach" given by the present-day rules. The present-day rules apply to all dikes equally. Introduction of a relation that depends on β_{norm} optimizes the semi-probabilistic assessment of dikes, because more dike's characteristics are taken into account when translating the safety factor into the corresponding reliability index (see section 9.1).

Furthermore, the achieved relations are also defined for safety factors lower than 1. The present-day relations are not defined for low safety factors. Recall, that the WTI 2017 semi-probabilistic assessment for the piping failure mechanism requires that any safety factor higher than zero can be translated into the corresponding reliability index. This is possible with the proposed relations.

Further differences between the studies are:

- Test sets - test set members based on the VNK2-data are used in this report. In OI 2014/study 2010 and OI 2014 v3 the test set members were artificial (artificial soil-scenarios) or were also based on the VNK2-data. In the latter case, the size of the data set was significantly smaller than in this report;
- Safety standards - the new safety standards are used in this report, whereas the current safety standards for dike-rings were applied in OI 2014/study 2010 and OI 2014 v3;
- Probabilistic engines - `Hydra-Ring` is used in this report, whereas `Excel`-based software for probabilistic computations was applied in OI 2014/study 2010 and OI 2014 v3.

10 Conclusions and recommendations

This chapter provides conclusions and recommendations regarding the final calibration exercise carried out for the piping mechanism. This calibration is envisaged for the new safety assessment framework: WTI 2017.

The calibration results include:

- Test set derived from the VNK2-databases (mean and coefficient of variation cov), with exception of the $cov(k)$=0.50 and $cov(d_{70})$=0.12;
- Design water levels estimated with `Hydra-Ring`, using TMR2006 databases;
- Designed values of the seepage length (piping) and the cover thickness (uplift and heave);
- Relations between the $\beta-$dependent safety factor and the reliability index on the cross-section level (β_{cross});
- Functional $\gamma - \beta$ relations to be used in the piping semi-probabilistic dike safety assessment, where uplift, heave and piping are studied separately.

Furthermore, comparison between the derived relations and the present-day ones is presented, as well as a study on the length-effect parameters for the piping mechanism (applicable to all sub-mechanisms). In a nutshell, the main conclusions are as follows.

CALIBRATION

- The considered test set covers a wide range of sub-soil scenarios and hydraulic regions in the Netherlands, and is considered as satisfactory for making proper conclusions about the semi-probabilistic rules. Cases that showed $FORM$-convergence problems were excluded from the analyses;
- In order to simplify the safety formats, only one safety factor per sub-mechanism is considered. All other (partial) safety factors are assumed equal to one;
- The characteristic values of the random variables are conform the WTI 2017 approach (*i.e.* typically 5%-quantile for the strength and 95%-quantile for the load). The characteristic values were consulted with experts;
- The seepage lengths derived in the piping calibration are quite long, which is a result from the piping model used (Sellmeijer *et al.*, 2011) and not from the calibration exercise itself;
- After the calibration, the relations were additionally differentiated with respect to water systems, safety standards and situations with and without a blanket layer. The differentiation with respect to safety standards of dike segments was chosen as plausible and was considered when defining the functional relations. The functional relations depend hence on the reliability index corresponding to the safety standard of a dike segment;
- Note that the relations have been derived separately for different safety levels (β_{norm}). This was done to prevent the semi-probabilistic assessment rules from becoming overly conservative. It is therefore expected that the recommended rules lead to an optimization of the semi-probabilistic assessment as it accounts for dike's characteristics.
- The functional relations for uplift and piping, were compared with the present-day ones (VTV (2007), Lopez de La Cruz *et al.* (2010), OI (2013) and OI (2015)) and the following can be concluded:
    - The functional relations depend on the reliability index corresponding to the safety standard of a dike segment and this is novel in case of the piping failure mechanism,

- In contrast to the present-day rules, the functional relations are also defined for low safety factors. This fulfills the requirements of the presented semi-probabilistic safety assessment for the piping failure mechanism.

LENGTH-EFFECT PARAMETERS

- The length-effect parameters were not part of the calibration exercise, but they are needed for the safety assessment;
- In this study, two approaches to estimate a and b values were considered. However, none showed conclusive results. This could be explained by the selected data but also by the complexity of the problem;
- Following the study of Lopez de La Cruz *et al.* (2010), the recommendation for the length-effect parameters is $b = 350$ m and $a = 1$, under the assumption that the *entire* dike segment is sensitive to piping. If this is not the case (*i.e.* if not the entire dike segment is sensitive to piping), the user can lower the value of a ($a \in [0, 1]$).

HYDRA-RING

- The model in `Hydra-Ring` was successfully applied in the calibration exercise and the obtained results (*i.e.* reliability indices and influence coefficients) are consistent with the results of previous studies;
- Problems with the uplift sub-mechanism, as detected during the preliminary calibration in 2014, were solved in the uplift kernel of `Hydra-Ring` at the beginning of 2015.

References

Calle, E. and W. Kanning, 2013. *WTI: Effecten ruimtelijke variabiliteit op geotechnische sterkte van waterkeringen*. Report 1207805-004-ZWS-005, Deltares.

de Bruijn, H., H. Knoeff and U. Förster, 2010. *Beschrijving toetsproces piping*. Report 1202341-001, Deltares.

Diermanse, F., K. Roscoe, J. Lopez de la Cruz, H. Steenbergen and T. Vrouwenvelder, 2013. *Hydra-Ring Scientific Documentation*. Report 1206006-004, Deltares.

DPV, 2015. *Synthesedocument deelprogramma veiligheid - achtergrondrapport bij deltaprogramma 2015*. Tech. rep., Dutch Ministry of Infrastructure and the Environment.

Förster, U., M. de Visser, H. de Bruijn, G. Kruse, M. Hijma and L. Vonhögen-Peeters, 2015. *Schematiseringshandleiding Piping bij dijken WTI 2017*. Report 1220084-006-GEO-0001, Deltares.

Förster, U., G. v. d. Ham, E. Calle and G. Kruse, 2012. *Technisch Rapport Zandmeevoerende Wellen*. Report 1202123-003, Deltares.

Jongejan, R., 2013. *Kalibratie van semi-probabilistische toetsvoorschriften: Algemeen gedeelte*. Report 1207803-003, Deltares.

Jongejan, R. and W. J. Klerk, 2015. *Functional design semi-probabilistic assessments Ringtoets*. Report 1209431-008-ZWS-0009, Deltares.

Jongejan, R. and J. Lopez de La Cruz, 2011. *Kalibratie semi-probabilistisch toetsvoorschrift voor piping*. Report 1204145-001-ZWS-0006-ha, Deltares.

Lopez de La Cruz, J., T. Schweckendiek, C. Mai Van and W. Kanning, 2010. *SBW Piping - HP8b Kalibratie van de veiligheidsfactoren*. Report 1202123-002-GEO-0005, Deltares.

OI, 2013. *Achtergrondrapport Ontwerpinstrumentarium 2014*. Tech. rep., Rijkswaterstaat Water, Verkeer en Leefomgeving.

OI, 2015. *Handreiking ontwerpen met overstromingskansen, Veiligheidsfactoren en belastingen bij nieuwe overstromingsnormen*. Report Concept vs. 2.5, Rijkswaterstaat Water, Verkeer en Leefomgeving.

Rackwitz, R., 2001. "Reliability analysis - a review and some perspectives." *Structural Safety* 23: 365-395.

Sellmeijer, J. B., J. Lopez de La Cruz, V. M. van Beek and H. Knoeff, 2011. "Fine-tuning of the backward erosion piping model through small-scale,medium-scale and IJkdijk experiments." *European Journal of Environmental and Civil Engineering* pages 1139-1154.

Teixeira, A. and K. Wojciechowska, 2015. *Analysis of effect uncertainty k and d70*. Memo 1220080-002-ZWS-0009, Deltares.

ter Horst, W., K. Wojciechowska and A. Teixeira, 2014. *Preliminary calibaration of safety factores for semi-probabilistic assessment of piping failure mechanism*. Report 1209431-007-ZWS-0004, Deltares.

Visschedijk, M. and T. Schweckendiek, 2013. *WTI 2017 Failure Mechanisms - Piping Kernel: Requirements and Functional Design (v0.3)*. Report, Deltares.

VNK2, 2013. *Van ruwe data tot overstromingsrisico - Handleiding ter bepaling van het overstromingsrisico van dijkringen binnen het project VNK2,*. Tech. Rep. Versienummer: 2.5, RWS Waterdienst.

VTV, 2007. *Voorschrift Toetsen op Veiligheid Primaire Waterkeringen*. Report ISBN: 978-90-369-5762-5, Ministerie van Verkeer en Waterstaat.

Wojciechowska, K. and A. Teixeira, 2014. *WTI 2017 Piping Calibration - issues*. Memo 1209431-007-ZWS-0006, Deltares.

A Final test set

This appendix presents the main assumptions, selection of the test set and derivation of design water levels for the purpose of the calibration exercise (uplift, heave and piping). Because the data from the VNK2-project is used in the calibration exercise, preparation of the calibration requires also translation of inputs from `PC-Ring` to `Hydra-Ring`. This translation is given in Appendix B.

A.1 General definitions and assumptions

The following definitions and assumptions hold in this study:

- A dike-ring consists of dike segments. For each dike segment, a certain safety standard applies. In this study, DPV segments are considered with the safety standards according to DPV (2015);
- A dike segment consists of dike sections that correspond to *bodemvakken* in the project VNK2. Each dike section has a representative cross-section.
- The probabilistic computations were performed with the available versions of the model `Hydra-Ring` that were available during the study (study period: January-July 2015) using the $FORM$-routine with the starting method 4;
- For the calculation purposes (`Hydra-Ring`), it is assumed that a cross-section of a dike has a length small enough to eliminate length-effects[1].

A.2 Test set

In this study, the test set consist of sub-soil scenarios within DPV segments(DPV, 2015). To select the test set the following criteria are applied:

1. The test set originate from the VNK2-project data with existing sub-soil scenarios, all available VNK2 databases are considered (Figure A.1),
2. There exists a link between HR[2] stations in VNK2 (`PC-Ring`) and HR stations in `Hydra-Ring`,
3. Dike-rings situated in the Eastern Scheldt are not considered in the calibration. This is because of a long computational time of probabilistic analyses with `Hydra-Ring` for this hydraulic region[3] and
4. Small dike-rings (e.g. 13b, 34a) are not considered.

[1] This is a practical trick to enable analysis of cross-section purely, without the length-effect using `Hydra-Ring`.

[2] *Hydraulische Randvoorwaarden*.

[3] Note that these computations require the $DirectionalSampling$ technique.

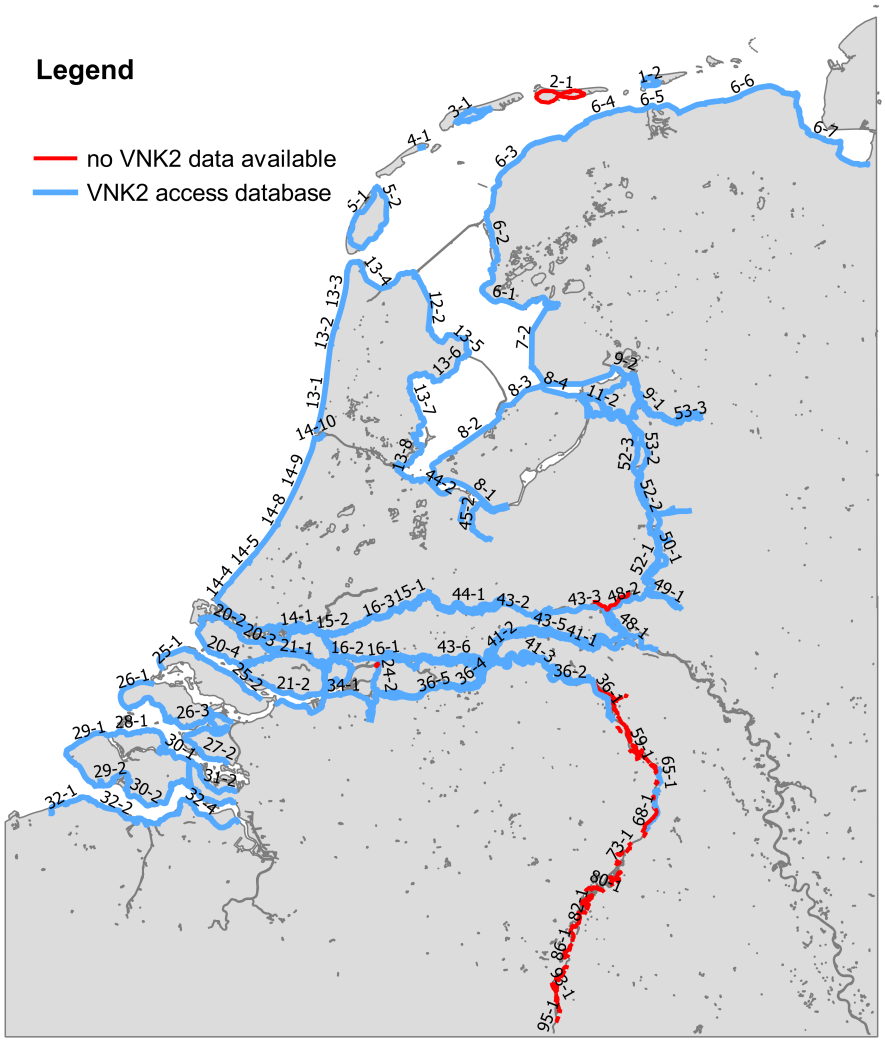

Figure A.1: Overview of available VNK2 databases per DPV segment.

The test set results from intersection of the above points. However, a direct link between HR stations in VNK2 and HR stations in `Hydra-Ring` could not be established for most of locations in the Wadden Sea (in particular dike-ring 6). Therefore, for this region, given a HR station in VNK2 the closest HR station in `Hydra-Ring` was found, the maximal considered distance was 250 m.

Figure A.2 and A.3 give an overview of the final test set differentiated with respect to hydraulic region and safety standard, respectively. Graphical presentation of the properties of the test set is given in Figure A.4, A.5 and A.6. Statistics of the test set are presented in Table A.1 and A.2.

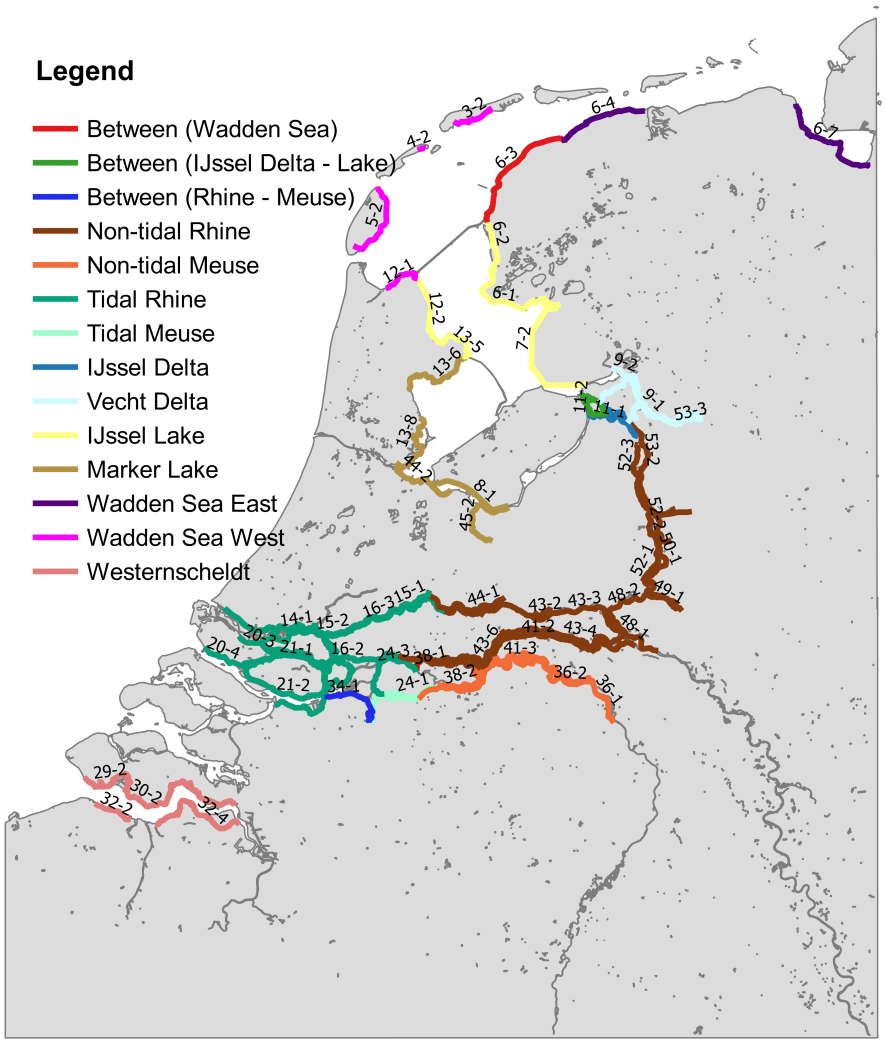

Figure A.2: DPV segments in the final test set for uplift, heave and piping (differentiation per hydraulic region).

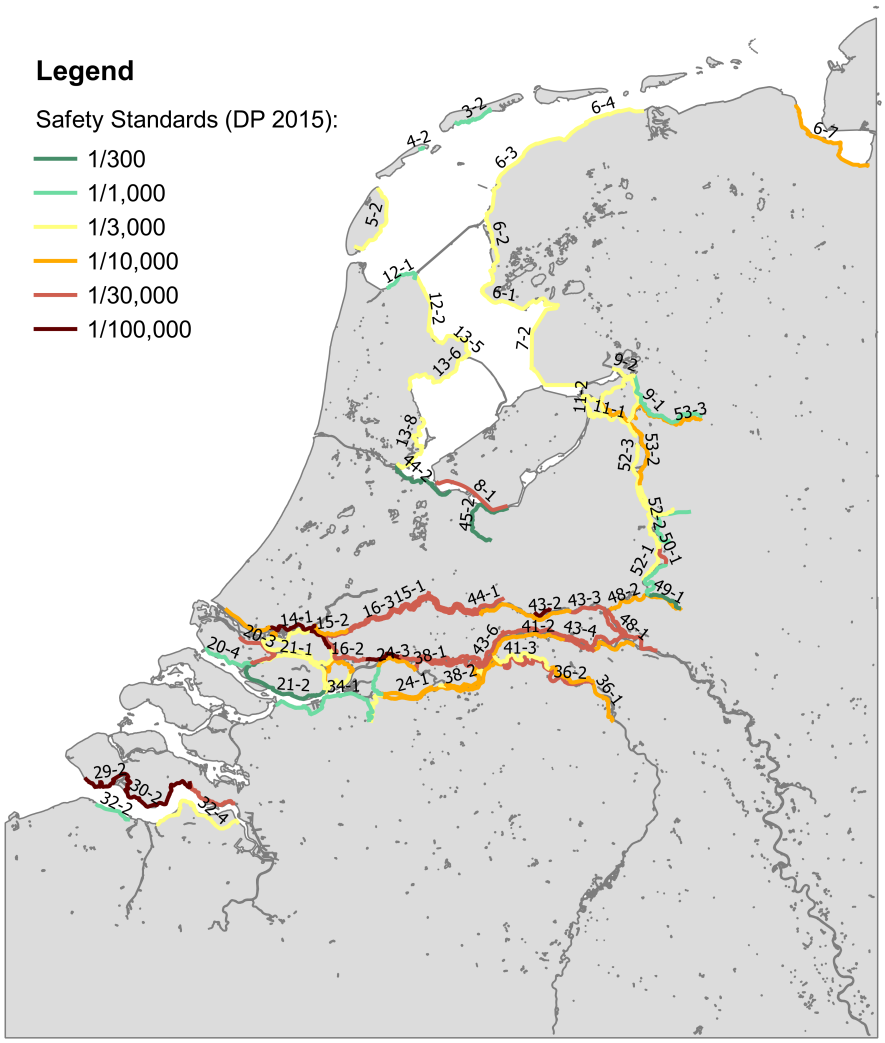

Figure A.3: DPV segments in the final test set for uplift, heave and piping (differentiation per safety standard).

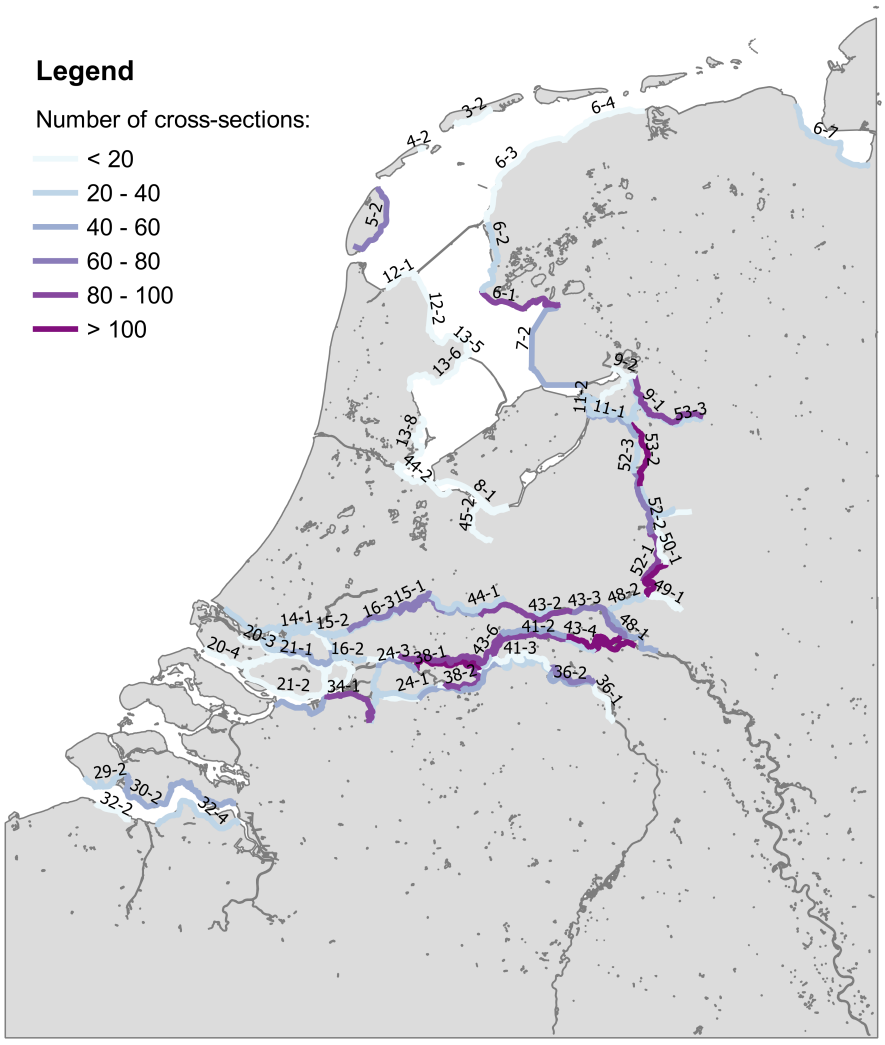

Figure A.4: Number of dike cross-sections (sub-soil scenarios) in the final test set per DPV segment.

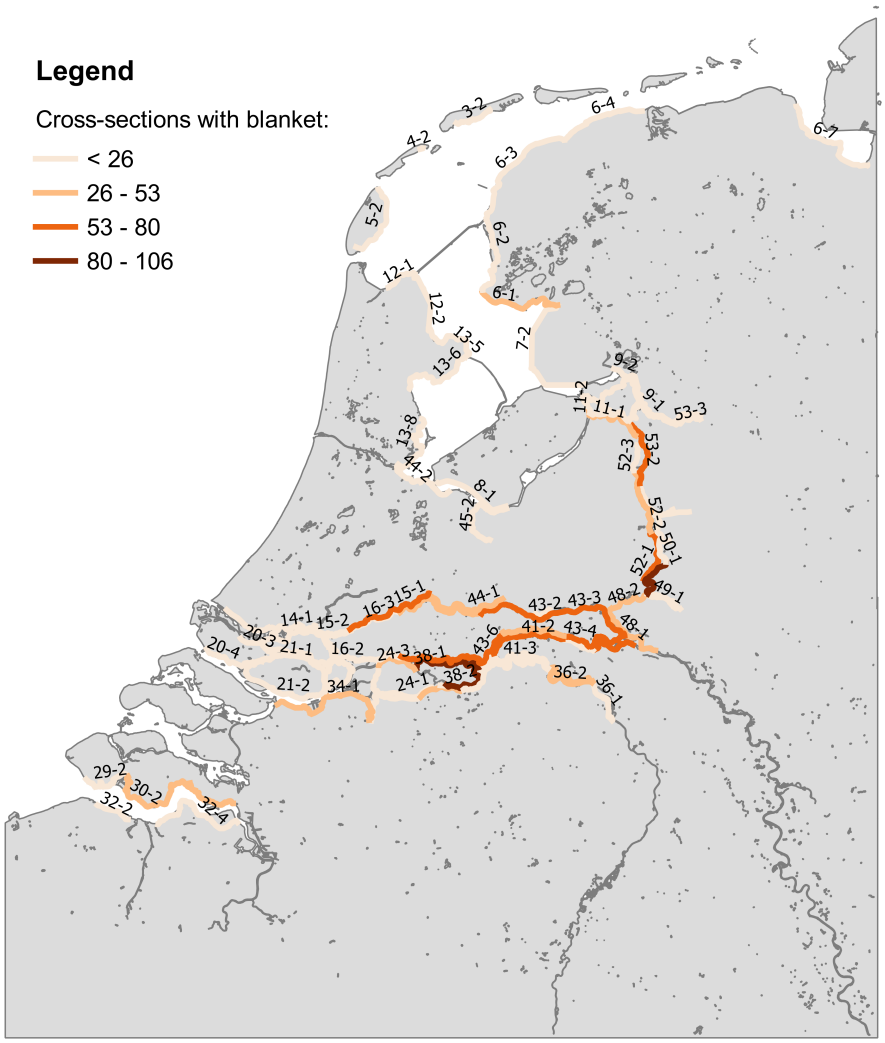

Figure A.5: Number of dike cross-sections (sub-soil scenarios) in the final test set with cover layer per DPV segment.

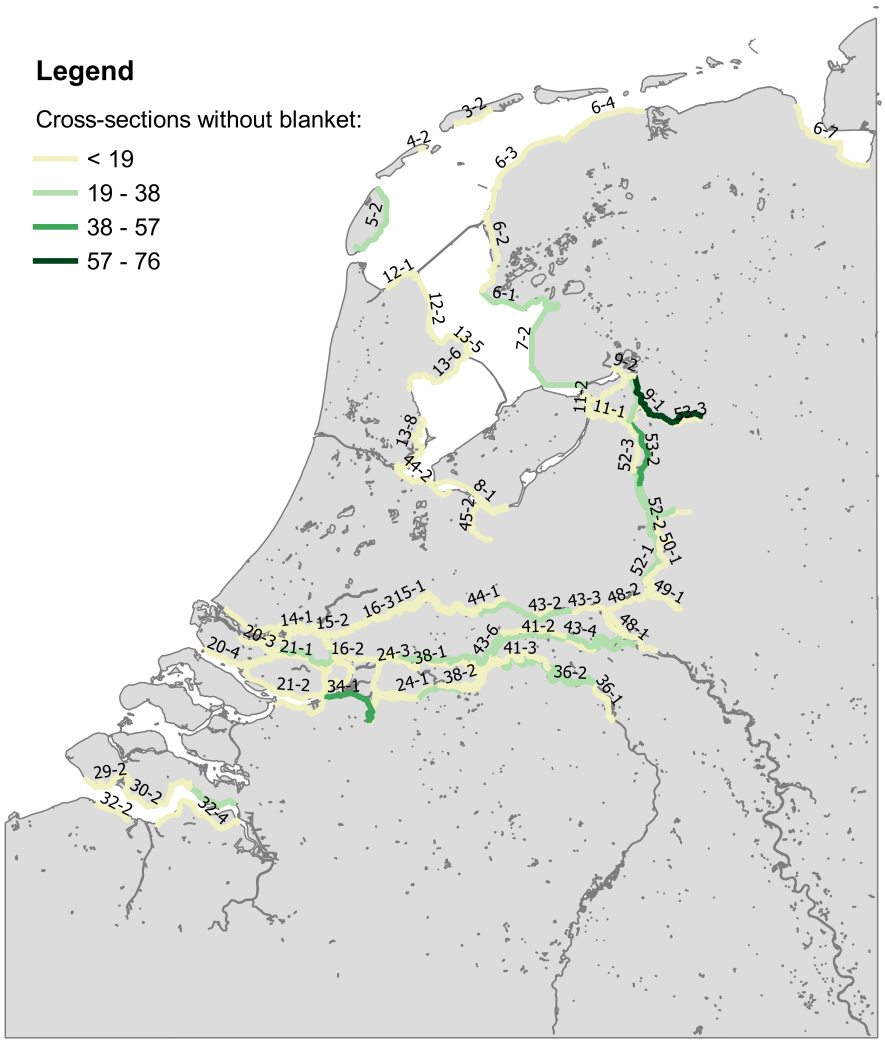

Figure A.6: Number of dike cross-sections (sub-soil scenarios) in the final test set without cover layer per DPV segment.

Table A.1: Statistics of the final test set per hydraulic region.

Id	Hydraulic region	# DPV segments	# sub-soil scenarios	# with cover	# without cover
1	Non-tidal Rhine	26	1466	973	493
2	Non-tidal Meuse	22	388	242	146
3	Tidal Rhine	21	584	382	202
4	Tidal Meuse	3	95	47	48
5	IJssel Delta	2	109	70	39
6	Vecht Delta	5	165	47	118
7	IJssel Lake	5	177	108	69
8	Marker Lake	5	43	33	10
9	Wadden Sea East	2	33	27	6
10	Wadden Sea West	4	93	53	40
11	Dutch Coast North	0	0	0	0
12	Dutch Coast Central	0	0	0	0
13	Dutch Coast South	0	0	0	0
14	Eastern Scheldt	0	0	0	0
15	Western Scheldt	5	168	105	63
3 and 4*		1	-	-	-
5 and 7*		1	-	-	-
9 and 10*		1	-	-	-
Total		**92**	**3321**	**2087**	**1234**

* Some dike segments are situated in more than one hydraulic region. Dike segment 34-1 is situated in regions 3 and 4; dike segment 11-2 is situated in regions 5 and 7; dike segment 6-3 is situated in regions 9 and 10.

Table A.2: Statistics of the final test set per safety standard.

Safety standard	# DPV segments	# sub-soil scenarios	# with cover	# without cover
300	4	42	33	9
1,000	11	420	233	187
3,000	29	806	459	347
10,000	22	925	589	336
30,000	20	984	669	315
100,000	6	144	104	40
Total	**92**	**3321**	**2087**	**1234**

A.3 Design water levels

To perform the calibration for uplift, heave and piping, design water levels needed to be derived first for all test set members. In this study, the water levels are derived with `Hydra-Ring` for the return periods T = [300; 1,000; 3,000; 10,000; 30,000; 100,000] using the TMR2006 hydraulic databases. Figure A.7 presents the resulting water levels corresponding to safety standards of the DPV segments. Each point in the graph represents a HR station that is used in the calibration exercise.

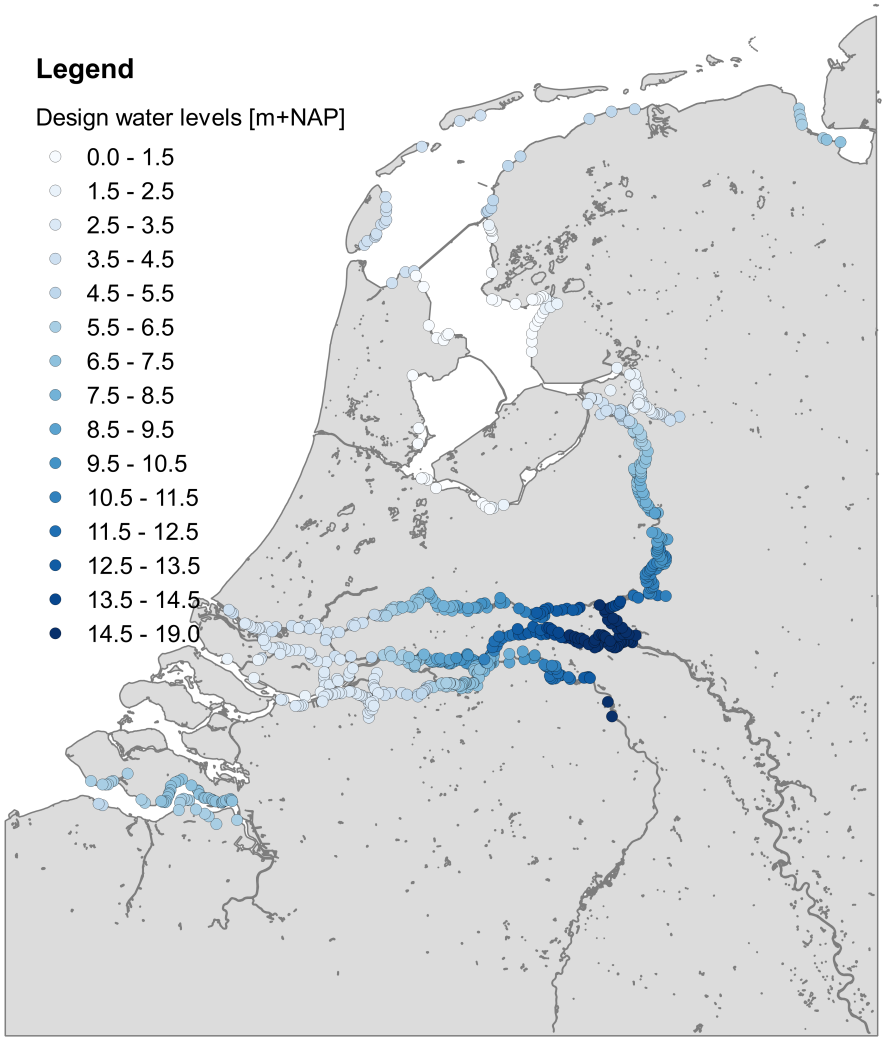

Figure A.7: Design water levels for HR stations considered in the calibration exercise.

To perform water level computations, `Hydra-Ring` requires as inputs the safety standard (in terms of reliability indices β), location of the dike cross-section and the corresponding HR station. As outputs, `Hydra-Ring` returns the design water level and the reliability index. The latter should be the same as the input (from the safety standard). The comparison of input and output reliability indices indicates if there were convergence problems during the computations and therefore informs about quality of the results. In general, these differences are small. As a remark, the difference of 0.17 for DPV segment 7-2 (one of the highest differences) corresponds to adjustments in the water level of less than 1 cm. Following figures show water levels for all return periods as well as the achieved reliability differences.

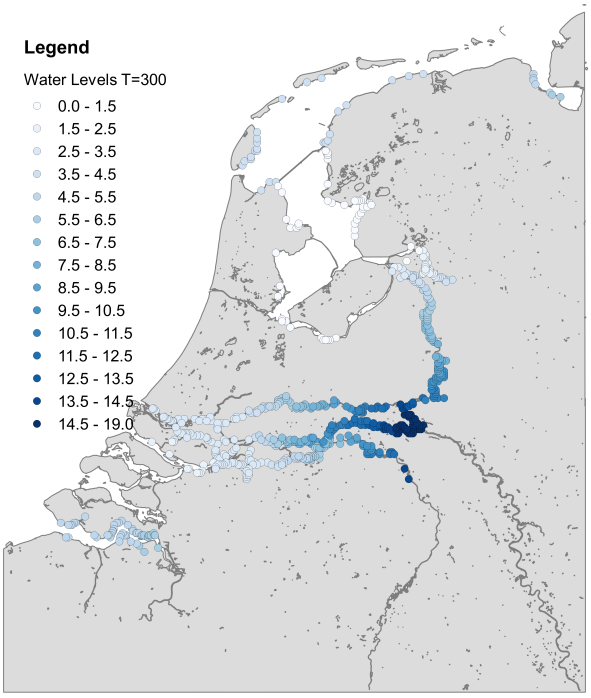

Figure A.8: Overview of water levels corresponding to T=300 years.

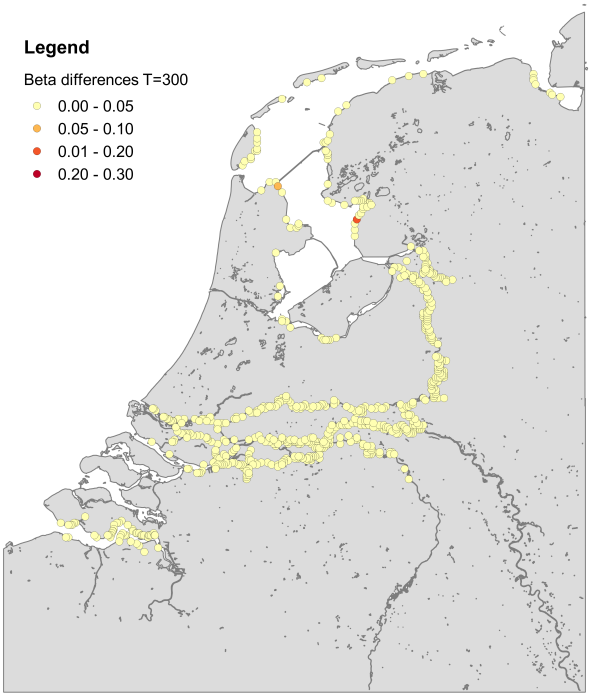

Figure A.9: Reliability differences in the water level calculations for T=300 years.

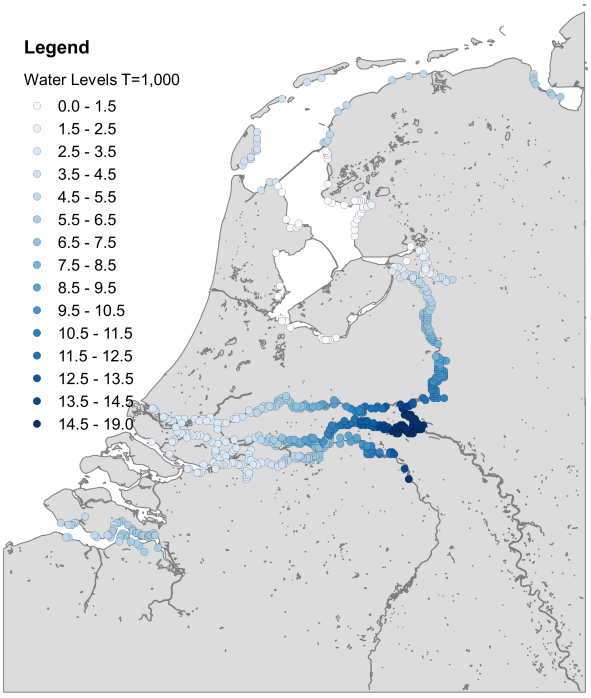

Figure A.10: Overview of water levels corresponding to T=1,000 years.

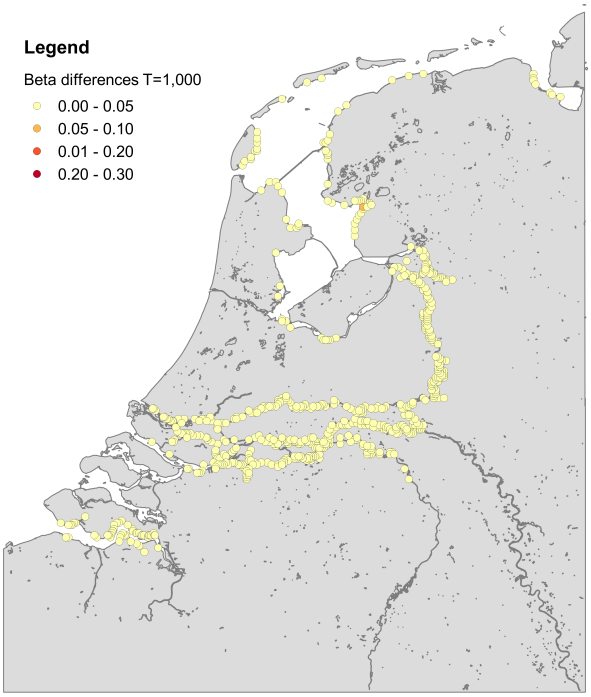

Figure A.11: Reliability differences in the water level calculations for T=1,000 years.

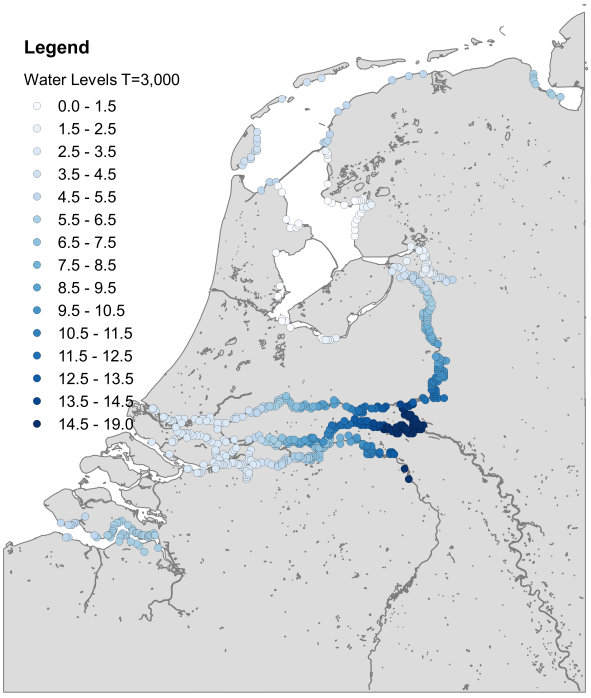

Figure A.12: Overview of water levels corresponding to T=3,000 years.

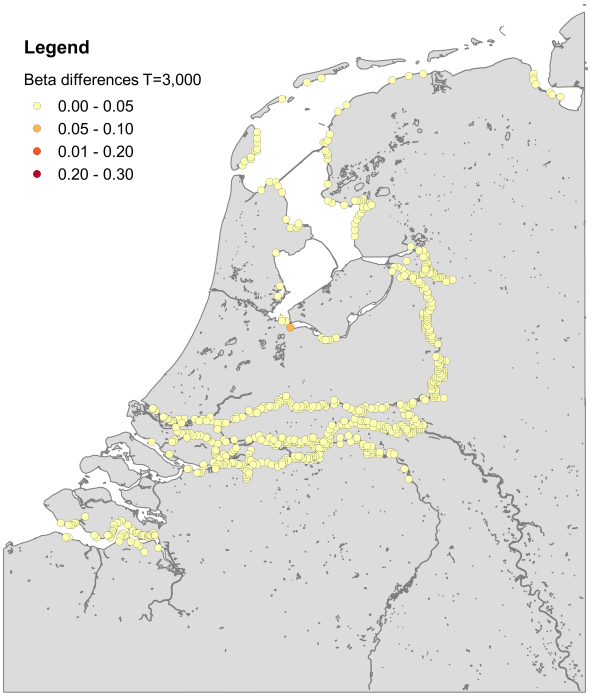

Figure A.13: Reliability differences in the water level calculations for T=3,000 years.

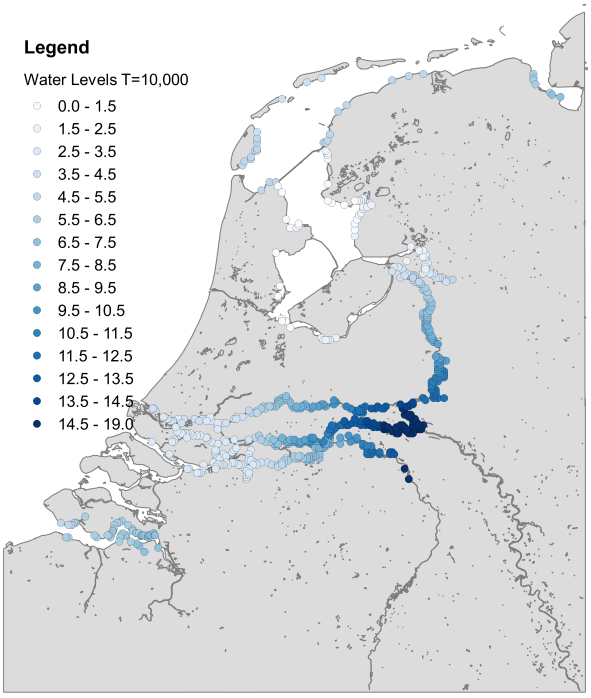

Figure A.14: Overview of water levels corresponding to T=10,000 years.

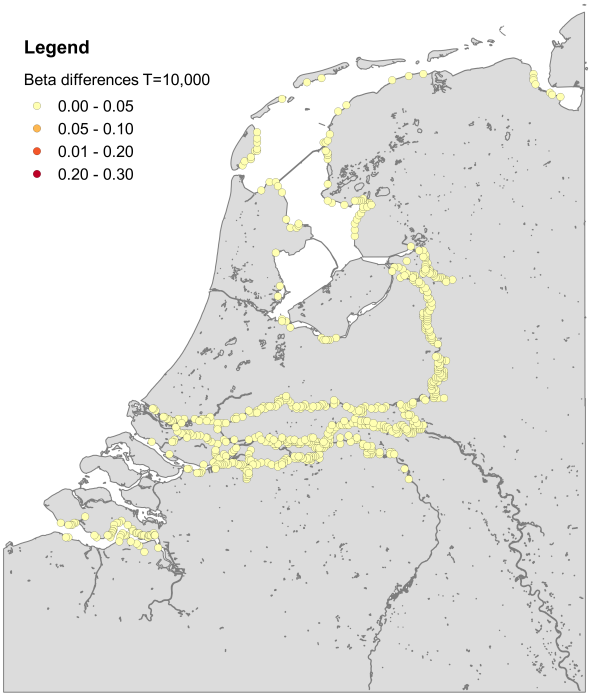

Figure A.15: Reliability differences in the water level calculations for T=10,000 years.

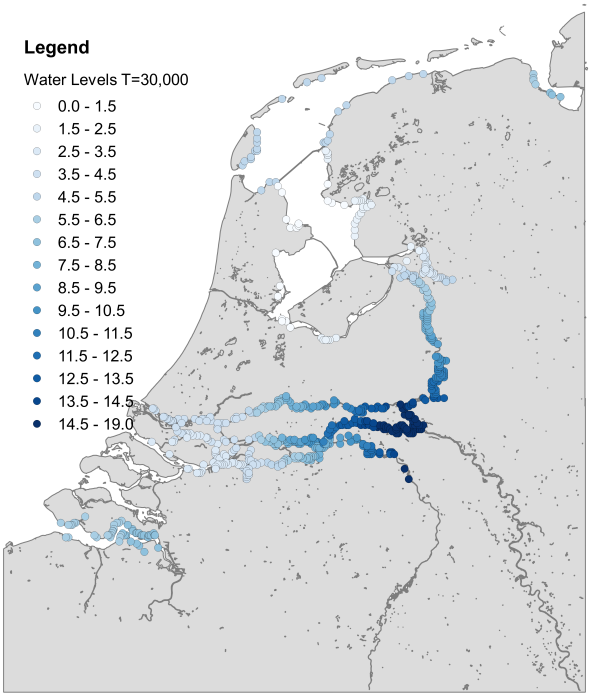

Figure A.16: Overview of water levels corresponding to T=30,000 years.

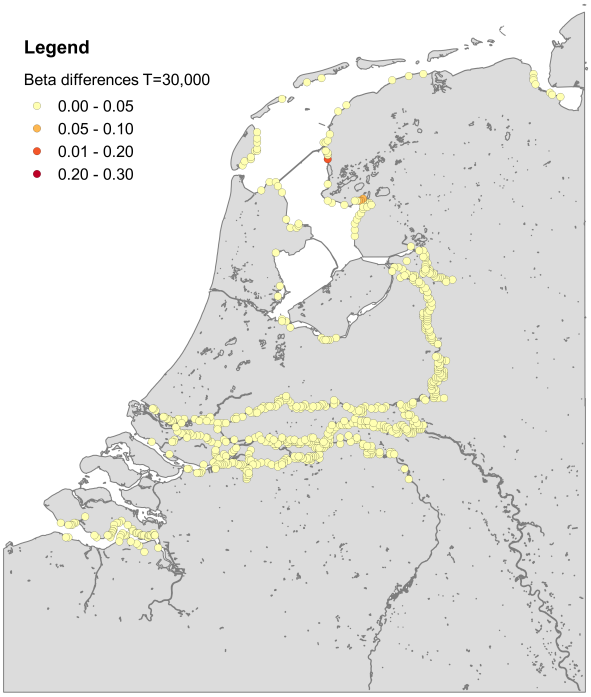

Figure A.17: Reliability differences in the water level calculations for T=30,000 years.

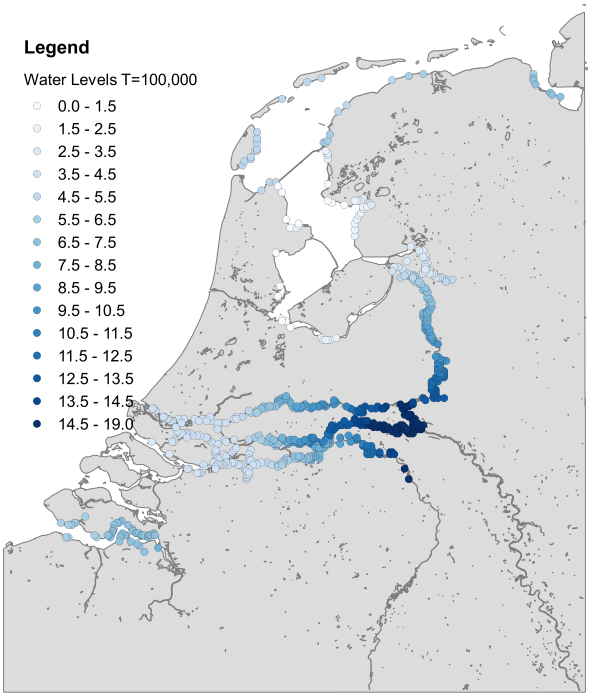

Figure A.18: Overview of water levels corresponding to T=100,000 years.

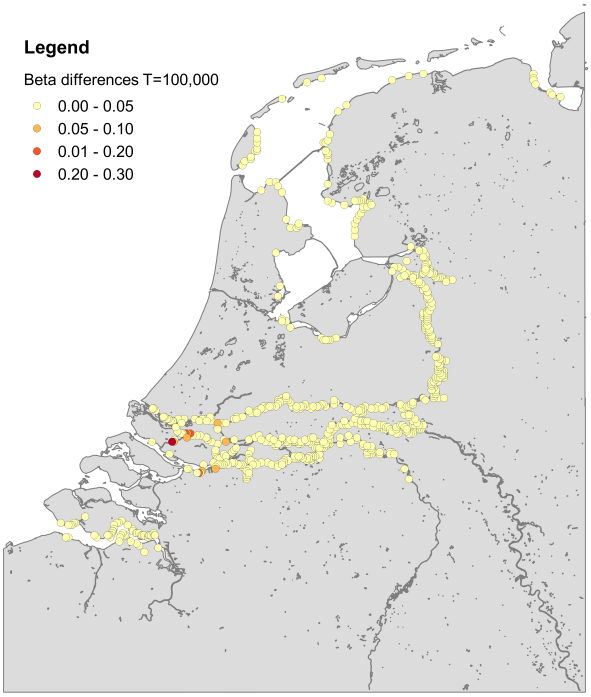

Figure A.19: Reliability differences in the water level calculations for T=100,000 years.

B Translation of inputs from PC-Ring to Hydra-Ring

This appendix presents translation of inputs from PC-Ring to Hydra-Ring performed in the calibration exercise. The translation of random variables from PC-Ring to Hydra-Ring is given in the following table.

Table B.1: Translation of random variables from PC-Ring to Hydra-Ring.

Variable	PC-Ring ID	Hydra-Ring ID	Distribution type in Hydra-Ring	Deviation type in Hydra-Ring
Phreatic level at the exit point (h_{exit})	99007	42	Normal (2)	σ
Total thickness of the cover layer (D_{cover})	3001	44	Log-normal (4)	cov
Saturated volumetric weight of the cover layer ($\gamma_{sat,cover}$)	3010	45	Log-normal (4$*$)	cov
Model factor for uplift (m_u)	3012	46	Log-normal (4)	cov
Damping factor at exit (r_{exit})	3014	47	Log-normal (4)	cov
Critical heave gradient ($i_{c,h}$)	-	127	Log-normal (4)	σ
Seepage length, from entry point to exit point (L)	3004	48	Log-normal (4)	cov
Thickness of the aquifer (D)	3002/3003	49	Log-normal (4)	cov
Model factor for piping (m_p)	3013	51	Log-normal (4)	cov
Darcy permeability (k)	3015/3016	55	Log-normal (4)	cov
70%-quantile of the grain size distribution of the piping-sensitive layer (d_{70})	3007	56	Log-normal (4)	cov

$*$ This variable is simulated with a shifted log-normal distribution (shift = 10).

The model Hydra-Ring is meant for probabilistic safety assessment of primary flood defences in the Netherlands. Currently, to perform computations with Hydra-Ring, VNK2 (PC-Ring) input databases need to be translated first to Hydra-Ring databases. This involves:

- Translation of random variables from PC-Ring to Hydra-Ring as presented in Table B.1 for uplift, heave and piping,
- Translation of a dike segment schematisation from PC-Ring to Hydra-Ring and
- Translation of 2-layer piping model (if present in PC-Ring) to 1-layer piping model (required by Hydra-Ring).

The translation of a dike segment schematisation is explained using the following example for piping failure mechanism.

Assume that a dike segment in PC-Ring consists of three sections (*dijkvakken*) and that each section contains two *bodemvakken*. Each *bodemvak* is described by two sub-soil scenarios and the corresponding weights. These three dijkvakken are translated to one presentation section in Hydra-Ring that consists of six sections. These sections in Hydra-Ring correspond to, in total, six bodemvakken in PC-Ring (3 *dijkvakken* x 2 *bodemvakken*). Each section in Hydra-Ring is then defined by two probability alternatives that correspond to the sub-soil scenarios in PC Ring[1].The procedure is also presented in Figure B.1.

[1] In the model PC-Ring, different sub-soil scenarios are denoted by 301, 302, . . . , 310. In the model Hydra-Ring these sub-soil scenarios are called probability alternatives.

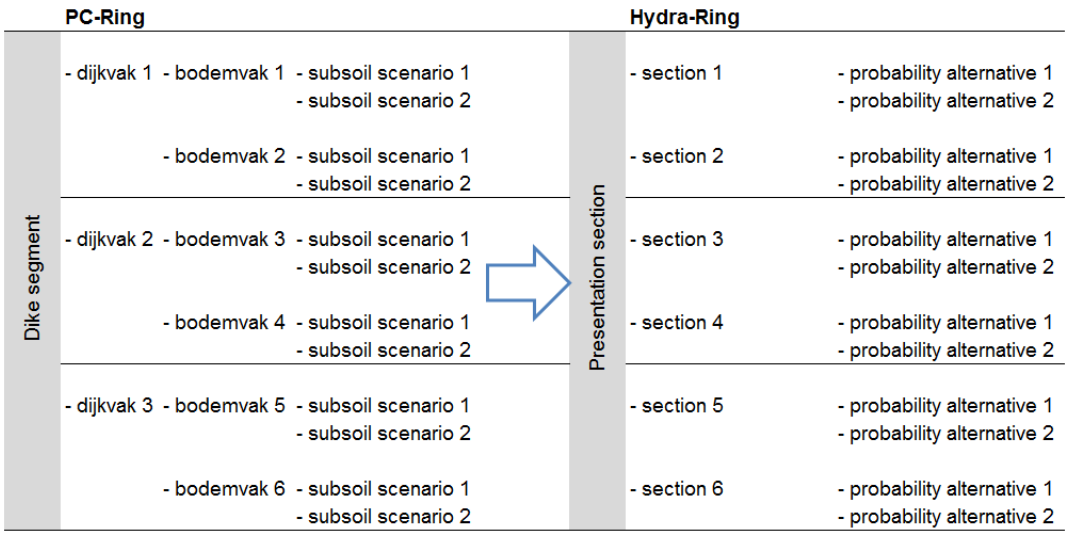

Figure B.1: Translation of a dike segment schematisation from `PC-Ring` *to* `Hydra-Ring`*.*

Contrary to `PC-Ring`, `Hydra-Ring` does not allow computations with the 2-layer piping model. In such model two sand layers, upper and lower, are present. If the 2-layer piping model is applied in `PC-Ring`, then the inputs (*i.e.* thickness of the upper and lower sand layers and permeability of these layers) are translated to the 1-layer piping in `Hydra-Ring` with the following assumptions:

$$\mu(D_1) = \mu(D_{2,lower}) + \mu(D_{2,upper}) \tag{B.1}$$

$$\sigma(D_1) = \sqrt{\sigma^2(D_{2,lower}) + \sigma^2(D_{2,upper})} \tag{B.2}$$

and

$$\mu(k_1) = \max\{\mu(k_{2,lower}), \mu(k_{2,upper})\} \tag{B.3}$$

$$\sigma(k_1) = \begin{cases} \sigma(k_{2,lower}) & \text{if } \mu(k_{2,upper}) > \mu(k_{2,lower}) \\ \sigma(k_{2,upper}) & \text{otherwise} \end{cases} \tag{B.4}$$

where:

μ	is the expected value operator,
σ	is the standard deviation operator,
D_1	is the thickness of the sand layer in 1-layer piping model,
$D_{2,lower}$	is the thickness of the lower sand layer in 2-layer piping model,
$D_{2,upper}$	is the thickness of the upper sand layer in 2-layer piping model,
k_1	is the permeability of the sand layer in 1-layer piping model,
$k_{2,lower}$	is the permeability of the lower sand layer in 2-layer piping model and
$k_{2,upper}$	is the permeability of the upper layer in 2-layer piping model.

It is important to note that this approach is logical for the thickness of the sand layer. On the other hand, for the permeability this is just one of the possible (logical) approaches. An alternative would be to consider the weighted average of the permeability values with the weights are based on the thickness of the sand layers:

$$\mu(k_{1,ave}) = \frac{\mu(k_{2,lower}) \cdot \mu(D_{2,lower}) + \mu(k_{2,upper}) \cdot \mu(D_{2,upper})}{\mu(D_{2,lower}) + \mu(D_{2,upper})} \tag{B.5}$$

Figure B.2 presents permeability values $\mu(k_{2,lower})$ and $\mu(k_{2,upper})$ present in the VNK2-data together with the values of $\mu(k_1)$ being the maximum of $\mu(k_{2,lower})$ and $\mu(k_{2,upper})$ (approach applied in the calibration exercise). For comparison, the weighted average permeability is also computed. Figure B.3 shows ratios of $\mu(k_1)$, based on the maximum, and $\mu(k_{1,ave})$, based on the weighted average. These ratios indicate that the differences between these two approaches are limited, the average ratio is 1.16. It is expected that the alternative approach would not lead to substantially different calibration results.

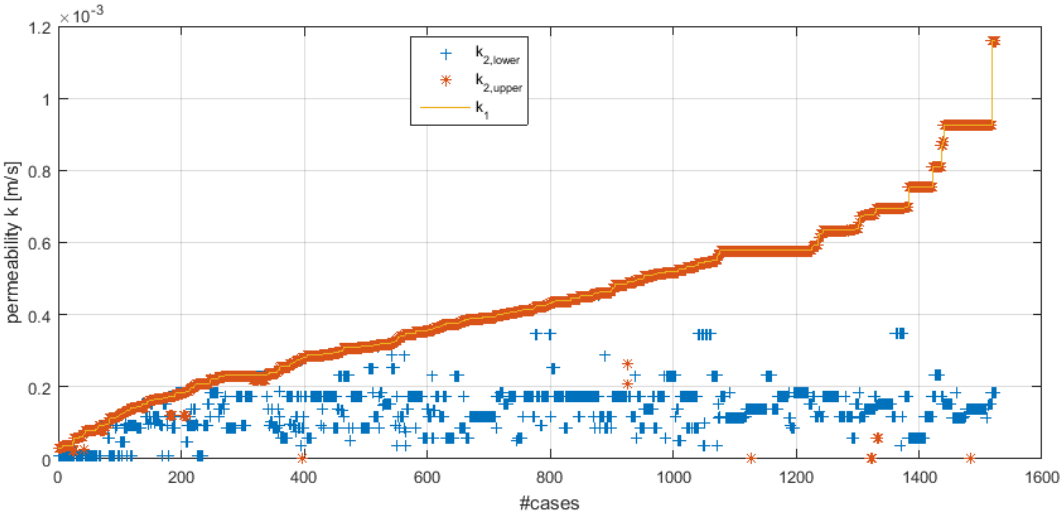

Figure B.2: Permeability values in the VNK2-databases (ordered).

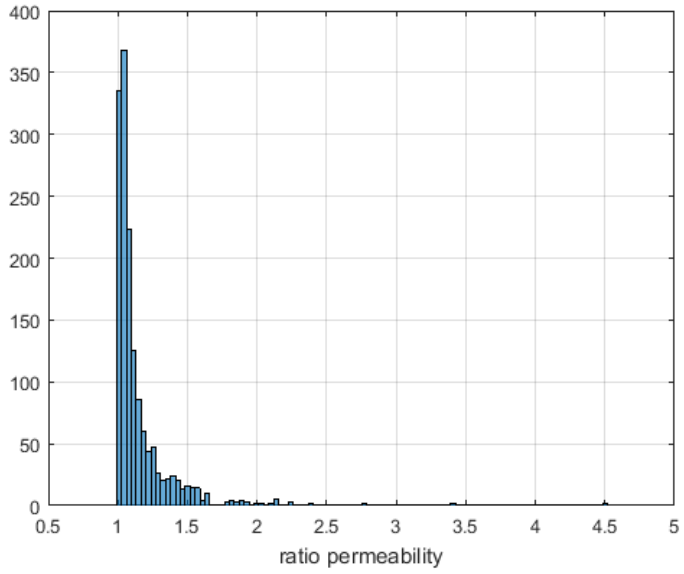

Figure B.3: Histogram of the permeability ratios $\mu(k_1)/\mu(k_{1,ave})$.

C Study on the length-effect parameters - Case 1

In the case of piping failure mechanism, the length-effect is characterised by the parameters a and b, and the relation between the reliability requirement for a dike cross-section and the reliability requirement for a dike segment is given as follows:

$$P_T = P_{T,cross} \cdot \left(1 + \frac{a \cdot L_{segm}}{b}\right) \tag{C.1}$$

$$P_T = f \cdot P_{norm} = \frac{f}{T} \tag{C.2}$$

where:

P_T	is the target failure probability of a dike segment for piping mechanism [yr^{-1}],
$P_{T,cross}$	the target failure probability of a dike cross-section for piping mechanism [yr^{-1}],
T	is the return period that corresponds to the safety standard of a segment [yr],
L_{segm}	is the total length of the segment [m],
a	is a fraction of the length that is sensitive to piping [-],
b	is a measure for the intensity of the length-effect within the part of the segment that is sensitive to piping (the length of independent, equivalent dike sections) [m],
P_{norm}	is the target failure probability (safety standard) [yr^{-1}] and
f	is the failure probability factor for piping failure mechanism [-].

Relation C.1 is used in WTI 2017 to transform the reliability requirement for a dike segment into the reliability requirement for a dike cross-section regarding the piping failure mechanism. Based on OI (2015), the recommended value of b is equal to 300 m. The recommended values of a are: 0.9 for the upper-river area and 0.4 for the remaining hydraulic regions in the Netherlands. Furthermore f is equal to 0.24.

This appendix shows a study with the goal of assessing the values of a and b for each sub-mechanism of piping. The analysis is performed for 12 DPV segments that were considered in the preliminary calibration study ter Horst *et al.* (2014) (real cases are hence used). The segments are situated in the non-tidal and tidal river areas, and in the delta of the river Vecht. See Table C.1 for more information on the segments. In the table, $\hat{a}$ represents the fraction of piping sensitive stretches within the dike segments based on the VNK2-data. These values are used to study the length effect parameters.

Table C.1: Input for the study on the length-effect parameters.

DPV segment	Hydraulic region in Hydra-Ring	Length of segment L_{segm} [m]	$\hat{a}$ [-]
9-1	Vecht delta	39,012	0.47
9-2	Vecht delta	8,010	0.22
15-1	Tidal Rhine	22,133	0.61
15-2	Tidal Rhine	24,562	0.16
16-1	Tidal Rhine	13,220	0.30
16-3	Tidal Rhine	19,946	0.43
36-2	Non-tidal Meuse	20,875	0.28
36-5	Non-tidal Meuse	17,596	0.36
50-1	Non-tidal Rhine	6,743	0.33
50-2	Non-tidal Rhine	6,231	0.28
53-2	Non-tidal Rhine	28,049	0.64
53-3	Vecht delta	29,822	0.11

Per dike segment, a one-to-one relation between the cross-sectional failure probability and the dike segment failure probability (combined) is analysed. This is done by first designing seepage lengths (cover thickness for uplift and heave) with the semi-probabilistic rule for all cross-sections in the segment. The designs are made for different values of the safety factor γ. Imposing the safety factor ensures that all cross-sections in the segment have the same safety level. Next, reliability computations are performed with Hydra-Ring for the entire segment using the designed values (corresponding to γ) and including the length-effect. These computations result in the reliability index for the segment $\beta_{segm,HYR}$ and lead to the relation:

$$\gamma - \beta_{segm,HYR} \tag{C.3}$$

Note that from chapter 8 we also have the relation between the cross-sectional reliability and the safety factor:

$$\gamma - \beta_{cross} \tag{C.4}$$

Since γ is common in both functions, the relation between β_{cross} and $\beta_{segm,HYR}$ can be established and hence the effect of the length (from $cross-section$ to $segment$) can be analysed. Note that the analysis concerns only the parameter b as the values of L_{segm} and a are given. Recall that the value of a is equal to $\hat{a}$. Furthermore, the analysis is performed for T = 3,000 years[1].

Figure C.1 shows the relations $\gamma - \beta_{segm,HYR}$ and $\gamma - \beta_{cross}$ found for the 12 DPV segments. The resulting values of b and the a/b ratios are given in Figure C.2. The values are shown only for dike segments in which high quality results were achieved. As a consequence, the following segments are not considered: [9-1, 9-2, 16-1, 16-3, 53-3] for uplift, [16-3, 53-3] for heave, and 53-3 for piping.

In summary, the following is observed:

- Uplift: b ranges from 25 m (DPV segment 36-5) to 600 m (DPV segment 50-2) and the mean value is 160 m. The a/b ratios vary between 0.0005 and 0.0138, and the mean value is 0.0055. Excluding of the outliers (*i.e.* DPV segment 36-5) leads to the mean value of 0.004.
- Heave: b ranges from 3 m (DPV segment 15-2) to 1030 m (DPV segment 50-2) and the mean value is 170 m. The a/b ratios vary between 0.0003 and 0.0574, and the mean value is 0.0134. Excluding of the outliers (*i.e.* DPV segment 9-1 and 15-2) leads to the mean value of 0.0053.

[1] In this appendix, T = 3,000 years is considered as the required safety standard for each of the 12 DPV segments.

- Piping: b ranges from 20 m (DPV segment 16-1) to 945 m (DPV segment 50-2). The mean value and the standard deviation are respectively 230 m and 340 m. The median is 100 m. The obtained a/b ratios vary between 0.0003 (DPV segments 9-2 and 50-2) and 0.0162 (DPV segment 16-1). The mean and the standard deviation of the a/b ratio are respectively equal to 0.0058 and 0.0053. Excluding of the outliers (*i.e.* DPV segments 16-1 and 16-3) leads to the mean value of 0.0037.

The applied approach differs from the one used in the preliminary calibration ter Horst *et al.* (2014). In 2014, `Hydra-Ring` was used to design cross-sections within a dike segment using a reliability index (ensuring the same safety level). The conclusion of the 2014 study was that b equal to 300 m is a good assumption. On the other hand, the conclusion of the current study is that a and b results have a high variability making it difficult to recommend one set of parameters. Only few of the considered segments gave recommendations similar to the recommendations from 2014.

Additionally, a detailed study on the a value is performed in this appendix. The value has been computed for every DPV segment in the calibration study (92 segments in total). Figure C.3 shows a histogram of the a values. The mean value is equal to 0.33 and the standard deviation is 0.23. Table C.2 presents results of the statistical analysis on a per hydraulic region. The analysis shows that the lowest values of a are found in the regions 'Marken Lake', 'IJssel Lake' and 'Wadden Sea east'. The highest values of a are found in the regions 'Non-tidal Rhine', 'IJssel delta' and 'Wadden Sea west'.

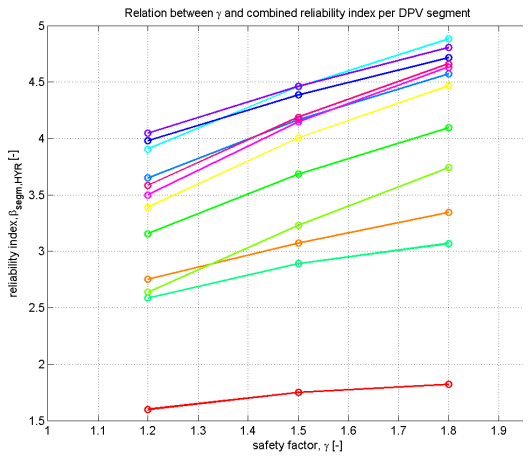

(a) γ - $\beta_{segm,HYR}$ relations, uplift

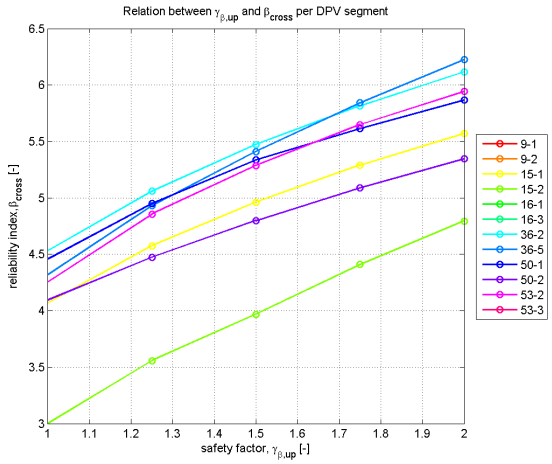

(b) $\gamma_{\beta,up}$ - β_{cross} relations, uplift

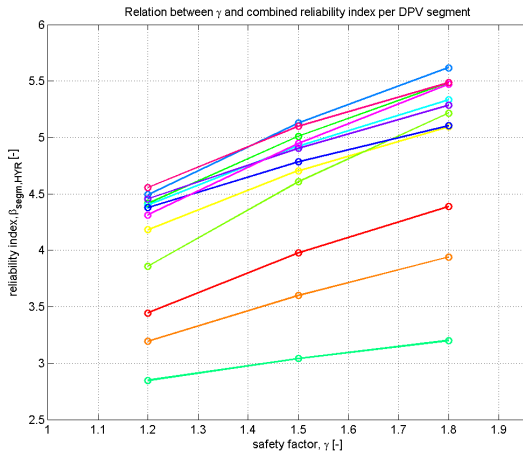

(c) γ - $\beta_{segm,HYR}$ relations, heave

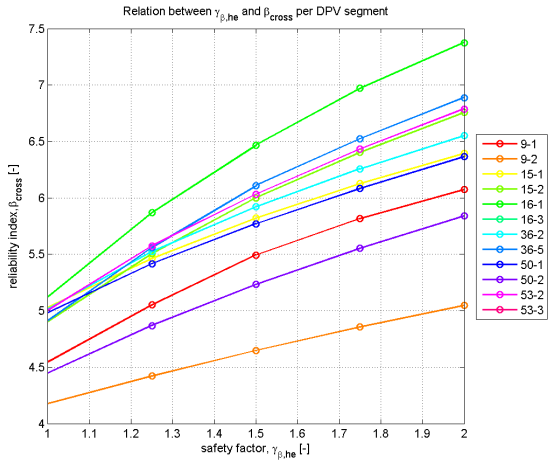

(d) $\gamma_{\beta,he}$ - β_{cross} relations, heave

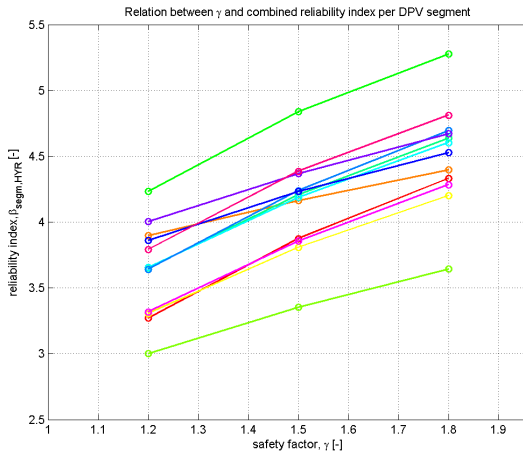

(e) γ - $\beta_{segm,HYR}$ relations, piping

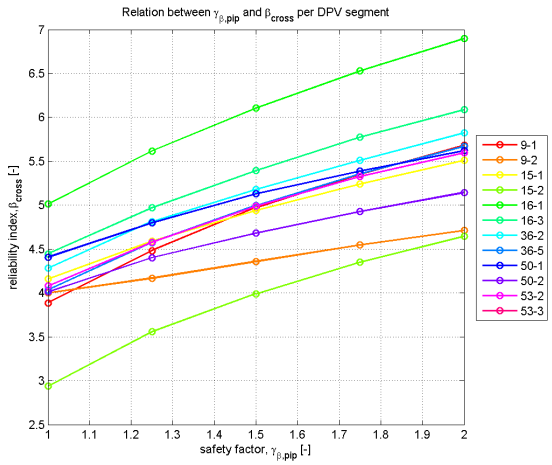

(f) $\gamma_{\beta,pip}$ - β_{cross} relations, piping

Figure C.1: Intermediate results of the length-effect parameters' analysis.

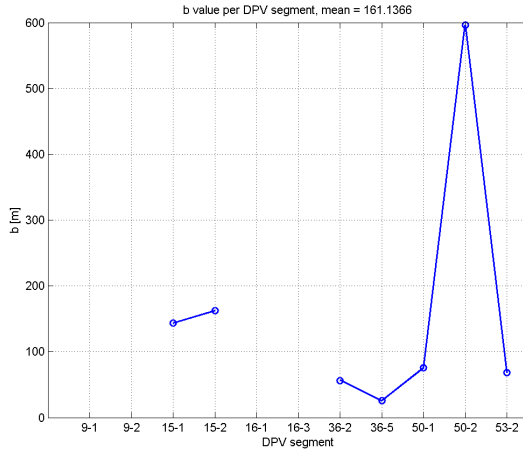

(a) b values, uplift

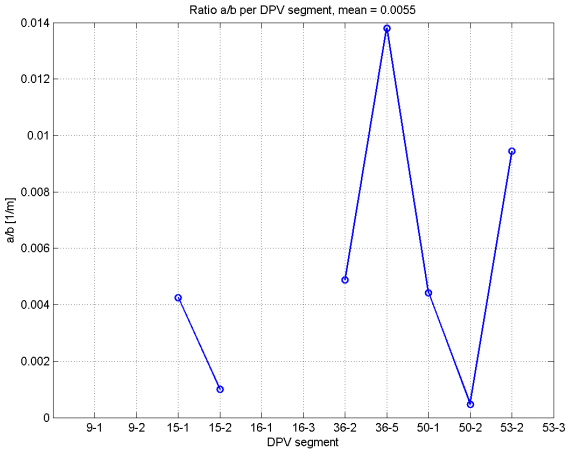

(b) a/b ratios, uplift

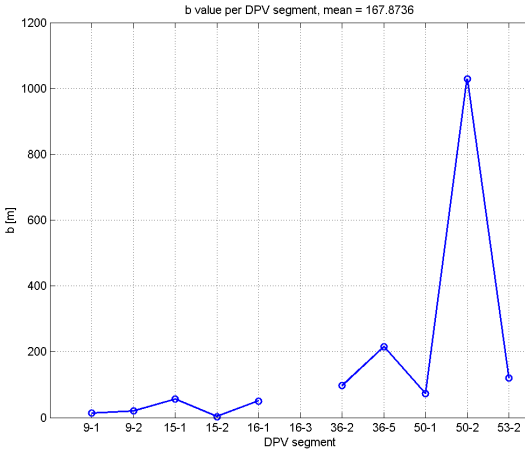

(c) b values, heave

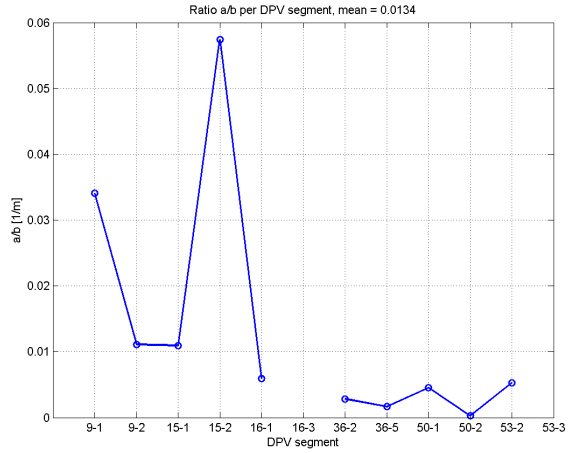

(d) a/b ratios, heave

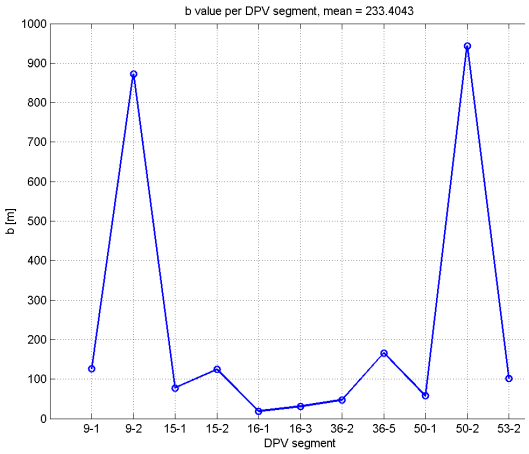

(e) b values, piping

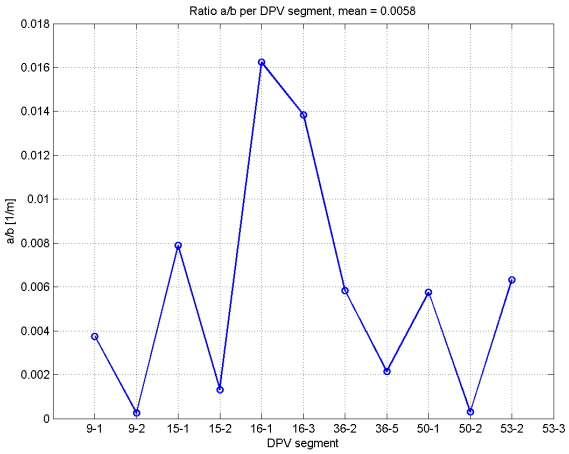

(f) a/b ratios, piping

Figure C.2: Final results of the algorithm that studies the parameters of the length-effect in piping sub-mechanism.

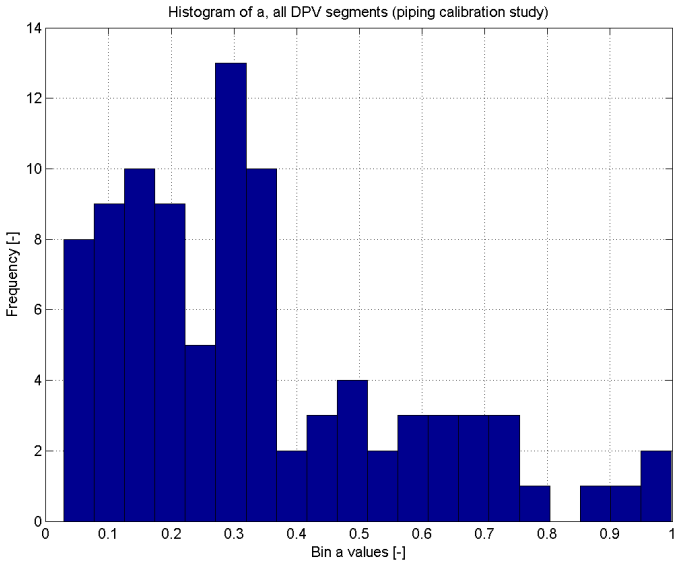

Figure C.3: Histogram of a values, all DPV segments considered in the calibration study.

Table C.2: Analysis of a values per hydraulic region

Hydraulic region in Hydra-Ring	a [-]					# of
	μ	σ	min	max	median	segments
Non-tidal Rhine	0.46	0.26	0.06	0.96	0.42	26
Non-tidal Meuse	0.34	0.27	0.03	0.999	0.28	11
Tidal Rhine	0.27	0.19	0.05	0.72	0.23	21
Tidal Meuse	0.32	0.02	0.31	0.34	0.31	3
IJssel delta	0.42	0.15	0.31	0.52	0.42	2
Vecht delta	0.24	0.16	0.07	0.47	0.22	5
IJssel Lake	0.19	0.11	0.11	0.38	0.15	5
Marken Lake	0.12	0.09	0.05	0.28	0.09	5
Wadden Sea east	0.17	0.04	0.15	0.2	0.17	2
Wadden Sea west	0.39	0.23	0.16	0.66	0.37	4
Western Scheldt	0.34	0.23	0.11	0.71	0.28	5

D Semi-proabilistic rules

This appendix presents the semi-probabilistic rules used in the calibration exercise (step 2) for piping, heave and uplift sub-mechanisms. The calibration exercise starts by gathering a data set and then for each member (cross-section), determine the required seepage length (or cover layer thickness) so that eq.(D.1) fulfills, for a range of values of the $\beta-$dependent safety factor.

$$\frac{R_{char}}{S_{char}} \geq \gamma_\beta \Leftrightarrow R_{char} \geq \gamma_\beta \cdot S_{char} \tag{D.1}$$

where R_{char} is the characteristic value of the resistance/strength, S_{char} is the characteristic value of the load and γ_β is the $\beta-$dependent safety factor.

Following, the semi-probabilistic rules are given for uplift, heave and piping sub-mechanisms.

SEMI-PROBABILISTIC RULE FOR UPLIFT

Knowing that the resistance and load terms of the uplift sub-mechanism read as follows (according to Visschedijk and Schweckendiek (2013)):

$$R = \Delta\phi_{c,u} = \frac{D_{cover} \cdot (\gamma_{sat,cover} - \gamma_{water})}{\gamma_{water}} \tag{D.2}$$

$$S = \Delta\phi = \phi_{exit} - h_{exit} = [h_{exit} + (h(T) - h_{exit}) \cdot r_{exit}] - h_{exit} \tag{D.3}$$

The semi-probabilistic rule for uplift is:

$$\Delta\phi_{c,u} \geq \gamma_{\beta,up} \cdot \Delta\phi \tag{D.4}$$

The calibration procedure aims to find the relation between the $\beta-$dependent safety factor ($\gamma_{\beta,up}$) and the cross-sectional target reliability index $\beta_{T,cross}$ by adjusting the 'thickness of the cover layer (D_{cover})', and then performing full probabilistic computations. Given the equations above and a value of $\gamma_{\beta,up}$, the characteristic value $D_{cover,char}$ can be derived based on eq.(D.5), when one cover layer is present.

$$D_{cover,char} \geq \frac{\gamma_{water} \cdot \gamma_{\beta,up} \cdot (h(T) - h_{exit,char}) \cdot r_{exit,char}}{\gamma_{eff,cover,char}} \tag{D.5}$$

SEMI-PROBABILISTIC RULE FOR HEAVE

Knowing that the resistance and load terms of the heave sub-mechanism read as follows (according to Visschedijk and Schweckendiek (2013)):

$$R = i_{c,h} \tag{D.6}$$

$$S = i = \frac{\phi_{exit} - h_{exit}}{D_{cover}} \tag{D.7}$$

The semi-probabilistic rule for heave is given in eq.(D.8).

$$i_{c,h} \geq \gamma_{\beta,he} \cdot i \tag{D.8}$$

The calibration procedure aims to find the relation between the $\beta-$dependent safety factor $\gamma_{\beta,he}$ and the target reliability index $\beta_{T,cross}$ by adjusting the 'thickness of the cover layer (D_{cover})', and then performing full probabilistic computations. Given the equations above and a value of $\gamma_{\beta,he}$, the characteristic value $D_{cover,char}$ can be derived based on eq.(D.9), when one cover layer is present.

$$D_{cover,char} \geq \frac{\gamma_{\beta,he} \cdot (h(T) - h_{exit,char}) \cdot r_{exit,char}}{i_{c,h,char}} \tag{D.9}$$

SEMI-PROBABILISTIC RULE FOR PIPING

The resistance and load terms of the piping sub-mechanism are defined by the following equations (according to Visschedijk and Schweckendiek (2013)):

$$R = H_c = F_{resistance} \cdot F_{scale} \cdot F_{geometry} \tag{D.10}$$

$$S = H = h(T) - h_{exit} - r_c \cdot D_{cover} \tag{D.11}$$

where:

$$F_{resistance} = \eta \cdot \frac{\gamma_{sub,particles}}{\gamma_{water}} \cdot \tan\theta_{sellmeijer,rev}$$

$$F_{scale} = \frac{d_{70.m}}{\sqrt[3]{\kappa \cdot L}} \cdot \left(\frac{d_{70}}{d_{70.m}}\right)^{0.4}, \kappa = \frac{\nu_{water}}{g} \cdot k \tag{D.12}$$

$$F_{geometry} = 0.91 \cdot \left(\frac{D}{L}\right)^{\frac{0.28}{\left(\frac{D}{L}\right)^{2.8}-1}+0.04}$$

Overlooking constants, the critical head difference (H_c) can be written as:

$$R = H_c = f(L, D, d_{70}, k) \tag{D.13}$$

and the semi-probabilistic rule for piping is given as follows:

$$H_c \geq \gamma_{\beta,pip} \cdot H \tag{D.14}$$

The calibration procedure for piping aims to find the relation between the $\beta-$dependent safety factor $\gamma_{\beta,pip}$ and the target reliability index $\beta_{T,cross}$ by adjusting the 'seepage length (L)'. Having the adjusted L according to eq.(D.15), full probabilistic computations are performed.

$$f(L_{char}, D_{char}, d_{70,char}, k_{char}) \geq \gamma_{\beta,pip} \cdot [h(T) - h_{exit,char} - r_{c,char} \cdot D_{cover,char}] \tag{D.15}$$

The meaning of each variable in the equations can be consulted in Table D.1. Furthermore, the $h(T)$ stands for the outside water level at the dike with the return period of T years (design water level), and subscript $char$ denotes the characteristic value of a variable.

Table D.1: Input parameters for piping analyses (norm = normal, log = log-normal).

Symbol [unit]	Description	Uplift	Heave	Piping	Distribution type	Default	$char$ value
m_u $[-]$	Model factor for uplift	x			log	μ 1.0 ,σ 0.10	1.0
γ_{water} $[kN/m^3]$	Volumetric weight of water	x		x	-	10	10
$\gamma_{sat,cover}$ $[kN/m^3]$	Saturated volumetric weight of the cover layer	x			shifted log (+10)	-	5%
r_{exit} $[-]$	Damping factor at exit	x	x		log	-	95%
$i_{c,h}$ $[-]$	Critical heave gradient		x		log	μ 0.5 ,σ 0.10	0.3
D_{cover} $[m]$	Effective thickness of the cover layer	x	x	x	log	-	5%
h_{exit} $[m + NAP]$	Phreatic level at the exit point	x	x	x	norm	-	5%
m_p $[-]$	Model factor for piping			x	log	μ 1.0 ,σ 0.12	1.0
h $[m+NAP]$	Outside water level	x	x	x	`Hydra-Ring`	-	Design water level*
r_c $[-]$	Reduction factor			x	-	0.3	0.3
L $[m]$	Seepage length, from entry point to exit point			x	log	-	5%
$\gamma_{sub,particles}$ $[kN/m^3]$	Submerged volumetric weight of sand particles			x	-	16.5	16.5
η $[-]$	White's drag coefficient			x	-	0.25	0.25
d_{70} $[m]$	70%-quantile of the grain size distribution of the piping-sensitive layer			x	log	cov 0.12	5%
k $[m/s]$	Darcy permeability			x	log	cov 0.50	95%
ν_{water} $[m^2/s]$	Kinematic viscosity of water			x	-	1.33×10^{-6}	1.33×10^{-6}
g $[m/s^2]$	Gravitational constant			x	-	9.81	9.81
D $[m]$	Thickness of the aquifer			x	log	-	95%
$d_{70;m}$ $[m]$	Mean value of the d_{70} in small scale tests			x	-	2.08×10^{-4}	2.08×10^{-4}
$\theta_{sellmeijer,rev}$ $[^\circ]$	Bedding angle of sand grains for the revised Sellmeijer rule (Sellmeijer *et al.*, 2011)			x	-	37	37

*Design water level is defined as the water level with an exceedance probability equal to the maximum allowable probability of flooding of a dike segment.

E Designed values derived in the calibration - Case 1 and 2

In this appendix, intermediate results of the calibration procedure are discussed. These results are the designed values of the seepage length (piping) and the cover thickness (uplift and heave) for all members of the test set. We emphasise that the term "designed" refers to the value that arises from a semi-probabilistic rule given a certain safety factor.

E.1 Uplift calibration: cover thickness

Table E.1 presents statistics of the designed cover thickness ($D_{cover,d}$) for $\gamma_{\beta,up}$ = [0.5; 1.0; 1.25; 1.5; 1.75; 2.0]. The values were achieved for all members of the test set with the semi-probabilistic uplift rule described in eq.((D.5)). Figure E.1 shows the cumulative distribution functions of the designed values. Additionally, the cumulative distribution function of the mean cover thickness, present in the VNK2-databases, is depicted in the graph with a bold black line. Note that around 30% of the VNK2 cases have no presence of a cover layer, nevertheless, these cases were also considered in the calibration exercise for uplift.

Note that the probability of obtaining a designed cover thickness larger than 20 m varies from 10% to 60%, depending on a safety factor (only $\gamma_{\beta,up} \geq 1$ is considered). Furthermore, the mean cover thickness values from the VNK2-databases are much lower than the designed values, as one can see in Figure E.1. This is (among others) caused by the low cover layer weight present in the VNK2-data.

Table E.1: Statistics of the designed cover thickness results for different safety factors, uplift calibration.

Safety factor	$D_{cover,d}$ [m]			
$\gamma_{\beta,up}$	average	deviation	min	max
0.50	6.1	3.2	0.2	34.3
1.00	12.2	6.3	0.5	68.5
1.25	15.2	7.9	0.6	85.7
1.50	18.3	9.5	0.7	102.8
1.75	21.3	11.1	0.8	119.9
2.00	24.4	12.7	0.9	137.1

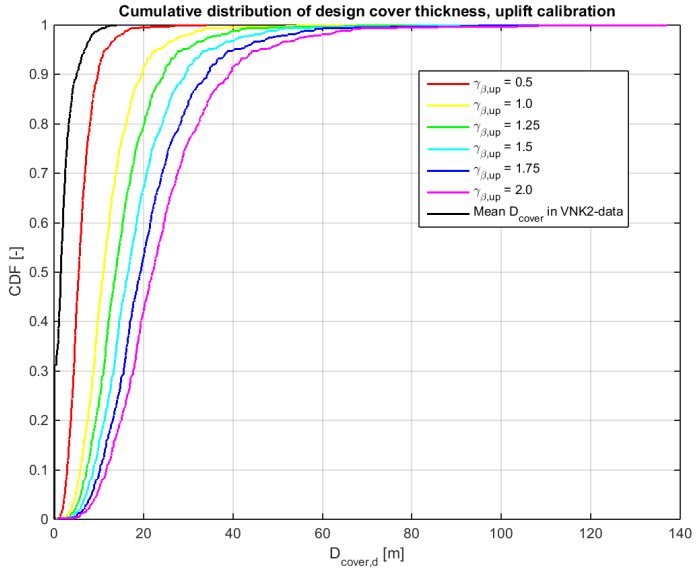

Figure E.1: Cumulative distribution functions of the designed cover layer thickness for different safety factors, uplift calibration.

E.2 Heave calibration: cover thickness

Table E.2 presents statistics of the designed cover thickness ($D_{cover,d}$) for $\gamma_{\beta,he}$ = [0.5; 1.0; 1.25; 1.5; 1.75; 2.0]. The values were achieved for all members of the test set with the semi-probabilistic heave rule described in eq.((D.9)). Figure E.2 shows the cumulative distribution functions of the designed values. Additionally, the cumulative distribution function of the mean cover thickness, present in the VNK2-databases, is depicted in the graph with a bold black line. Here, VNK2 cases with no cover layer were also considered in the calibration exercise for heave.

The probability of obtaining a designed cover thickness larger than 20 m vary from 40% to 90%, depending on a safety factor (only $\gamma_{\beta,he} \geq 1$ considered). Furthermore, the mean cover thickness values from the VNK2-databases are much lower than the designed values. As for uplift, this is (among others) caused by the fact that designs are also made for test sets without a cover layer (*i.e.* D_{cover} = 0 m).

Table E.2: Statistics of the designed cover thickness results for different safety factors, heave calibration.

Safety factor	$D_{cover,d}$ $[m]$			
$\gamma_{\beta,he}$	average	deviation	min	max
0.5	9.3	3.5	0.4	21.8
1.0	18.7	7.0	0.9	43.5
1.25	23.3	8.8	1.1	54.4
1.5	28.0	10.5	1.3	65.3
1.75	32.7	12.3	1.6	76.2
2.0	37.4	14.0	1.8	87.1

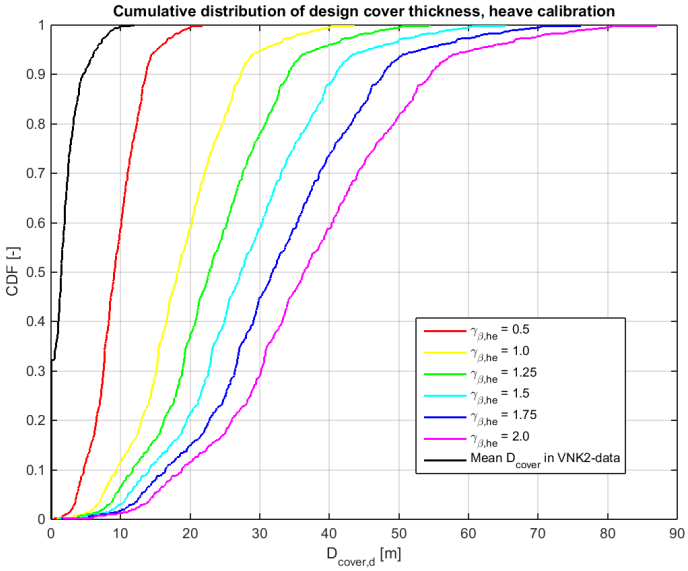

Figure E.2: Cumulative distribution functions of the designed cover thickness for different safety factors, heave calibration.

E.3 Piping calibration: seepage lengths

Table E.3 and Table E.4 present statistics of the designed seepage lengths (L_d) for Case 1 and Case 2, respectively, and $\gamma_{\beta,pip}$ = [0.5; 1.0; 1.25; 1.5; 1.75; 2.0]. The values were achieved for all members of the test sets with the semi-probabilistic piping rule as described in eq.(D.15). The resulting designed values are presented in Figure E.3 and Figure E.4 as cumulative distribution functions. Additionally, the cumulative distribution functions of the mean seepage lengths, present in the VNK2-databases, are depicted in the graphs (bold black lines).

Table E.3: Statistics of the designed seepage lengths results for different safety factors, piping calibration (Case 1 - all inputs from the VNK2-databases).

Safety factor	L_d [m]			
$\gamma_{\beta,pip}$	average	deviation	min	max
0.50	59.2	33.0	0.04	169.6
1.00	134.3	72.6	0.13	366.6
1.25	173.1	93.1	0.19	469.2
1.50	212.6	113.9	0.25	573.8
1.75	252.7	135.0	0.32	680.2
2.00	293.4	156.5	0.40	788.3

Table E.4: Statistics of the designed seepage lengths results for different safety factors, piping calibration (Case 2 - adjusted cov values of k and d_{70}).

Safety factor	L_d [m]			
$\gamma_{\beta,pip}$	average	deviation	min	max
0.50	50.1	27.3	2.2	186.3
1.00	114.9	61	6.7	404.4
1.25	148.5	78.3	9.5	517.8
1.50	182.6	95.9	12.7	633.5
1.75	217.2	113.8	16.2	751.1
2.00	252.2	131.9	20	870.4

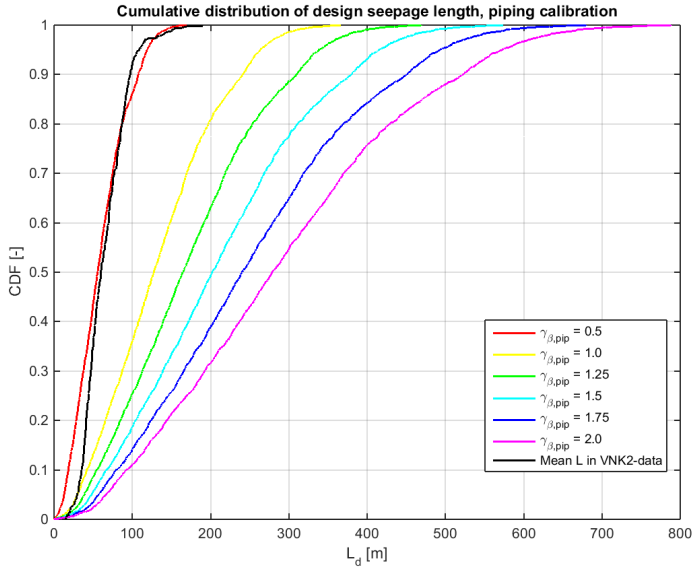

Figure E.3: Cumulative distribution functions of the designed seepage lengths for different safety factors, piping calibration (Case 1 - all inputs from the VNK2-databases).

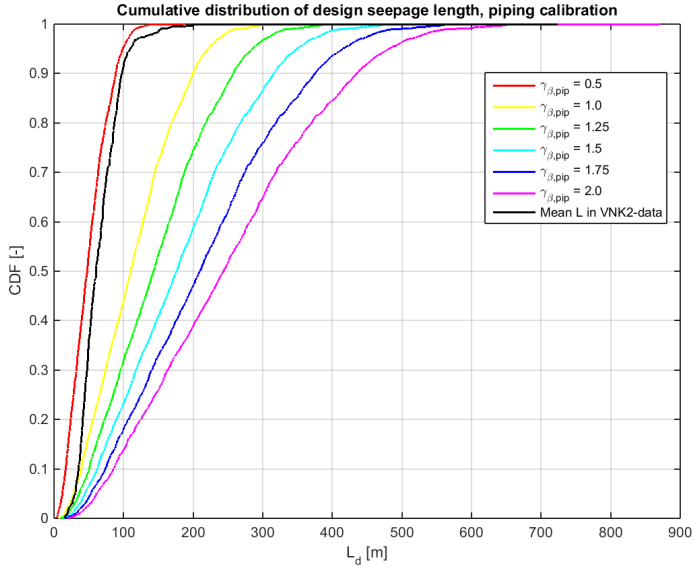

Figure E.4: Cumulative distribution functions of the designed seepage lengths for different safety factors, piping calibration (Case 2 - adjusted cov values of k and d_{70}).

Geographical distribution of the designed values (L_d) is presented in Figure E.5 for Case 1 and $\gamma_{\beta,pip}$ = 1.5. The points in the map represent the maximal seepage lengths found for each dike cross-section.

It can be observed that the values of L_d are considerable for most of the test cases. The probability of obtaining a designed seepage length L_d longer than 100 m varies from approximately 65% to 90% for both cases, depending on a safety factor considered (only $\gamma_{\beta,pip} \geq 1$ is considered). Furthermore, extremely long seepage lengths occur, up to 788.3 m (Case 1) and 870.4 (Case 2) for $\gamma_{\beta,pip}$ = 2. We note that the mean seepage lengths from the VNK2-database roughly correspond to designed seepage lengths found for $\gamma_{\beta,pip}$ = 0.5.

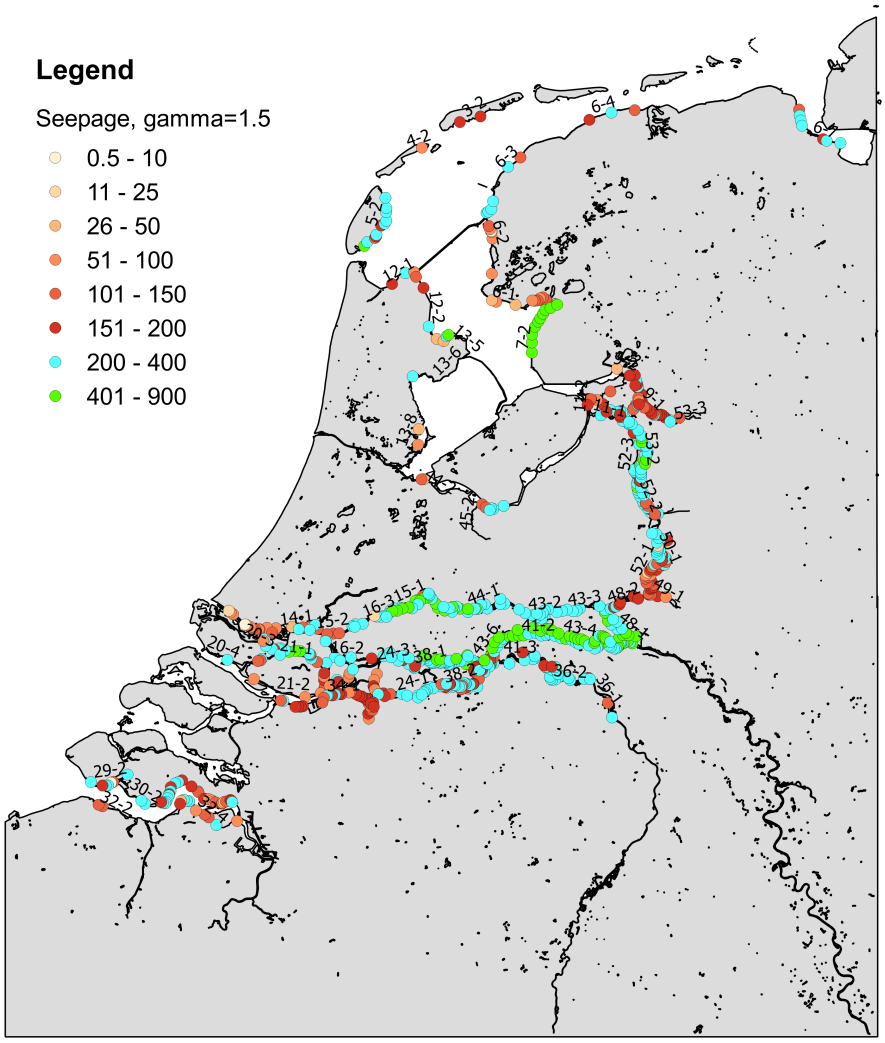

Figure E.5: Overview of the designed seepage lengths for $\gamma_{\beta,pip}$ = 1.5, piping calibration (Case 1 - all inputs from the VNK2-databases).

F Cluster alternatives study - Case 1

F.1 Clustering alternatives

The test set selected for the calibration of piping includes different characteristics, which help to divide the results per intuitive groups (which we call clusters). In summary, the following clusters can be considered:

- Cluster R: refers to analyses of the results per hydraulic Region (15 regions/classes),
- Cluster W: refers to analyses of the results per Water system (6 water systems/classes),
- Cluster T: refers to analyses of the results per return period (6 T/classes),
- Cluster S: refers to analyses of the results per Safety standard level (3 levels/classes),
- Cluster C: refers to analyses of the results per Cover layer thickness class (3 classes).

Note that each cluster mentioned above has a classification, which is explained next. Cluster W is a simplification(merge) of the classes of cluster R, while cluster S is a simplification of cluster T. As previously referred, 11 out of 15 hydraulic regions are represented in the test set (Table A.1). These belong to 6 different water systems:

- Upper-river area: hydraulic regions 1 (Non-tidal Rhine) and 2 (Non-tidal Meuse),
- Lower-river area: hydraulic regions 3 (Tidal Rhine) and 4 (Tidal Meuse),
- Vecht and IJssel deltas: hydraulic regions 5 (IJssel Delta) and 6 (Vecht Delta),
- Lake area: hydraulic regions 7 (IJssel Lake) and 8 (Marker Lake),
- Wadden Sea: hydraulic regions 9 (Wadden Sea east) and 10 (Wadden Sea west),
- Western Scheldt: hydraulic region 15 (Western Scheldt).

Furthermore, the following safety levels are defined within cluster S:

- Low safety standard level for T =[300;1,000] years,
- Medium safety standard level for T =[3,000;10,000] years,
- High safety standard level for T =[30,000;100,000] years.

The following classes of cover layer thickness are considered for cluster C [1]:

- 'No cover' defined by cases with $\mu(D_{cover}) <$ 0.1 m,
- 'Thin cover thickness' defined by cases with 0.1 m $\leq \mu(D_{cover}) <$ 6 m,
- 'Thick cover thickness' defined by cases with $\mu(D_{cover}) \geq$ 6 m.

But one can also consider the following cluster C':

- 'Thin or no cover thickness' defined by cases with $\mu(D_{cover}) <$ 6 m,
- 'Thick cover thickness' defined by cases with $\mu(D_{cover}) \geq$ 6 m.

[1] These classes are the same as considered in the study Lopez de La Cruz *et al.* (2010).

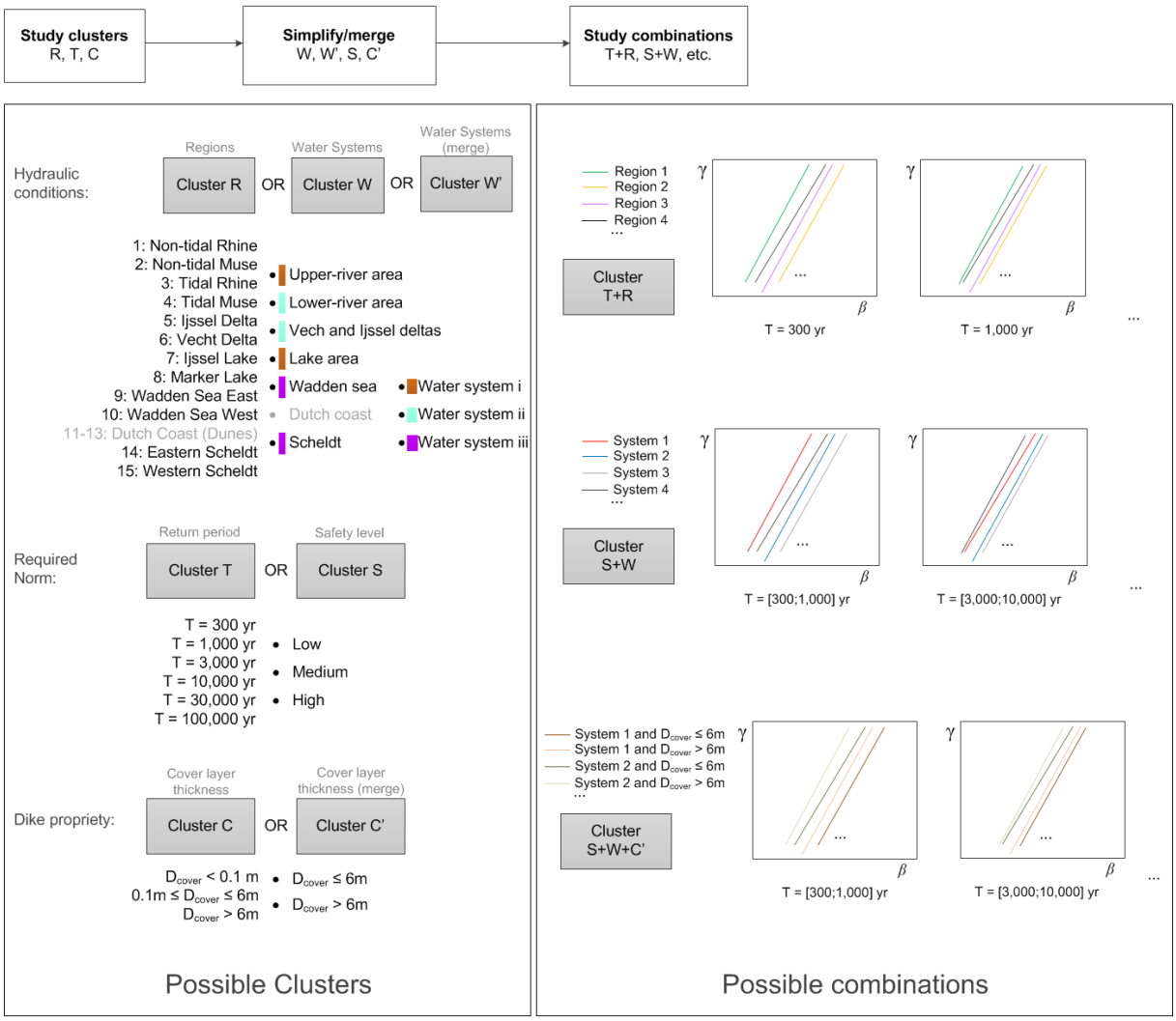

Figure F.1: Representation of the clusters in a summarised way (left) and schematic representation of possible combinations of clusters (right), as the basis for the rationalisation and recommendation for the semi-probabilistic assessment of piping.

Merging clusters (or classes) can be considered an advantage, since the data set's number of points increases, which influences (increases) the quality of the statistical inference of the 20%-quantile. This is however not the case when significantly different clusters are merged.

In the following analysis (section F.2), care was taken to not merge significantly different clusters. The next section presents the conclusions of such as analysis - individual clustering and combinations (as shown in Figure F.1). All plots are analysed next to each other, in order to check if merging is acceptable (*i.e.* if the two sets of data to be merged have a similar behaviour). In Figure F.1 a schematisation of the analysis is done, also, one can see representation of the clusters in a summarised way and a schematic representation of 3 possible combinations of clusters is shown, which is the basis for the rationalisation and recommendation (next section).

Herein, the following acronym definitions (for clustering) are/can be used:

- T+R: clustering per hydraulic region within a cluster per return period,
- T+W: clustering per water system within a cluster per return period,
- S+R: clustering per hydraulic region within a cluster per safety standard level,

- S+W: clustering per water system within a cluster per safety standard level,
- S+W+C: clustering per cover layer class within a water system which is within a safety standard level,
- etc.

F.2 Rationalization of the results and clustering combination

The following analysis was applied per sub-mechanism. The analysis starts by plotting the clusters R, W, T and C (see Appendix G, H and I). In each plot, also a 20%-quantile curve for all results (continuous black line) is presented. After a critical look into these plots, the following can be concluded:

- for Cluster W, the positioning of the 20%-quantile curves (based on the point-results per water system) with respect to the continuous black line (all results) is difficult to explain. This is because many factors contribute to the final positioning, such as (i) differences in variables per water system, (ii) differences in influence coefficients of the variables per water system, (iii) variability of the water level and decimate heights (*decimering-shoogtes*), (iv) safety standards and also (v) the statistical uncertainty introduced by the test set size per water system[2];
- the positioning of the 20%-quantile curves for Cluster C is intuitive. Considering the curve for cases with a thick cover thickness (mean higher than 6 m) and given a reliability index, the corresponding required safety factor is lower than the safety factor according to the overall curve (continuous black line - all results). Meaning that to achieve a certain safety level, a lower safety factor is needed in the case of the thick cover layer than in the case of the thin cover layer;
- in the case of Cluster T, the positions of the 20%-quantile curves with respect to the continuous black line can be explained as follows. Given a safety factor, a higher required safety standard leads to a higher outside water level, which entails a higher seepage length or cover thickness according to the semi-probabilistic rules. This consequently leads to a higher reliability index.

After analysing and concluding this, combinations of clusters were studied (T+W, S+W, etc.). The following steps were taken:

1. all cases (presented in Figure 8.2, 8.6 and 8.5) are plotted taking into account clustering type T, this was the starting point, *i.e.* one 20% curve per T (see e.g. in Figure F.2 for heave sub-mechanism),
2. within each T we applied clustering type R, but also clustering type W (separate), these are compared to each other, T+R vs T+W. This clustering results in 6 plots (1 per T), each with multiple lines (see e.g. in Figure F.3 for the heave sub-mechanism),
3. per safety standard level (low, medium, high), the corresponding T+W (or T+R[3]) are compared (see e.g. in Figure F.4 for the heave sub-mechanism),
4. the resultant clustering (e.g. S+W) can be further merged/simplified, e.g. resulting in S+W'. Here, the W' cluster considers the following merged/simplified groups: (i) Upper-river area and lakes, (ii) Lower-river and river deltas and (iii) Sea and sea deltas[4]. In this case the clustering graphs result in 3 lines per S, so, a total of 3×3=9 lines (S+W') - see e.g. in Figure F.5 for the heave sub-mechanism,

[2] In Appendix J, influence coefficients found for $\gamma_{\beta,pip}$ = 1.5 are summarized, and in Appendix K the ranges of each one of the random variables that intervene in each sub-mechanism are presented.

[3] Cluster R was at this point not considered any more, because some of the hydraulic regions did not provide enough points for the analysis.

[4] Correspondent hydraulic regions to these groups are (i) regions 1, 2, 7 and 8, (ii) regions 3, 4, 5 and 6 and (iii) regions 9, 10 and 15.

5 finally, the resultant S+W', can be divided/detailed taking into account the cover layer class: S+W/W'+C or S+W/W'+C'. The C' cluster considers only 2 classes instead of 3 (cluster C), these 2 classes are (i) cover layer thickness < 6 m and (ii) cover layer thickness > 6 m - see e.g. in Figure F.6 for the heave sub-mechanism.

Once again, we aim for practical and sufficient representative $\gamma_\beta - \beta_{cross}$ relations, and such a multi-combination of clusters (such as S+W'+C/C') is to be avoided. Also, note that the merging is based on the analysis of the data-points. As a consequence merging of e.g. upper-river area and lakes was proposed. This may be considered unexpected due to the differences between these water systems, however it is not unexpected when looking at the behaviour of the data-points.

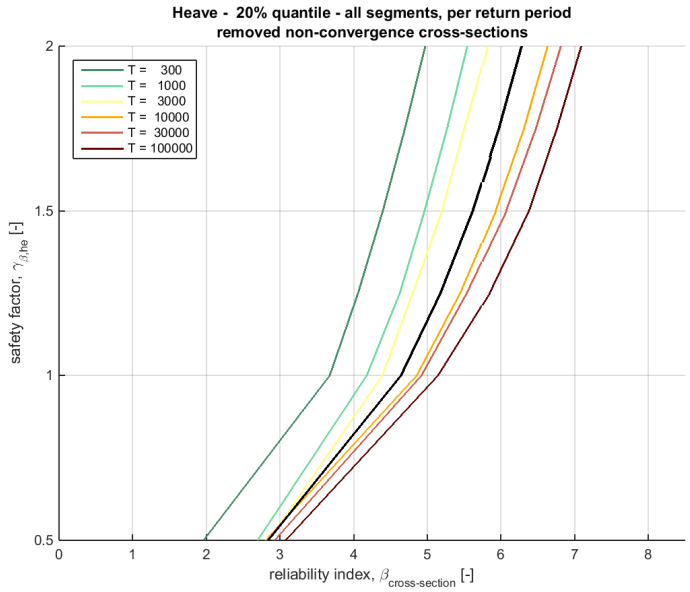

Figure F.2: Cluster step 1 example: Heave calibration results with 20%-quantile curve (all results - black line), and curves per class return period (Cluster T).

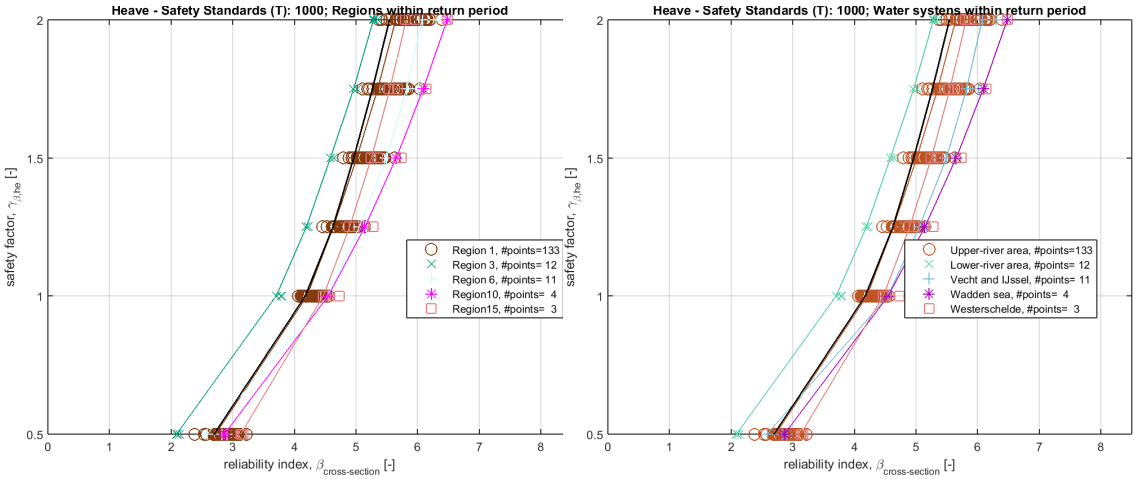

(a) Cluster T+R *(b) Cluster T+W*

Figure F.3: Cluster step 2 example: Heave calibration results with 20%-quantile curves per region and water system for T = 1,000 years.

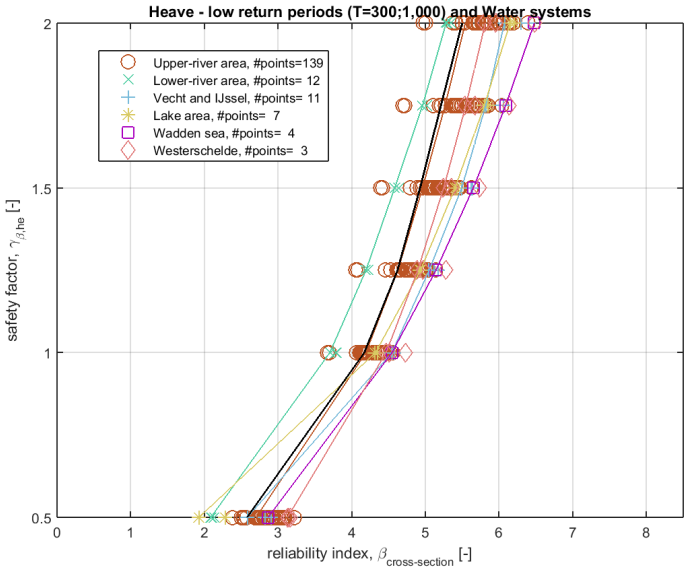

Figure F.4: Cluster step 3 example: Heave calibration results with 20%-quantile curves per water system for low safety standard (Cluster S+W).

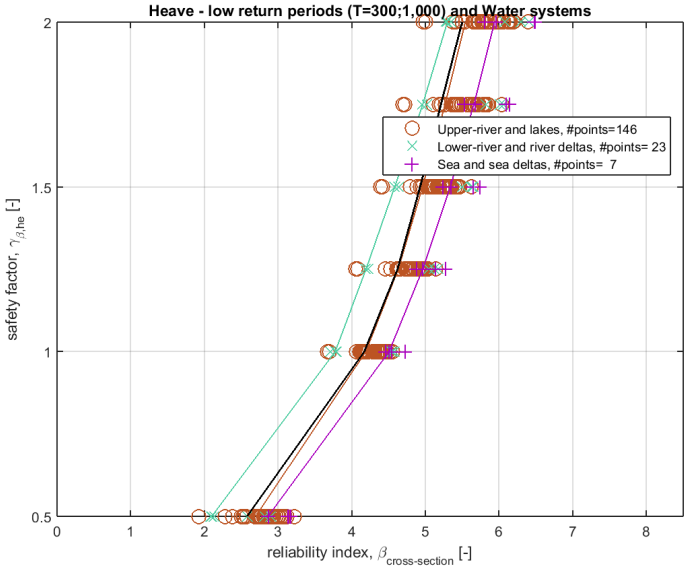

Figure F.5: Cluster step 4 example: Heave calibration results with 20%-quantile curves per water system for low safety standard (Cluster S+W').

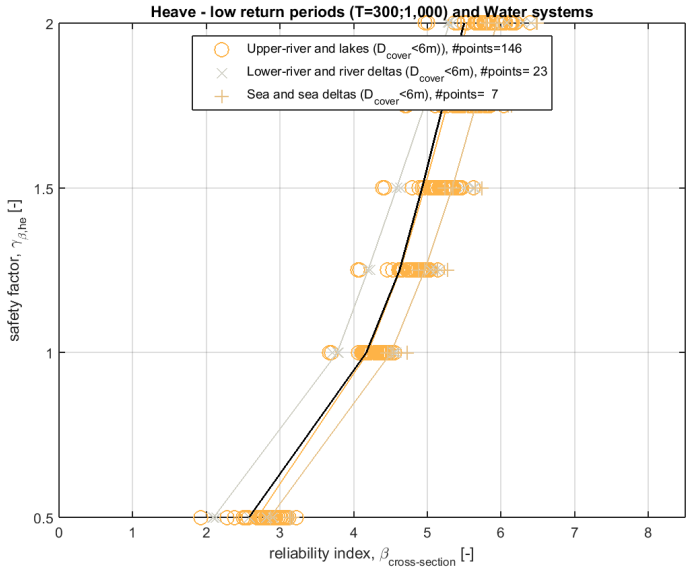

Figure F.6: Cluster step 5 example: Heave calibration results with 20%-quantile curves for low safety standard (Cluster S+W'+C).

For each one of the sub-mechanisms (see all details in Appendix L, M and N), these considerations lead to the following results(each paragraph below corresponds directly to the steps presented earlier, in page 87):

1 this step results in a picture where it is easy to understand the effect of T in the $\gamma - \beta$ relation. From left to right we have the lowest T to the highest T,

2 comparison between T+R and T+W shows that T+W represents a good merge of the hydraulic regions into water systems, and also a bigger data set per cluster for a more reliable inference of the 20%-quantile line is achieved,

3 when merging/simplifying T+W into S+W we see a better representation of all the water systems relevant to a certain safety standard level. Here, the merging of the return periods is considered acceptable,

4 when comparing S+W to S+W', it is seen that there is a recognizable pattern of the results. It happens for all sub-mechanisms that the water system group (ii) is the one most on the left, followed by (i) and then (iii), which is the line most on the right side (*i.e.* W'(ii) > W'(i) > W'(iii)), however, the following is also detected

   (a) UPLIFT: behaviour is as described above,

   (b) HEAVE: behaviour is as described above, except for medium safety level, where line W'(i) coincides with W'(iii),

   (c) PIPING: behaviour is as described above, except for the low safety level where W'(ii) coincides with W'(iii) and for high safety level where W'(ii) coincides with W'(i).

   Note that, if one was to take a more detailed clusterting (e.g. T+W or T+R for the low safety level) the data set number would affect the confidence in the recommended 20%-quantile curve (as one can see in the number of points indicated in each one of the figures in Appendix L, M; N). This also might have affected the results presented for S+W' and also justify the break in the pattern W'(ii) > W'(i) > W'(iii),

5 finally, another clustering (C') was applied, however this did not show any advantages to the calibration recommendations (especially in terms of simplicity).

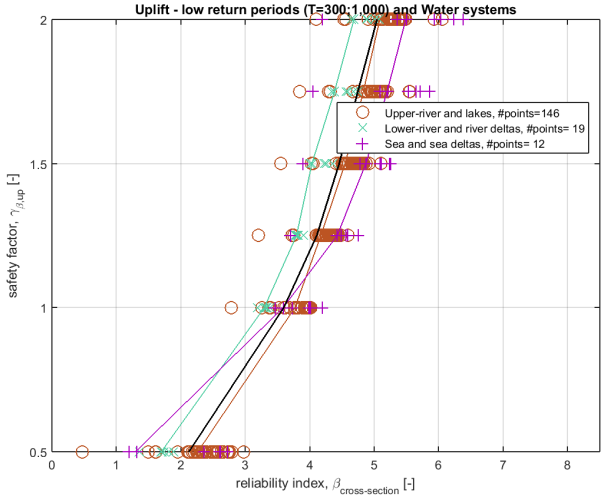

(a) Low safety standard level

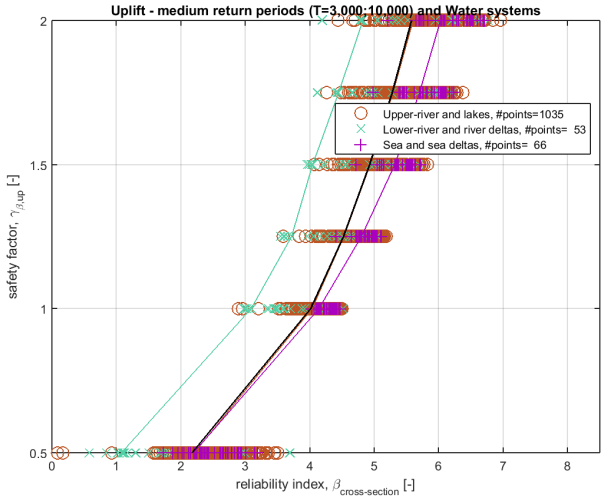

(b) Medium safety standard level

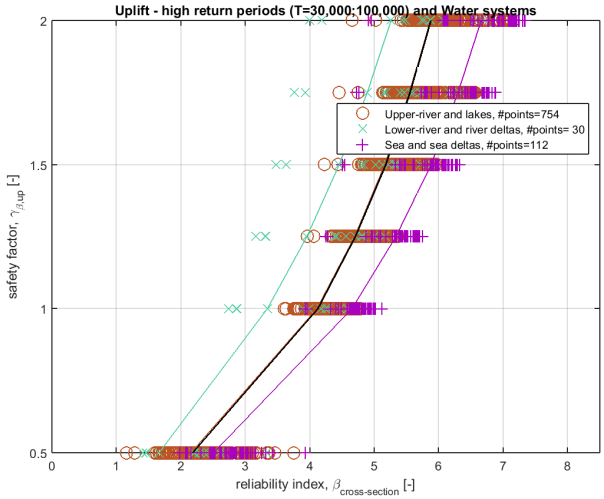

(c) High safety standard level

Figure F.7: Cluster S+W' and respective 20%-quantile curves, uplift calibration. The black line represents the 20%-quantile curve based on all data points in the respective plot. Notice that for the medium and high safety standard levels, the brown and black curves overlap.

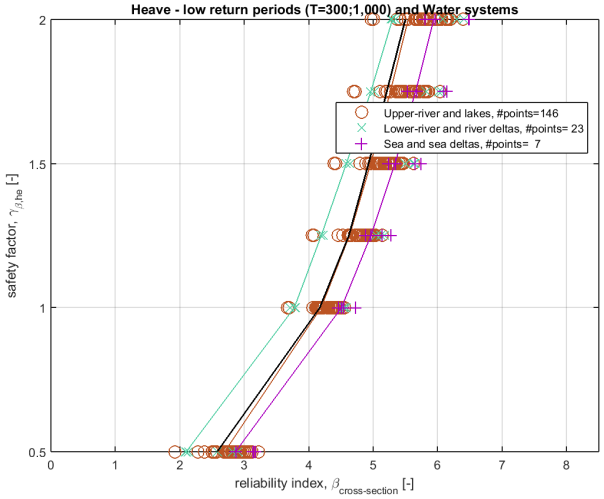

(a) Low safety standard level

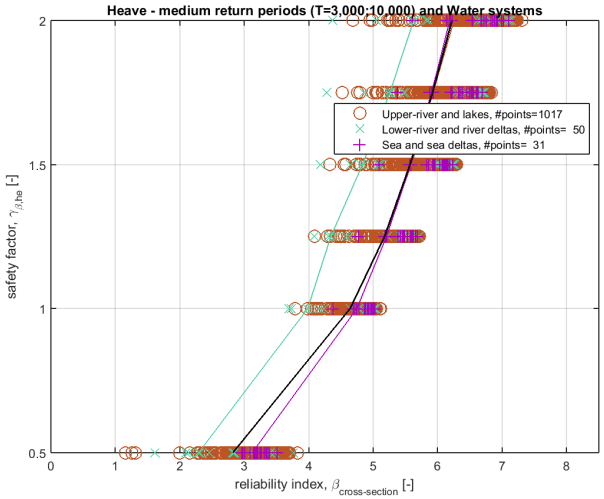

(b) Medium safety standard level

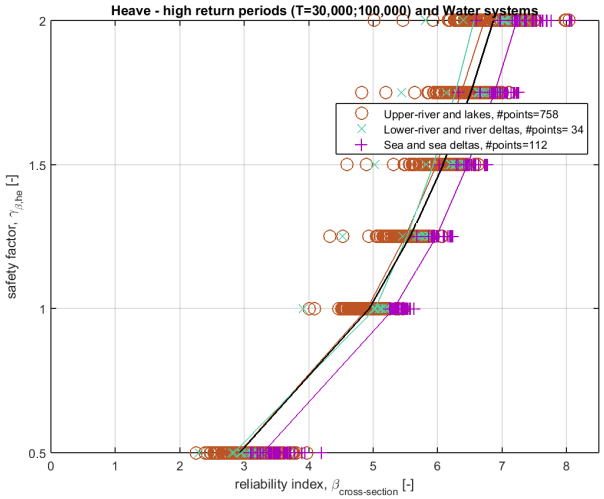

(c) High safety standard level

Figure F.8: Cluster S+W' and respective 20%-quantile curves, heave calibration. The black line represents the 20%-quantile curve based on all data points in the respective plot. Notice that for the medium safety standard level, the brown and black curves overlap.

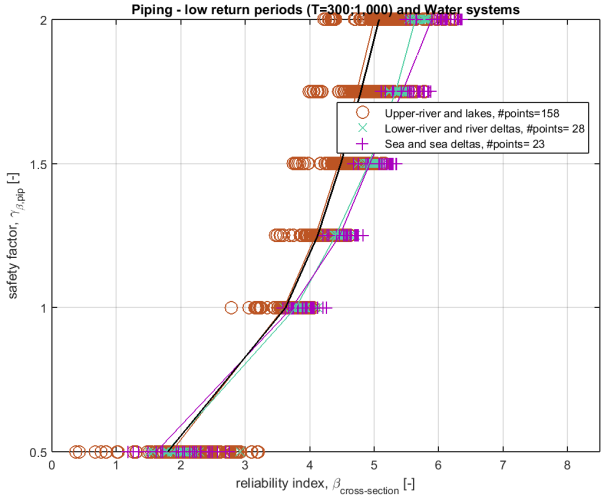

(a) Low safety standard level

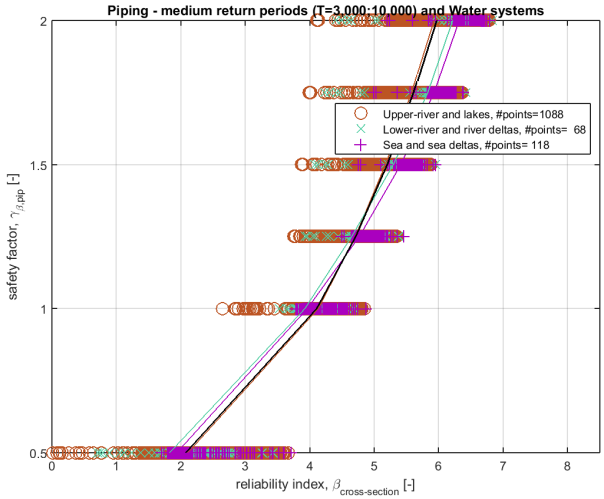

(b) Medium safety standard level

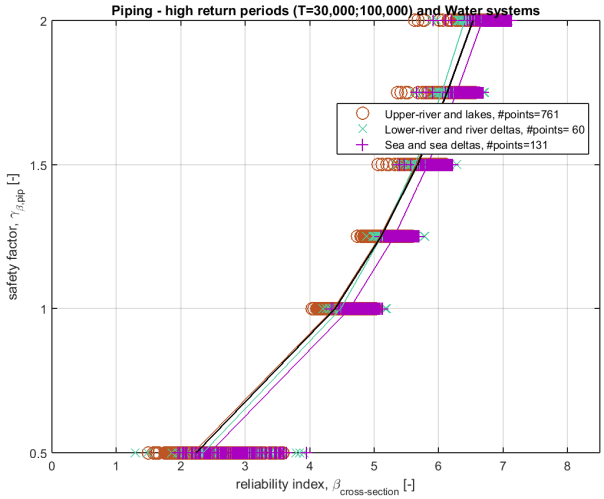

(c) High safety standard level

Figure F.9: Cluster S+W' and respective 20%-quantile curves, piping calibration. The black line represents the 20%-quantile curve based on all data points in the respective plot. Notice that for the low safety standard level, the brown and black curves overlap.

G Uplift: calibration results per cluster W, T and C - Case 1

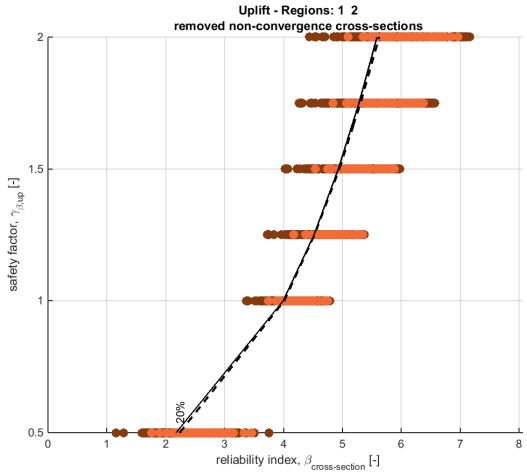

(a) Upper-river area

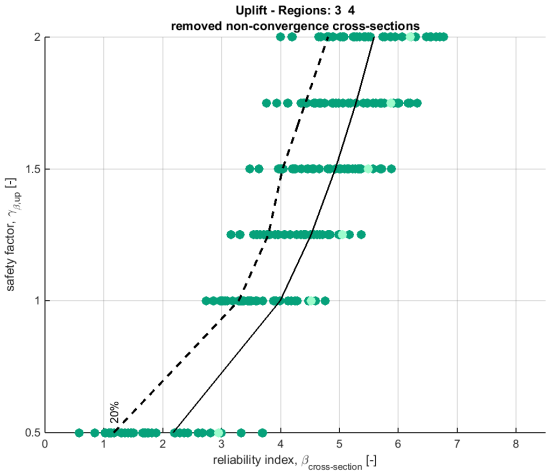

(b) Lower-river area

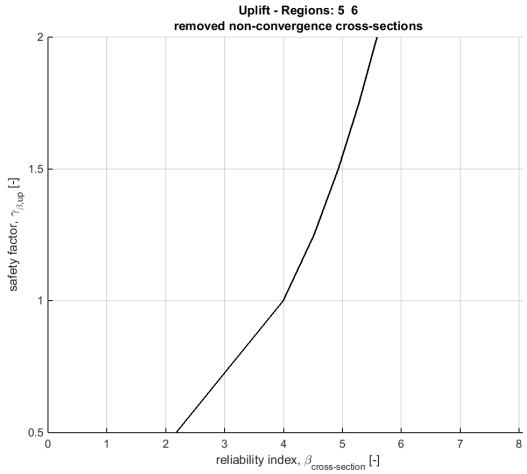

(c) Vecht and IJssel deltas

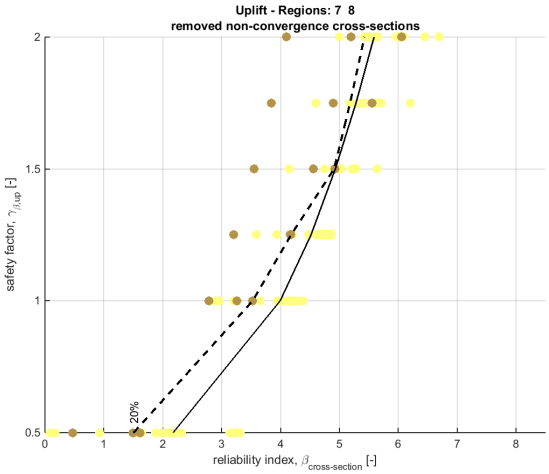

(d) Lake area

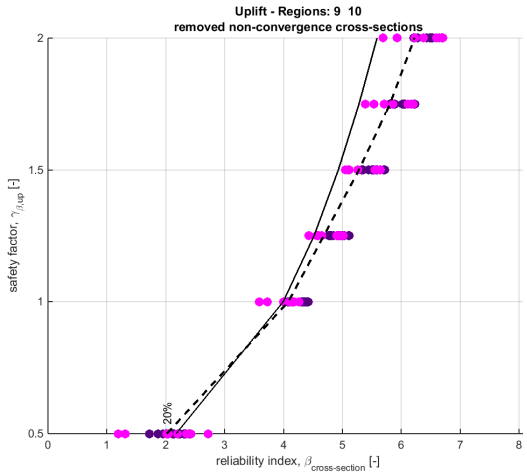

(e) Wadden Sea

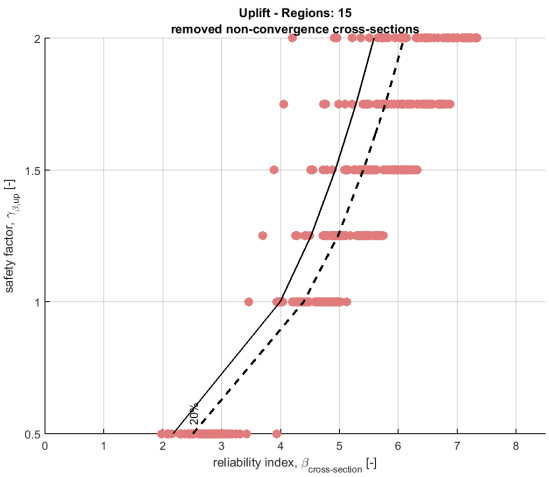

(f) Western Scheldt

Figure G.1: Uplift calibration results with 20%-quantiles - Cluster W.

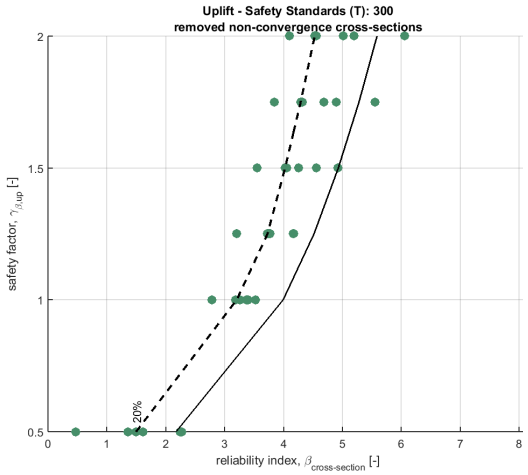

(a) Return period T = 300 years

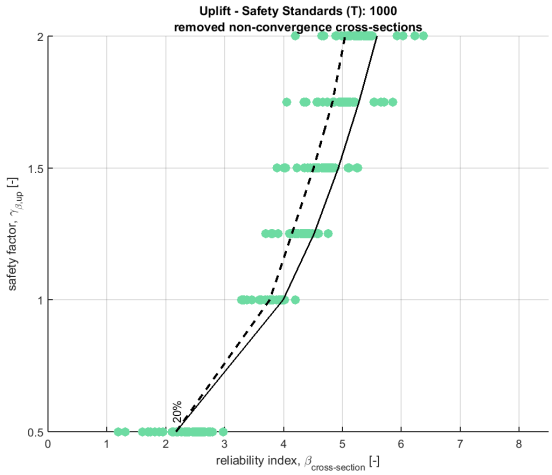

(b) Return period T = 1,000 years

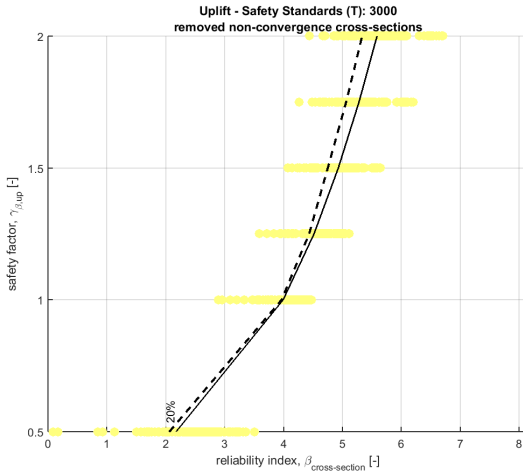

(c) Return period T = 3,000 years

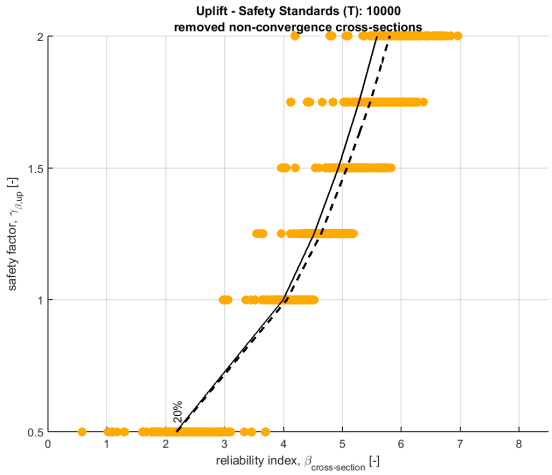

(d) Return period T = 10,000 years

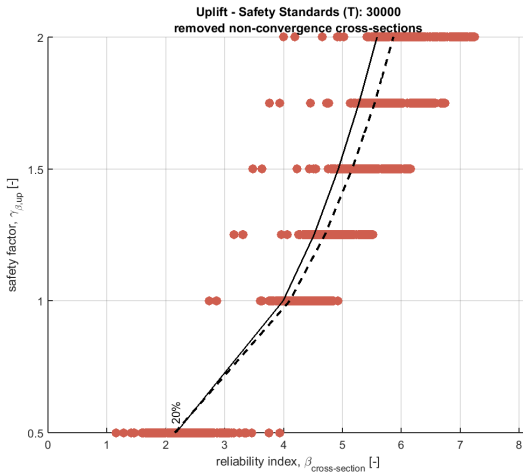

(e) Return period T = 30,000 years

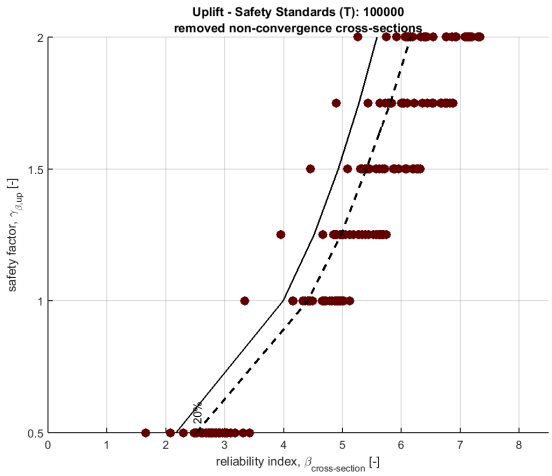

(f) Return period T = 100,000 years

Figure G.2: Uplift calibration results with 20%-quantiles - Cluster T.

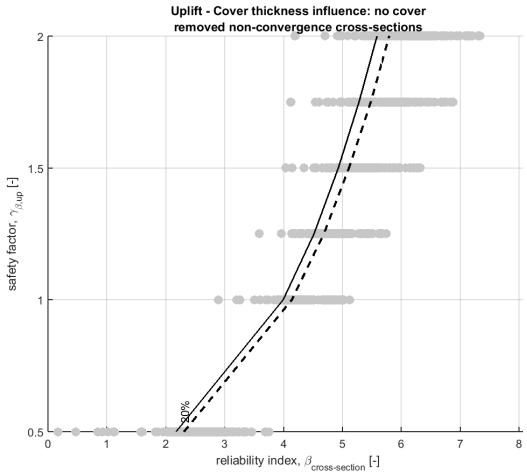

(a) No cover

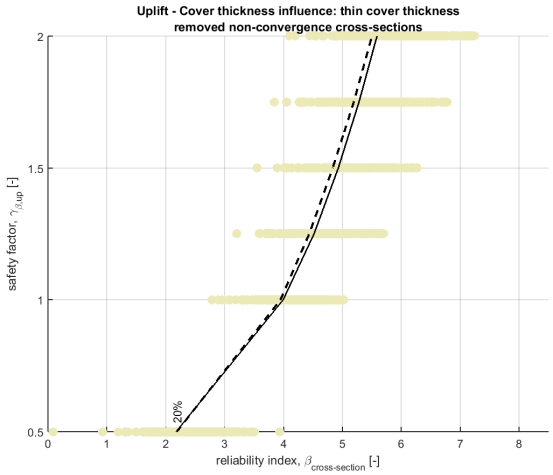

(b) Thin cover thickness

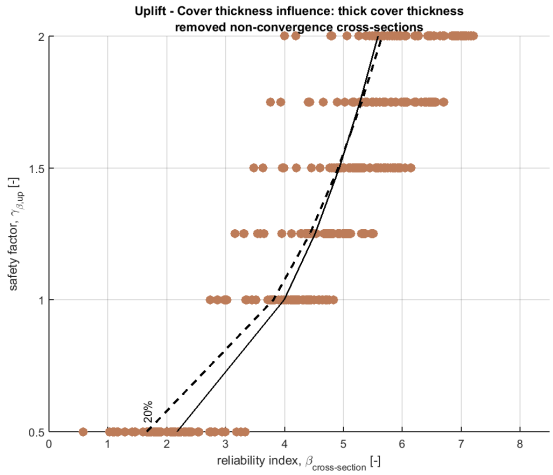

(c) Thick cover thickness

Figure G.3: Uplift calibration results with 20%-quantiles - Cluster C.

H Heave: calibration results per cluster W, T and C - Case 1

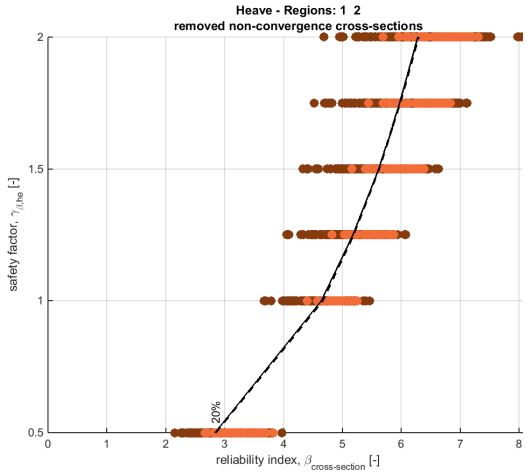

(a) Upper-river area

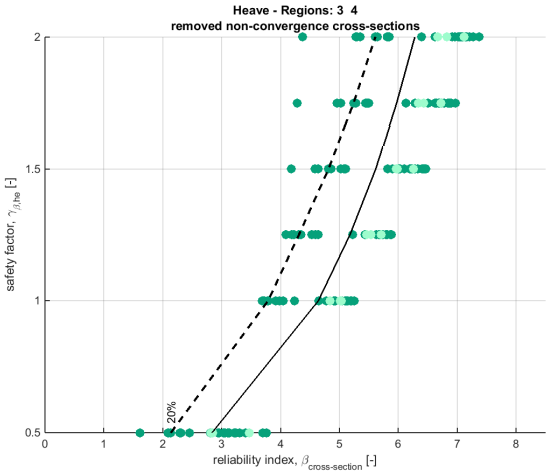

(b) Lower-river area

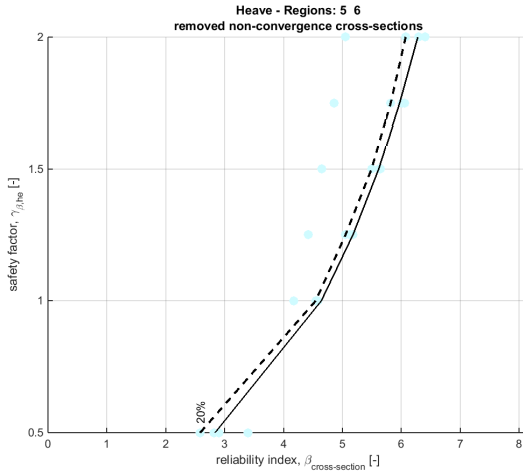

(c) Vecht and IJssel deltas

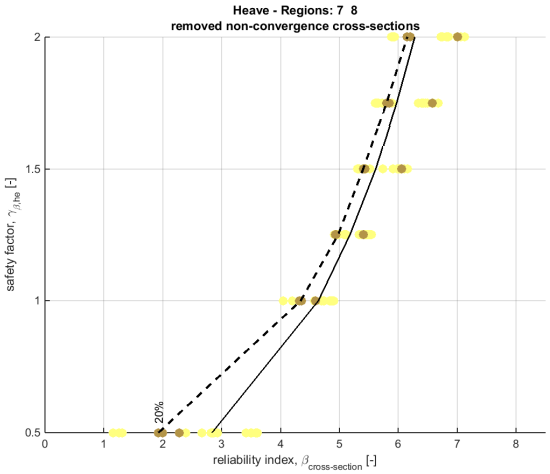

(d) Lake area

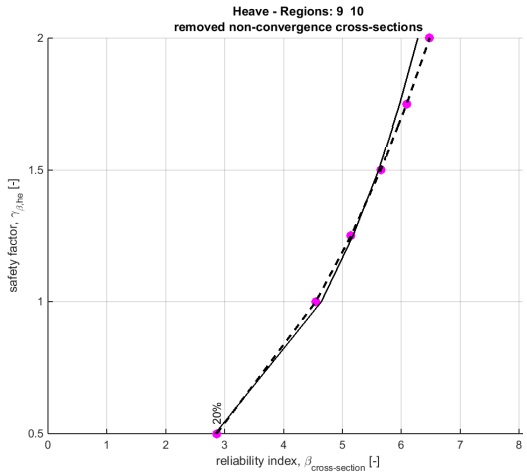

(e) Wadden Sea

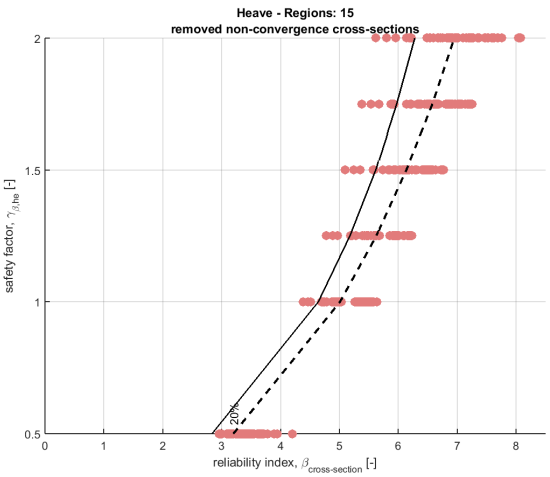

(f) Western Scheldt

Figure H.1: Heave calibration results with 20%-quantiles - Cluster W.

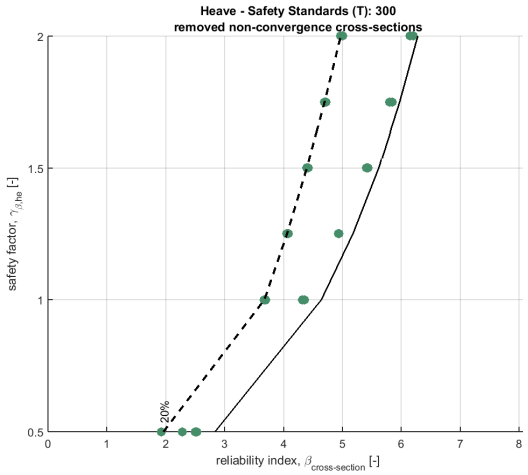

(a) Return period T = 300 years

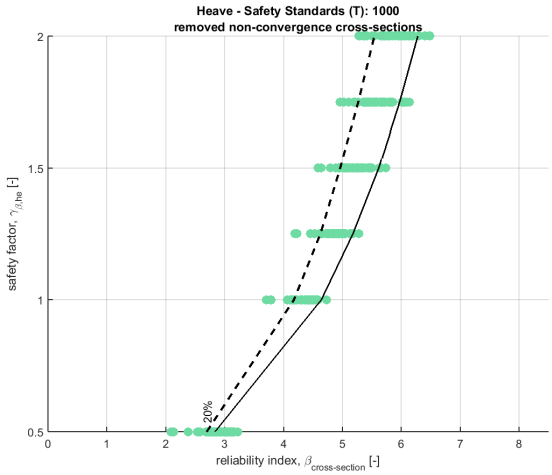

(b) Return period T = 1,000 years

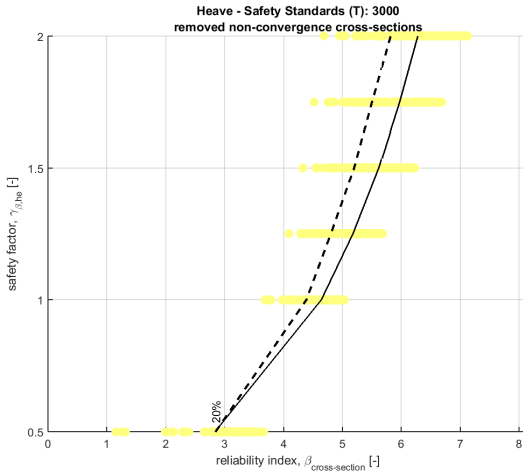

(c) Return period T = 3,000 years

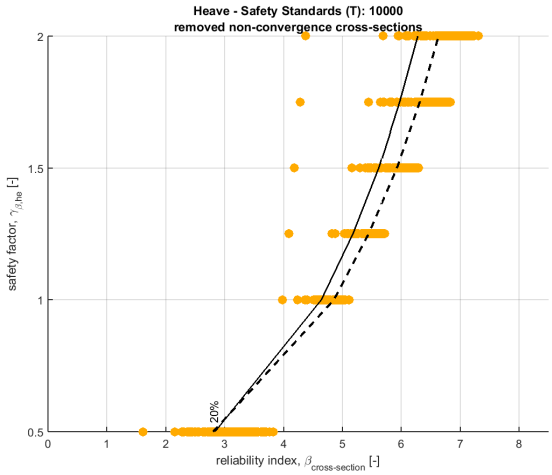

(d) Return period T = 10,000 years

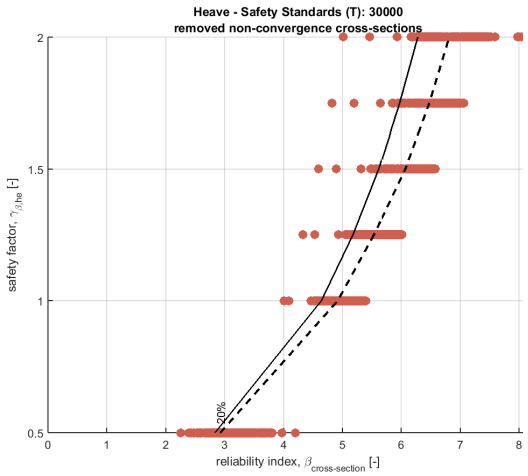

(e) Return period T = 30,000 years

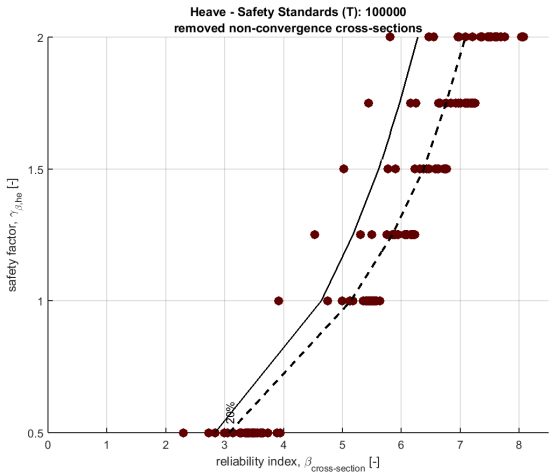

(f) Return period T = 100,000 years

Figure H.2: Heave calibration results with 20%-quantiles - Cluster T.

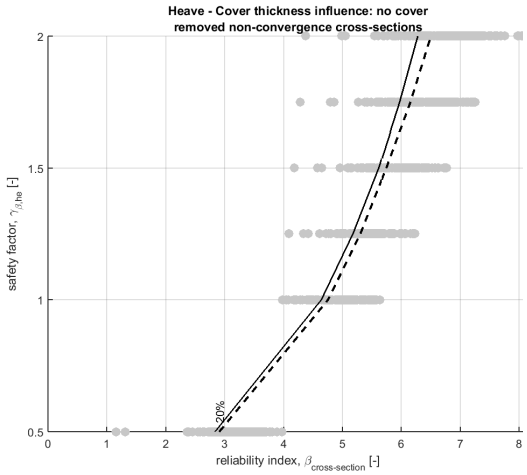

(a) No cover

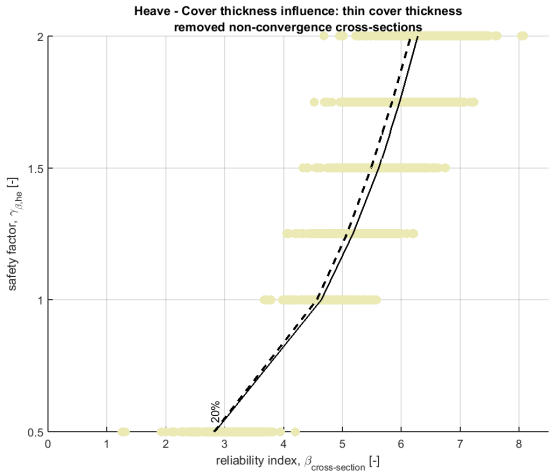

(b) Thin cover thickness

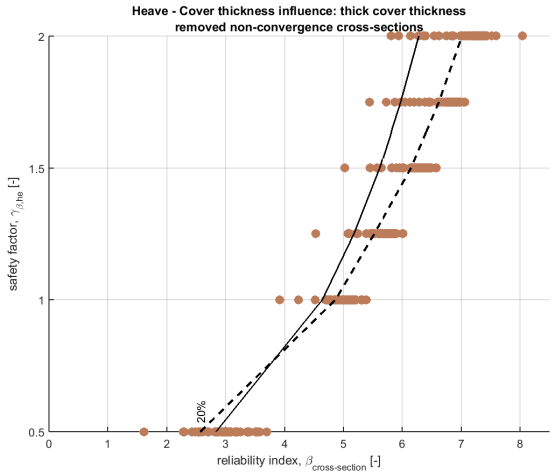

(c) Thick cover thickness

Figure H.3: Heave calibration results with 20%-quantiles - Cluster C.

I Piping: calibration results per cluster W, T and C - Case 1

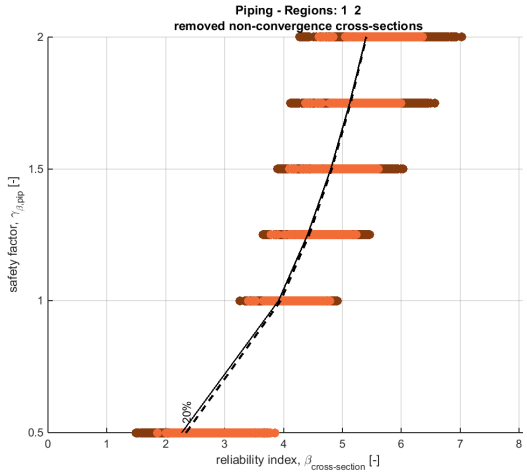

(a) Upper-river area

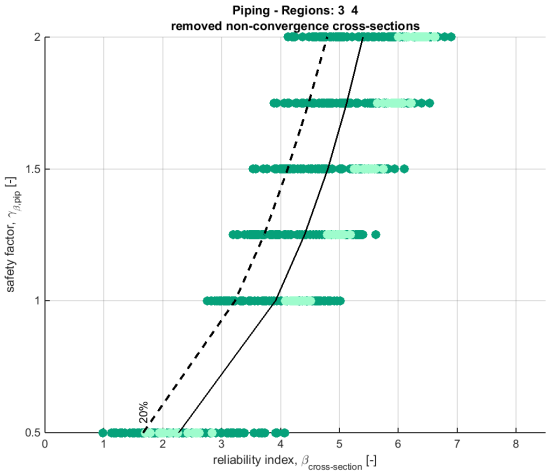

(b) Lower-river area

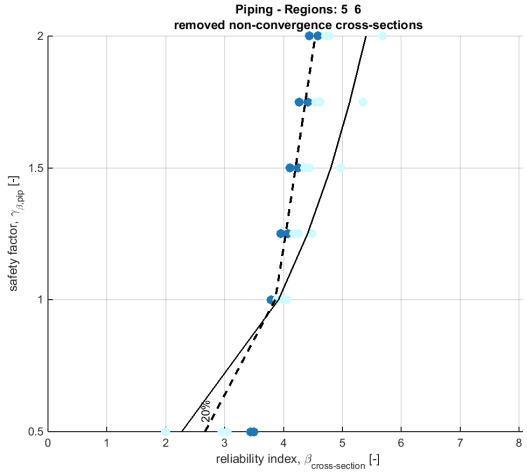

(c) Vecht and IJssel deltas

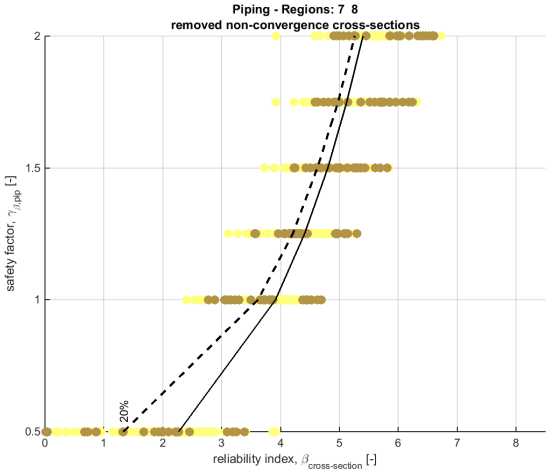

(d) Lake area

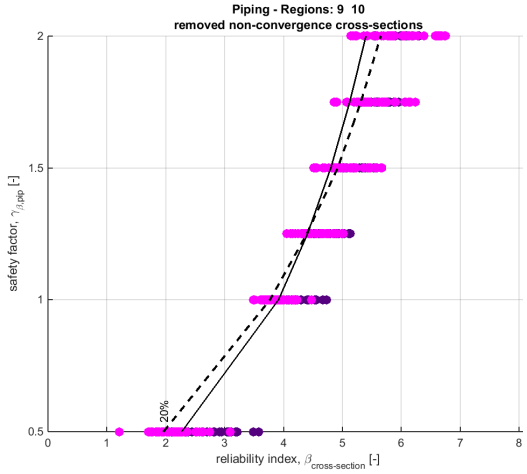

(e) Wadden Sea

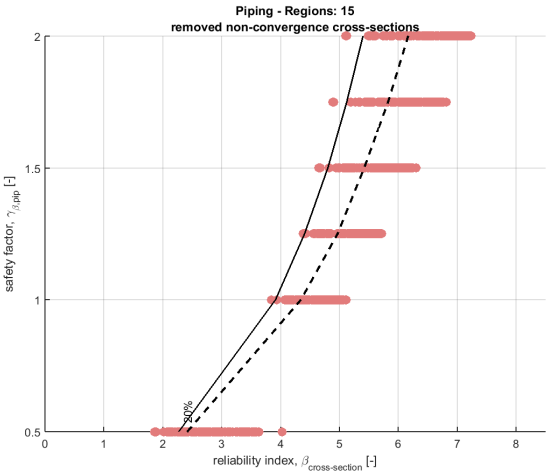

(f) Western Scheldt

Figure I.1: Piping calibration results with 20%-quantiles - Cluster W.

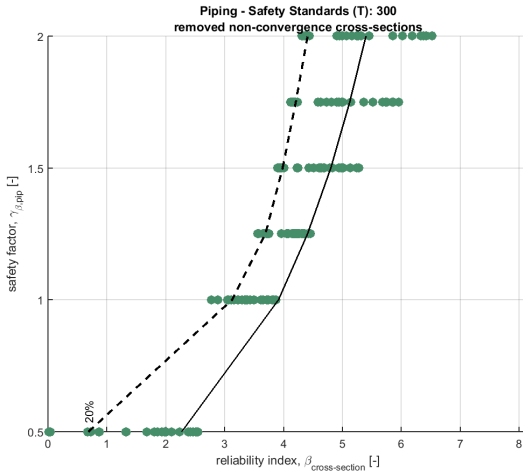

(a) Return period T = 300 years

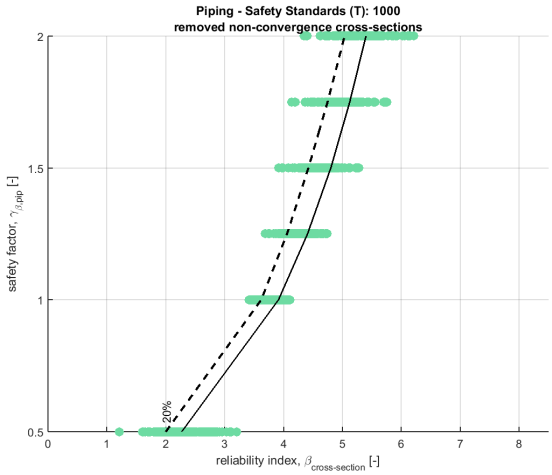

(b) Return period T = 1,000 years

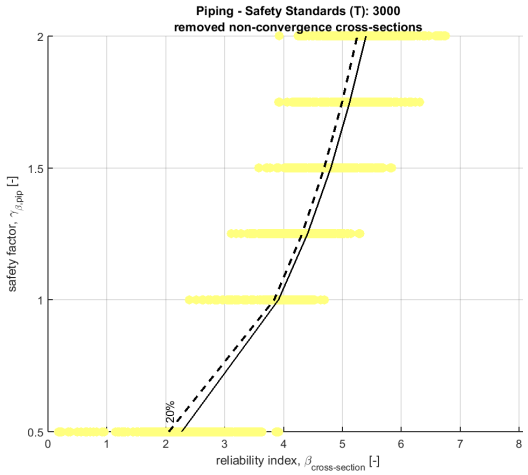

(c) Return period T = 3,000 years

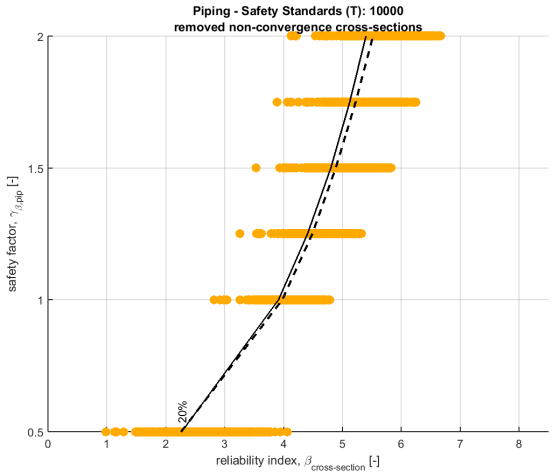

(d) Return period T = 10,000 years

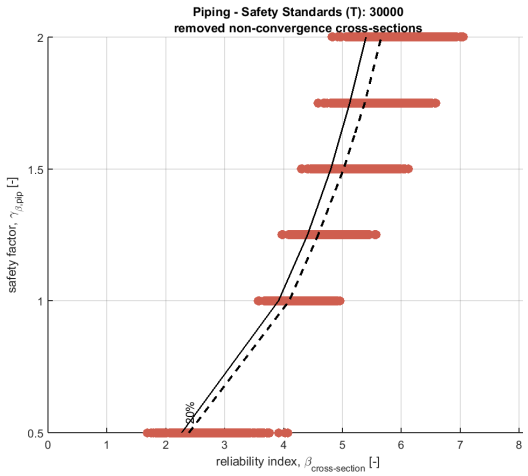

(e) Return period T = 30,000 years

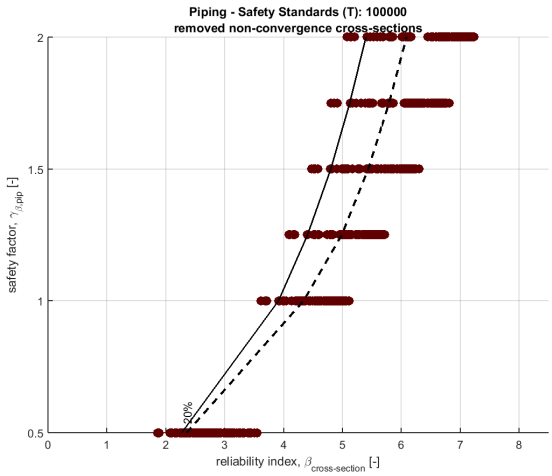

(f) Return period T = 100,000 years

Figure I.2: Piping calibration results with 20%-quantiles - Cluster T.

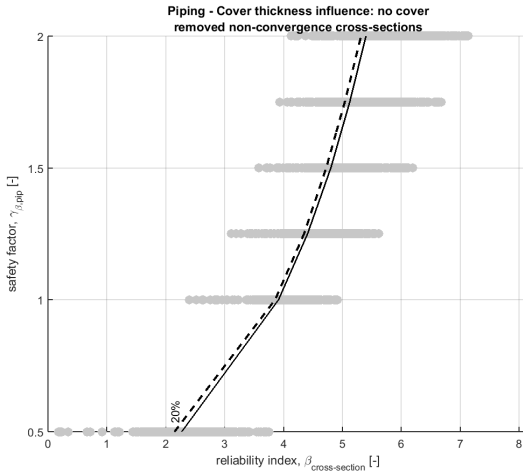

(a) No cover

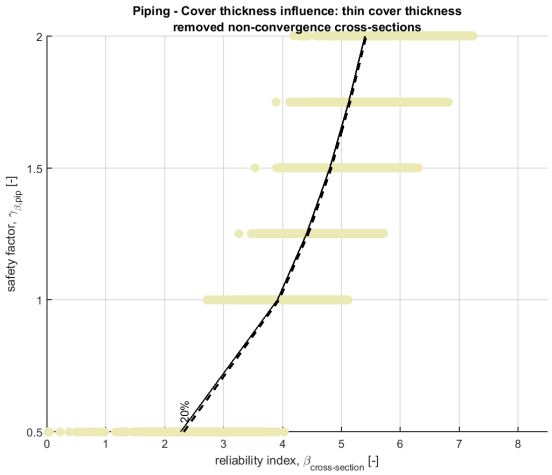

(b) Thin cover thickness

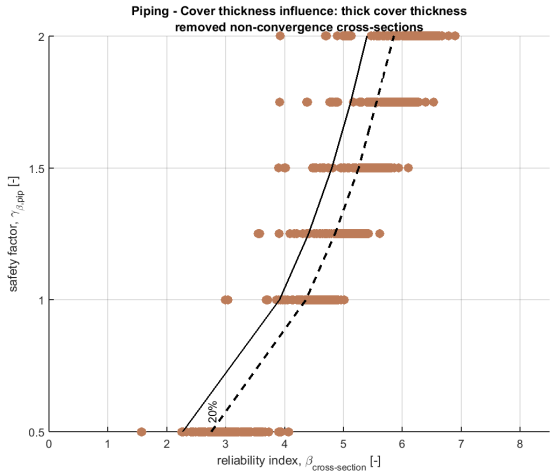

(c) Thick cover thickness

Figure I.3: Piping calibration results with 20%-quantiles - Cluster C.

J Influence coefficients (Step 3) - Case 1

J.1 Uplift - clustering per water system

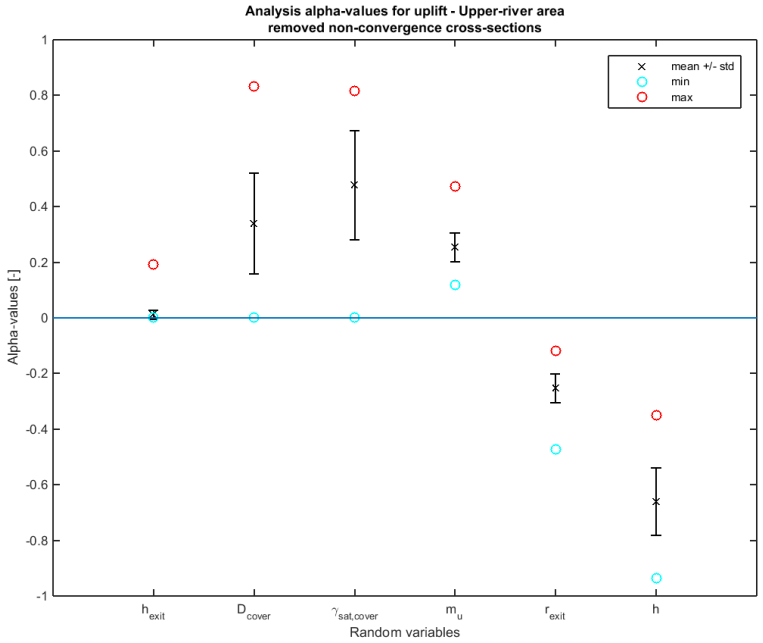

(a) Upper-river area

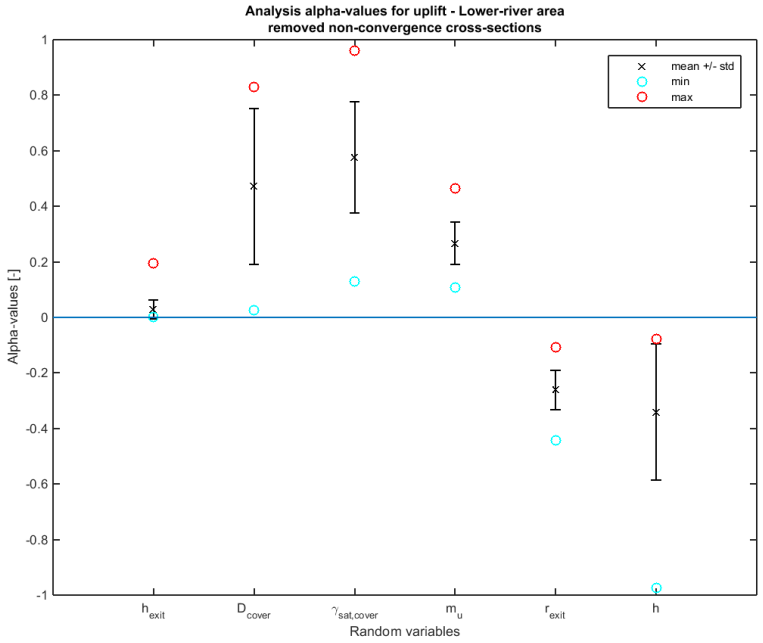

(b) Lower-river area

Figure J.1: Analysis of influence coefficients for $\gamma_{\beta,up}$ = 1.5, uplift calibration.

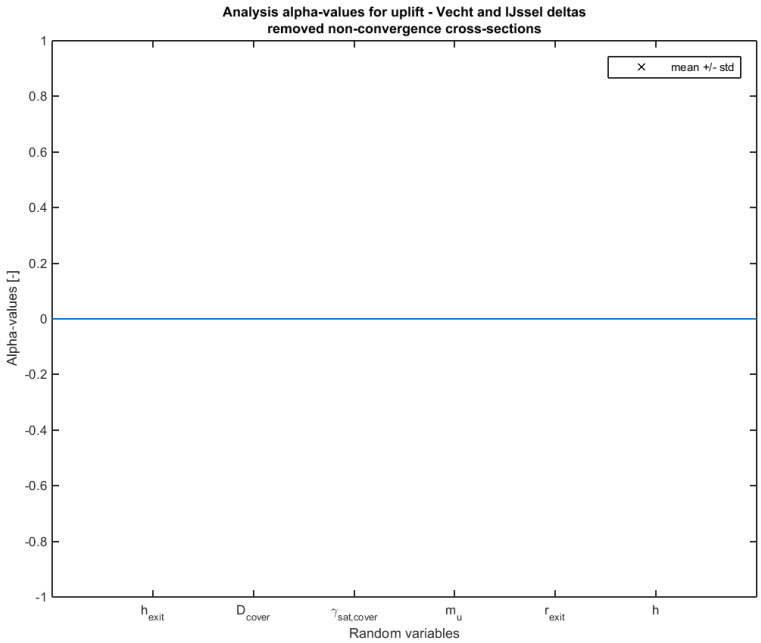

(a) Vecht and IJssel deltas

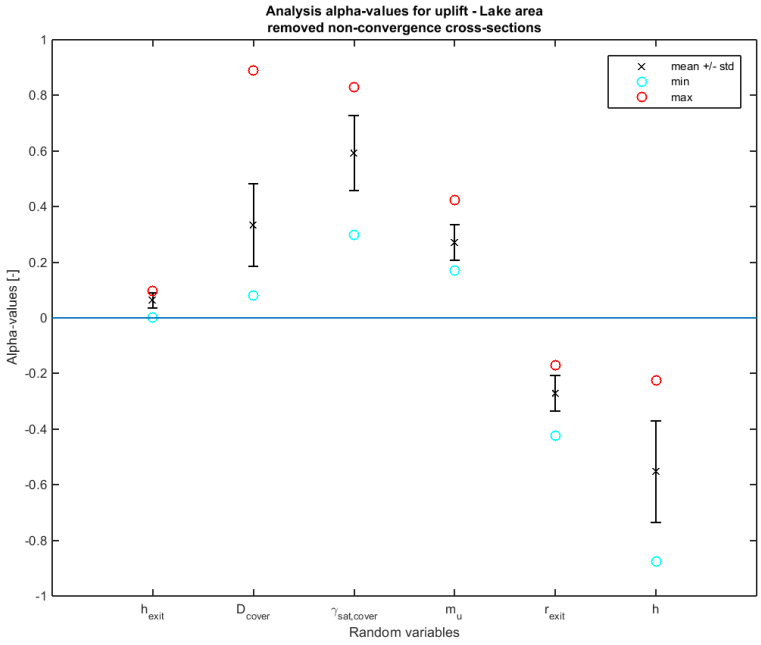

(b) Lake area

Figure J.2: Analysis of influence coefficients for $\gamma_{\beta,up}$ = 1.5, uplift calibration.

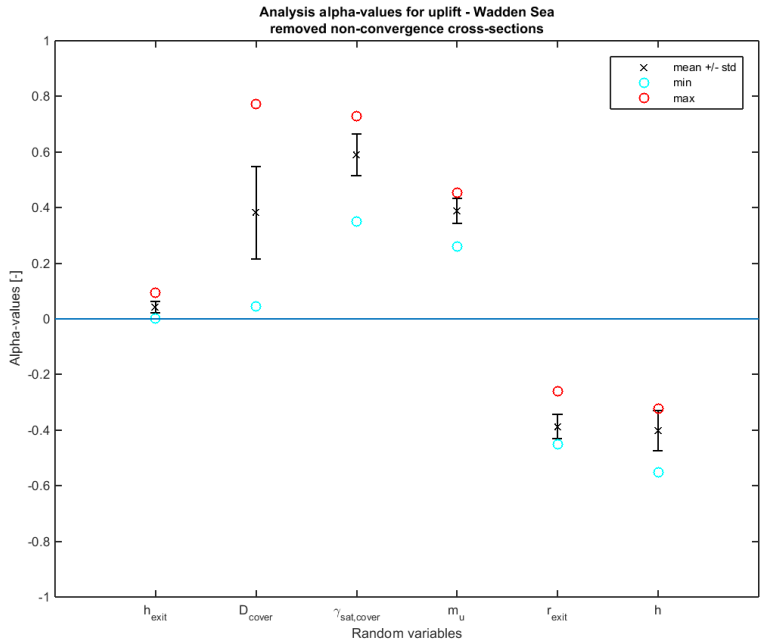

(a) Wadden Sea

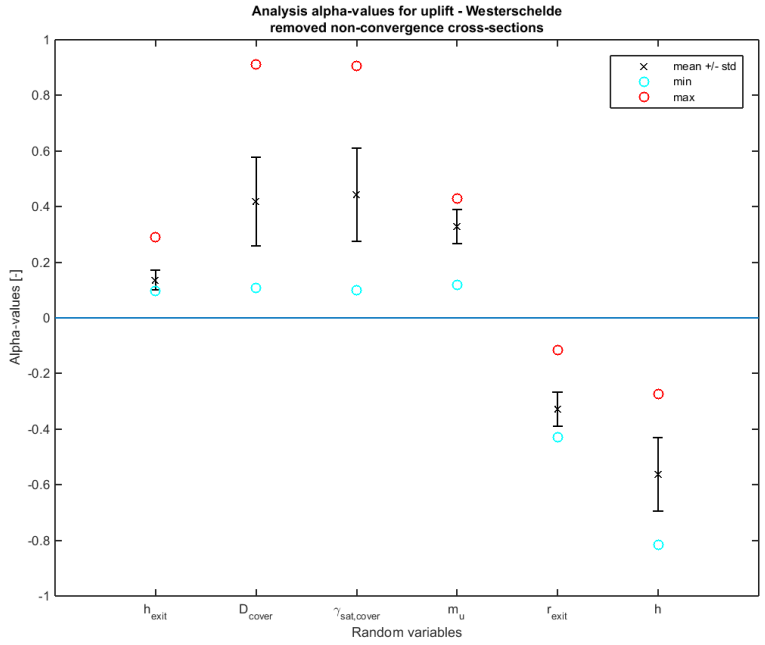

(b) Western Scheldt

Figure J.3: Analysis of influence coefficients for $\gamma_{\beta,up}$ = 1.5, uplift calibration.

J.2 Uplift - clustering per cover thickness class

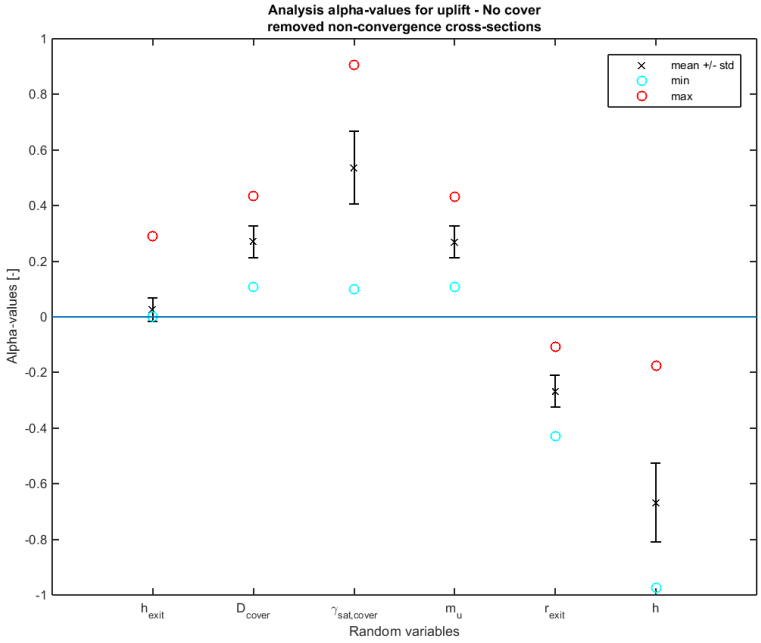

(a) No cover

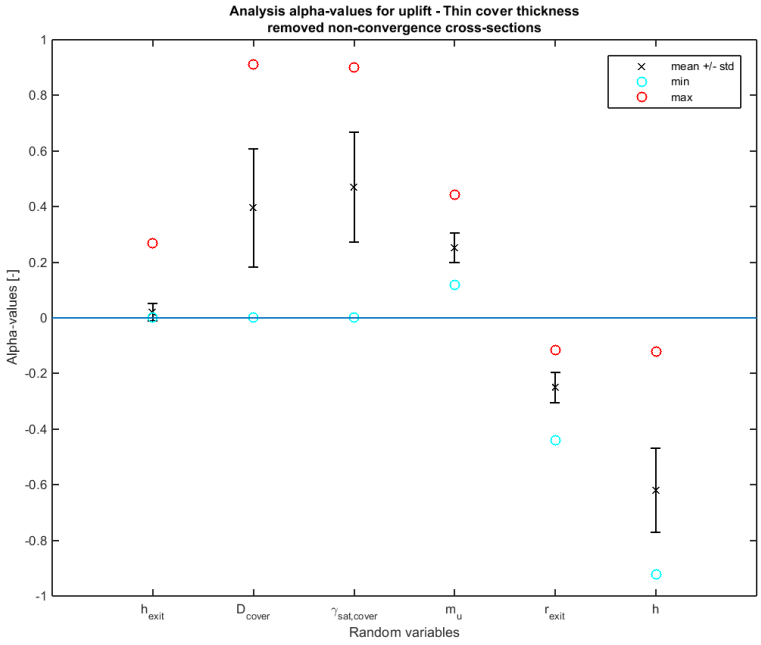

(b) Thin cover thickness

Figure J.4: Analysis of influence coefficients for $\gamma_{\beta,up}$ = 1.5, uplift calibration.

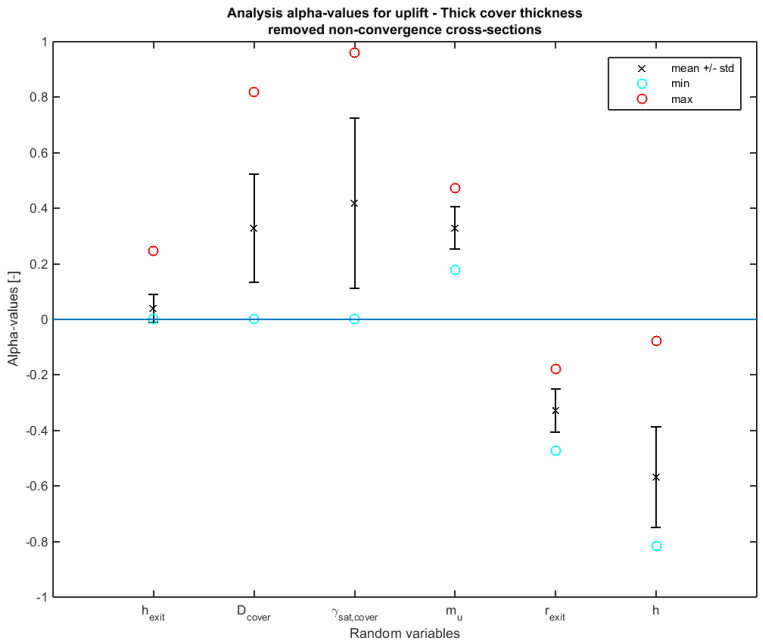

(a) Thick cover thickness

Figure J.5: Analysis of influence coefficients for $\gamma_{\beta,up}$ = 1.5, uplift calibration.

J.3 Heave - clustering per water system

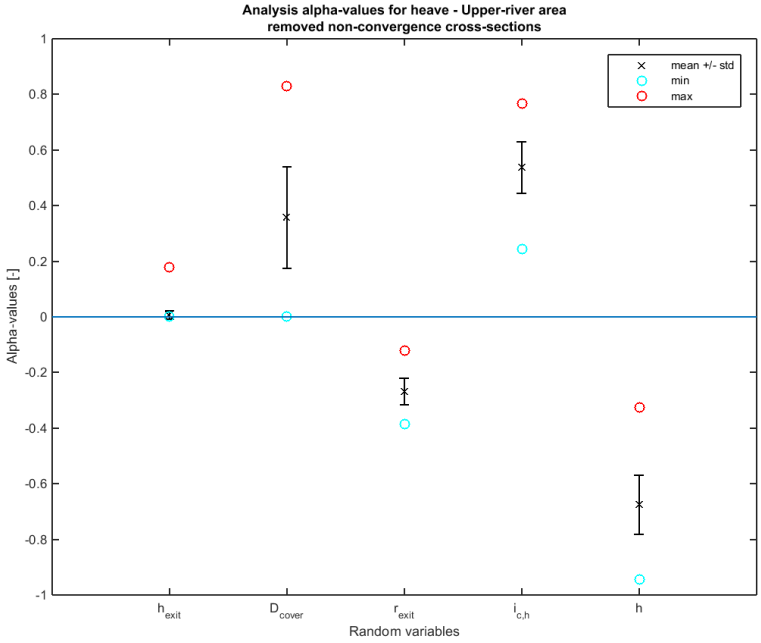

(a) Upper-river area

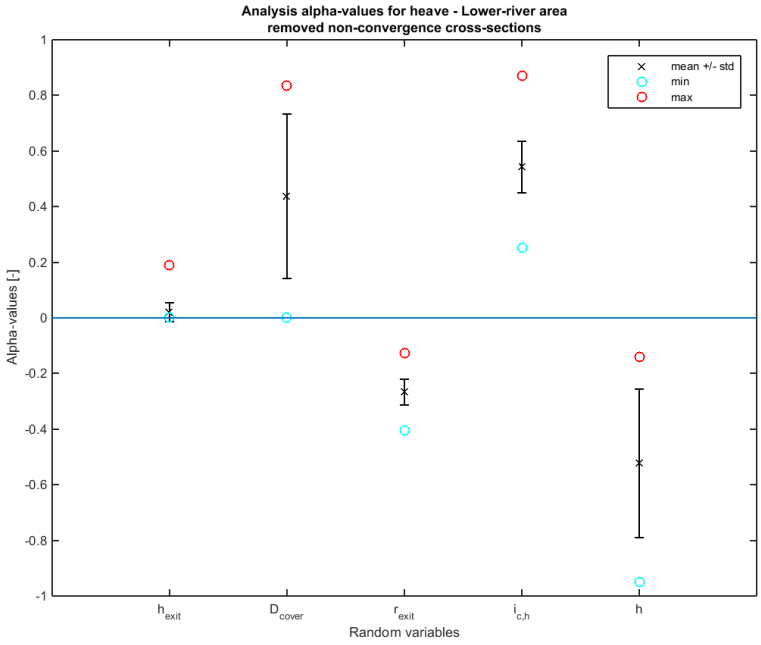

(b) Lower-river area

Figure J.6: Analysis of influence coefficients for $\gamma_{\beta,he}$ = 1.5, heave calibration.

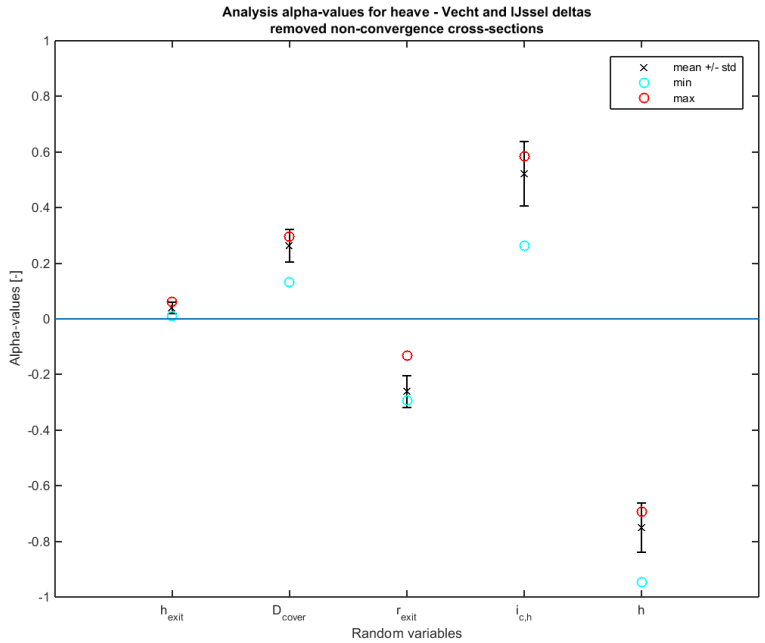

(a) Vecht and IJssel deltas

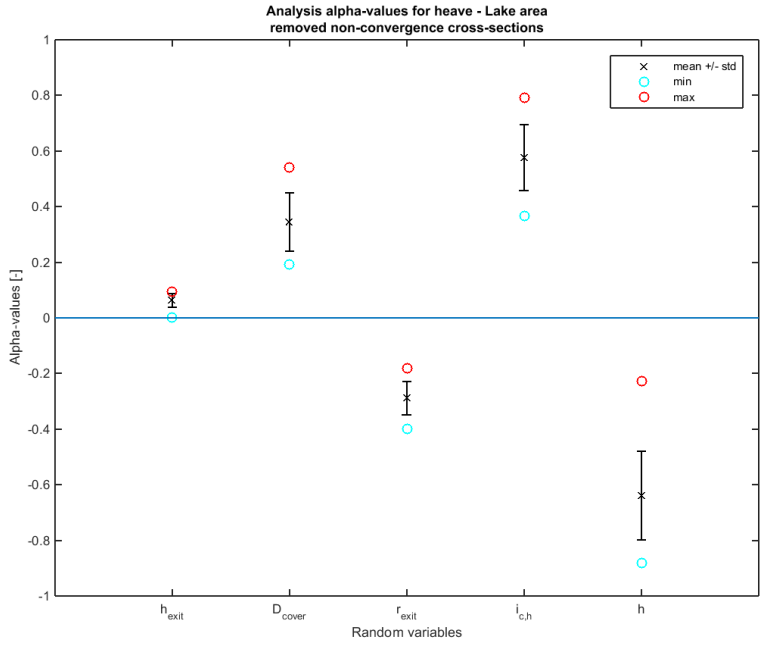

(b) Lake area

Figure J.7: Analysis of influence coefficients for $\gamma_{\beta,he}$ = 1.5, heave calibration.

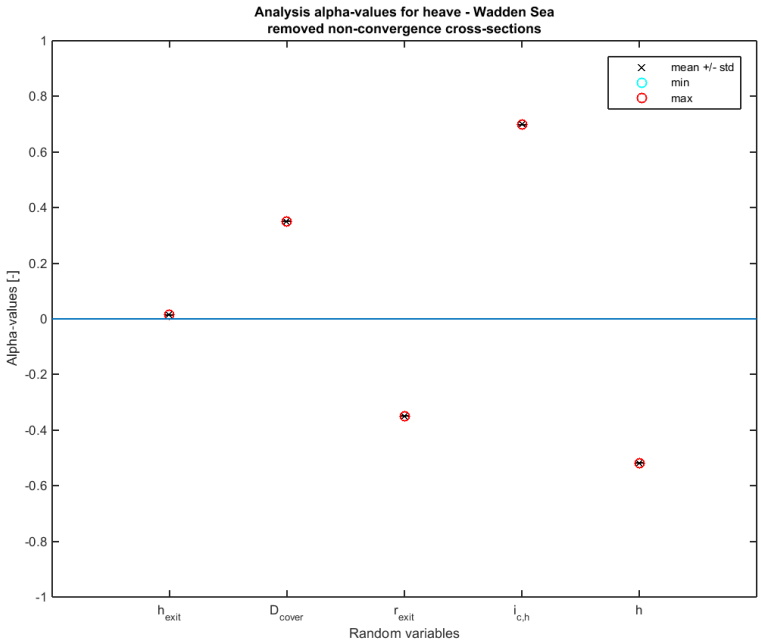

(a) Wadden Sea

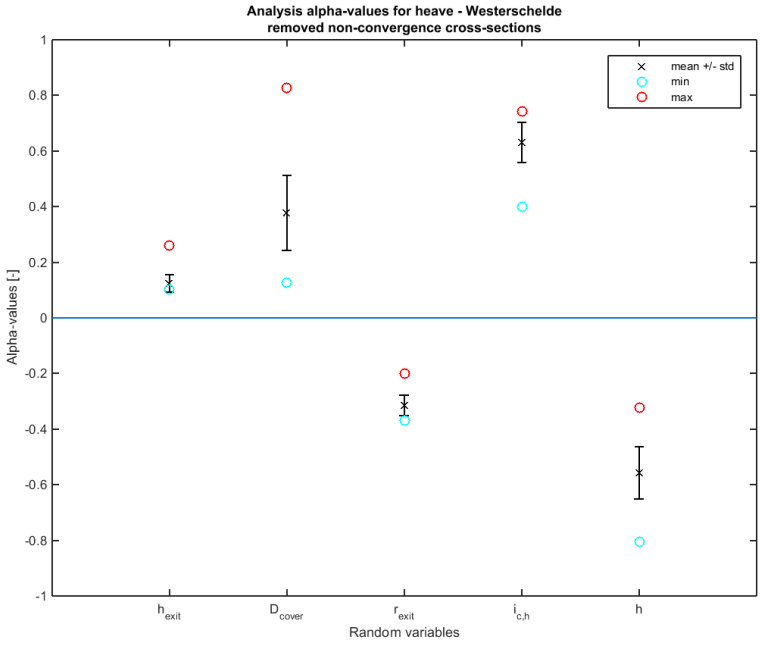

(b) Western Scheldt

Figure J.8: Analysis of influence coefficients for $\gamma_{\beta,he}$ = 1.5, heave calibration.

J.4 Heave - clustering per cover thickness class

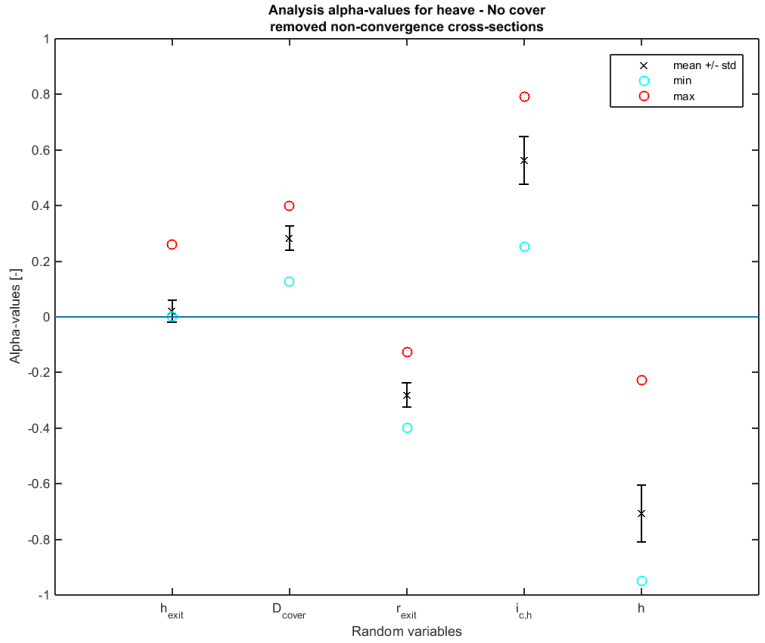

(a) No cover

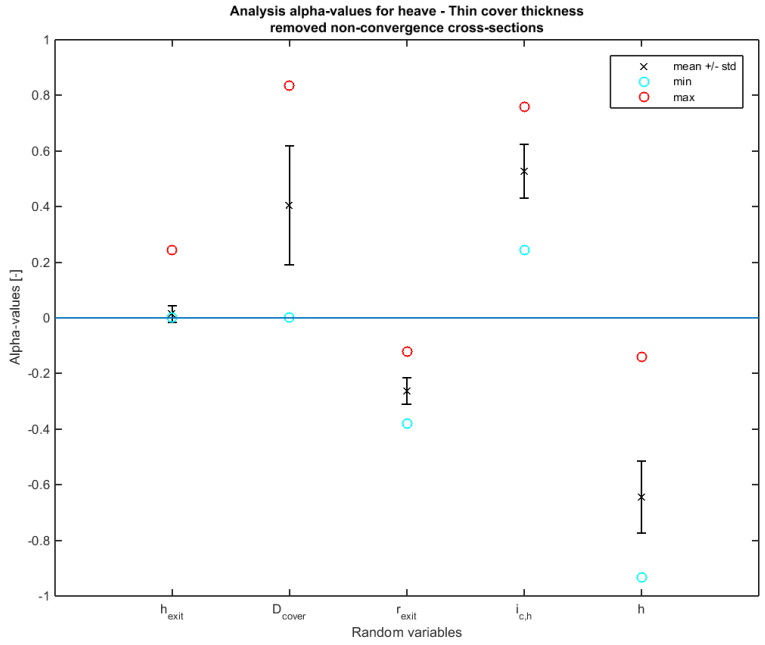

(b) Thin cover thickness

Figure J.9: Analysis of influence coefficients for $\gamma_{\beta,he}$ = 1.5, heave calibration.

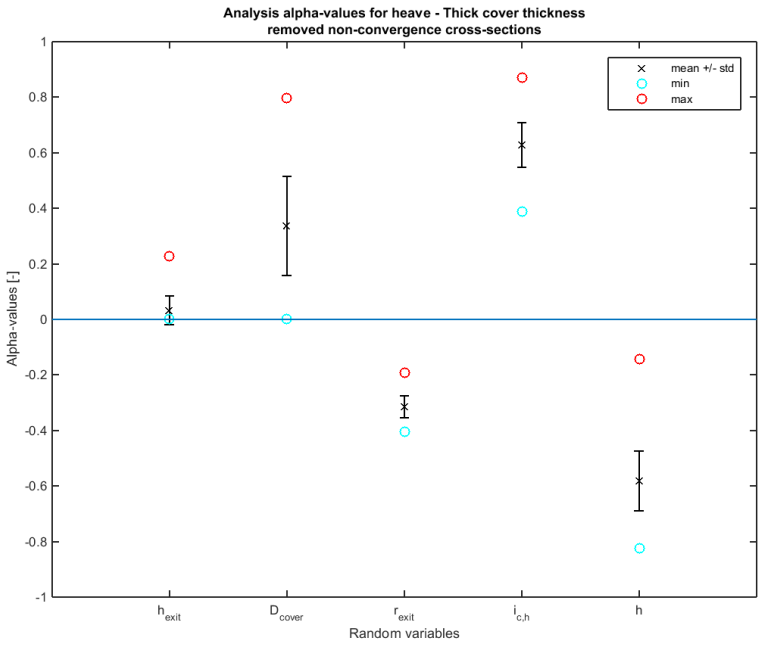

(a) Thick cover thickness

Figure J.10: Analysis of influence coefficients for $\gamma_{\beta,he}$ = 1.5, heave calibration.

J.5 Piping - clustering per water system

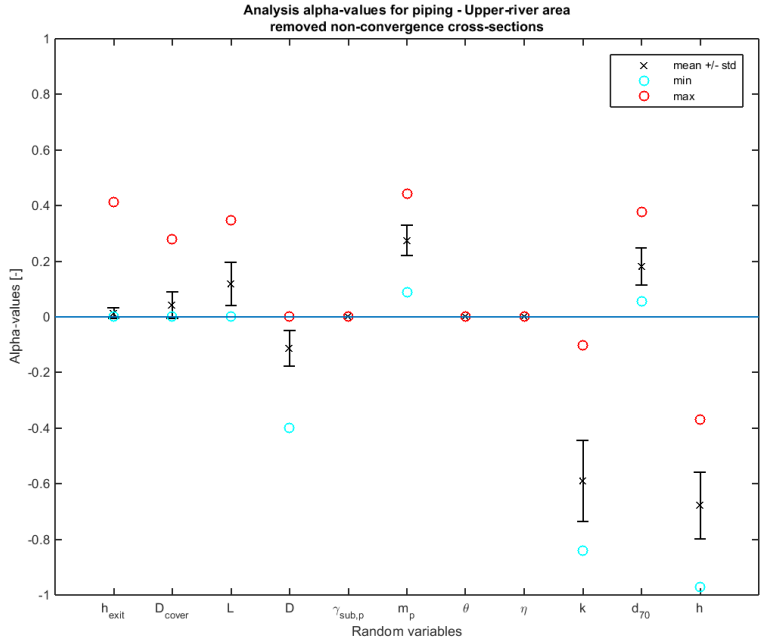

(a) Upper-river area

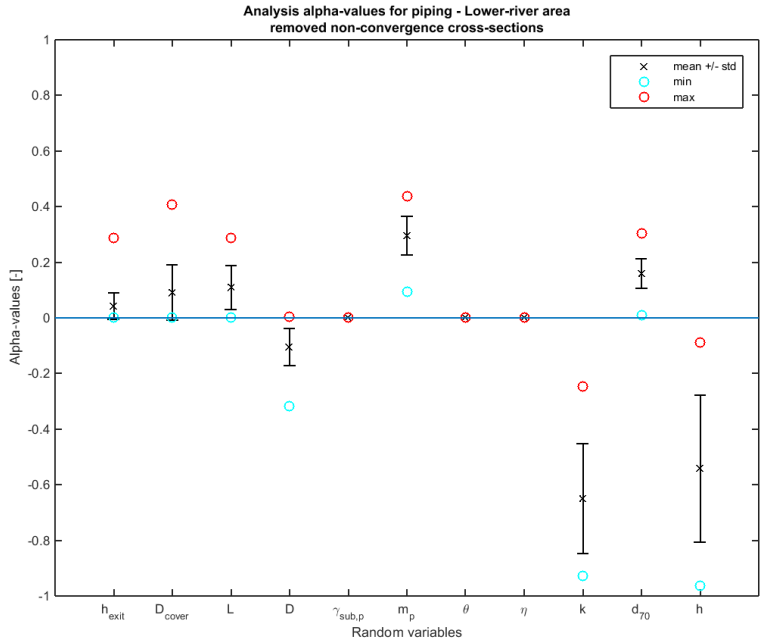

(b) Lower-river area

Figure J.11: Analysis of influence coefficients for $\gamma_{\beta,pip}$ = 1.5, piping calibration.

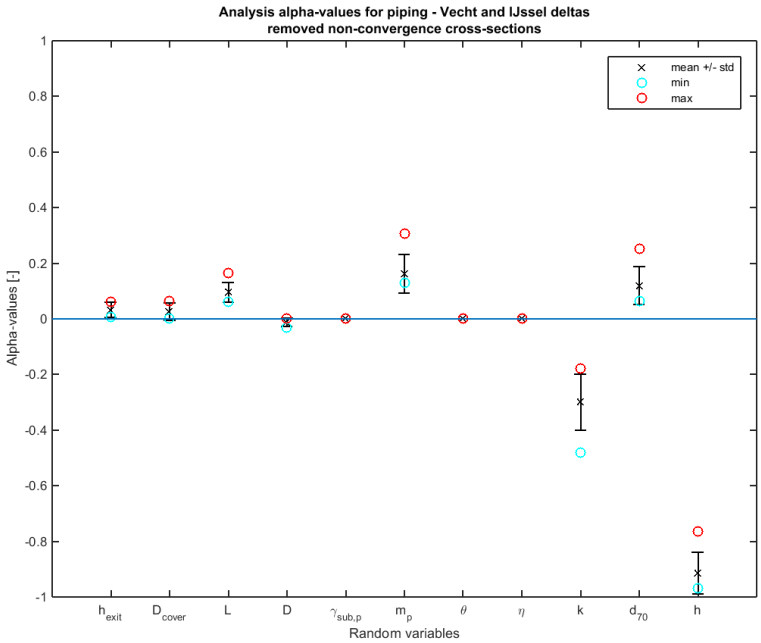

(a) Vecht and IJssel deltas

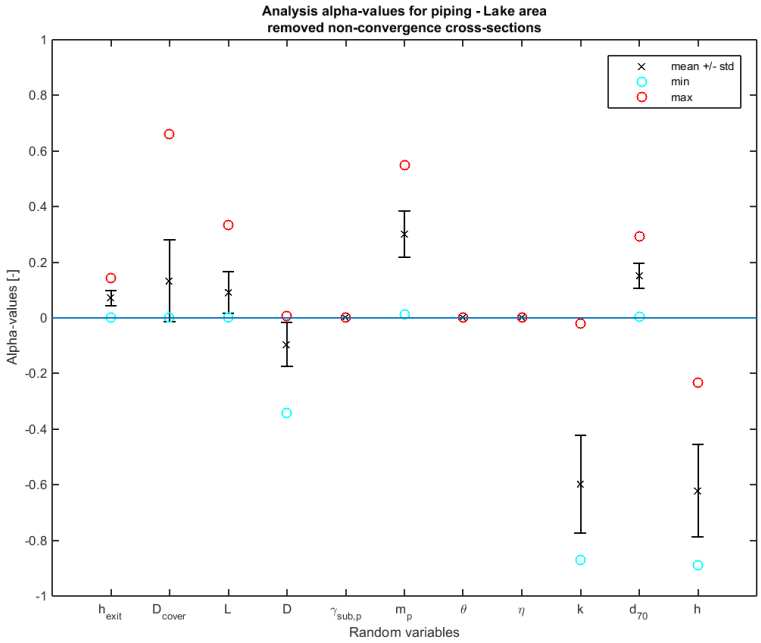

(b) Lake area

Figure J.12: Analysis of influence coefficients for $\gamma_{\beta,pip}$ = 1.5, piping calibration.

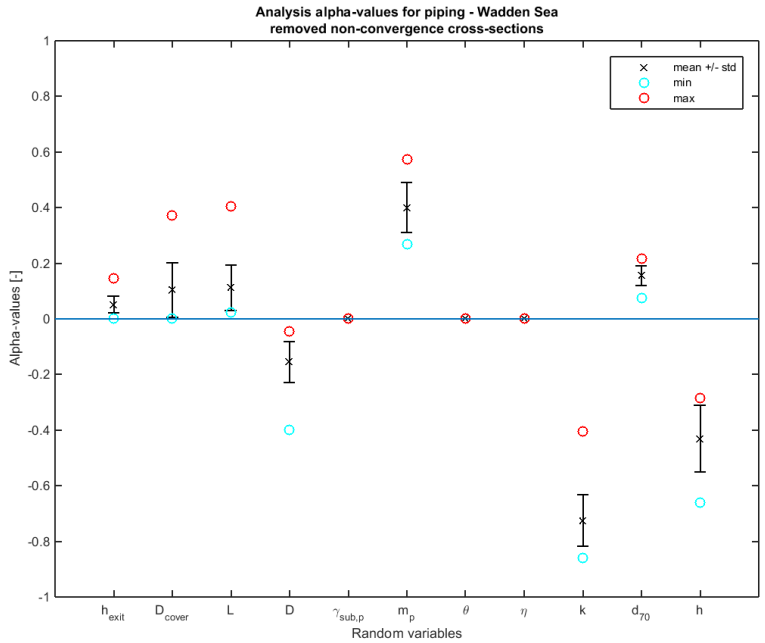

(a) Wadden Sea

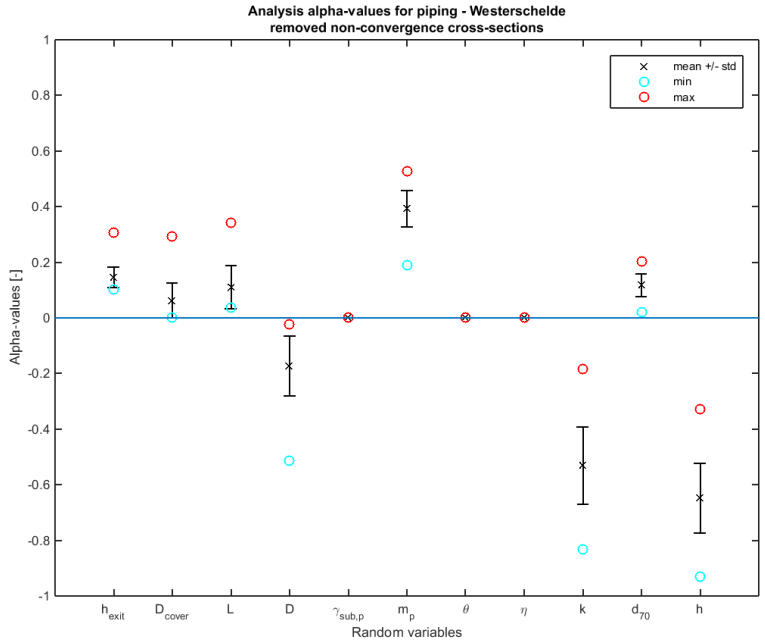

(b) Western Scheldt

Figure J.13: Analysis of influence coefficients for $\gamma_{\beta,pip}$ = 1.5, piping calibration.

J.6 Piping - clustering per cover thickness class

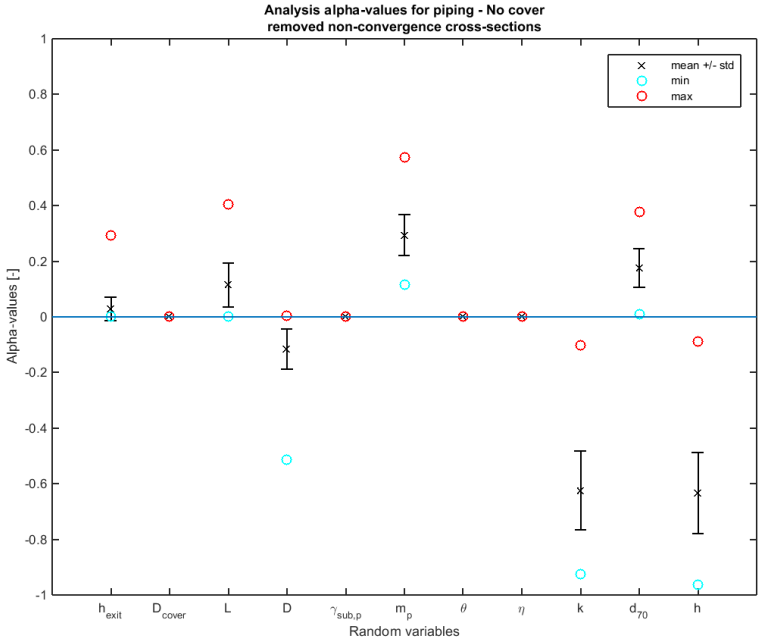

(a) No cover

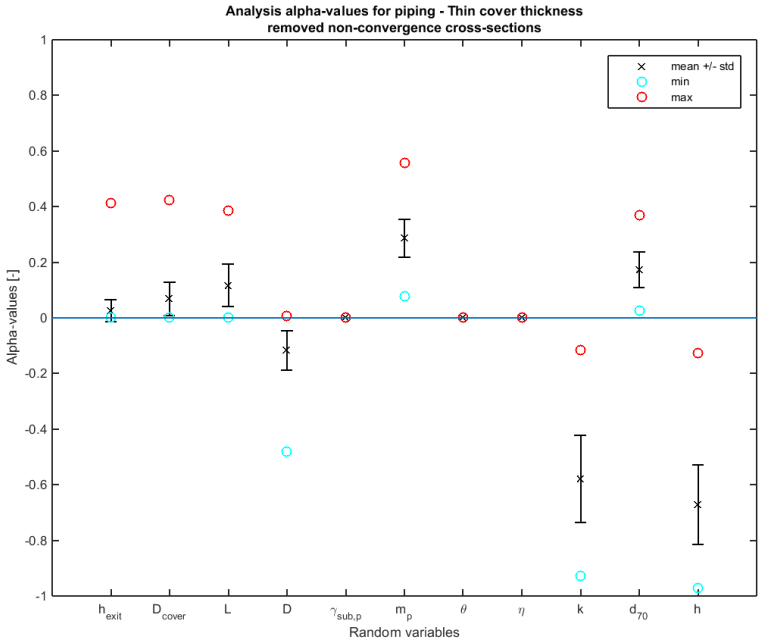

(b) Thin cover thickness

Figure J.14: Analysis of influence coefficients for $\gamma_{\beta,pip}$ = 1.5, piping calibration.

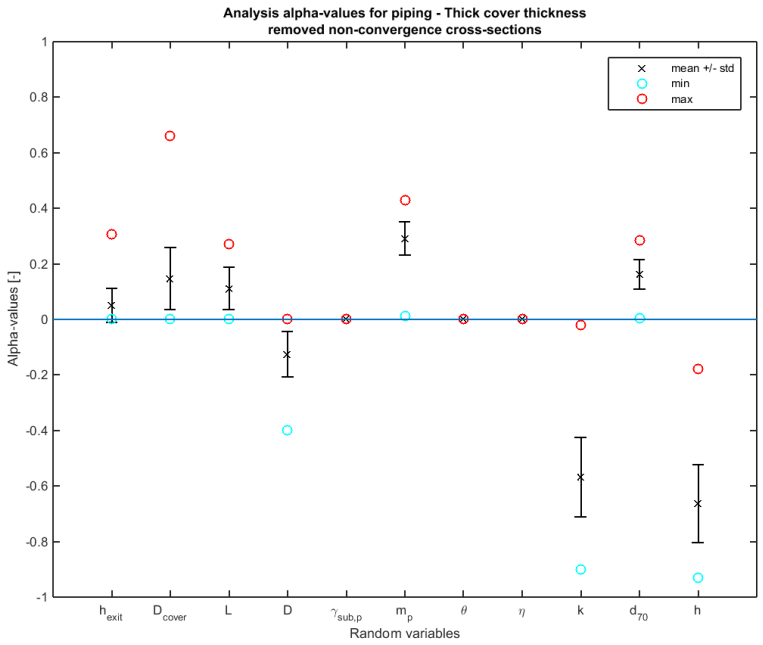

(a) Thick cover thickness

Figure J.15: Analysis of influence coefficients for $\gamma_{\beta,pip}$ = 1.5, piping calibration.

K Variables in the calibration

K.1 Decimate heights

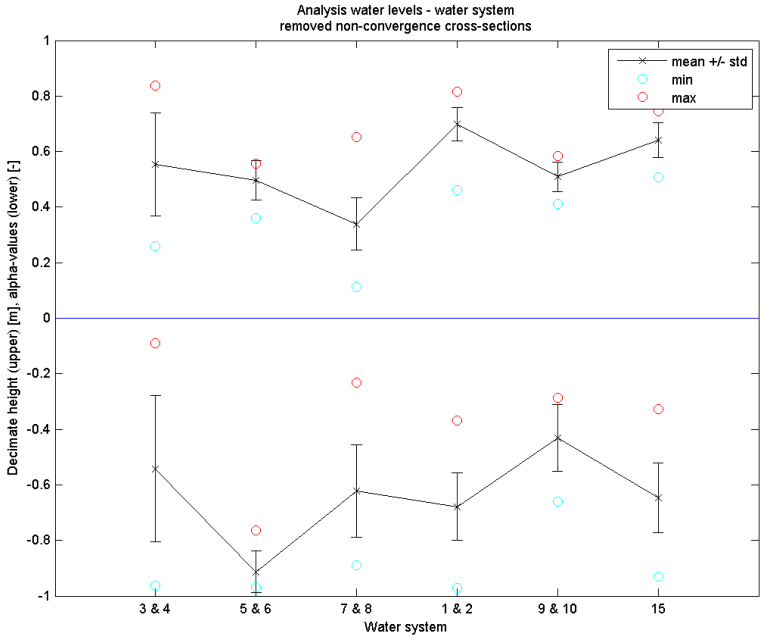

(a) Clustering per water system

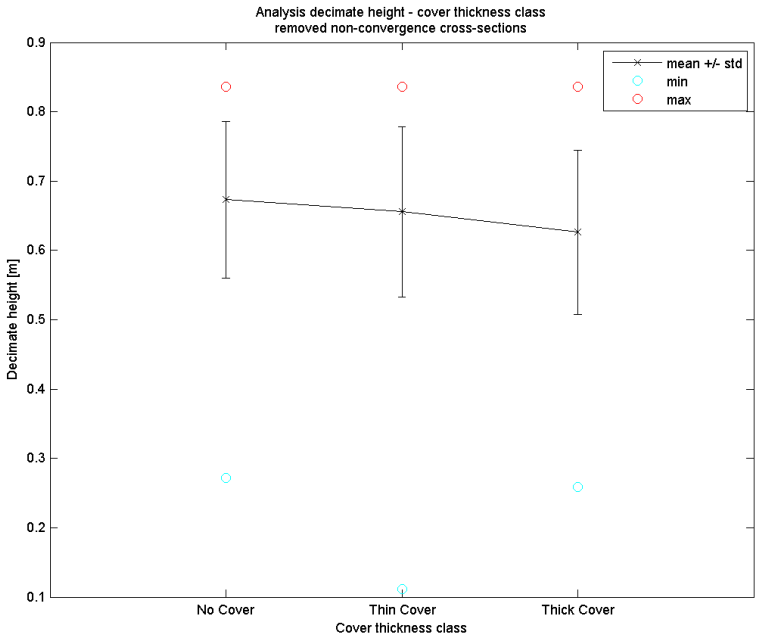

(b) Clustering per cover thickness class

Figure K.1: Decimate heights.

K.2 Uplift - clustering per water system

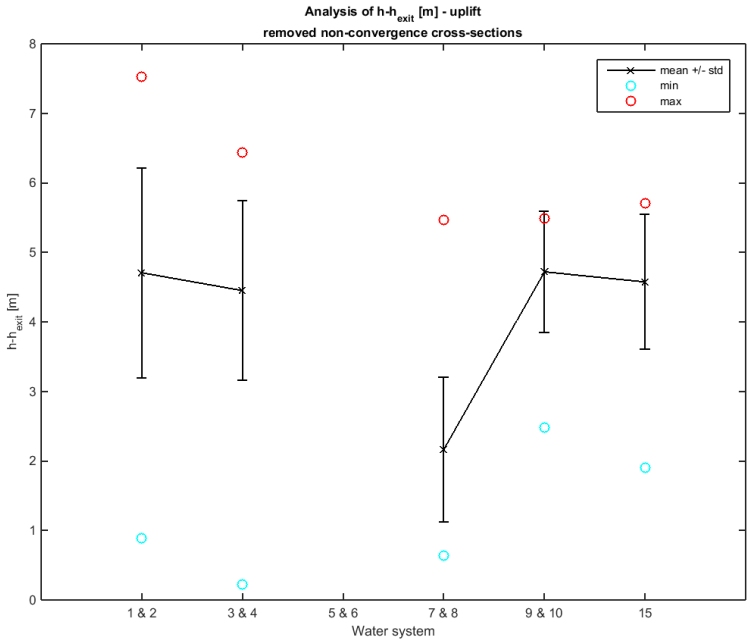

(a) $h - h_{exit}$

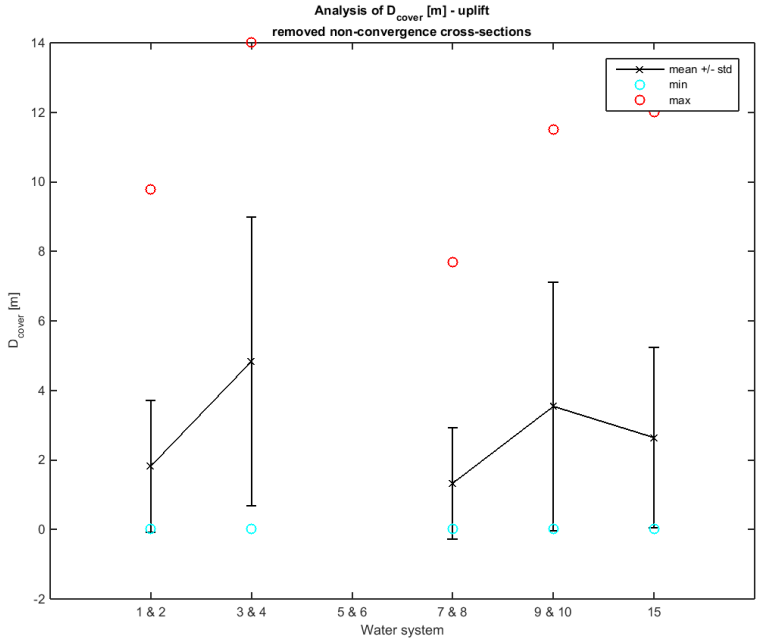

(b) D_{cover}

Figure K.2: Analysis of mean values of variables, uplift calibration.

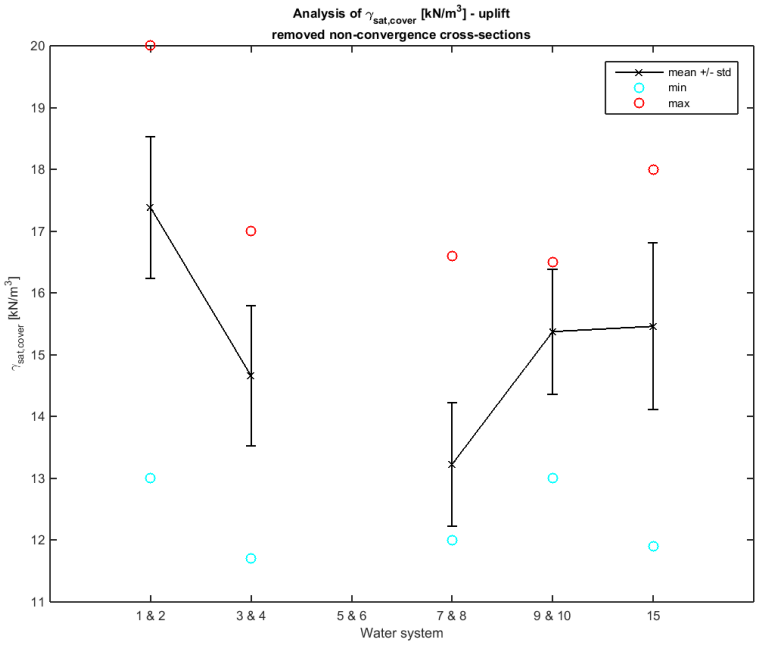

(a) $\gamma_{sat,cover}$

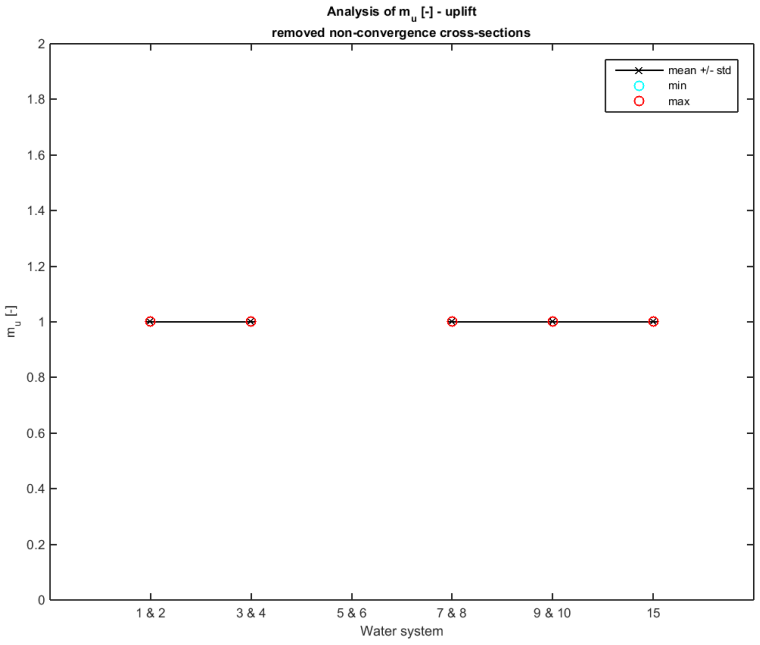

(b) m_u

Figure K.3: Analysis of mean values of variables, uplift calibration.

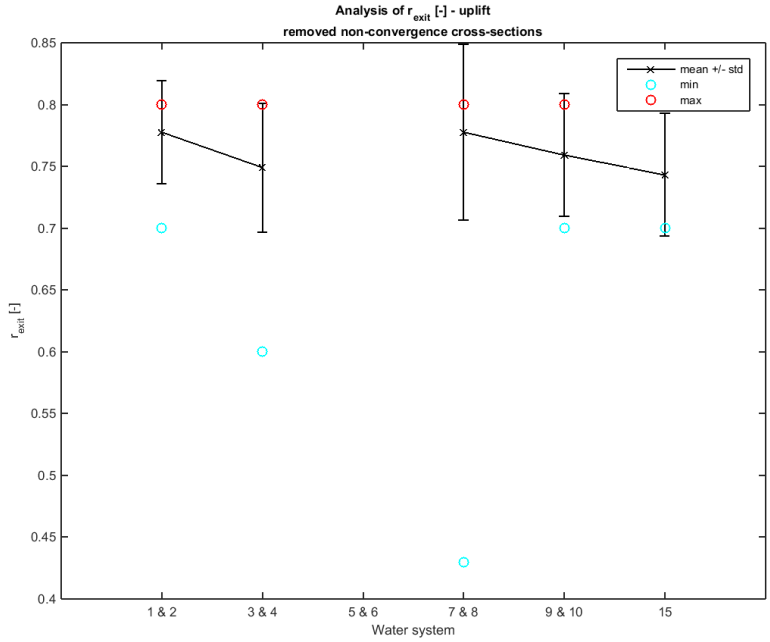

(a) r_{exit}

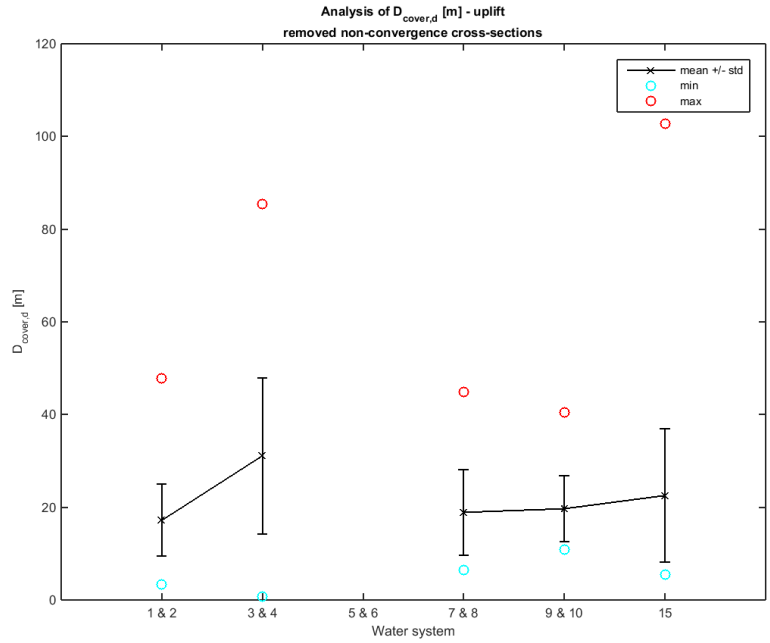

(b) $D_{cover,d}$ *for* $\gamma_{\beta,up}$ *= 1.5*

Figure K.4: Analysis of mean values of variables, uplift calibration.

K.3 Uplift - clustering per cover thickness class

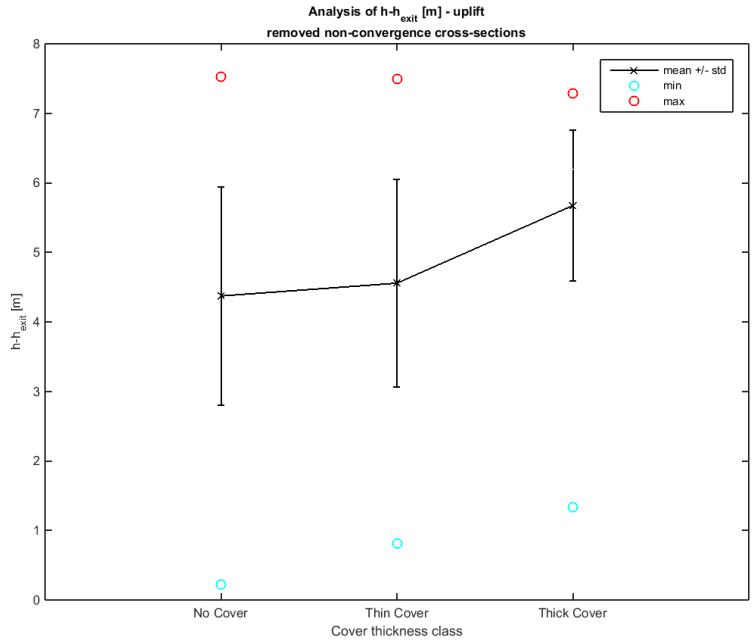

(a) $h - h_{exit}$

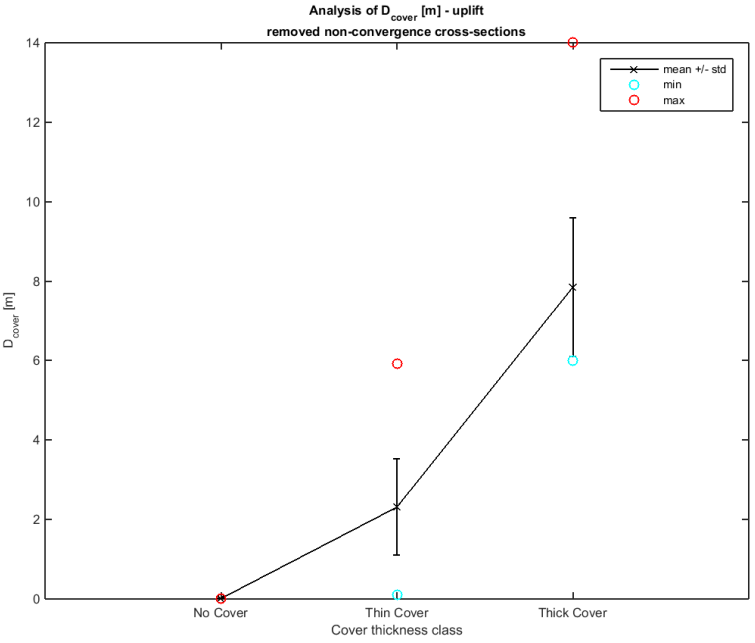

(b) D_{cover}

Figure K.5: Analysis of mean values of variables, uplift calibration.

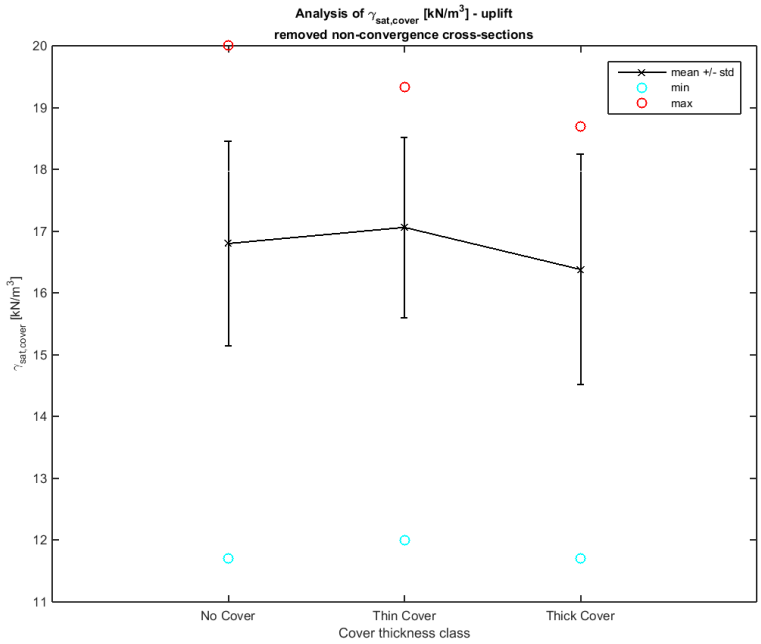

(a) $\gamma_{sat,cover}$

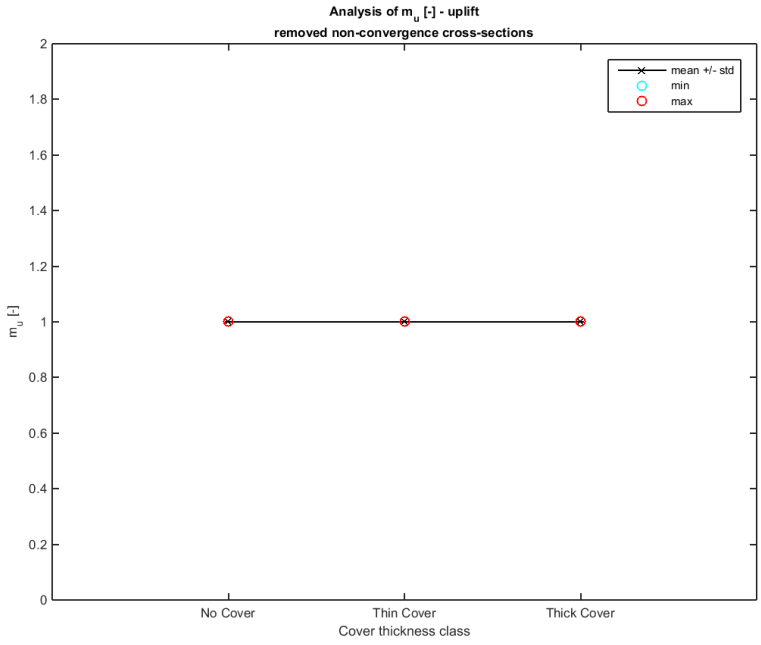

(b) m_u

Figure K.6: Analysis of mean values of variables, uplift calibration.

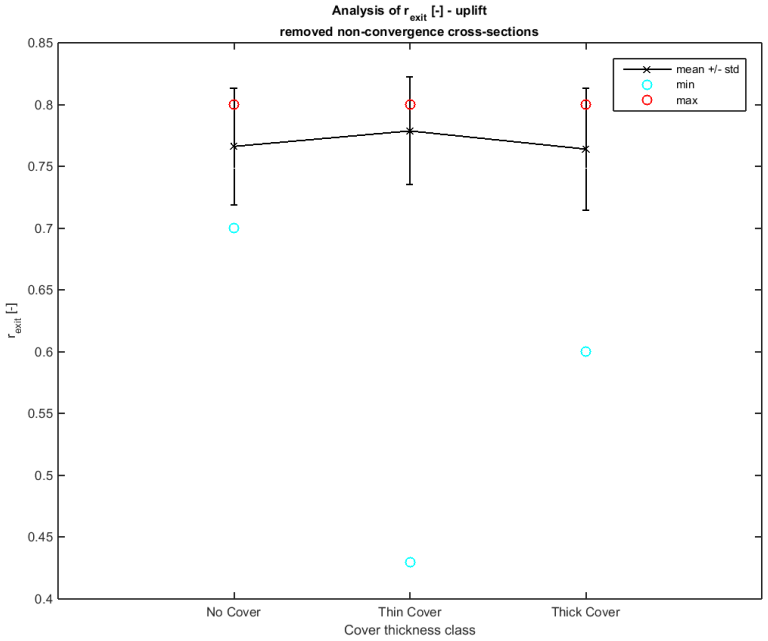

(a) r_{exit}

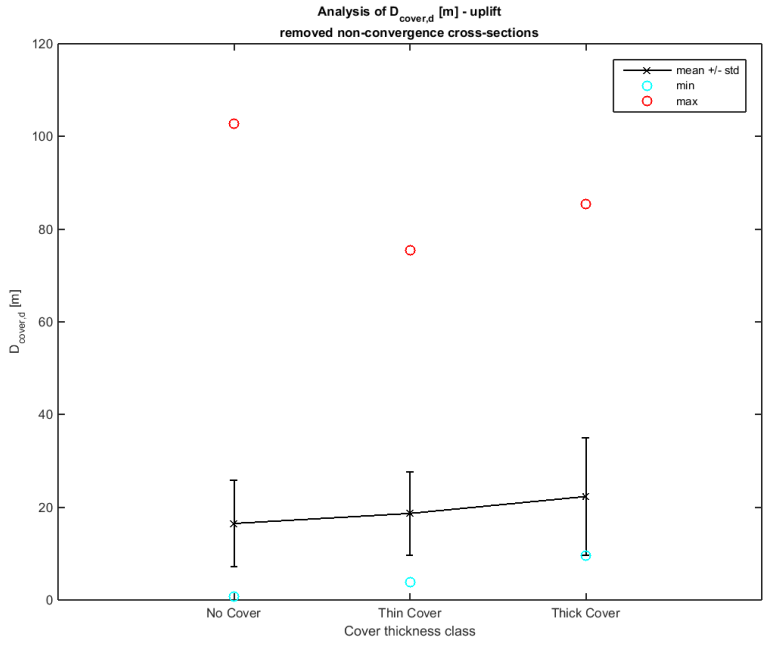

(b) $D_{cover,d}$ *for* $\gamma_{\beta,up}$ *= 1.5*

Figure K.7: Analysis of mean values of variables, uplift calibration.

K.4 Heave - clustering per water system

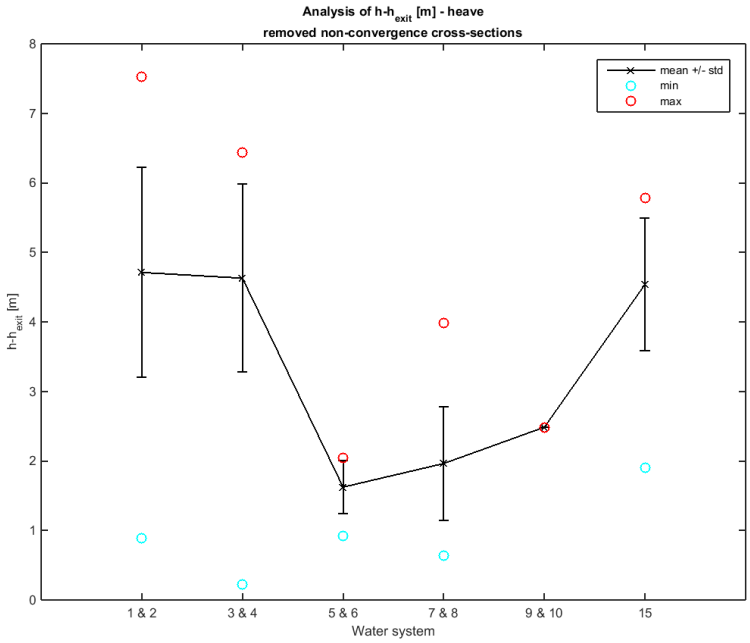

(a) $h - h_{exit}$

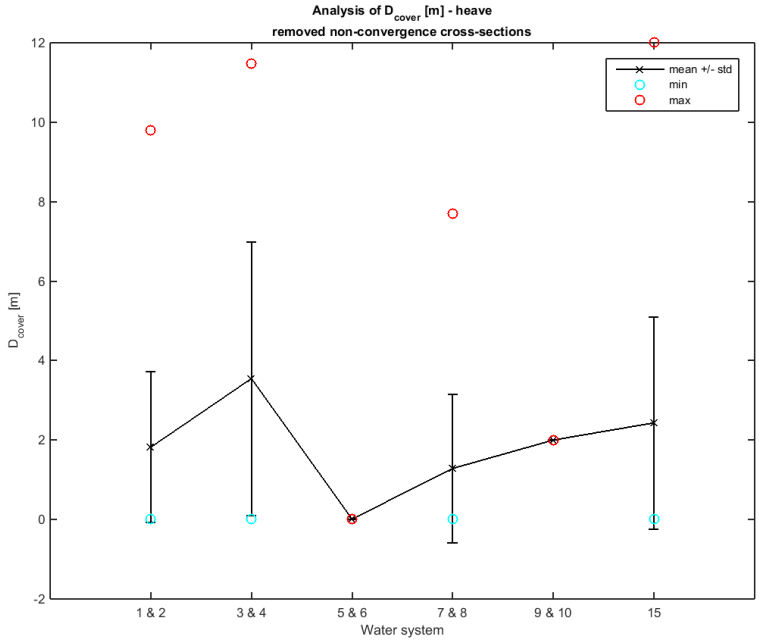

(b) D_{cover}

Figure K.8: Analysis of mean values of variables, heave calibration.

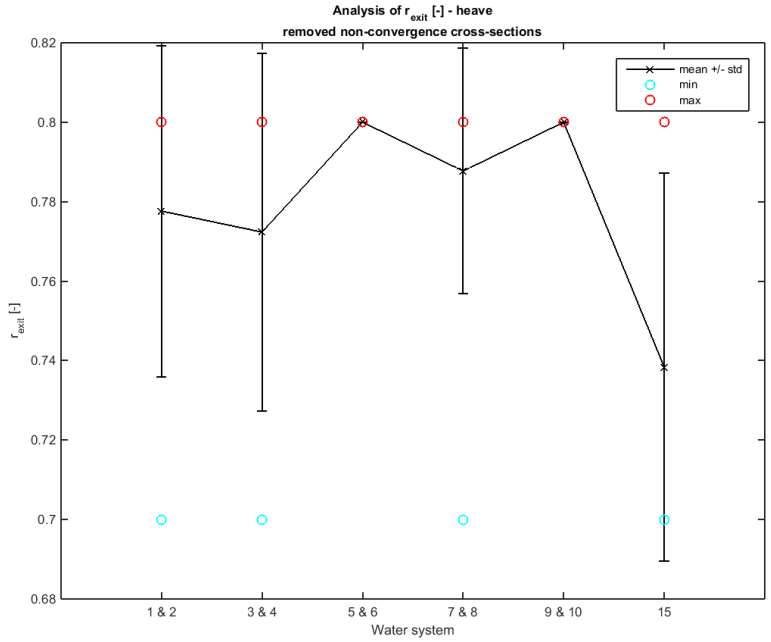

(a) r_{exit}

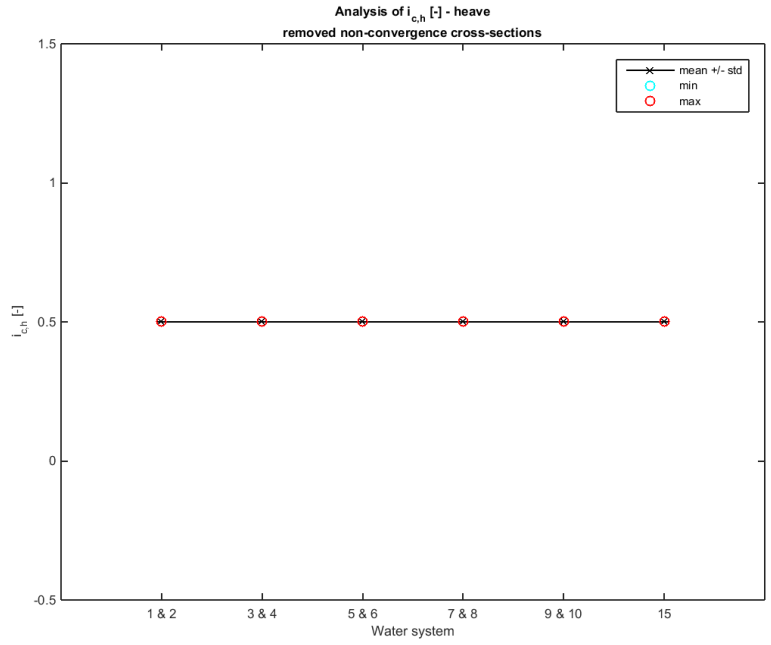

(b) $i_{c,h}$

Figure K.9: Analysis of mean values of variables, heave calibration.

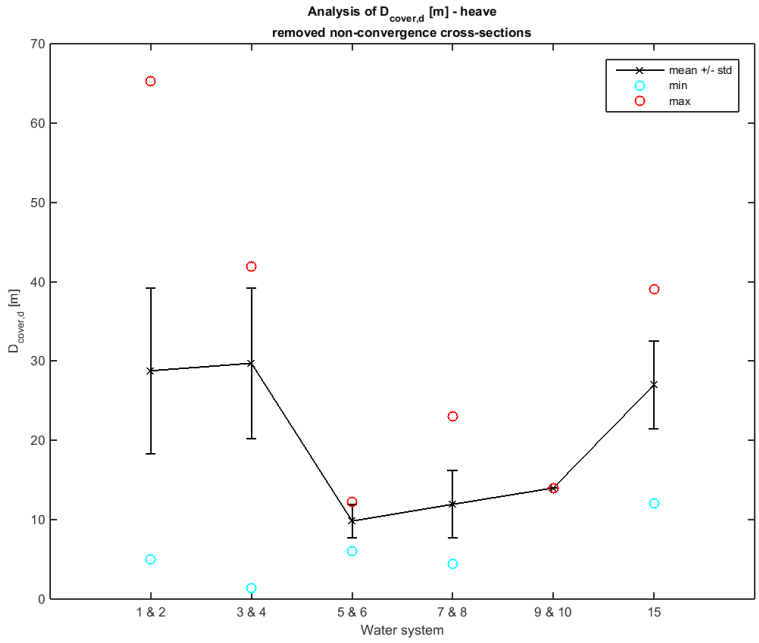

(a) $D_{cover,d}$ *for* $\gamma_{\beta,he}$ *= 1.5*

Figure K.10: Analysis of mean values of variables, heave calibration.

K.5 Heave - clustering per cover thickness class

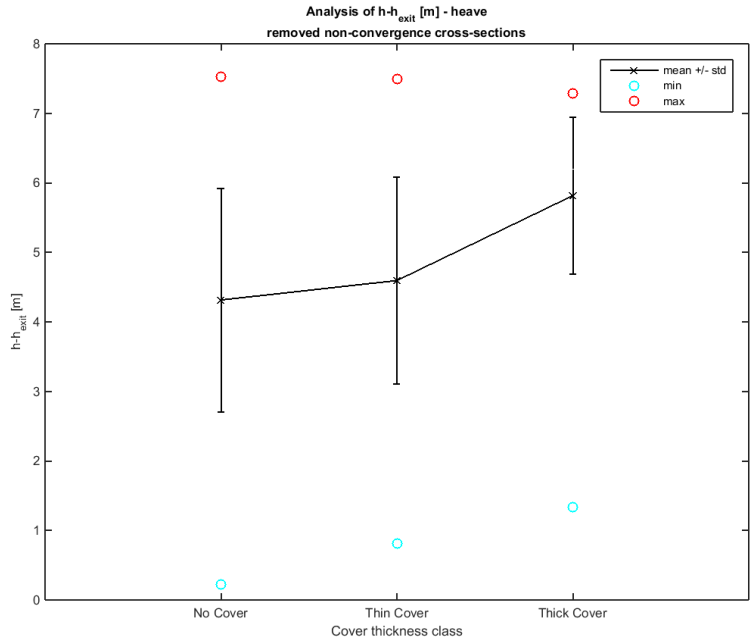

(a) $h - h_{exit}$

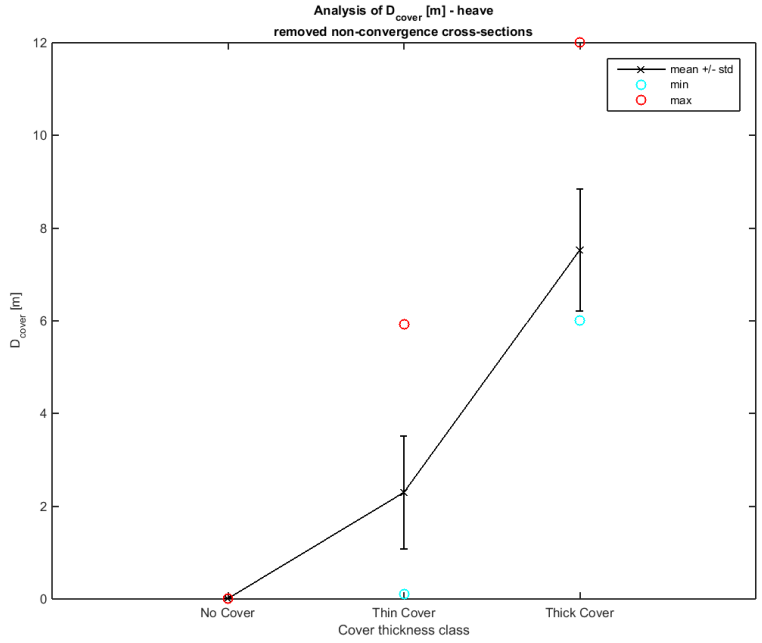

(b) D_{cover}

Figure K.11: Analysis of mean values of variables, heave calibration.

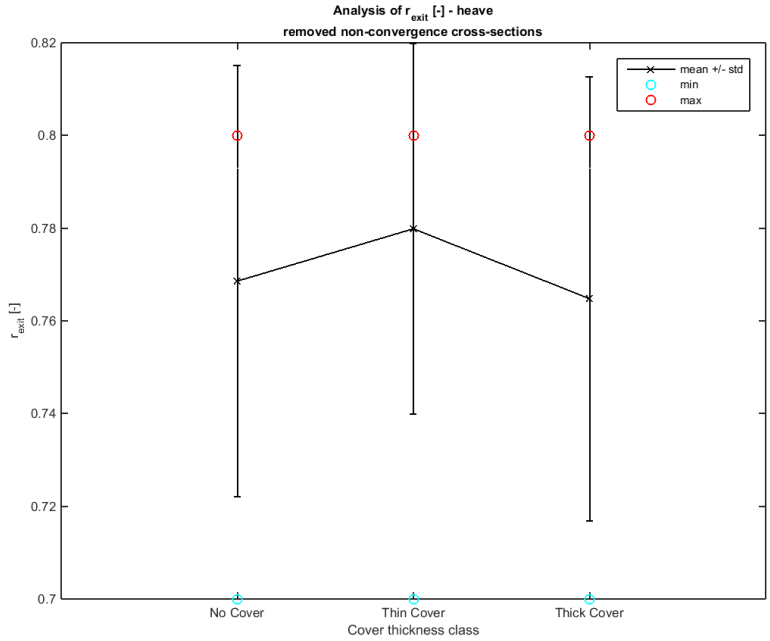

(a) r_{exit}

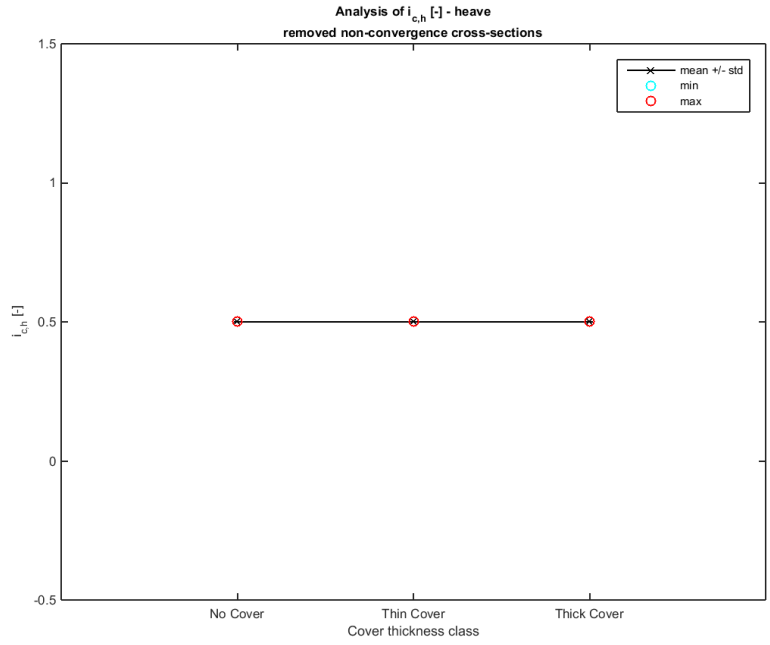

(b) $i_{c,h}$

Figure K.12: Analysis of mean values of variables, heave calibration.

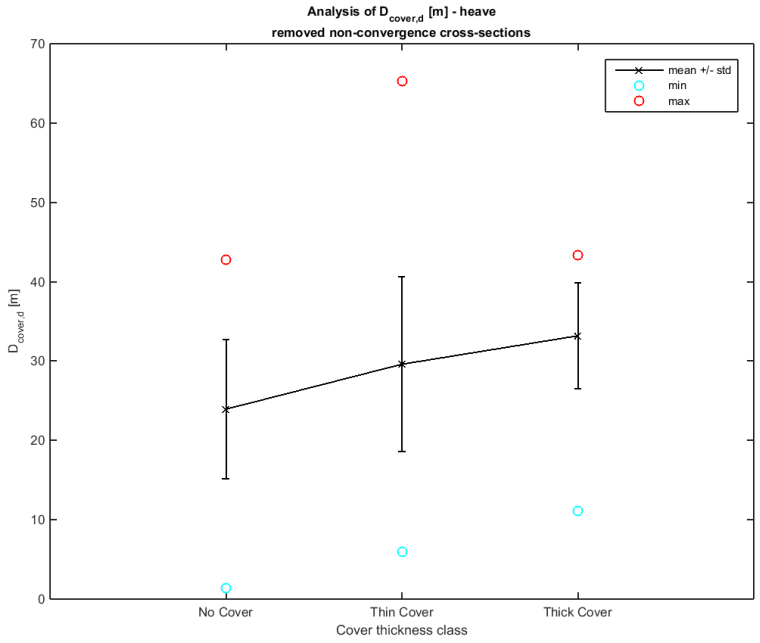

(a) $D_{cover,d}$ *for* $\gamma_{\beta,he}$ *= 1.5*

Figure K.13: Analysis of mean values of variables, heave calibration.

K.6 Piping - clustering per water system

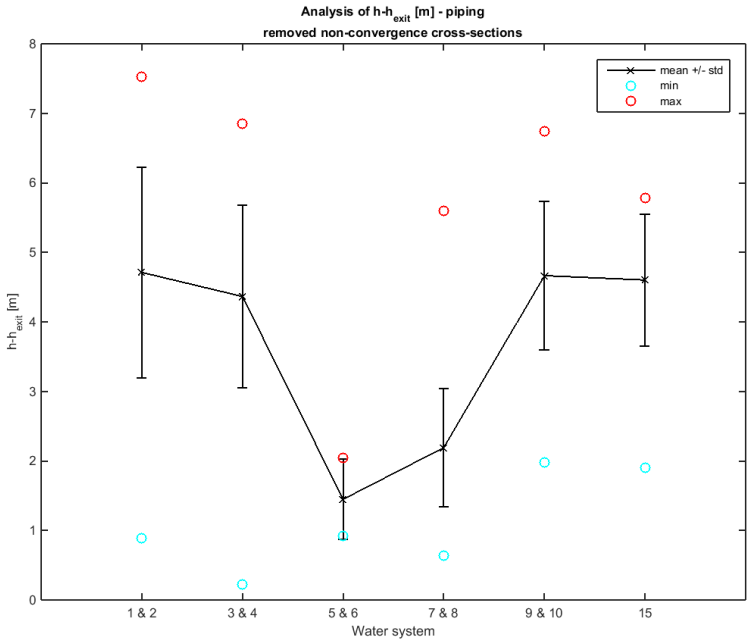

(a) $h - h_{exit}$

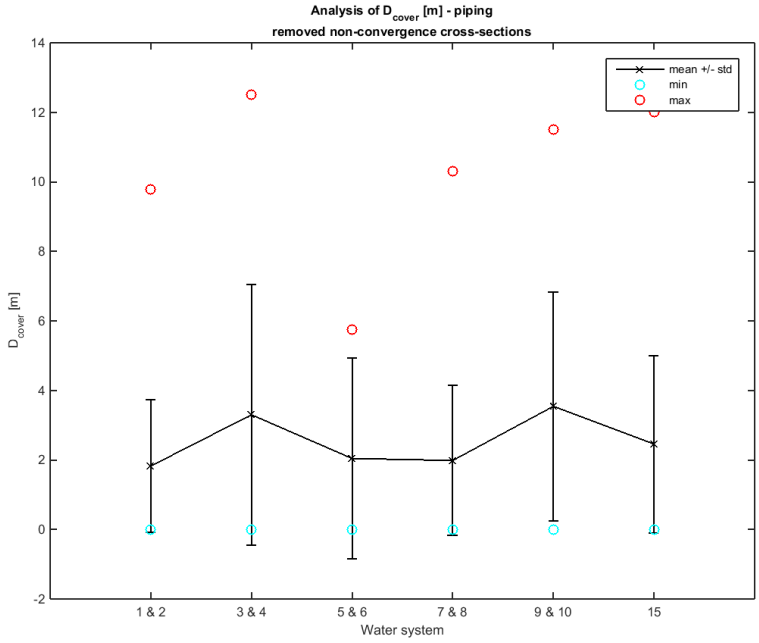

(b) D_{cover}

Figure K.14: Analysis of mean values of variables, piping calibration.

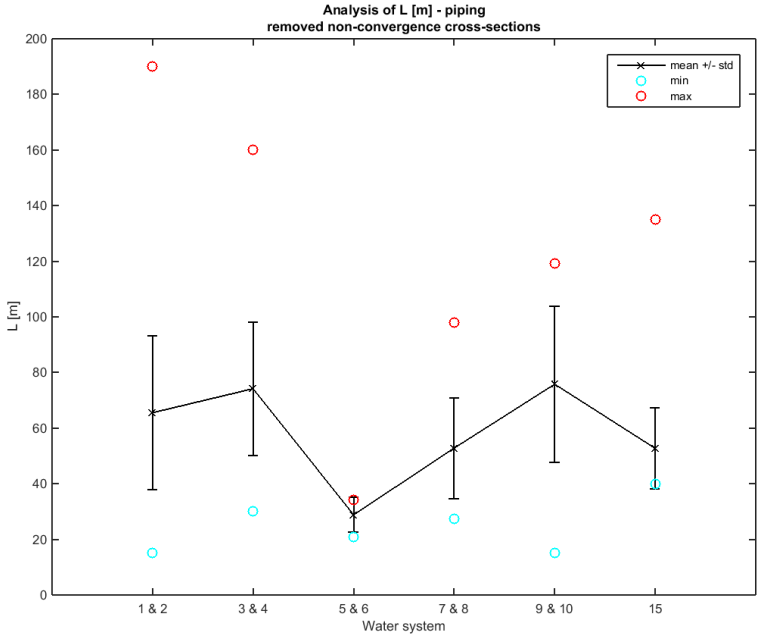

(a) L

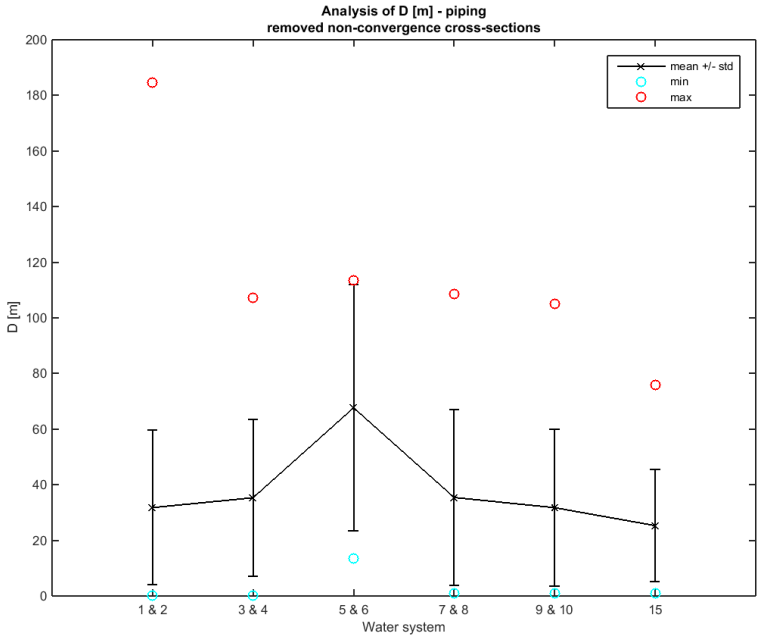

(b) D

Figure K.15: Analysis of mean values of variables, piping calibration.

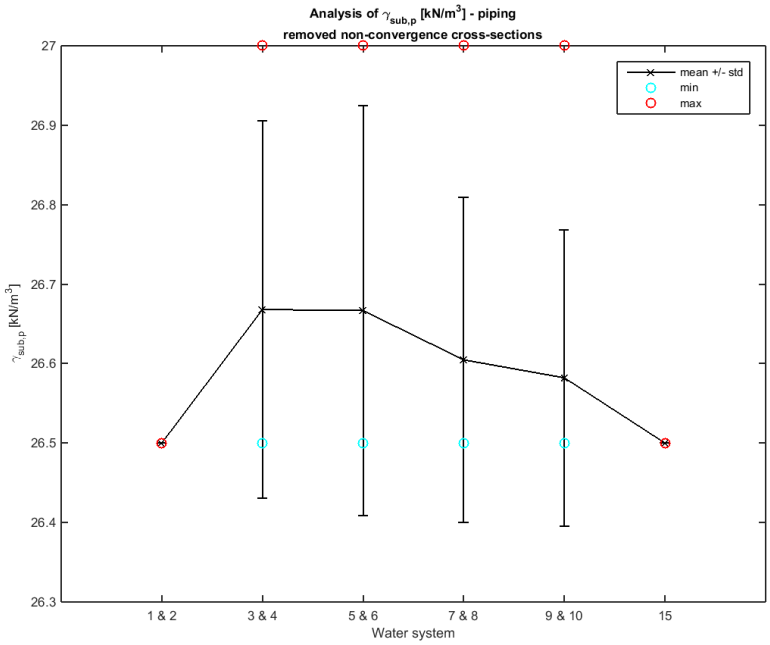

(a) $\gamma_{sub,p}$

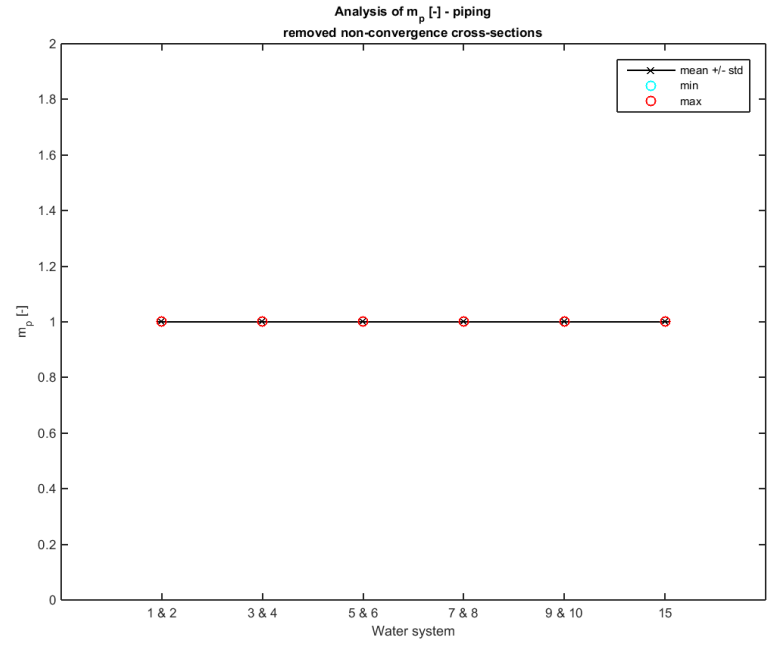

(b) m_p

Figure K.16: Analysis of mean values of variables, piping calibration.

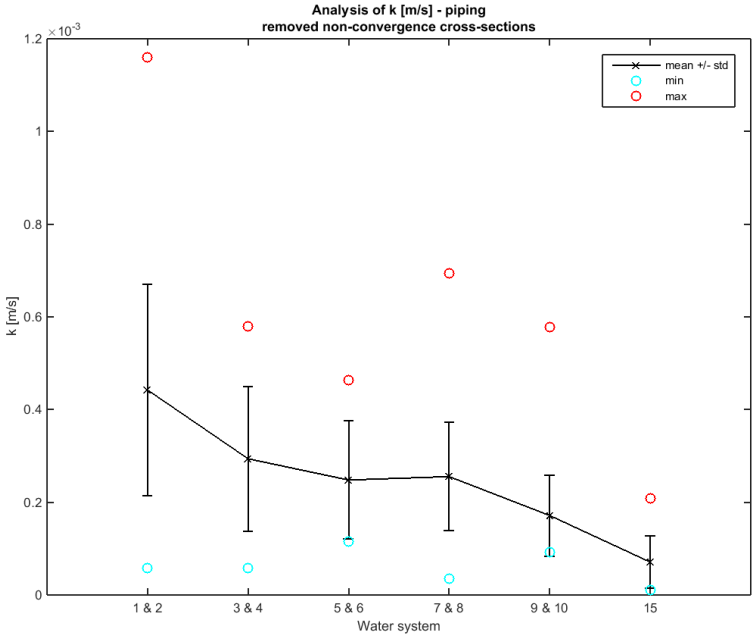

(a) k

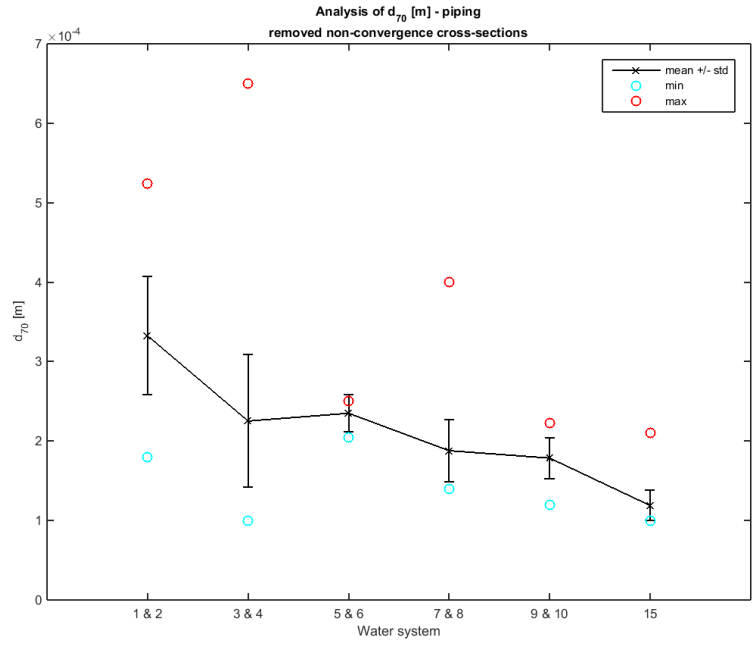

(b) d_{70}

Figure K.17: Analysis of mean values of variables, piping calibration.

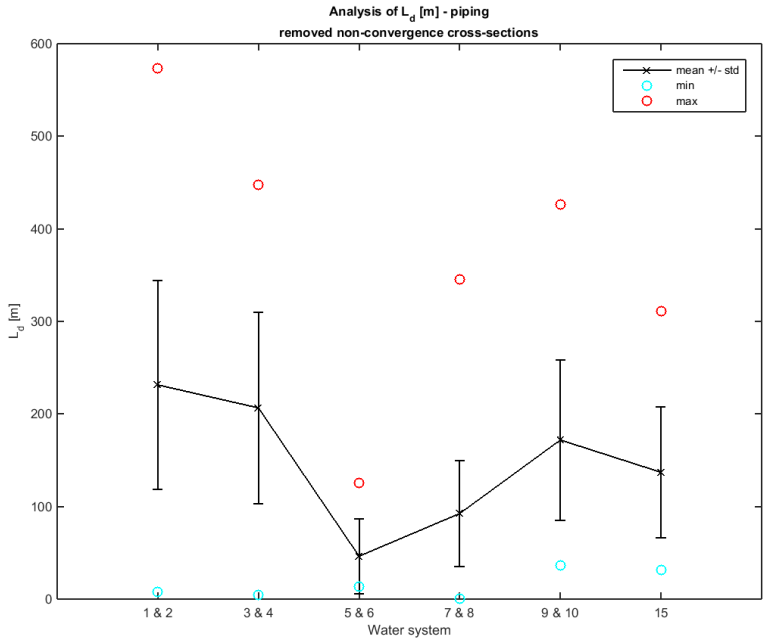

(a) L_d for $\gamma_{\beta,pip}$ = 1.5

Figure K.18: Analysis of mean values of variables, piping calibration.

K.7 Piping - clustering per cover thickness class

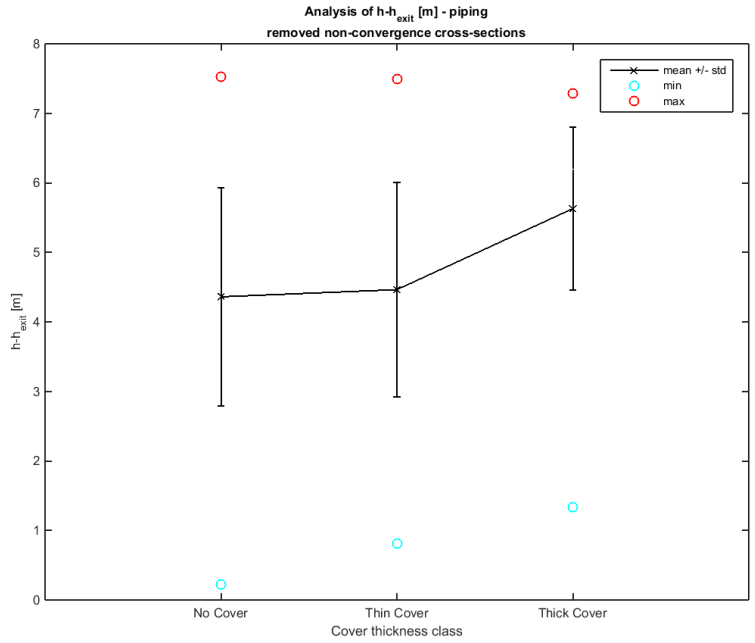

(a) $h - h_{exit}$

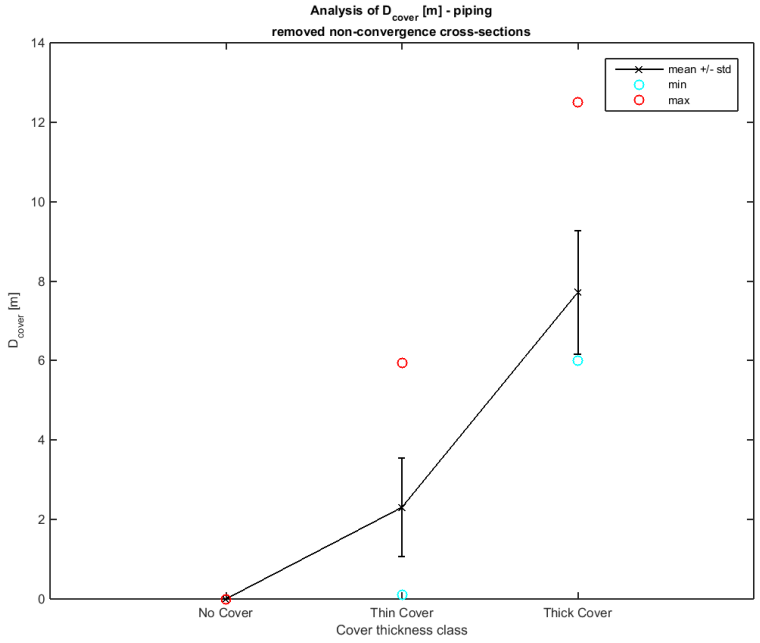

(b) D_{cover}

Figure K.19: Analysis of mean values of variables, piping calibration.

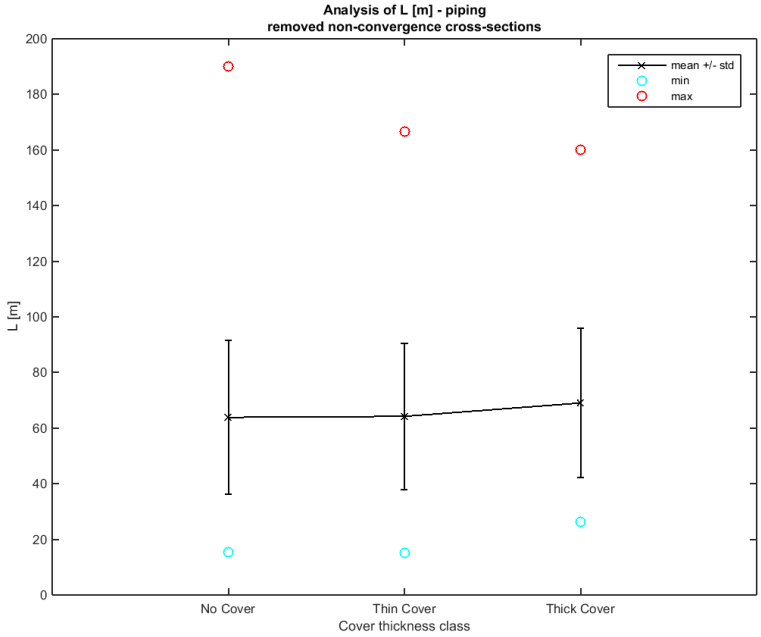

(a) L

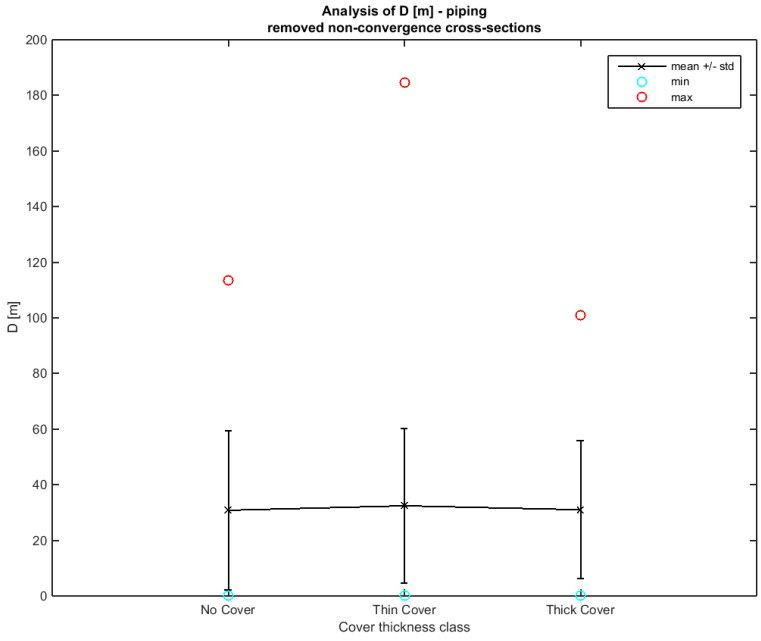

(b) D

Figure K.20: Analysis of mean values of variables, piping calibration.

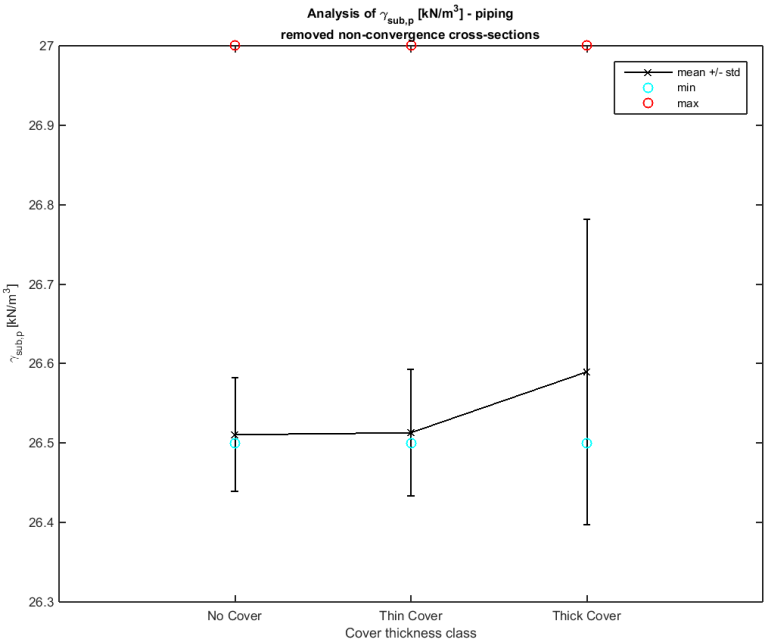

(a) $\gamma_{sub,p}$

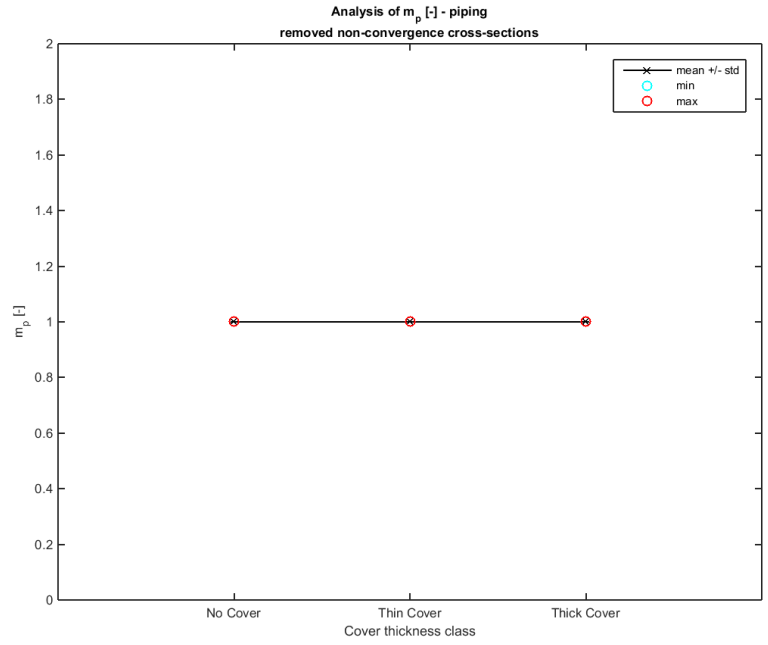

(b) m_p

Figure K.21: Analysis of mean values of variables, piping calibration.

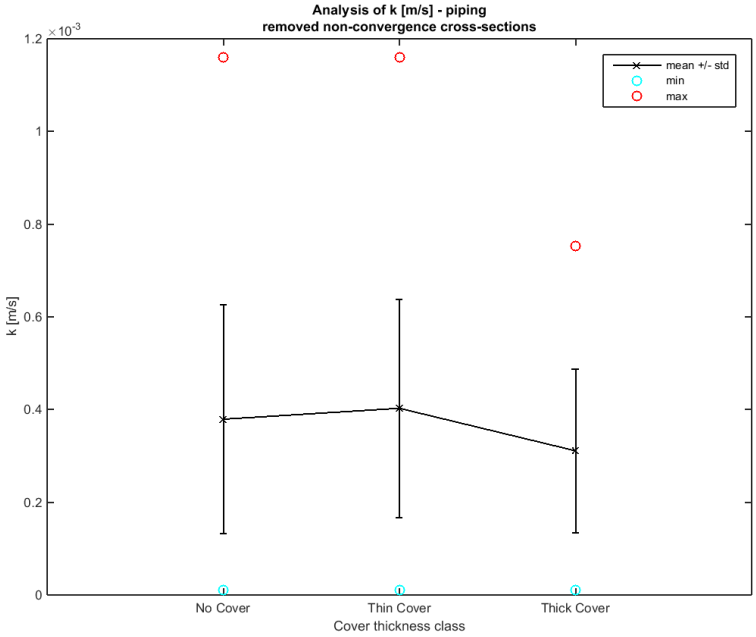

(a) k

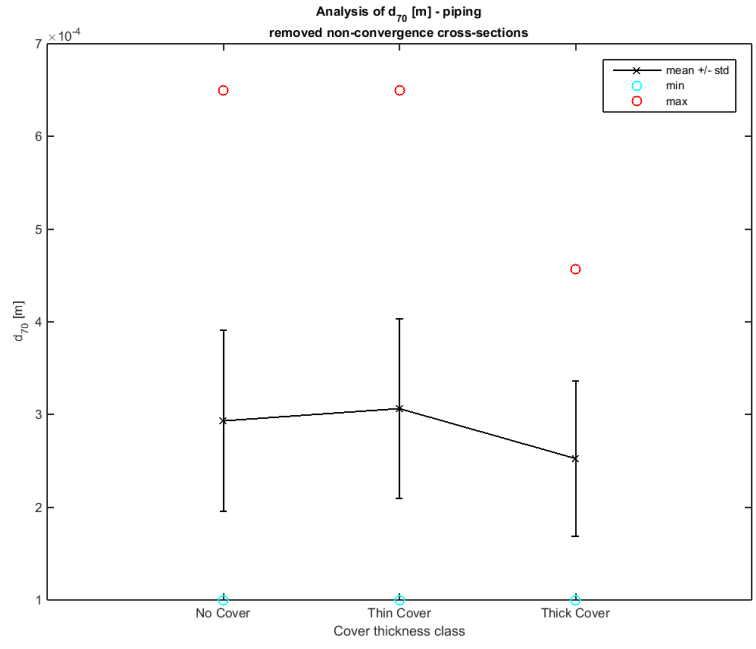

(b) d_{70}

Figure K.22: Analysis of mean values of variables, piping calibration.

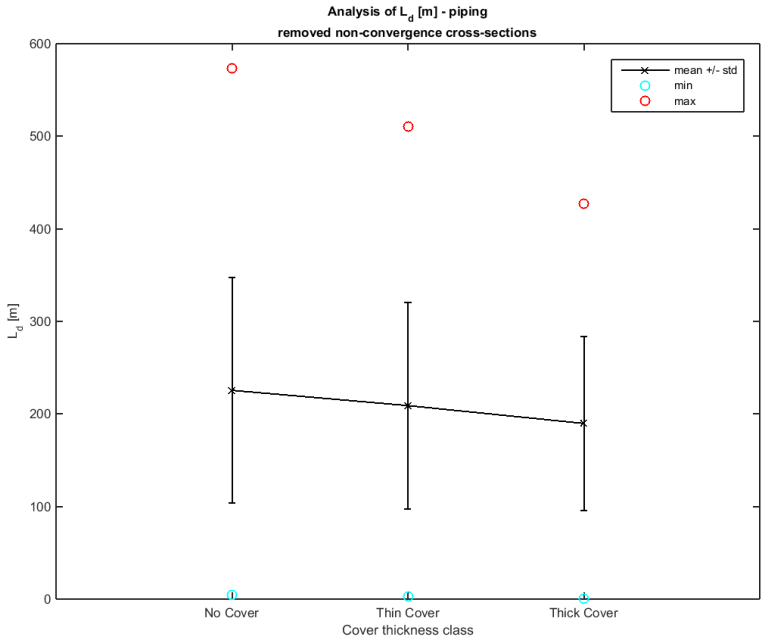

(a) L_d *for* $\gamma_{\beta,pip}$ *= 1.5*

Figure K.23: Analysis of mean values of variables, piping calibration.

L Uplift: calibration results and cluster alternatives - Case 1

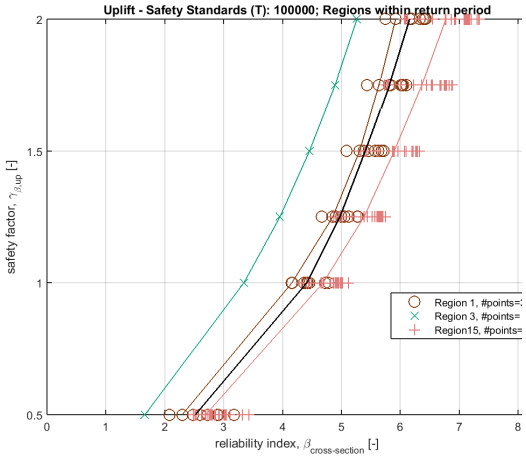

(a) Return period T = 300 years

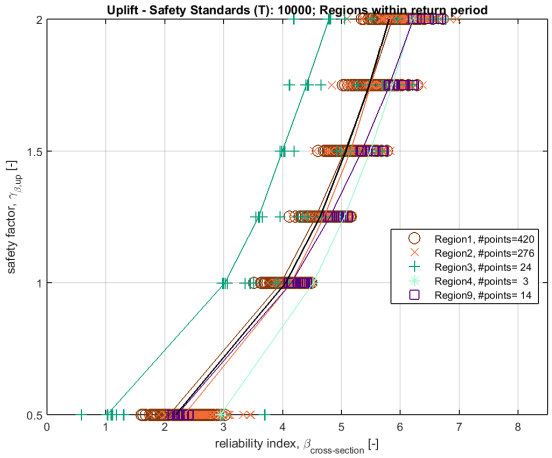

(b) Return period T = 1,000 years

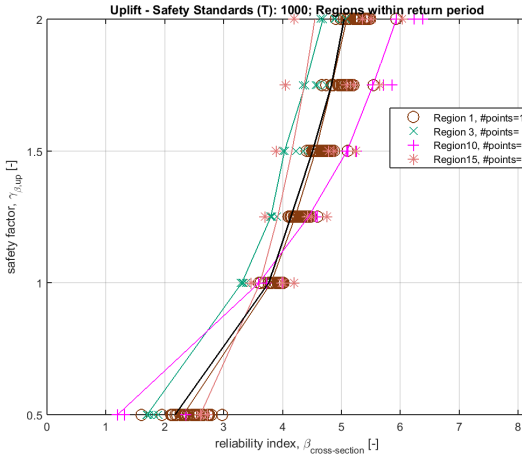

(c) Return period T = 3,000 years

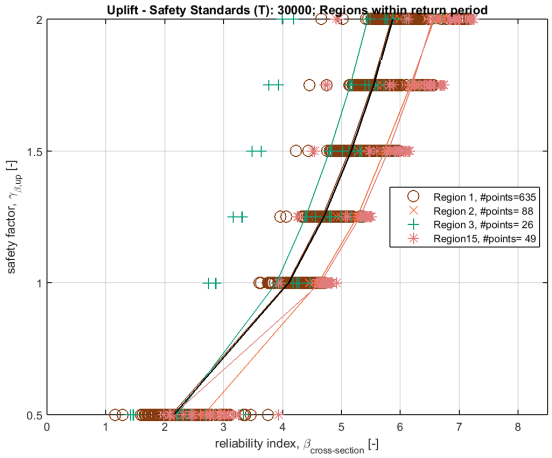

(d) Return period T = 10,000 years

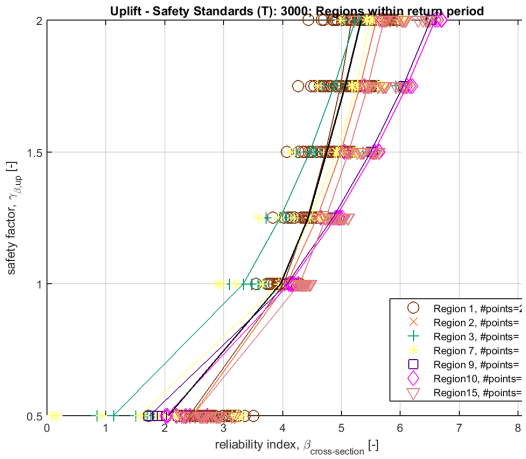

(e) Return period T = 30,000 years

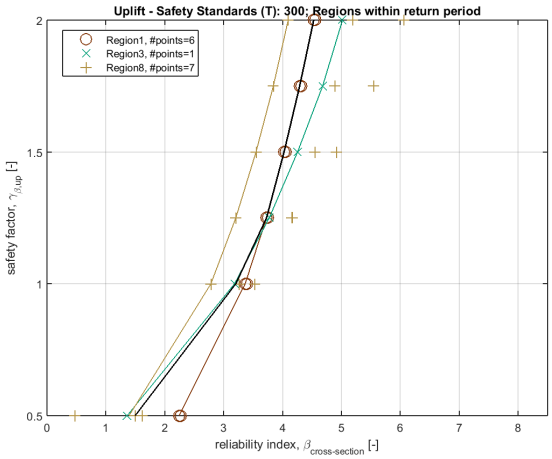

(f) Return period T = 100,000 years

Figure L.1: Uplift calibration results with 20%-quantiles - clustering per hydraulic region within a cluster per return period (T+R).

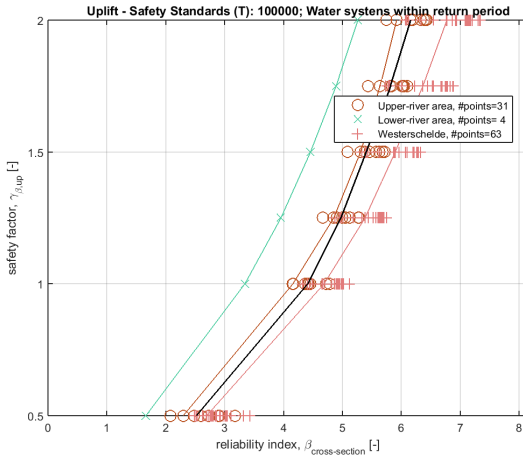

(a) Return period T = 300 years

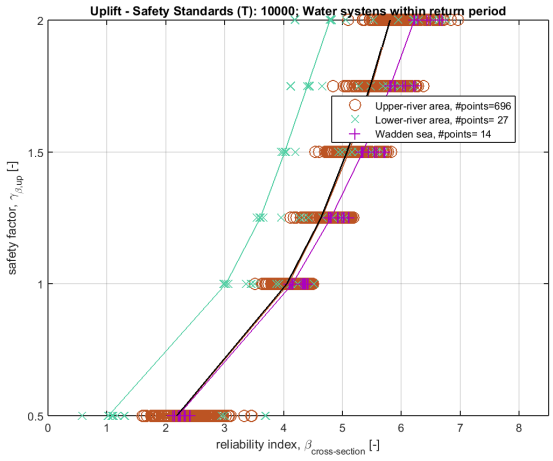

(b) Return period T = 1,000 years

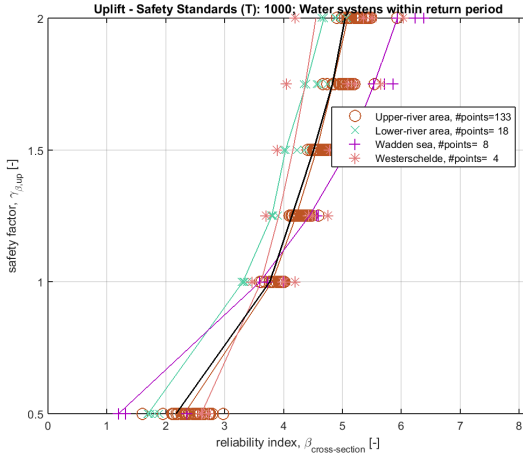

(c) Return period T = 3,000 years

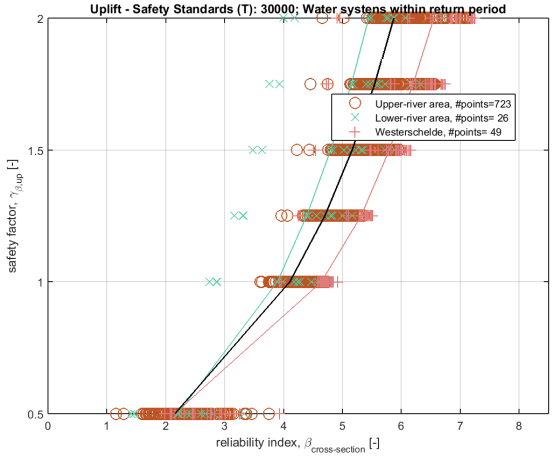

(d) Return period T = 10,000 years

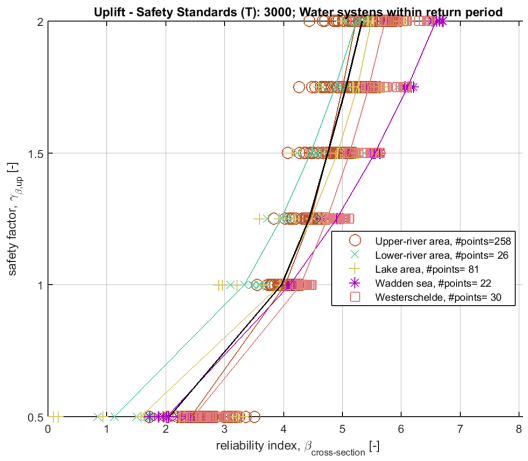

(e) Return period T = 30,000 years

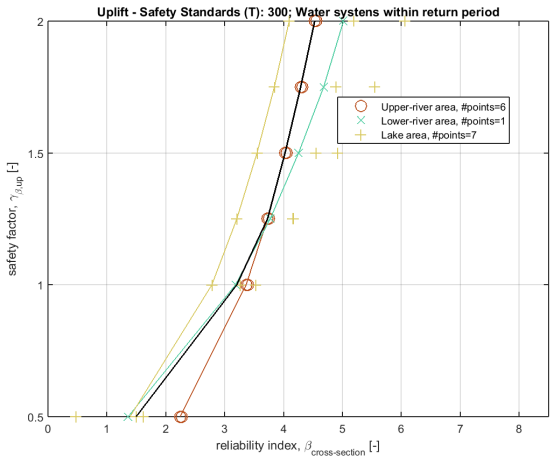

(f) Return period T = 100,000 years

Figure L.2: Uplift calibration results with 20%-quantiles - clustering per water system within a cluster per return period (T+W).

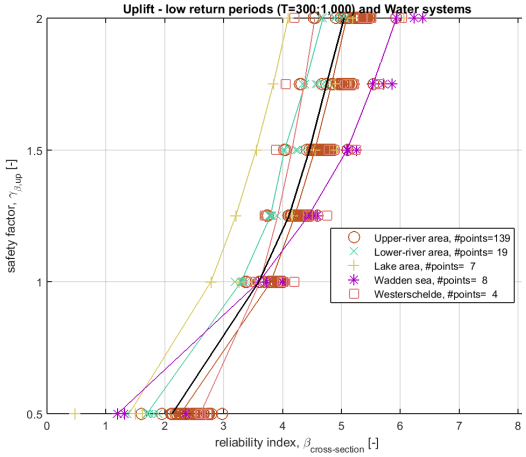

(a) Low safety standard level

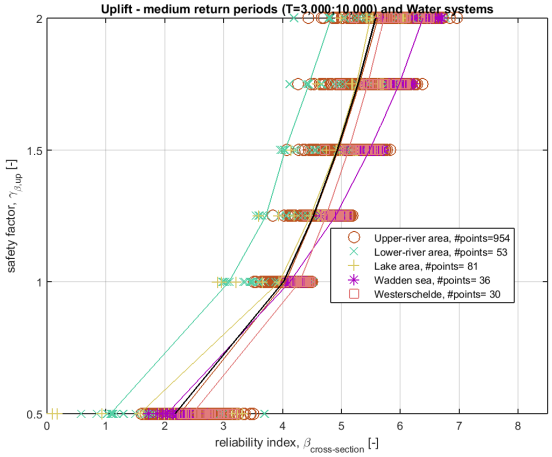

(b) Medium safety standard level

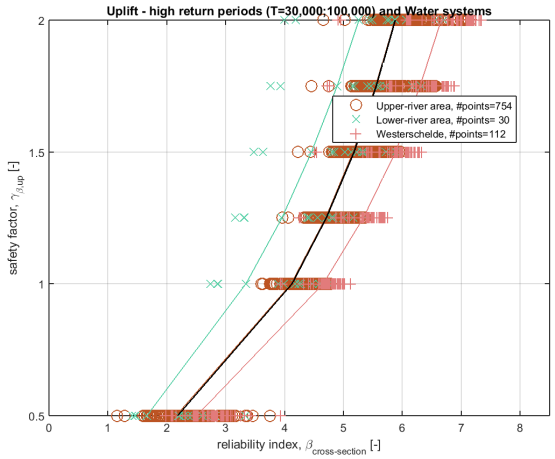

(c) High safety standard level

Figure L.3: Uplift calibration results with 20%-quantiles - clustering per water system within a cluster per safety standard level (S+W).

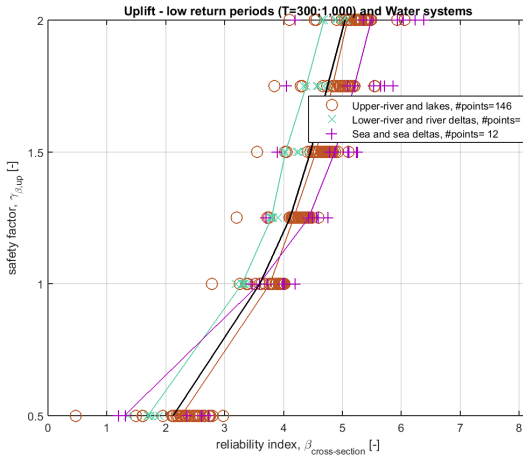

(a) Low safety standard level

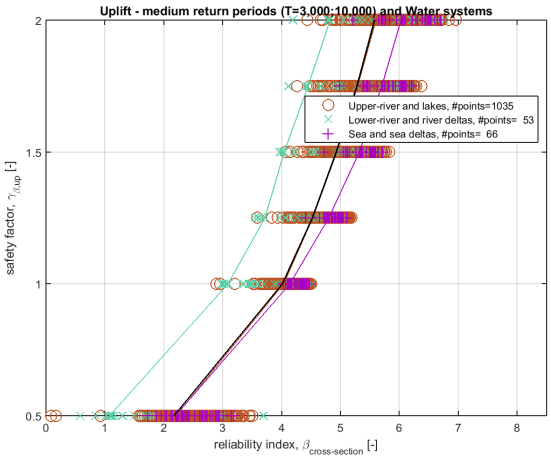

(b) Medium safety standard level

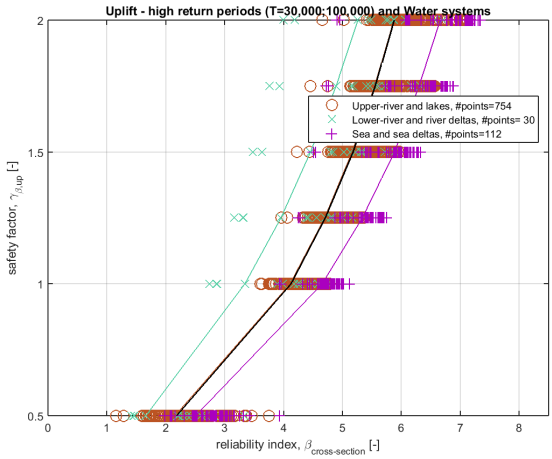

(c) High safety standard level

Figure L.4: Uplift calibration results with 20%-quantiles - clustering per water system (Wb) within a cluster per safety standard level (S+Wb).

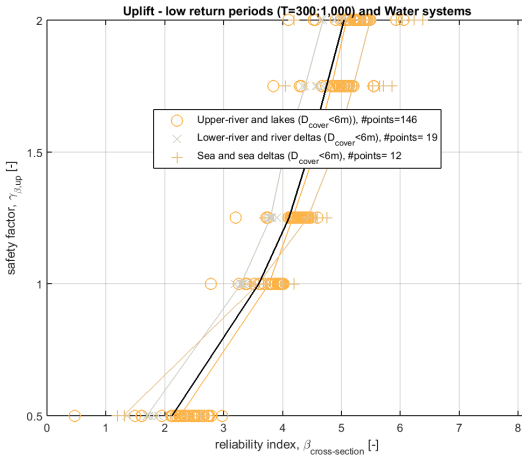

(a) Low safety standard level

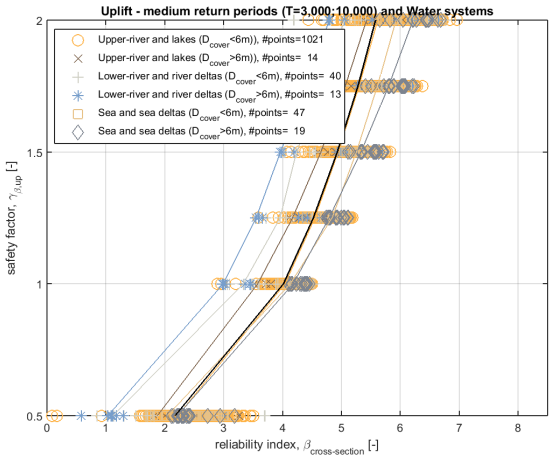

(b) Medium safety standard level

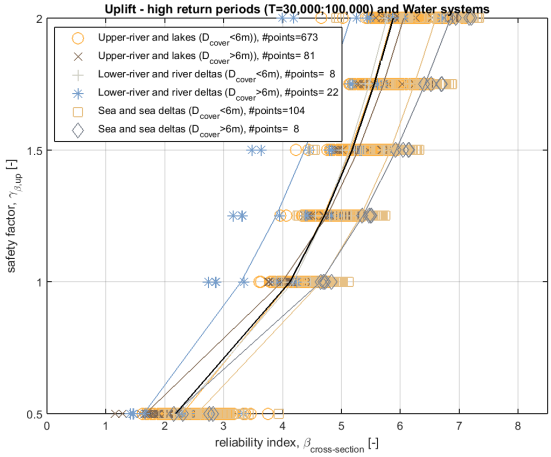

(c) High safety standard level

Figure L.5: Uplift calibration results with 20%-quantiles - clustering per cover layer class (Cb) within a water system (Wb) which is within a safety standard level (S+Wb+Cb).

M Heave: calibration results and cluster alternatives - Case 1

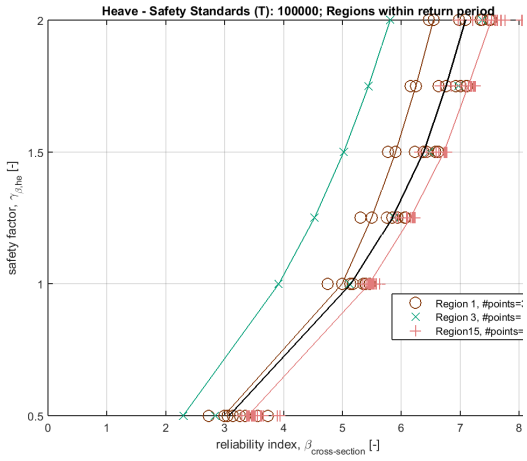

(a) Return period T = 300 years

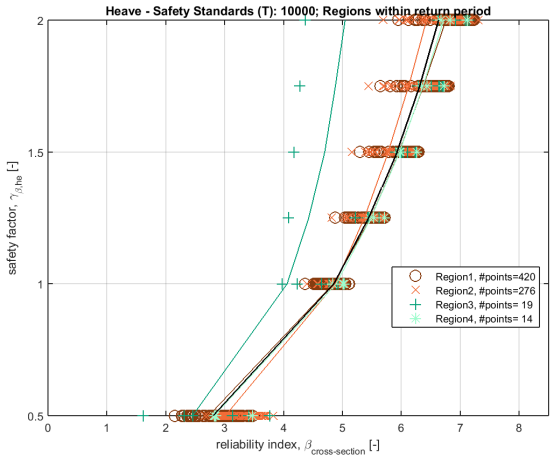

(b) Return period T = 1,000 years

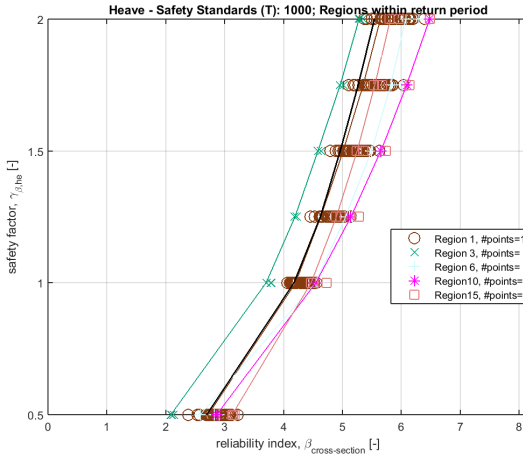

(c) Return period T = 3,000 years

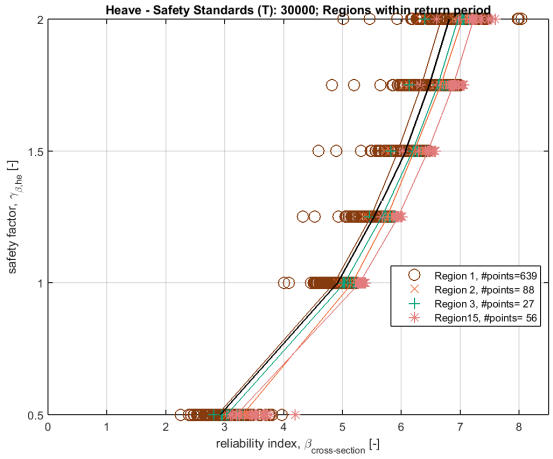

(d) Return period T = 10,000 years

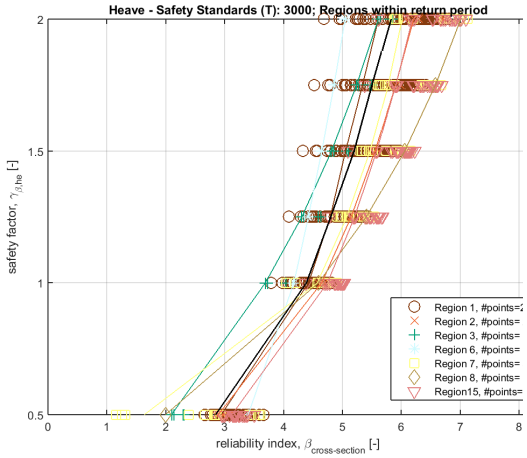

(e) Return period T = 30,000 years

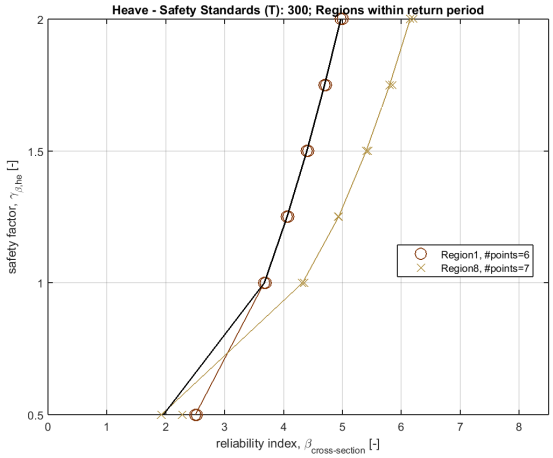

(f) Return period T = 100,000 years

Figure M.1: Heave calibration results with 20%-quantiles - clustering per hydraulic region within a cluster per return period (T+R).

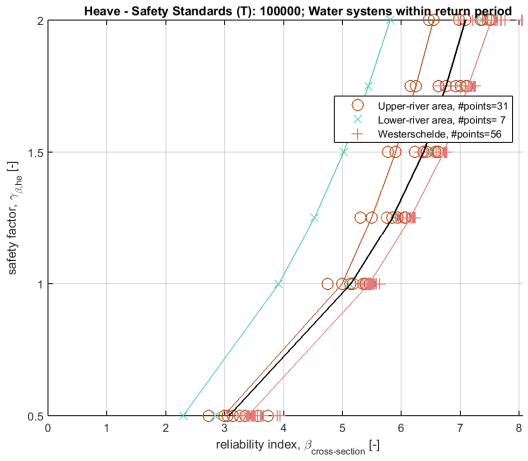

(a) Return period T = 300 years

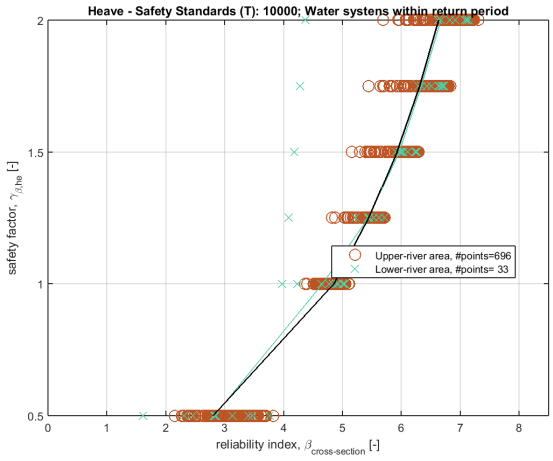

(b) Return period T = 1,000 years

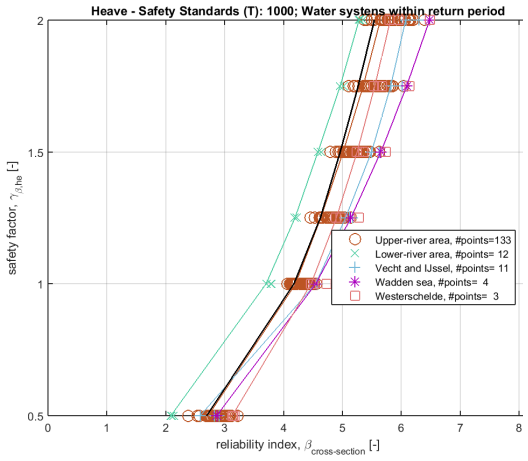

(c) Return period T = 3,000 years

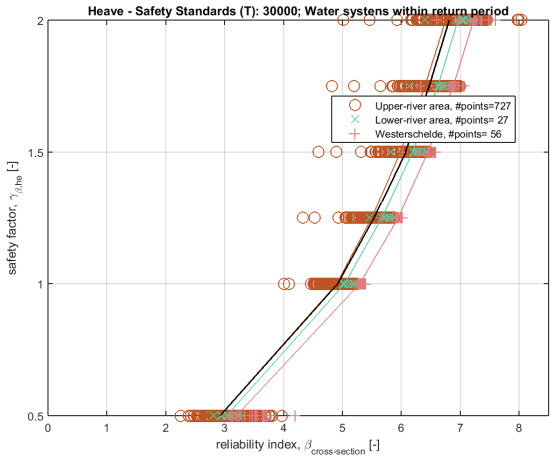

(d) Return period T = 10,000 years

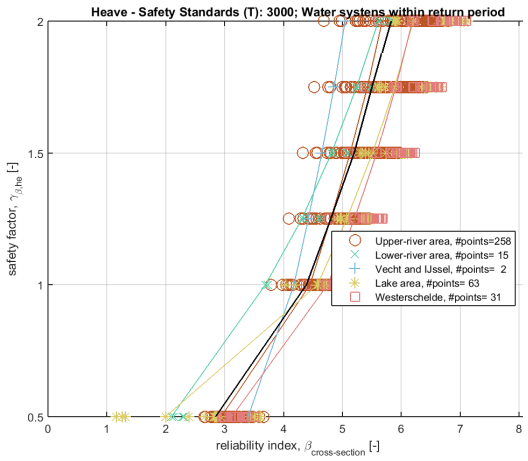

(e) Return period T = 30,000 years

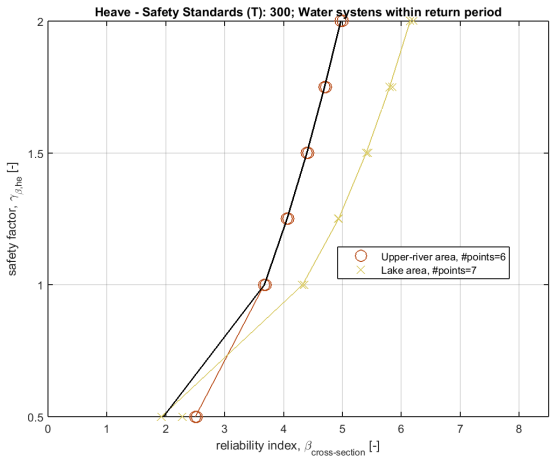

(f) Return period T = 100,000 years

Figure M.2: Heave calibration results with 20%-quantiles - clustering per water system within a cluster per return period (T+W).

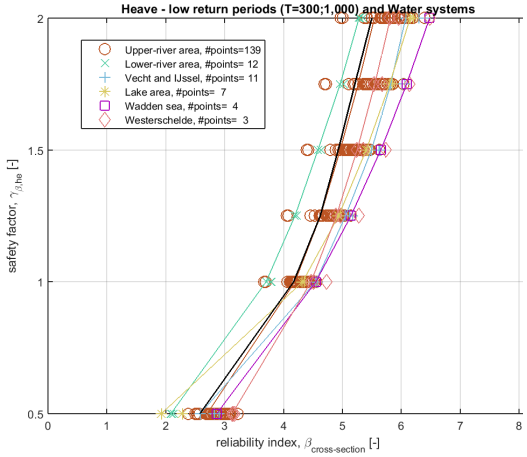

(a) Low safety standard level

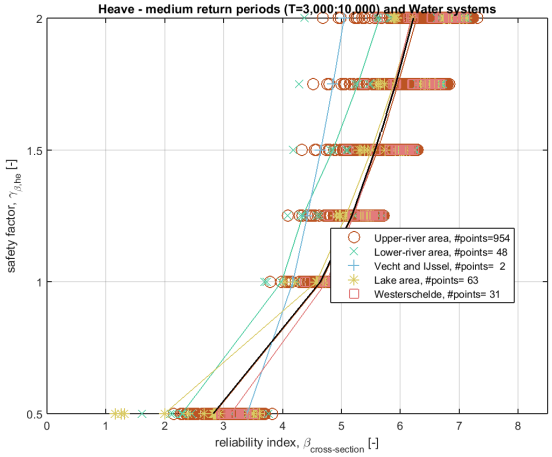

(b) Medium safety standard level

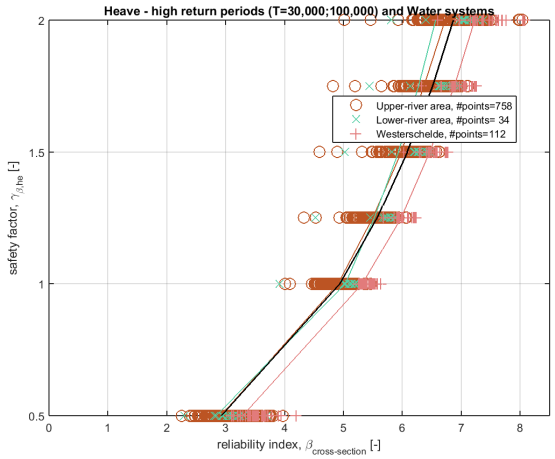

(c) High safety standard level

Figure M.3: Heave calibration results with 20%-quantiles - clustering per water system within a cluster per safety standard level (S+W).

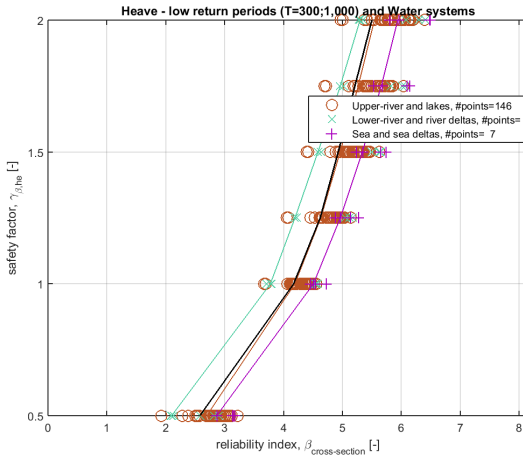

(a) Low safety standard level

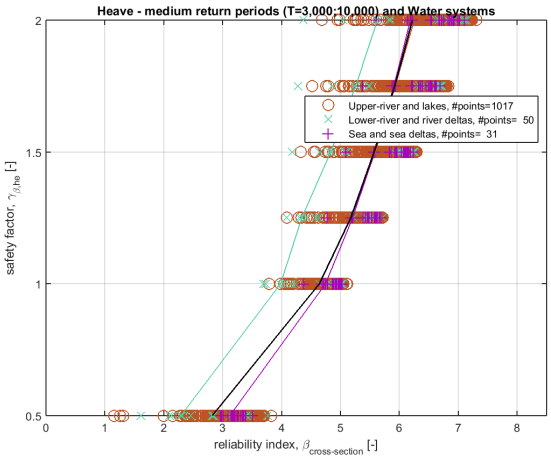

(b) Medium safety standard level

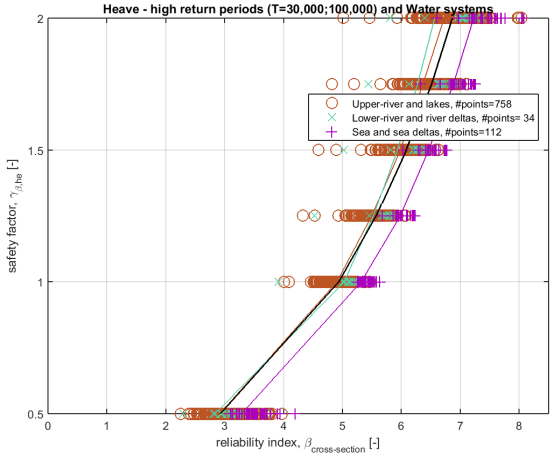

(c) High safety standard level

Figure M.4: Heave calibration results with 20%-quantiles - clustering per water system (Wb) within a cluster per safety standard level (S+Wb).

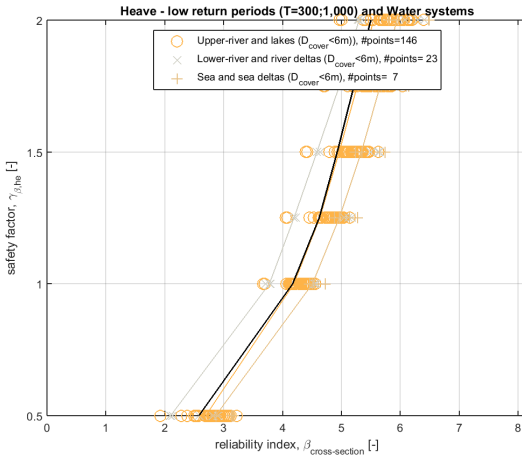

(a) Low safety standard level

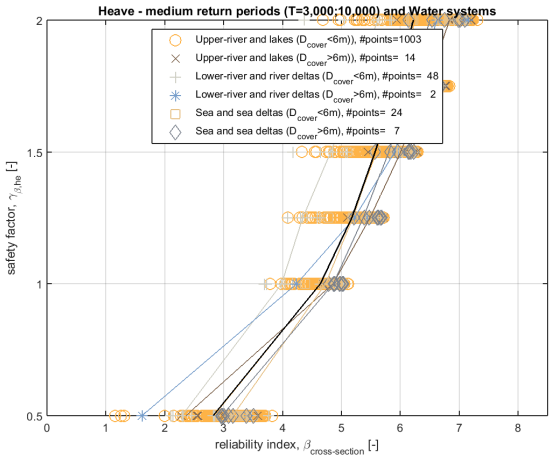

(b) Medium safety standard level

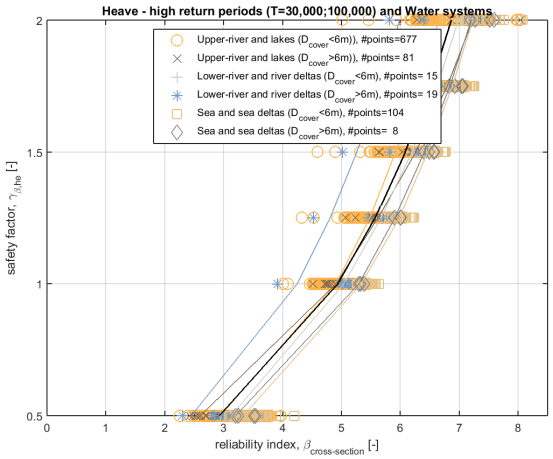

(c) High safety standard level

Figure M.5: Heave calibration results with 20%-quantiles - clustering per cover layer class (Cb) within a water system (Wb) which is within a safety standard level (S+Wb+Cb).

N Piping: calibration results and cluster alternatives - Case 1

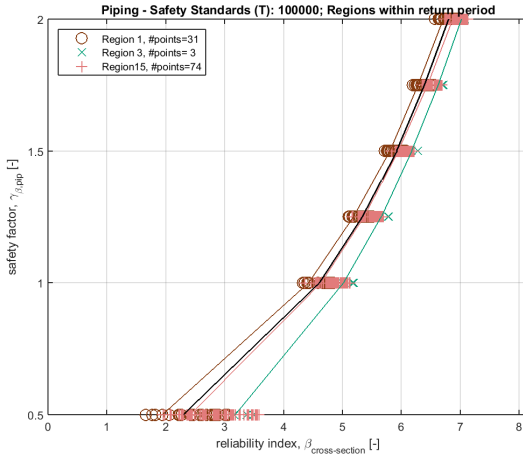

(a) Return period T = 300 years

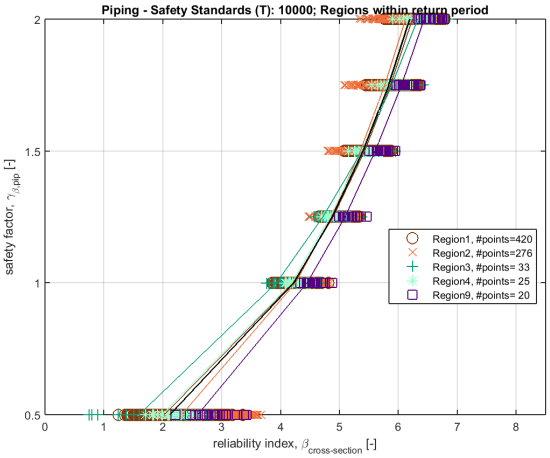

(b) Return period T = 1,000 years

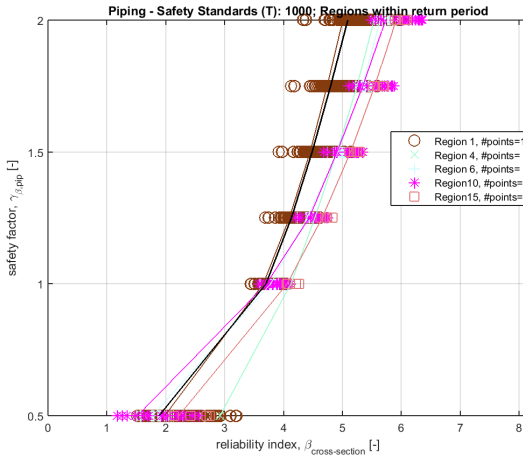

(c) Return period T = 3,000 years

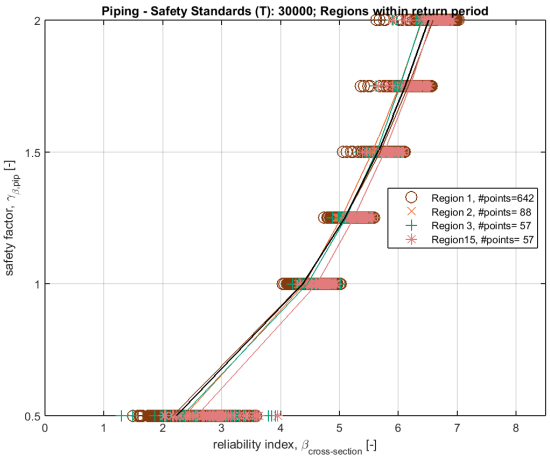

(d) Return period T = 10,000 years

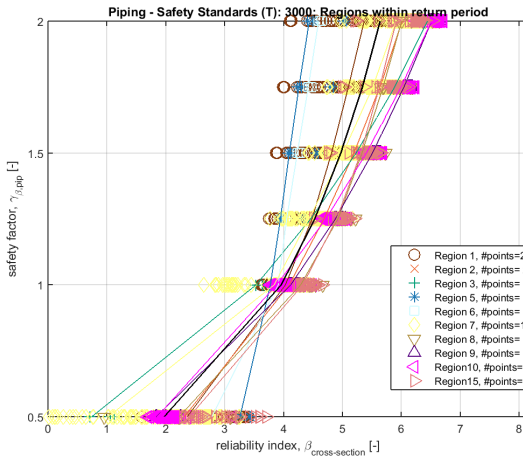

(e) Return period T = 30,000 years

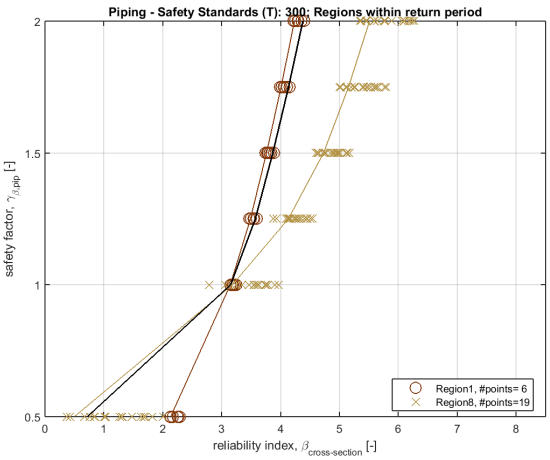

(f) Return period T = 100,000 years

Figure N.1: Piping calibration results with 20%-quantiles - clustering per hydraulic region within a cluster per return period (T+R).

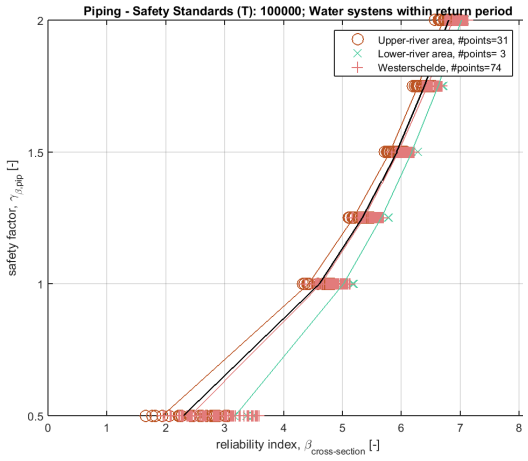

(a) Return period T = 300 years

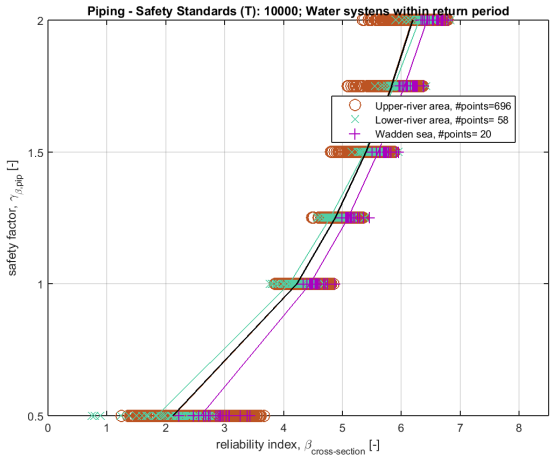

(b) Return period T = 1,000 years

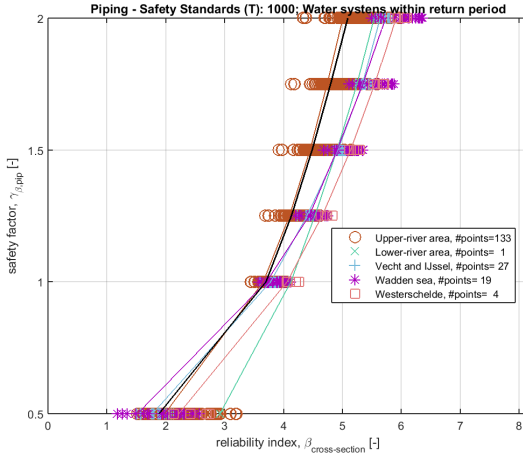

(c) Return period T = 3,000 years

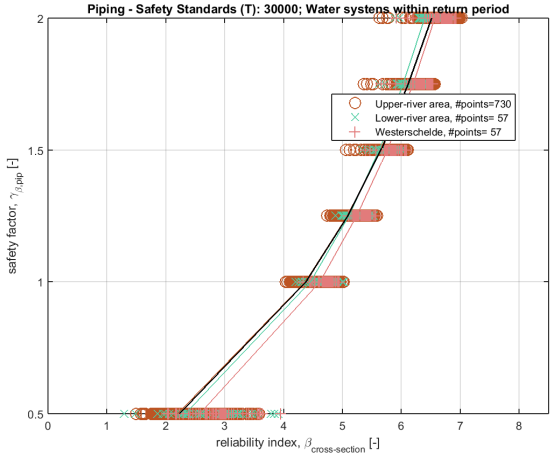

(d) Return period T = 10,000 years

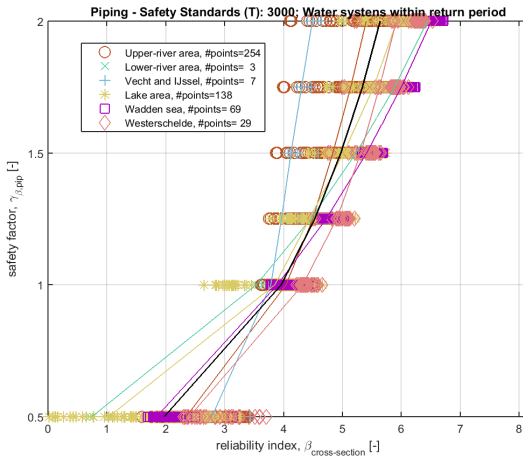

(e) Return period T = 30,000 years

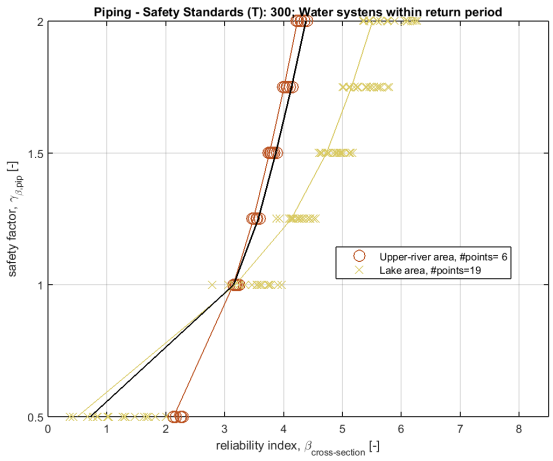

(f) Return period T = 100,000 years

Figure N.2: Piping calibration results with 20%-quantiles - clustering per water system within a cluster per return period (T+W).

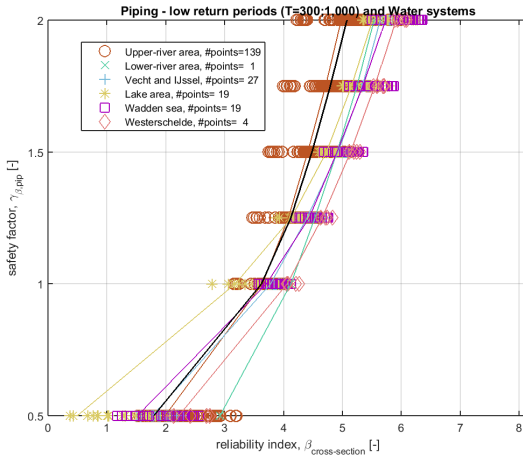

(a) Low safety standard level

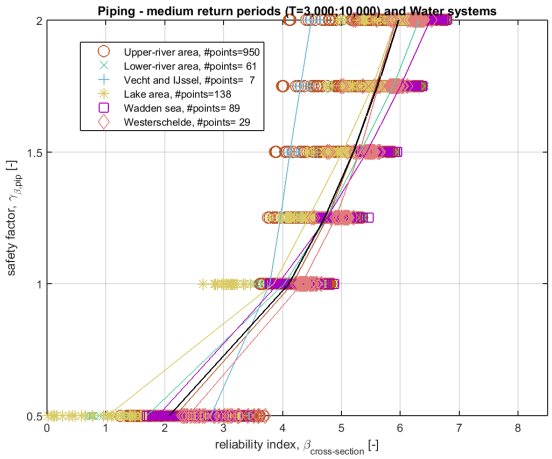

(b) Medium safety standard level

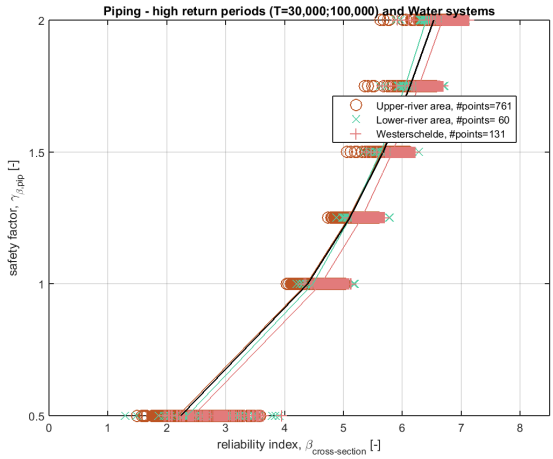

(c) High safety standard level

Figure N.3: Piping calibration results with 20%-quantiles - clustering per water system within a cluster per safety standard level (S+W).

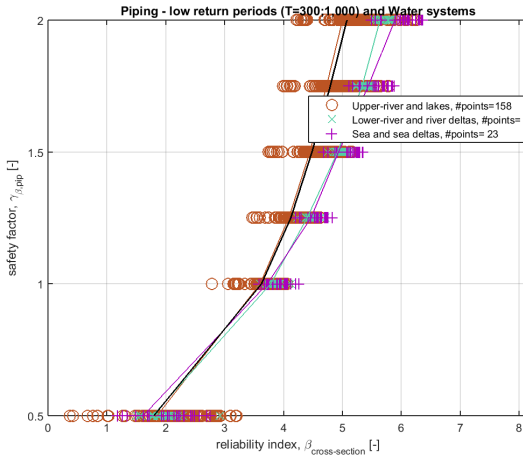

(a) Low safety standard level

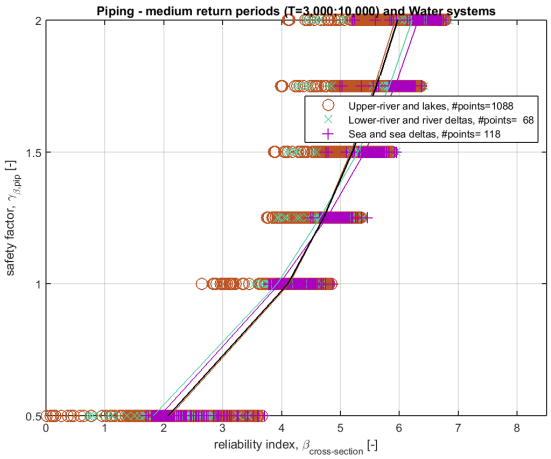

(b) Medium safety standard level

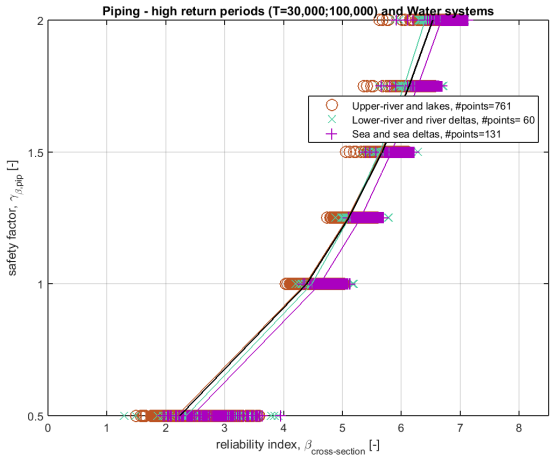

(c) High safety standard level

Figure N.4: Piping calibration results with 20%-quantiles - clustering per water system (Wb) within a cluster per safety standard level (S+Wb).

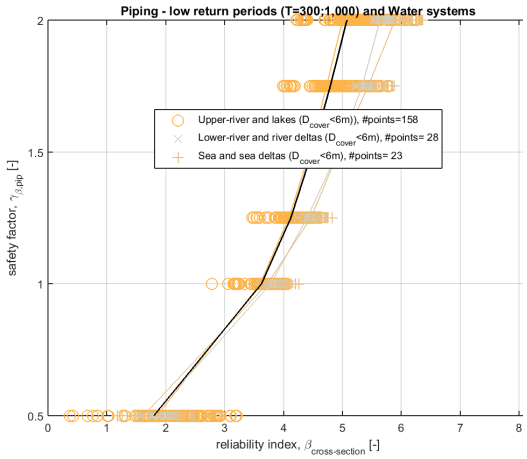

(a) Low safety standard level

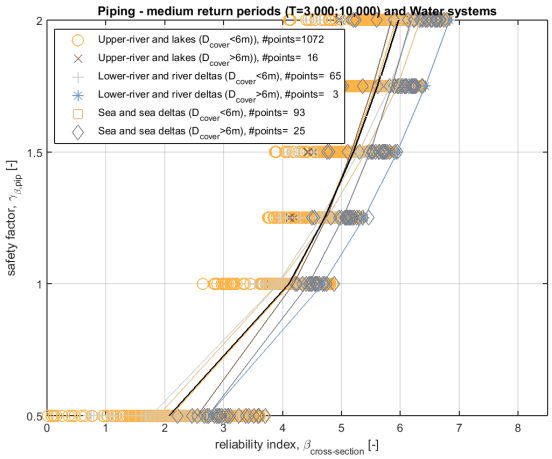

(b) Medium safety standard level

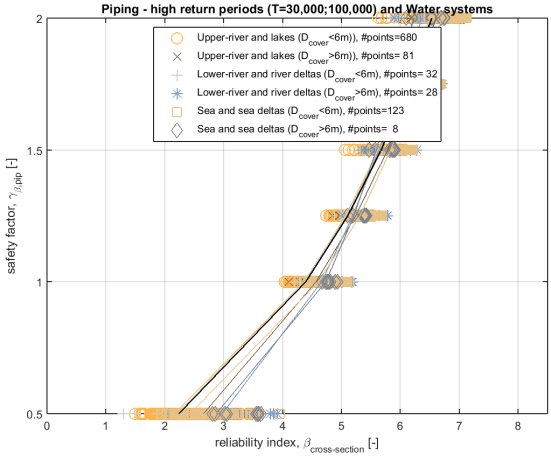

(c) High safety standard level

Figure N.5: Piping calibration results with 20%-quantiles - clustering per cover layer class (Cb) within a water system (Wb) which is within a safety standard level (S+Wb+Cb).

O Calibration for Eastern Scheldt - Case 1

This appendix presents the results of the calibration exercise of the semi-probabilistic rule for piping sub-mechanism applied to the area of the Eastern Scheldt (*Oosterschelde*). This area requires $Directional\ \ Sampling$ computations due to the loading characteristics *i.e.* the presence of the storm surge barrier. The method leads to a considerable computational time. Therefore, we considered only one dike segment in this area, *i.e.* segment 28-1 (leading to about 30 test cases). The exact same calibration procedure presented in chapter 4 was followed.

The Figure O.1 shows the results of the calibration for dike segment 28-1 together with the results of the calibration of the 2352 cases (remaining areas) for which probabilistic computations were carried out with the $FORM$ method. The analysis refers to Case 1 - all inputs come from the VNK2 databases. The two curves in the figure refer to the 20%-quantiles of the reliability indices achieved per safety factor; the red curve corresponds to dike segment 28-1 and the black curve corresponds to the remaining areas in the Netherlands.

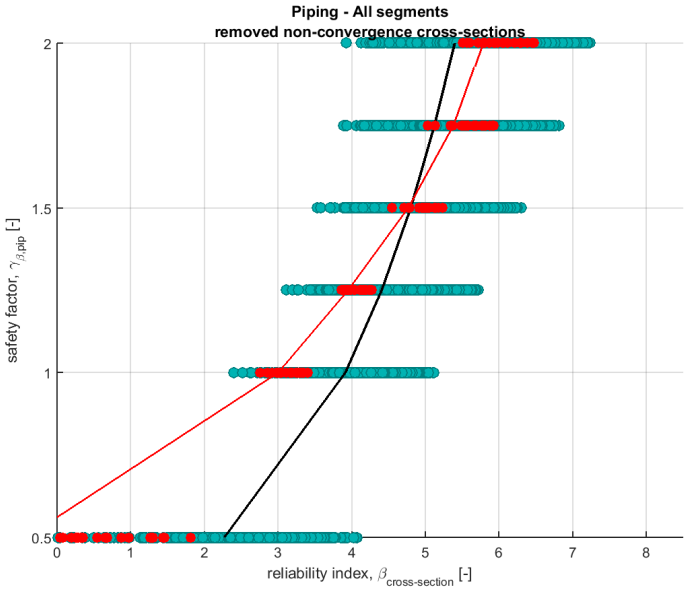

Figure O.1: Piping calibration results, 20%-quantile curve for dike segment 28-1 (red line) and remaining areas (black line), Case 1.

In this report, we recommend functional relations based on more than 2000 test cases (see chapter 8). Adding of the extra test cases in the Eastern Scheldt will not change the derived relations (this also holds for the uplift and heave sub-mechanisms). Therefore, the recommendation for dike segments in the Eastern Scheldt in case of the semi-probabilistic piping assessment, is to follow the steps from chapter 9. Note that the derived relations are novel as they depend on the reliability index corresponding to the safety standard of a dike segment β_{norm}. Introduction of a relation that depends on β_{norm} optimizes the semi-probabilistic assessment of dikes (also in the Eastern Scheldt), because more dike's characteristics are taken into account.